Universidade do Minho
Escola de Engenharia

Thomas Alwart de Bruijn

Recycling of Continuous Fibre Reinforced Thermoplastic Composites

Setembro de 2020

Recycling of Continuous Fibre Reinforced Thermoplastic Composites
Thomas A. de Bruijn
UMinho | 2020

TPAC THERMOPLASTIC COMPOSITES APPLICATION CENTER
Regieorgaan SIA

Universidade do Minho
Escola de Engenharia

Thomas A. de Bruijn

Recycling of Continuous Fibre Reinforced Thermoplastic Composites

Tese de Doutoramento
Ciência e Engenharia de Polimeros e Compósitos

Trabalho efetuado sob a orientação do
Dr. João Pedro Lourenço Gil Nunes

Co-orientador
Dr. Ferrie Wander Joseph van Hattum

Setembro de 2020

"We do not inherit the Earth from our ancestors; we borrow it from our children."

– Native American Proverb

Acknowledgements

The work presented in this thesis would not have been possible without the support of many people, institutions and companies.

First, I would like to express my strong gratitude to my supervisors. Dr. João Pedro Nunes for the guidance, encouragement and help throughout my PhD and allowing to pursue my PhD at the University of Minho. I thank Dr. Ferrie W.J. van Hattum for the support, vision and confidence during the project and making my time at the Thermoplastic Composites Applications Centre (TPAC) a great experience.

This work is part of the TPC-Cycle project, financed by the Dutch Organization of Applied Research – Regieorgaan SIA (RAAK 2014-01-72PRO), Netherlands Organization for Scientific Research (NWO).

I am grateful to the TPC-Cycle project partners for giving their valuable input and support. The partners involve industrial compagnies and knowledge institutes representing the total value chain in thermoplastic composite: Arnt Offringa, Michael Wielandt and Johan Meuzelaar of GKN Fokker, Menno Hensbroek of Cato Composites, David Manten, Marko Vreeling and Peter Boer of Dutch Thermoplastic Components, Winand Kok, Frank ten Napel and Richard Bergman of Toray Advanced Composites, Chris Volkmann of NRT, Prof. Remko Akkerman, Dr. Sebastiaan Wijskamp, Dr. Iqbal Rasheed, the technical advisory board and technicians of the Thermoplastic Composites Research Center (TPRC), TPAC and Saxion University of Applied Sciences. I also acknowledge various compagnies, e.g. OEMs in aerospace, for making the access panel possible or showing interest in e.g. the workshop. I am especially thankful to Johan Meuzelaar for the opportunity, effort and collaboration on the access panel and enabling it to fly.

This dissertation would not have been possible without my research partner, colleague and friend Dr. Guillaume Vincent. It was a great time working, learning and traveling throughout our PhD period. The discussions about scrap vs waste, goodness of mixing, the word *"chocolatine"* and the fact that France is a five-star shaped country will stay with me my entire life.

Many thanks to all colleagues of the TPAC and people of Saxion, with whom I worked, for their help and the wonderful time in general. I want to thank Rik Voerman, Franziska Regel, Marieke Voordouw, Remi Hoefman and all involved students, including Ilse, Kevin and Matteo.

I want to acknowledge the people at the University of Minho and University of Twente. I am grateful to the staff, PhD students and technicians for their time during and outside working hours.

I would like to thank everyone who directly or indirectly supported me throughout the last years and encouraged me in the completion of this work, for example Arne and Anna, for their support on modelling. Finally, I want to thank Ellen for her endless support and love. Lastly, dear Yfke and Michiel thank you both for giving perspective to my life and helping me to strive for future generations.

STATEMENT OF INTEGRITY

I hereby declare having conducted this academic work with integrity. I confirm that I have not used plagiarism or any form of undue use of information or falsification of results along the process leading to its elaboration.

I further declare that I have fully acknowledged the Code of Ethical Conduct of the University of Minho

University of Minho, 25 Sep 2020

Full name: Thomas Alwart de Bruijn

Signature: 

Abstract

Due to the material's intrinsic benefits, the volume of continuous fibre reinforced thermoplastic composites (TPCs) is growing and leading to a rise of industrial waste, though a high-quality recycling route is not yet available. TPC recycling enables reclaiming the high economic value, reducing the environmental impact and to be in-line with environmental directives. In this study a new TPC recycling route was developed and successfully validated allowing to achieve, maximum cost effectiveness and minimum environmental impact.

The trade-off between mechanical performance and processability or degree of mixing for long and short fibres respectively, is optimised by developing a micromechanical model. The model was used to predict stiffness and strength and includes distributions for fibre length and the degree of mixing, by local fibre volume variation and fibres per bundle. An appropriate recycling route consisting of shredding, low-shear mixing and compression moulding, was established to experimentally validate the mechanical performance of recycled TPCs. G/PP and C/PPS at various fibre orientations, contents and length distributions and waste material consolidation stages were processed both without mixing and by different levels of low-shear mixing. Characterisation was performed by flexural, impact and cross-sectional microscopy testing. The experimental properties of the recycled material were found to be in-line with theoretical predictions and increase with degree of mixing.

Three demonstrator products were designed, produced and tested to prove their technical and application feasibility; a bracket, a safety shoe nose cap and an aerospace access panel. While made of recycled material with inferior material properties, the panel was even lighter than the current solution and gave enough confidence to be flight tested. Life cycle analysis and cost assessment were used to compare the recycled material and demonstrators to currently used alternatives. A significant reduction in cost and environmental impact was found for both the panel and nose cap. The panel made from recycled material offered reductions of over 80% in greenhouse gases (GHG) and 60% in cost, when compared to the virgin C/epoxy benchmark.

The work carried out demonstrates that recycling is feasible and enables applications currently made by using virgin materials at a significant reduction in costs and environmental impact and already led to the world's first flying fully recycled thermoplastic composite application in aerospace*.

Keywords: *Environmental impact, LCA, Mechanical behaviour, Recycling, Thermoplastic matrix composites.*

* JEC Group, "A rotorcraft access panel made from recycled carbon PPS," HOW IT'S MADE, 2020. [Online, Accessed: 01-Jul-2020]. Available: http://www.jeccomposites.com/knowledge/international-composites-news/how-its-made-rotorcraft-access-panel-made-recycled-carbon.

Resumo

Face às suas vantagens intrínsecas, a aplicação de termoplásticos reforçados com fibras contínuas (TPCs) tem aumentado e contribuído para o crescimento do lixo industrial, dada a inexistência duma solução eficaz para a sua reciclagem. A reciclagem dos TPCs deve recuperar o alto valor económico do material, reduzir o impacto ambiental e estar em linha com as diretivas ambientais existentes. Este estudo desenvolveu e validou com sucesso um novo método de reciclagem de TPCs com máximo custo-benefício e mínimo impacto ambiental.

Desenvolveu-se um modelo micromecânico para otimizar o equilíbrio entre desempenho mecânico e processabilidade ou grau de mistura para, respetivamente, fibras longas e curtas. Sendo usado para prever da rigidez e a resistência mecânica, o modelo incorpora a influência que a variação da fração volúmica localizada de fibras e o seu número nas mechas têm na distribuição dos comprimentos de fibras e grau de mistura obtidos. Definiu-se uma reciclagem adequada envolvendo trituração, mistura com baixa taxa de corte e fabrico por compressão para validar o desempenho mecânico de TPCs reciclados. Fabricaram-se compósitos G/PP e C/PPS reciclados com diferentes teores, orientações, comprimentos e distribuição de comprimentos de fibras, estágios de consolidação de resíduos, sem mistura ou com diferentes níveis de mistura a baixa taxa de corte para caracterização por ensaios de flexão, impacto e microscopia da sua seção transversal. Os TPCs reciclados apresentaram propriedades em linha com as previsões teóricas e que aumentavam com o grau de mistura. Projetaram-se, fabricaram-se e testaram-se três produtos demonstradores para comprovar a sua viabilidade técnica e aplicação: um suporte, uma biqueira de sapato de segurança e um painel de acesso para a indústria aeroespacial. Embora usando material reciclado de propriedades inferiores, o painel mostrou ser ainda mais leve que a solução atualmente existente e ofereceu suficiente confiança para ter já sido testado em voo. A análise de ciclo de vida e a avaliação de custos foram usadas para comparar demonstradores com as suas alternativas atuais. Tanto o painel como a biqueira permitiram reduzir significativamente o custo e impacto ambiental. O painel reciclado, comparado à solução em material virgem, diminuiu as emissões de gases de estufa e o custo em mais de 80% e 60%, respetivamente. Este trabalho comprova que a reciclagem é viável e que a substituição de materiais virgem em muitas aplicações atuais pode reduzir significativamente custos e o impacto ambiental e já contribuiu para a realização do primeiro voo mundial integrando um produto destinado à indústria aeroespacial totalmente fabricado em TPC reciclado*.

Palavras-chave: *Comportamento mecânico, Compósitos de matriz termoplástica, Impacto ambiental, LCA, Reciclagem.*

* JEC Group, "A rotorcraft access panel made from recycled carbon PPS," HOW IT'S MADE, 2020. [Online, Accessed: 01-Jul-2020]. Available: http://www.jeccomposites.com/knowledge/international-composites-news/how-its-made-rotorcraft-access-panel-made-recycled-carbon.

Contents

List of figures

List of Tables

Nomenclature

Acronyms

2D	Two-dimensional
2D random	Two-dimensional random (fibre orientation)
5HS	5 harness satin
BMC	Bulk moulding compound
BSD	Bundle size distribution
C/PPS	Carbon fibre reinforced polyfenyleensulfide
CED	Cumulative energy depletion
CFRP	Carbon fibre reinforced polymer
CM	Compression moulding
CoV	Coefficient of variation
DCM	Direct compression moulding
EoL	End-of-Life
FEM	Finite element method
FLBSD	Combined fibre length and bundle size distribution
FLD	Fibre length distribution
FRPC	Fibre reinforced polymer composite
FVD	Fibre volume fraction distribution
FVF	Fibre volume fraction
G/PP	Glass fibre reinforced polypropylene
GFRP	Glass fibre reinforced polymer
GHG	Greenhouse gases (GHG)
GM	Good mix (or well mixed) material
GMT	Glass mat reinforced thermoplastic
IoS	Intensity of Segregation
L/d	Length over diameter
LCA	Life-cycle-assessment
LCCA	Life-cycle-and-cost-assessment
LFT	Long fibre thermoplastic
LL	Lower limit

MCM	Mixing compression moulding
MROM	Modified rule of mixtures
PEAK	(family of) Polyaryletherketone
PEEK	Polyetheretherketone
PEI	Polyetherimide
PM	Poorly mixed (material)
PMMA	Polymethylmethacrylate
PP	Polypropylene
PPS	Polyphenylene sulfide
ROM	Rule of mixtures
SD	Standard deviation
SEM	Stereo electron beam microscope
SFT	Short fibre thermoplastic
TPC	Thermoplastic composite
TPU	Thermoplastic polyurethane
TSC	Thermosetting composite
UD	Unidirectional (fibre orientation)
UL	Upper limit

Coordinate system

1, 2, 3	Coordinate system with direction 1 indicating the main fibre direction, 2 perpendicular to this direction and 3 perpendicular to the 1-2-plane

Greek symbols

η_e	mechanical efficiency
η_l	fibre length efficiency factor
η_o	fibre orientation factor
ρ	density
Ψ_p	probability density function
Θ	fibre orientation

θ_d	draft angle
σ_c,	composite strength
σ_{cL}	longitudinal strength of a composite
σ_f	fibre strength
σ'_m	matrix strength at fibre failure
τ	interfacial shear strength (between fibre and matrix)
θ	fibre orientation angle with direction 3 (out of plane)
φ	fibre orientation angle with direction 1 in the 1-2 plane (in plane)

Roman Symbols

$\mathbf{a}_{ij}$	second order fibre orientation tensor describing the state at any point (ij = 1, 2, 3)
d	fibre diameter
D	bundle diameter
E_c,	Young's modulus composite
E_f	Young's modulus fibre
E_m	Young's modulus matrix
h	height
K	bending stiffness
I	moment of inertia
l	fibre length
l_c.	critical fibre length
$\boldsymbol{p}_i$	unit vector to describe the orientation state of a single fibre in space (i = 1, 2, 3)
r_B	radius at bottom (of rib)
r_T	radius at top (of rib)
t	thickness
T	base thickness (of rib)
V_f	fibre volume
w	width

1 Introduction

1.1 Background and motivation

Composite materials are on a rise. The material offers lightweight potential and can contribute to a reduction of emissions, especially in very defined areas of application such as the transportation sector [1]. This will contribute to reach the European Green Deal [2]: 1) at least a 50% cut in greenhouse gas (GHG) emissions in 2030 compared to 1990 levels [3] and, 2) net-zero GHG emissions in 2050 [4]. Lightweight is not the only advantage. Other benefits, such as possibilities for integrating components into existing systems, decreasing the complexity of the manufacturing process, are becoming increasingly important [1].

The global demand for carbon fibre reinforced polymer (CFRP) was 114kt (approx. 15bn US$) in 2017 and showed an average annual growth rate of 12.8% in volume since 2010 [1]. The European market for glass fibre reinforced polymers (GFRP) with a length over 2 mm was 1.118 kt in 2017, having increased at rates of more than 2% per year in Europe and well over this figure in the rest of the world [1].

Within the continuous fibre composites' market, thermoplastic composites (TPC) account for an increasing market share in comparison to their thermosetting equivalent. For example, the carbon fibre based TPCs is growing from 24% in 2014 to 29% in 2018 compared to carbon fibre thermoset composites, which represents an average annual growth rate of 17% related to overall revenue [1]. For the total TPC market, a growth rate of 3.7% is foreseen for 2018-2023, driven by growing demand for lightweight and environmentally sustainable materials, and the replacement of metals with composites in different end use industries [5]. Beneficial characteristics, like superior toughness, fast processing, possibility to weld, automate the production and recycling potential result in a rising interest and application [6, 7]. Beside the current small volumes in several minor sectors of the past, the recent success of applications in high-end, but low to medium volume markets, like aerospace [6, 8, 9], sporting goods [10] and defence [11] have proven the technology ready for high volume and serial production in, for example, the automotive industry [5, 6]. Since the volumes are increasing, large material supplying companies like Sabic [14] and Ten Cate [15] are increasing their efforts to provide continuous fibre TPCs.

The increased scale will likely bring the material and processing costs down, accelerating the growth and enabling opportunities in other segments.

Due to this increasing demand, large amounts of waste will follow in the (near) future: first in form of production waste and at a later stage as end-of-life waste. Since the production processes in continuous fibre reinforced composites often involve activities like stamp forming, usually incorporating nesting and trimming, the generated industrial waste is considerable [16]. As an illustration, the global demand and estimated waste of carbon fibre only is given in Figure 1.1.

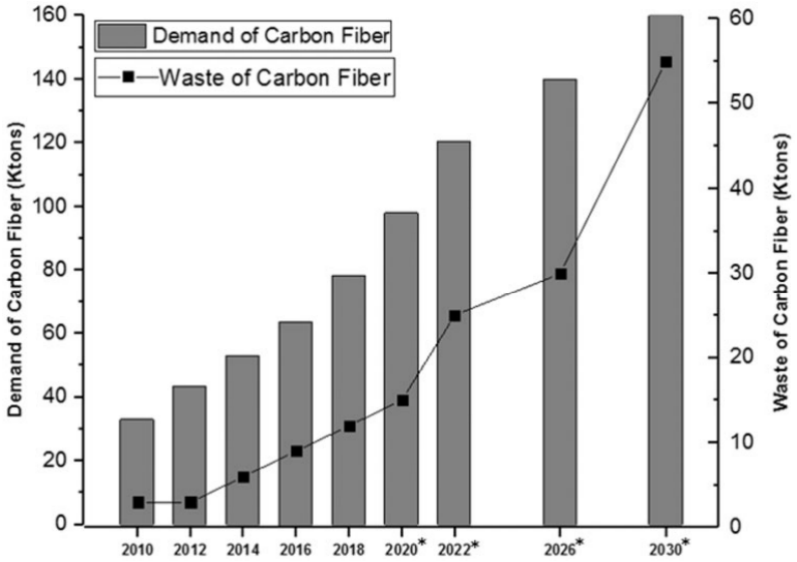

Figure 1.1 - Global demand of carbon fibre and estimated waste of carbon fibre (*estimates) [1, 17, 18]

Current continuous fibre processing techniques for high-end applications can incorporate a product to industrial waste ratio up to 40% and the waste is often incinerated [19, 20]. The term buy-to-fly ratio is used in aerospace to describe the procured material weight to the weight of the finished product. For metal production in aerospace, buy-to-fly ratios between 10:1 and 5:1 are common and the low buy-to-fly ratio of composites, ranging between 1.2:1 and 2:1 are seen as a driver to choose for composite material [21–24]. The expectation is that the figure may decline in the future due to process optimisation by e.g. the use of fibre placement, however, the growing volume will result in an increasing waste stream.

It is found to be difficult to acquire precise data on thermoplastic waste volumes and cost, especially since most numbers include thermosetting plastics, representing the major part of the composite market. Using the general numbers stated previously and the waste ratio for composites, a rough indication of waste volume can be made. Based on the numbers discussed in this section, a very rough indication of post-industrial waste is 10 kt/yr or 1.3bn US$ (based on the mentioned 114 kt/yr and 15bn US$/yr

CFRP, 29% with a thermoplastic matrix and 30% waste). Considering Dutch companies only, the total amount of waste is expected to grow from 50 t/yr in 2015 to 100 t/yr in 2024 and this waste is currently treated as general waste due to the absence of adequate recycling technologies [25].

These values concern the high-end and low-volume market typically found in aerospace. Nevertheless, recycling is a topic of concern in the low-end high-volume market as well. Beside the economical and general environmental impact of the waste, legislation is becoming an increasingly important factor. Several European directives and regulations are concerning polymer waste management and recycling (e.g. 99/31/EC on Landfill of Waste; 2000/53/EC on End-of-life vehicles; 2004/35/EC on Environmental Liability; 2019 The European Green Deal [2]). As an example: in the automotive industry, 85% of the weight of cars produced as of the year 2015, needs to be reused or recycled. Furthermore, the Dutch government aims to transform the linear economy to a circular economy by reducing the use of primary materials with 50% by 2030 and to become completely circular by 2050 [26]. The linear economy and sustainable economy are visualised in Figure 1.2 [27]. This thesis aims to recycle post-industrial waste – indicated in Figure 1.2 by the highlighted, dark-green circle - which is a first step towards a fully circular economy, where all materials are fully recycled and no raw material and waste exist. The European Climate ambitions are recently increased in The European Green Deal [2] to "transform EU's economy for a sustainable future" and "striving to be the first climate-neutral continent". Besides the previous stated reductions on GHG emission, the goals include "mobilising industry for a clean and circular economy" and "a zero-pollution ambition for a toxic free environment". These general goals are likely to be translated in more specific directives and regulations of nations and companies, resulting in an increased request for energy efficient processes and recycling solutions.

Beside cost and legislation, the environmental aspect of recycling is the third motivation for recycling. The environmental awareness and knowledge on the impact of e.g. GHG on the earth is growing and can offer a reason for clients of customer at several locations in the value chain to choose for solutions incorporating recycling. But most of all, recycling typically helps to reduce the use of materials and energy, hence it generally offers a reduction on the negative environmental impact improving the lives of us and our future generations.

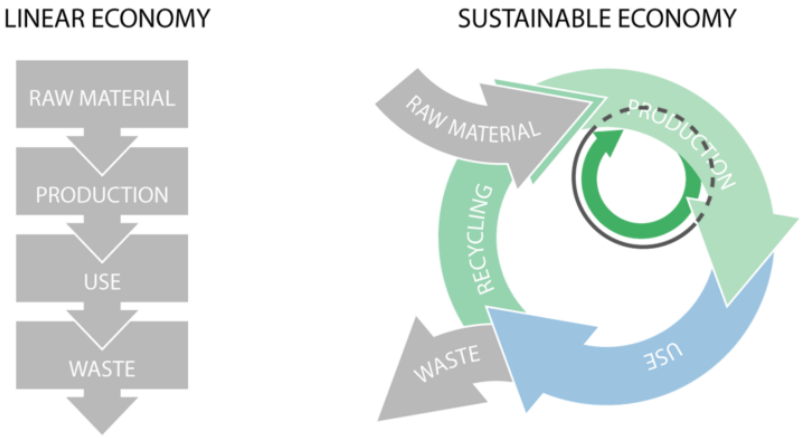

Figure 1.2 - Transition of a linear economy (left) towards a sustainable economy (right). This thesis will focus on the post-industrial production waste, highlighted on the righthand side. Adapted from [27]

1.2 Recycling of continuous fibre thermoplastic composites

Over decades, the hierarchy of waste management is used as a basis for ranking waste disposal options from least favourable to most favourable (see Figure 1.3) [28]. Whereas metal and thermoplastic materials are rather straightforward to recycle, the addition of continuous fibres to thermoplastics makes recycling increasingly complicated and most of the waste is disposed by landfill and energy recovery. While this is often also stated for TPCs, there seems to be more research dedicated to thermosetting composites (TSC). For TSCs various studies were performed, i.e. Oliveux et al. [29], Pickering [30] and Zhang et al. [31] presented overviews of recycling routes. Thermal and chemical methods are used to separate fibres and matrix to perform fibre reclamation, unnecessary for TPCs. For both thermosets and thermoplastic composites, mechanical grinding is commonly used to reduce the waste to small particles used as filler, often in cement kilns leading to significant controversy concerning the environmental impact and in some occasions to higher value products by injection moulding [29]. Within injection moulding, fibre lengths are typically reduced by high shear forces to around 0.2 to 0.3 mm, resulting in reasonable fibre efficiency regarding stiffness, but low efficiency regarding strength and impact [32]. Therefore, the recycling of thermoplastic composites by injection moulding does not lead to structural applications. Although this route offers a solution in new applications and is likely to have a lower environmental impact compared to the current widely applied incineration method, the mechanical performance of the fibres is only marginally exploited. Since thermoplastic composites offer direct recycling possibilities by melting and forming, it opens the possibility for a higher quality recycling route in terms of fibre length and mechanical performance. This study aims at a practical approach to research such a high-quality recycling

route retaining the mechanical properties through preserving long fibre length (>5 mm), unaffected fibre sizing and impregnation, leading to a more economical and environmental solution.

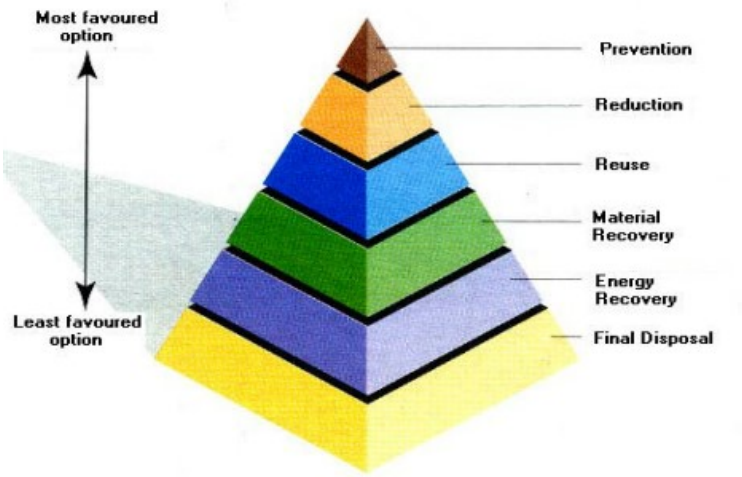

Figure 1.3 - Hierarchy of waste management [28]

1.3 Continuous fibre thermoplastic composites waste

To cover a broad range of the TPC market, one carbon fibre-based material is selected to represent the high-end market and one glass fibre-based material is selected to represent the high-volume market. The high-end market is dominated by aerospace [1] and the main TPC material used in this sector is C/PPS [33]. The most used TPC material in the composite sector is G/PP [34].

Three types of TPC manufacturing processes found in aerospace are studied to identify the origin and type of waste. Figure 1.4 shows a material flowchart of the three processes including the production steps where waste is generated. The top row in the figure represents a process with a simultaneous forming and consolidation step, typically found in autoclave or press consolidation of prepregs. The second row in the figure shows the material flow for separate consolidation and forming, typically found in stamp forming. The third and bottom row illustrates a process of UD tapes placed in tailored blanks, typically found in tailored banks, which are recently researched to, amongst others, reduce waste [35]. The ratio of waste at the processing steps is estimated by, amongst others, taking dimensions of available waste material when available. Although waste is created at various stages throughout the manufacturing process, the majority of the waste consist of nesting offcuts and trimmed edged, which is pre-dominantly consolidated multiply material. Hence, the focus will be on this type of waste material, although also semipreg is considered for comparison reasons.

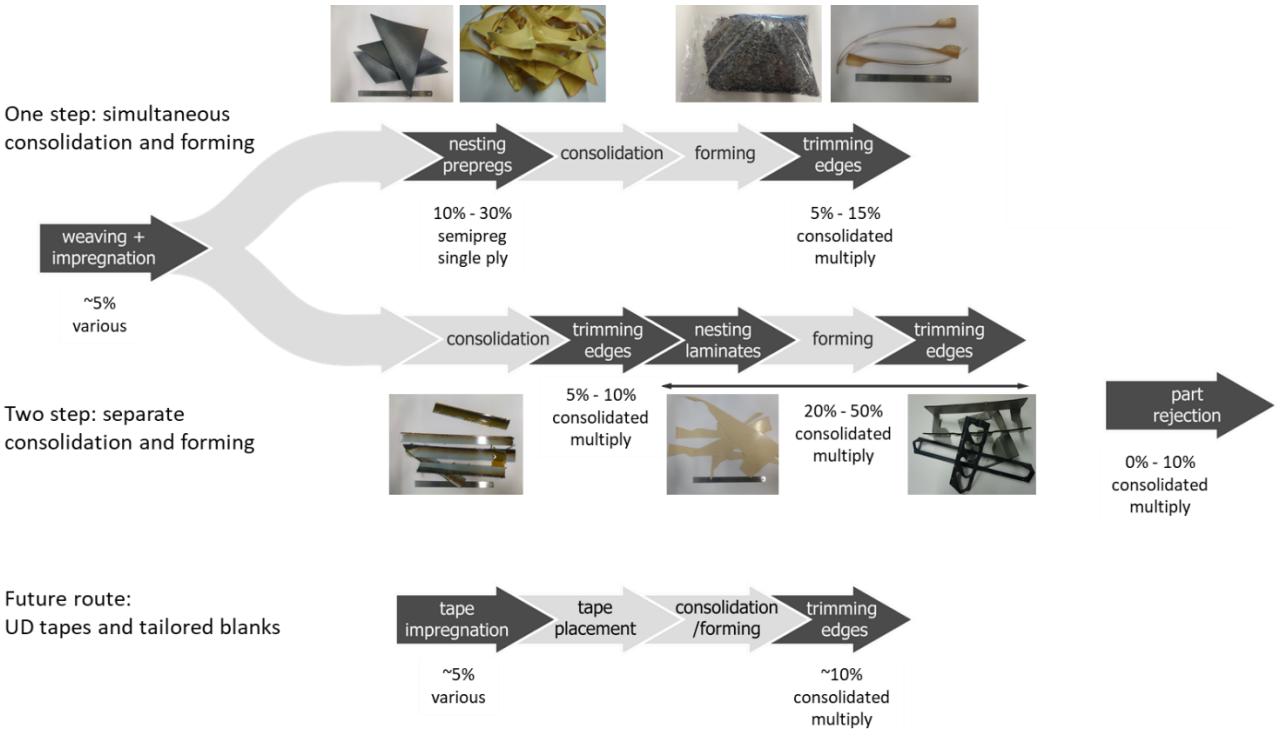

Figure 1.4 - A material flowchart of three types of TPC manufacturing routes. The dark coloured manufacturing stages represent production steps at which waste is produced, including the type of waste and estimated waste ratio.

1.4 TPC-Cycle project

Continuous fibre reinforced TPCs started to be widely used by several companies and institutes in the Netherlands [36]. The sector is recognised by the Dutch government as a field of high priority in the High-Tech Systems and Materials program, resulting in various financial incentives for industrial research, creating a suitable climate to perform recycling studies on TPCs. This research is executed as part of the TPC-Cycle project, led by Saxion, University of Applied Sciences and its ThermoPlastic composites Application Center - TPAC, both located in Enschede, the Netherlands. The project further involves multiple Dutch companies and institutes from the total value chain in TPC: material supplier Toray Advanced Composites (previously known as Ten Cate), Nido Recycling Techniek (NRT) focussed on size reduction, manufacturer Dutch Thermoplastic Components (DTC), CATO Composites covering development and manufacturing, GKN Fokker (previously known as Fokker Aerostructures) focussed on design and manufacturing and the ThermoPlastic composites Research Center (TPRC) as a fundamental research centre. This thesis is part of the TPC-Cycle project and its funding by the Dutch organisation of Applied Research, Regieorgaan SIA, part of the Netherlands Organisation for Scientific Research (NWO) through the research grant SIA-RAAK 2014-01-72PRO is gratefully acknowledged.

1.5 Objective and scope

The goal of this PhD study is to obtain a better understanding of the possibilities of continuous fibre TPC recycling and develop a new recycling route this material. The research focuses on the optimum process for TPC waste to obtain the highest performance possible at lowest economic and environmental cost. The performance is measured by the value of the application, from the material quality towards the value and cost of a product. Costs are both economic and environmental. The study can be concentrated to the following research question:

Which recycling route for processing post-industrial TPC waste will lead to maximum cost effectiveness and minimum environmental impact?

An important boundary condition of the study is to include both low-end and high-end materials, e.g. glass fibre reinforced polypropylene (G/PP) and carbon fibre reinforced polyphenylene sulphide (C/PPS). Since the majority of the post-industrial (and later end-of-life) waste consists of consolidated multiply laminates of various geometries, this will be the focus throughout the thesis. Occasionally, a single ply semipreg structured material will be used for comparison reasons.

1.6 Outline

The core of this thesis is schematically outlined in Figure 1.5. It contains four chapters and is preceded by an introduction including a state of the art.

In Chapter 3, the analytical modelling of the mechanical performance is studied. Current models are applied to investigate the influence of fibre length, fibre content and fibre orientation. The models are extended to include fibre dispersion and distribution. Theoretically constructed distributions of fibre length, fibre volume and bundle size are used to span the area of potential mechanical properties, including the upper and lower bound. Distributions based on experimental work offer insight in the influence of the variable's distributions based on the studied recycling route. The information obtained is used to define the most suitable processing settings for the recycling route.

The experimentally validation and technical feasibility on material level is described in Chapter 4. The developed recycling route is used to recycle post industrial waste and benchmarked to the commonly described manufacturing method of direct compression moulding. G/PP and C/PPS materials having various volumes, orientations, lengths and length distributions of fibres, flake dimensions and consolidation stages are processed at various processing variables to create samples. These are tested

to determine the mechanical performance. Results are compared to the theoretical prediction found in Chapter 3.

Chapter 5 concerns the application of real products processed from the recycling route developed. A rotorcraft access panel, a safety shoe nose cap and a bracket are developed to analyse the technical feasibility of the recycling route on part level. The design, manufacturing and testing is described. Results are compared to current parts to validate if all demanded requirements are met.

The cost effectiveness and environmental impact are studied in Chapter 6. A life cycle and cost assessment of the developed access panel, safety shoe nose cap and their currently used counterparts is performed. The commonly described recycling route of direct compression moulding is added for comparison. The results offer insight into the cost effectiveness and environmental impact of parts produced by the developed recycling solution, in comparison the current solutions of virgin material and the recycling process of direct compression moulding.

In Chapter 7, the results and conclusions of the previous chapters are discussed and, finally, the conclusions and recommendations are presented in Chapter 8.

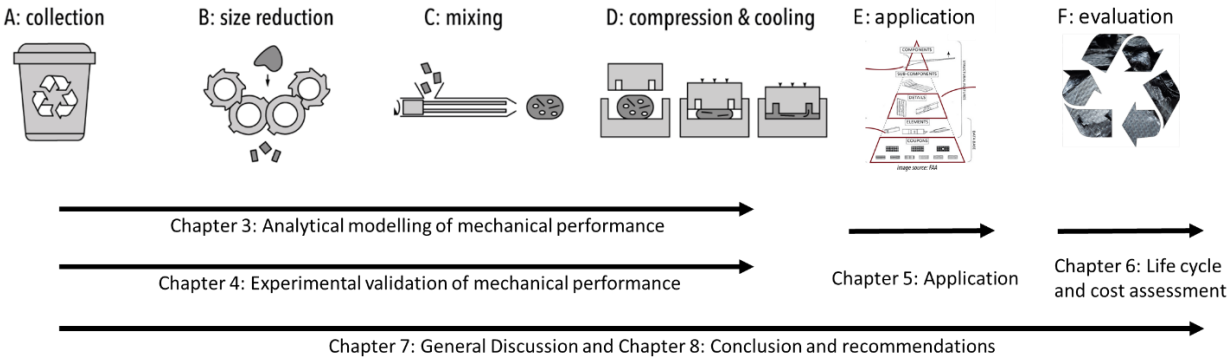

Figure 1.5 - Outline of the thesis

1.7 References

[1] D. E. Witten, V. Mathes, M. Sauer, and M. Kühnel, "Composites Market Report 2018," *AVK – Ind. Verstärkte Kunststoffe e.V. Carbon Compos. e.V.*, no. November, 2019.

[2] European Commision, "The European Green Deal," Brussels, Januari 2020.

[3] European Council, "European Council (23 and 24 October 2014) – Conclusions," 2014.

[4] European Commision, "A Clean Planet for all - A European strategic long-term vision for a prosperous, modern, competitive and climate neutral economy," 2018.

[5] Lucintel, "Thermoplastic Composites Market Report: Trends, Forecast and Competitive Analysis," 2020.

[6] A. R. Offringa, "Thermoplastic applications composites-rapid processing applications," *Compos. Part A*, vol. 27, no. 4, pp. 329–336, 1996, doi: https://doi.org/10.1016/1359-835X(95)00048-7.

[7] A. Staff, "Exponential Growth Expected for Thermoplastic Composites | Composites Manufacturing Magazine." [Online]. Available: http://compositesmanufacturingmagazine.com/2012/07/exponential-growth-expected-thermoplastic-composites/. [Accessed: 01-Jun-2016].

[8] C. Red, "The Outlook for Thermoplastics in Aerospace Composites, 2014-2023," *Composites World, High-Performance Composites*, 2014. [Online]. Available: http://www.compositesworld.com/articles/the-outlook-for-thermoplastics-in-aerospace-composites-2014-2023. [Accessed: 28-Jun-2016].

[9] G. Gardiner, "Thermoplastic composite demonstrators — EU roadmap for future airframes," *CompositesWorld*, 2018. [Online]. Available: https://www.compositesworld.com/articles/thermoplastic-composite-demonstrators-eu-roadmap-for-future-airframes-.

[10] "The markets: Sports and recreation (2016)," 2016. [Online]. Available: http://www.compositesworld.com/articles/the-markets-sports-and-recreation-2016. [Accessed: 28-Jun-2016].

[11] D. Campbell and D. Cramer, "Hybrid Thermoplastic Composite Ballistic Helmet Fabrication Study," *SAMPE J.*, vol. 44, pp. 1–11, 2008.

[12] J. Markarian, "Long fibre reinforced thermoplastics continue growth in automotive," *Plast. Addit. Compd.*, vol. 9, no. 2, pp. 20–24, 2007, doi: 10.1016/S1464-391X(07)70025-9.

[13] F. Henning *et al.*, "LFTs for automotive applications," *Reinf. Plast.*, vol. 49, no. 2, pp. 24–33, 2005, doi: 10.1016/S0034-3617(05)00546-1.

[14] W. Schijve and G. Francato, "New thermoplastic composite solutions for automotive lightweighting," *JEC Compos. Mag.*, no. 103, pp. 96–98, 2016.

[15] Toray Advanced Composites, "Advanced Composite Materials Selector Guide," 2019.

[16] J. Day, A. K. Wood, and S. F. Pang, "Recycling of APC-2 offcuts," *Compos. Manuf.*, vol. 5, no. 3,

pp. 187–193, 1994.

[17] S. Pickering and T. Turner, "Research and development in support of carbon fibre recycling," in *CAMX 2014 – composite and advanced materials expo, USA*, 2014.

[18] M. F. Khurshid and M. Hengstermann, "Recent developments in the processing of waste carbon fibre for thermoplastic composites – A review," 2019, doi: 10.1177/0021998319886043.

[19] S. Pimenta, S. T. Pinho, and P. Robinson, "Micromechanics of Recycled Composites for Material Optimisation and Eco-Design," *18th Int. Com. Compos. Mater.*, pp. 1–6, 2011.

[20] E. Asmatulu, J. Twomey, and M. Overcash, "Recycling of fiber-reinforced composites and direct structural composite recycling concept," *J. Compos. Mater.*, vol. 48, no. 5, pp. 593–608, 2013, doi: 10.1177/0021998313476325.

[21] B. W. G. Somi Seong, Obaid Younossi, "Titanium: Industrial Base, Price Trends, and Technology Initiatives," 2009.

[22] Airbus, "Metals and composites: finding the right material for each application," *Airbus Commercial aircraft*, 2018. [Online]. Available: https://www.airbus.com/newsroom/stories/metals-and-composites–finding-the-right-material-for-each-appli.html.

[23] K. Michaels, "Aerospace composites in 'the more for less' era," *CompositesWorld*, 2017. [Online]. Available: https://www.compositesworld.com/columns/aerospace-composites-in-the-more-for-less-era.

[24] R. Lahr and M. P. Päßler, "Workshop Recycling von CFK-Komponenten – Herausforderungen und Chancen," in *Workshop Recycling von CFK-Komponenten – Herausforderungen und Chancen*, 2016.

[25] TPC-Cycle project partners *et al.*, "Internal communication within TPC-Cycle project meetings."

[26] Ministry of Infrastructure and Ministry of Economic Affairs and Climate Policy, "Netherlands circular in 2050," 2016.

[27] L. Jetten and L. de Roos, "Knowledge meeting: From waste to raw material (VANG)," Utrecht, 2014.

[28] W. Hansen, "EU Waste Policy and Challenges for Regional and Local Authorities," *Institute for International and European Environmental Policy*. 2002.

[29] G. Oliveux, L. O. Dandy, and G. a. Leeke, "Current Status of Recycling of Fibre Reinforced Polymers: review of technologies, reuse and resulting properties," *Prog. Mater. Sci.*, vol. 72, pp. 61–99, 2015, doi: 10.1016/j.pmatsci.2015.01.004.

[30] S. J. Pickering, "Recycling technologies for thermoset composite materials-current status," *Compos. Part A Appl. Sci. Manuf.*, 2006, doi: 10.1016/j.compositesa.2005.05.030.

[31] J. Zhang, V. S. Chevali, H. Wang, and C. Wang, "Current status of carbon fibre and carbon fibre composites recycling," *Compos. Part B*, p. 108053, 2020, doi: 10.1016/j.compositesb.2020.108053.

[32] W. Schijve, "High performance at medium fibre length in long glass fibre polypropylene," *Plast. Addit. Compd.*, vol. 2, no. 12, pp. 14–21, 2000, doi: 10.1016/S1464-391X(00)80121-X.

[33] J. Sloan, G. Gardiner, and M. Favaloro, "Webinar: Thermoplastic Composites in Aerospace Parts and Structures," *CompositesWorld*, 2019. [Online]. Available: https://www.compositesworld.com/events/details/41eef0b7-4495-492b-bb35-5ab94c961dfe. [Accessed: 16-Jun-2020].

[34] M. Biron, *Thermoplastics and Thermoplastic Composites: Technical Information for Plastics Users*. Elsevier Science & Technology, 2018.

[35] T. K. Slange, "Rapid Manufacturing of Tailored Thermoplastic Composites by Automated Lay-up and Stamp Forming," University of Twente, 2019.

[36] S. Black, "Thermoplastic composites technology: A view from Europe," *CompositesWorld*, 2015. [Online]. Available: https://www.compositesworld.com/articles/thermoplastic-composites-technology-a-view-from-europe.

2 State of the art

A better understanding of the relationship between mechanical performance, fibre length and mixing enables optimising all stages of a recycling route. Micromechanical modelling is important for the research on recycling of continuous fibre thermoplastic composites for various reasons. First to check if common models for discontinuous fibres may be also applied to the recycled thermoplastic composites (TPC). Modelling may also lead to an increased understanding of the influence of variables, by including differences between the recycled a virgin material, like material structure and, thus, enabling the potential optimisation of the recycling route. Predicting the effect of the fibre length distribution and degree of mixing on the mechanical properties provides as well important information to make choices regarding the trade-off between mechanical performance and processability. With increasing fibre aspect ratio (length/diameter), first the stiffness, then strength and finally impact properties increase, as shown in Figure 2.1 [1–3]. Nevertheless, while a longer fibre length results in a higher mechanical performance, the processability of recycled TPC becomes negatively affected.

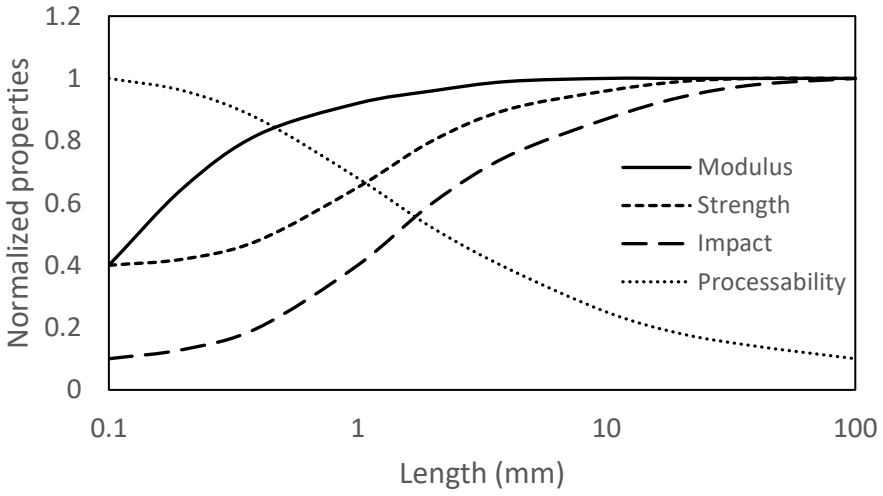

Figure 2.1 - Influence of fibre length on normalised mechanical properties [2, 3]

The processability of the material is related to the degree of mixing, which is dependent on the process and material used. In this study, the degree of mixing is considered as the distribution and dispersion of fibres. Distribution is related to the local fibre volume variation and the dispersion to the amount of fibres per bundle. The latter is in literature also known as filamentation. Among others, the amount of shear stress during the process affects the degree of mixing. Higher shear stresses will generally result in better mixing, but also in increased fibre attrition [4]. Therefore, the processability declines when long fibre lengths are required in the final product [3]. In this study, consolidated multi-layered woven flakes are considered to be the main material to be recycled (see Section 1.3). These flakes become more difficult to mix than LFT pellets due to the internal structure of the reinforcement. The fibre bundles in the latter can be directly dispersed, whereas the flake needs to be delaminated and woven bundles of the resulting layers need to be disentangled before dispersion can take place. As Figure 2.2 shows, fibre bundles can be observed in poorly dispersed material.

Literature on recycling of thermoplastic composite materials predominately consider non-mixed approaches [5, 6]. A specific process, including a previously designed low shear mixing process, was developed and applied to recycle TPC material with limited fibre friction in this research project [7, 8]. Although this process uses mixing rods instead of a conventional extrusion screw, it is similar to long fibre thermoplastic (LFT) processing, which is a technology thoroughly studied and embraced by industry for virgin discontinuous materials (see Section 2.2.4). It is known for the excellent formability, short cycle times and net shape manufacturing compared to continuous fibre materials, although the final obtained mechanical properties were been found to be lower [9–11].

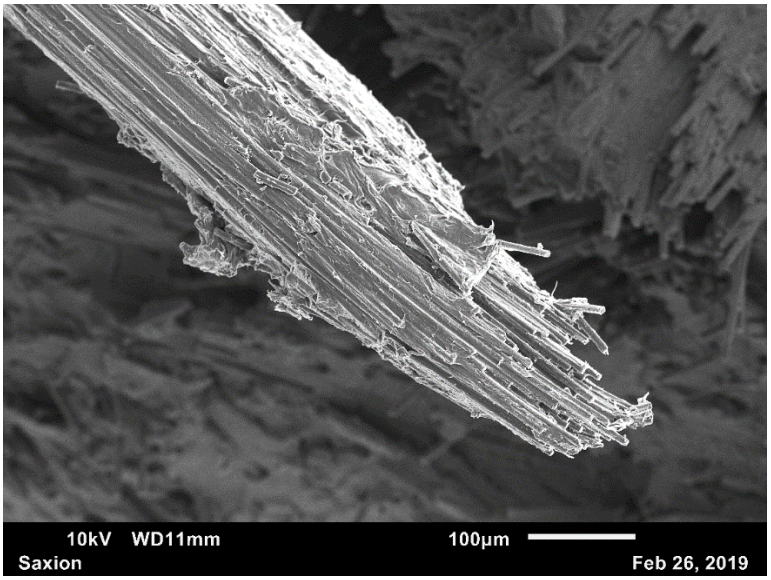

Figure 2.2 - SEM image of a large bundle in a poorly-mixed material

Higher degrees of mixing result in a more homogeneous composite with less rich areas, both in resin as well as in fibres. Hence the strength is improved by limiting the stress concentrations, crack paths and potential weakest links. Processing technologies using mixing also feature manufacturing benefits such as a shorter cycle time, improved flow and therefore filling of interstices, less fibre bridging and reduced jamming.

More insight on the balance between fibre length and degree of mixing is necessary to determine the optimal required fibre length and fraction for comminution and processing. Hence this topic serves to focus subsequent research and provide boundary conditions for requirements of specific processing steps, for instance the size reduction step. Being able to predict the mechanical properties provides a reference for experimental data and aids the design process of applications made from recycled TPC, building confidence to choose applications for recycled materials.

While it is known that the most important variables for mechanical properties are fibre orientation, its length and volume fraction (FVF) [12], other interesting effects to include when considering TPC waste as input material should be the bundle size, fibre length and its volume distribution.

2.1 Mechanical modelling of discontinuous fibres

Multiple models have been proposed to predict mechanical properties of discontinuous fibre reinforced composites [13, 14]. The widely accepted models of Cox [15] and Kelly-Tyson [16] are shear lag models and require the following assumptions: no fibre–matrix debonding or interfacial slip; ideal elastic conditions; micro-cracking and voids present in the composite are not taken into account; fibre interactions and stress concentrations are neglected; the composite matrix properties are the same as those of the unreinforced matrix and the matrix has a lower modulus than the reinforcement.

As a first step, properties of a unidirectionally (UD) aligned discontinuous fibre composite are derived from the constituent properties and expressed as a function of fibre length. Secondly, the properties can be adjusted for fibre length by simply using an average fibre length, or averaging the fibre length by integrating over a given length distribution. These properties are then applied accordingly to a certain orientation distribution to the discontinuous fibre reinforced thermoplastic matrix composites by considering the orientation averaging determined on them [14].

This study looks to integrate the degree of mixing by considering a bundle size distribution referred to as dispersion and local fibre volume averaging referred to as distributions.

2.1.1 *Stiffness*

Models of, amongst others, Cox [15], Halpin-Tsai [17] and Tandon Weng [18] are available to calculate the composite stiffness. The Cox model introduces a fibre length efficiency factor η_l in the equation known as 'rule-of-mixtures' (ROM). The model is extended by Krenchel [19] to include fibre orientation by an orientation factor η_o. This factor can be derived using a $\cos^4(\Theta)$, where Θ is the fibre orientation [19]. For commonly used in-plane random orientation this results in a value for η_o of 3/8. The Cox model extended by Krenchel is:

$$E_c = \eta_l \eta_o V_f E_f + \left(1 - V_f\right) E_m \qquad \text{eq. 1.}$$

where E_c, E_f and E_m are, respectively, the composite, fibre and matrix moduli, and V_f is the fibre volume fraction. Thomason and Vlug [20] compared the theoretical predictions of the Cox – Krenchel [20] model to experimental data and found excellent agreement within their study on the influence of fibre length (0.1-12mm) in composites with 10% to 40% fibre weight fractions. However, other studies show shortcomings of the Cox model when used to predict stiffness [13, 21].

The model of Halpin-Tsai is the most widely applied, possibly because of its relative simplicity and proven accurate prediction of stiffness [17]. The Tandon-Weng [18] model is based on a combination of Eshelby's and Mori-Tanaka's [22, 23] theories of inclusions and is much more computational time-consuming, but gives slightly better predictions [21] .

2.1.2 *Strength - Kelly Tyson*

Although many models are available, tensile strength is found to be a property more difficult to predict accurately compared to stiffness [24]. The simple modified model of the ROM, commonly used to predict the stiffness of a composite, can also be applied for the prediction of strength for UD continuous fibre reinforced composites.

$$\sigma_c = \eta_l \eta_o V_f \sigma_f + \left(1 - V_f\right) \sigma_m \qquad \text{eq. 2.}$$

where σ_c, σ_f and σ_m are, respectively, the composite, fibre and matrix strengths. The most widely applied models for predicting the strength of a discontinuous fibre composites are the shear-lag models proposed by Cox [15, 20] and Kelly-Tyson [16]. Both shear-lag models consider a shear stress at the fibre-matrix interface as a result from a higher modulus of the reinforcement compared to the matrix. Hence, the stress in the matrix is transferred by the shear stress at the interface to a normal stress in the fibre. Cox

assumes an elastic linear behaviour both for the matrix and reinforcement, but a non-linear evolution of the shear stress at both fibre ends. While the model of Kelly-Tyson adopts the linear adjustment of the shear stress at the fibre ends. In Figure 2.3, the load transfer for both models is given for subcritical and supercritical fibre length. Theoretical results of the Kelly-Tyson model for long fibre reinforced thermoplastics correlate well with experimental data [25].

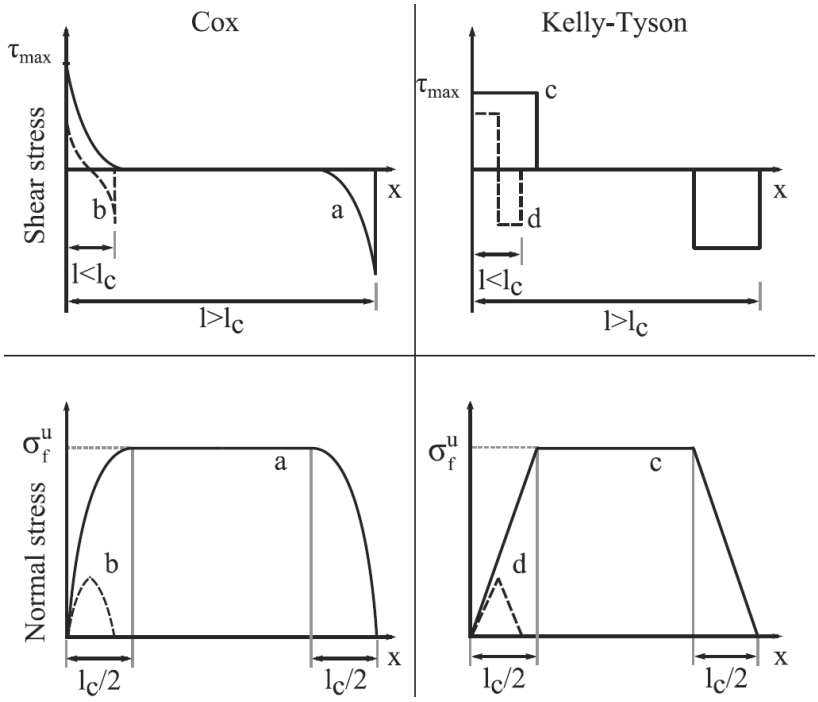

Figure 2.3 - Load transfer mechanisms (dotted lines show the case when the fibre is shorter than the critical length). X-axis is along the fibre length and shear stress is at the fibre-matrix interface. [26]

An important parameter in both models is the critical fibre length l_c. The failure mode for a fibre length below l_c is a fibre pull-out, since the interface area is insufficient to load the fibre to the maximum stress level. Therefore, failure occurs at the interface. Above l_c the fibre breaks. The critical fibre length is then given by [16]:

$$l_c = \frac{\sigma_f d}{2\tau} \qquad \text{eq. 3.}$$

where σ_f and d are the fibre strength and diameter respectively, and τ is the interfacial shear strength between fibre and matrix. The latter is limited by the shear strength of the matrix when a strong interfacial bond is present. Assuming the matrix to be isotropic, according to the well-known Distortion-Energy Theory, shear strength can be defined as [14]:

$$\tau = \frac{\sigma_m}{\sqrt{3}} \qquad \text{eq. 4.}$$

This expression results in values which are matching experimental values in literature [27]. The critical fibre length can be determined based on experimental tests by means of the single fibre fragmentation test [28] or by the extension of Bowyer and Bader to the Kelly-Tyson model [29]. In this study, the expression stated above is used.

From the Kelly-Tyson model, the longitudinal strength of a composite σ_{cL} in the principal direction can be expressed by:

$$\sigma_{cL} = \sum_{l_i=0}^{l_i=l_c} \frac{\tau l_i V_f}{d} + \sum_{l_j=l_c}^{l_j=\infty} \sigma_f V_f \left(1 - \frac{l_c}{2l_j}\right) + \left(1 - V_f\right)\sigma'_m \qquad \text{eq. 5.}$$

where l and σ_f are the fibre length and strength respectively, σ'_m is the matrix strength at fibre failure, and V_f is the fibre volume fraction. Note that below the critical fibre length the composite strength is dominated by the matrix shear strength. The subcritical and supercritical fibre lengths are handled separately by two summation terms. Furthermore, the composite strength at the critical fibre length is only half of the strength potential of the fibre in case of constant shear stress of the Kelly-Tyson model. Although the strength potential of the fibre will approach the value of an infinite fibre, it will never be fully utilised. Thomason et al. concluded that a length of more than 5 times the critical fibre length is necessary to obtain 90% of the maximum attainable strength [24].

Note that the Weibull-type dependency of fibre strength on fibre length can result in declining strength values at increasing fibre lengths. Van Hattum [14] proposed a method to integrate such a Weibull distribution function in the Kelly-Tyson model. In this study, this latter method was not used for simplification and more clear relationship between the input and output of the model.

A failure criterion is required to deal with multiple loading conditions and predict failure due to simultaneous loads in the principal directions. The relatively simple Tsai-Wu [30] failure criterion for anisotropic materials was selected to account for arbitrary fibre orientation which is not limited to in-plane stresses.

2.1.3 *Length averaging*

In recycled thermoplastic composites, the feedstock contains material with non-uniform fibre length. In high shear processing technologies, the length is reduced, resulting in a shorter fibre length distribution. Because of the non-linear relationship between the fibre length and mechanical properties, the use of a fibre length distribution improves the accuracy of the prediction over using a single average value [14, 31]. A distribution of the feedstock material can be obtained from image analysis of flakes, as is described in a related study by Vincent et al. [32]. The property of the unidirectional composite is then weighted over the determined distribution of fibre lengths to include a fibre length distribution.

2.1.4 *Fibre orientation*

The expressions for modulus and strength are given for a unidirectional fibre orientation. To account for other fibre orientations, multiple approaches can be applied. Although the Krenchel orientation factor η_o (3/8 for 2D random orientation) can be applied to the simple ROM and the more advanced shear lag model, Thomason [24] notes that the value results in an overprediction for the strength of short fibre composites. Therefore, a factor of η_o = 0.2 should be used to find a good fit with experimental data. Garkhail et al. [33] notes that this adjustment transforms the orientation factor η_o to a fitting parameter without a physical meaning. To improve the effect of fibre orientation, the more advanced fibre orientation averaging method of Advani and Tucker [34] was applied in this study.

The foundations for fibre orientation prediction have been established by Jeffery [35], as an extension on Einstein's study on behaviour of spherical particles in a fluid. The approach of taking ellipsoidal particles and describe their rotation in a diluted Non-Newtonian flow was adapted by Folgar and Tucker [36]. They applied the idea to fibres in a concentrated suspension to calculate the orientation distribution of a composite. The model is most frequently used and integrated in popular commercial process simulation software like Moldflow™ and Moldex3D™ for modelling the orientation of short fibres in composites [37].

The 'orientation averaging method' presented by Advani and Tucker [38] can be followed to account for the effect of fibre orientation for an arbitrary fibre length distribution. To describe the orientation state of a single fibre in space a unit vector $\boldsymbol{p}$ is defined. This vector can be described with two angles φ and θ, see Figure 2.4. The elements of $\boldsymbol{p}$ are:

$$\boldsymbol{p} = \begin{pmatrix} p_1 \\ p_2 \\ p_3 \end{pmatrix} = \begin{pmatrix} \cos\phi \sin\theta \\ \sin\phi \sin\theta \\ \cos\theta \end{pmatrix} \qquad \text{eq. 6.}$$

The 1- axis is chosen as the main fibre orientation direction, 2-axis perpendicular to this direction and 3-axis perpendicular to the 1-2-plane. The latter is physically representing the through-thickness direction. A probability density function Ψ_p is introduced such that the probability of a fibre positioned in the range $\boldsymbol{p}$ and ($\boldsymbol{p}$+$d\boldsymbol{p}$) equals $\Psi_p(\boldsymbol{p})d\boldsymbol{p}$. Advani and Tucker [34] introduced a fourth order and second order orientation tensor to represent the orientation of a large population of fibres. The second order tensor is defined as:

$$\boldsymbol{a_{ij}} = \oint \Psi(\boldsymbol{p})\, \boldsymbol{pp}d\boldsymbol{p} = \begin{bmatrix} \boldsymbol{a_{11}} & \boldsymbol{a_{12}} & \boldsymbol{a_{13}} \\ \boldsymbol{a_{21}} & \boldsymbol{a_{22}} & \boldsymbol{a_{23}} \\ \boldsymbol{a_{31}} & \boldsymbol{a_{23}} & \boldsymbol{a_{33}} \end{bmatrix} \qquad \text{eq. 7.}$$

where $\mathbf{a}_{ij}$ is a second order fibre orientation tensor describing the state at any point. The trace of the matrix $a_{11}+a_{22}+a_{33} = 1$ [14, 39].

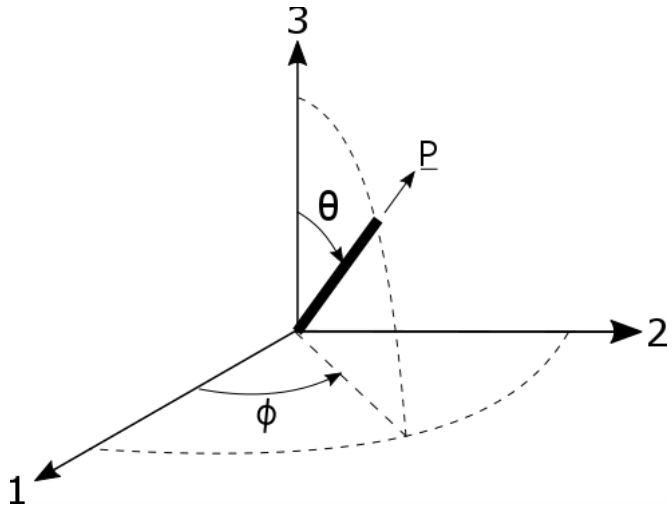

Figure 2.4 - Coordinate system and definitions for a single fibre [38]

Orientation averaging and closure approximation

A fourth order fibre orientation tensor is required to calculate the composite strength and stiffness. As the computation of this tensor is often time consuming a closure approximation is often used to derive the fourth order tensor from a second order one [14, 40]. Several approximations are available. The first-generation closure hypotheses are the linear, quadratic, and hybrid. The linear approximation is exact for a completely isotropic fibre orientation distribution, the quadratic approximation is exact for aligned fibres and the hybrid one is a weighted intermediate of the other two [41]. Cintra-Tucker [42] proposed an orthotropic fitted closure approximation to calculate the fourth-order orientation tensor. According to comparisons of Dray [41] and Chen [43], this type gives the best approximation in comparison to other

orthotropic closure approximations. Dray concluded that the results are very close to those obtained with the experimentally measured fourth-order orientation tensor.

Effect of material flow on orientation

Flow can have an effect on the fibre orientation. Wall effects can lead to a layered structure presenting skin, shell and core. These observations are known in short fibre composites and are found to result in through-thickness variations in orientation distribution. Fibres are predominantly aligned in flow direction at the skin and in cross-flow direction in the core [14, 39]. It has been observed that the core of long fibre materials is significantly larger and is more randomly in-plane oriented compared to short-fibre thermoplastic composites [44, 45]. Overall, long fibres are more limited to move and are therefore more randomly oriented in plane with a higher level of orientation perpendicular to the flow direction, especially at higher contents [46]. This cross-flow orientation is also found by experimental work carried out by Vincent and al. when using the same process as the one studied in the present research [47]. According to Nguyen [48], while the wall effect is important, it is also possible that fibre-fibre interactions will be developed in the LFTs which make the wall effect become negligible [39].

2.1.5 *Degree of mixing*

The models described in the previous section are assuming a perfect degree of mixing, although this is not the case in practice. Material and process have a profound influence on the degree of mixing. The structure and constituents of the initial recycled material influence the initial degree of mixing and the required effort for homogenisation. The applied processing method determines the homogenisation speed and, possibly, the final degree of mixing obtainable.

A poor degree of mixing is known to have a negative influence on the mechanical performance of a composite [7, 49, 50]. The degree of mixing is often stated as a multiscale phenomenon that illustrates the combination of fibre distribution and dispersion [51, 52]. This is well-worded by Kim et al. [50]: “Mixing has two aspects, dispersion and distribution; dispersive mixing is to break down agglomerates of fillers into aggregates and particles and distributive mixing is to distribute the particles uniformly throughout the polymeric matrix without affecting particle size.” Various levels of dispersion and distribution are visualised by schematic cross-sections in Figure 2.5 [53]. Dispersion and distribution should be taken into account in the models when considering the often complex structure of waste material, e.g. woven or consolidated materials.

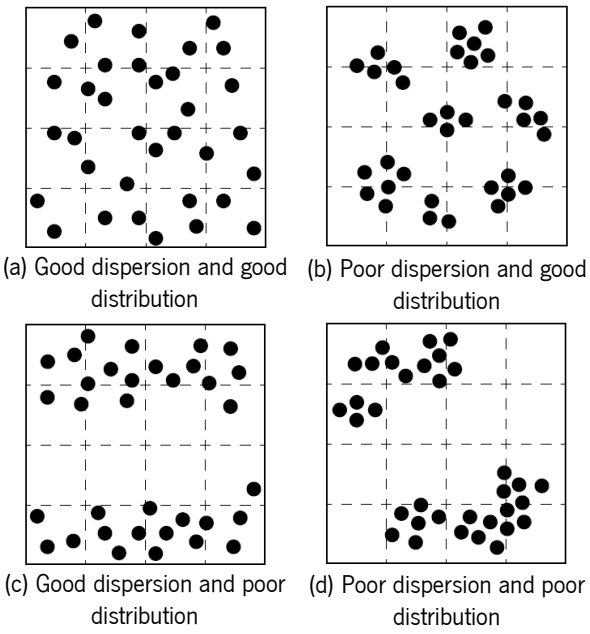

Figure 2.5 - Schematic cross-sections with various degrees of mixing [53]

2.1.6 *Characterisation of the Degree of mixing*

The characterisation of the two above mentioned effects was done using methods proposed in the already referred study of Vincent et al. [53], which gives an overview of various methods to analyse the degree of mixing from cross-sectional microscopic images.

Three methods are used to measure the degree of mixing on different scales, although the terminology is slightly different to the one used in the above-mentioned study. The intensity of segregation (IoS) relates to the coefficient of variation (CoV) of FVF and is therefore a measure of its local evenness. Cross-sectional micrographs were segmented to identify the fibre, matrix and porosity fractions. By applying a grid over the image and calculating the average fibre volume content of each division, the fibre volume distribution (FVD) can be obtained. The results vary depending on cell size. A visualisation of this method is shown in Figure 2.6. Figure 2.6a and e show the initial cross-sectional image of a poorly mixed and good mixed sample. Figure 2.6b to d and f to h display the fibre fraction in grey scale for each cell and with increasing grid size.

The number of fibres per bundle is captured in the bundle size distribution (BSD). The BSD is obtained by identifying every fibre and connecting it to neighbouring fibres by a refined Delaunay triangulation. Bundles are identified by removing connections longer than three times the fibre diameter (see Figure 2.7). In this study the IoS was used to create the local FVD and is a measure for the distribution of fibres on a meso scale. The BSD is a measure for the dispersion and therefore homogenisation at micro scale.

The output data on mixing of Vincent et al. [53] is used to include realistic FVD and BSD data of C/PPS material mixed by the developed recycling route.

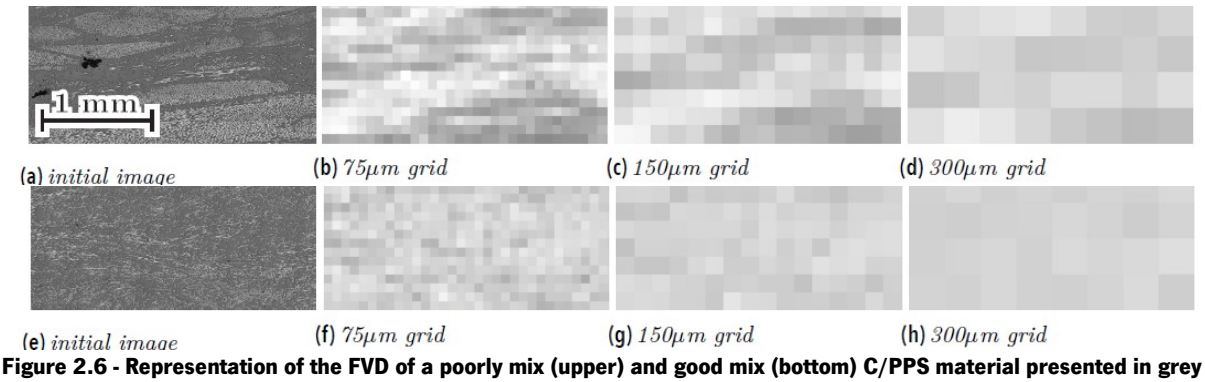

Figure 2.6 - Representation of the FVD of a poorly mix (upper) and good mix (bottom) C/PPS material presented in grey scale at various cell sizes. Source Vincent et al. [53]

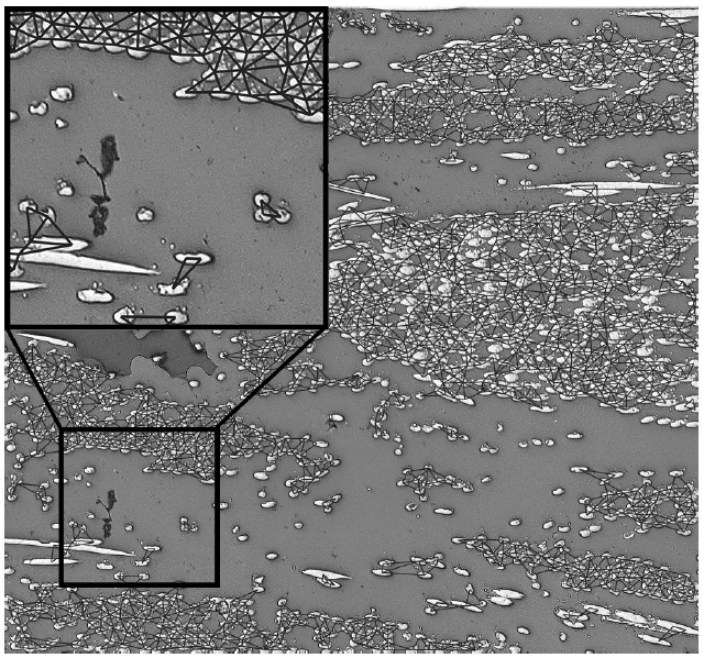

Figure 2.7 - The BSD is computed by capturing the location of every fibre and applying refined triangulation based on Delaunay. Neighbouring fibres are seen as a bundle when the distance between them is below three times the fibre diameter. Source: Vincent et.al . [53]

2.1.7 *Dispersion by bundle size averaging (BSA) (+critical bundle length)*

The effect of bundle size on the performance of composites was studied by various authors [33, 43, 45, 54–56]. The presence of larger bundles usually decreases the mechanical properties and can originate, amongst others, difficulties in dispersing bundles or the decision to use larger tow sizes for cost reasons, for example. Continuous tows larger than 12K (tows with 12000 fibres) bundles are available at half price of the smaller ones [56, 57].

The decrease of mechanical performance can be attributed to two main effects. Among others, Rondeau et al. [56] described that at the end of larger bundles, stress concentrations lead to larger decreases in strength and minor decreases in stiffness. The bundle itself is assumed to act as a large-diameter fibre.

The second effect originates from the relative decreased surface area of fibres in an undispersed bundle compared to fully dispersed bundles. Following the shear-lag theory this surface area is important to transfer stress at the fibre-matrix interface and directly related to the strength of discontinuous fibres, especially for fibres having lengths several times below the critical fibre length. Various studies confirm the positive influence of smaller bundles on the mechanical performance and their effect on lower levels of variability [43, 45, 54–56, 58, 59]. These studies used non-mixed fibre bundles between 3k and 24k in combination with a thermosetting matrix.

For well-mixed long fibre thermoplastic processes the feedstock is often a LFT pellet with a UD morphology, and is optimised for easy dispersion [1]. However, a level of undispersed fibre bundles was also found by Chen et al. [43] after processing these materials. These undispersed fibres have a higher effective diameter resulting in a smaller bundle aspect ratio and therefore affect material properties [45, 54, 55]. Chen et al. [43] claimed that it is essential for accurate predictions of composite properties to incorporate the effect of the presence of fibre bundles. Garkhail et al. [33] saw a large and significant influence of dispersion of flax bundles compared to the effect of coupling agents.

Previous studies on non-mixed thermoset composite materials [55, 56, 58, 59] also concluded that the effect of bundles is substantial. The effect of bundles in studies on mixed LFT was observed at high fibre loadings and long fibres, but was not intensively studied [45, 54]. Because the current study is focused on long fibre lengths, and low-shear mixing likely results in difficulties to disperse the complex material structure, the effect of bundles is a focus in this study.

2.1.8 *Distribution by local fibre volume distribution*

Local FVDs or the spatial distribution uniformity of a reinforcement is frequently studied and linked to the mechanical performance in the field of metallic matrix and nanocomposites [49, 51, 60]. Fibre reinforced plastics are generally higher-filled and more adequately distributed in comparison to nanocomposites. The dispersion of the considered recycled TPC material and recycling route might be low, however the main reason for this is the structure of the reinforcing material: it is often a woven flake structure with dimensions in the centimetre range, which is diluted with virgin polymer and mixed at low shear levels to prevent fibre attrition. For this reason, the effect of FVD on the mechanical performance by fibre volume content averaging is included in this study, although it is known that the relation between fibre content and mechanical properties is often linear.

2.2 Processing discontinuous fibre thermoplastic composites

In the current section multiple processing methods for discontinuous fibres are discussed to give insight in the options to select the most suitable recycling method.

2.2.1 *Direct compression moulding*

Several studies have researched manufacturing routes for thin thermoplastic composites processed by direct compression moulding (DCM) [5, 61–64]. Most of these studies consider virgin material. Rasheed et al. [5] studied the recycling of chopped woven flakes of single ply semipreg C/PPS originating from nesting waste. All these studies describe a similar process, consisting of several steps which are illustrated in Figure 2.8a. First, the material was directly placed in a mould. Then, the mould is heated to a temperature above the materials melting temperature. The material is kept under limited pressure inside the heated mould to assure contact until the desired temperature is reached. When the desired temperature is reached a previously established moulding pressure was applied to the material for a certain dwell time. Finally, the mould and material are cooled with constant moulding pressure before the final part was released. This relatively simple recycling process for thermoplastic composites is similar to the process used for Bulk moulding compounds (BMC). Results showed a manufacturing route providing a design freedom not feasible with continuous fibres: introduction of design features including ribs, thickness variations and bosses, offers function integration and geometrically optimised structures. This approach is commercially offered by Ten Cate [63].

However, stress concentrations at flake edges can lead to a large variation of strength values [5]. In this research thin flexible prepreg flakes were used. It was possible to mould parts with high fibre volume fractions (>50% FVF) resulting in relatively high stiffness [5]. However, low levels of homogeneity were observed in parts manufactured by DCM, i.e. voids, pit holes, jamming and resin ridge areas occurred often [5]. The meso-structure of the flakes can result in a poor load transfer load, causing limitation of properties [65]. Also during manufacturing issues occur: e.g. jamming can result in potential damage of the mould [5]. However, adding polymer to decrease the fibre content, e.g. to make processing easier, can lead to irregular and localised fibre contents due to the absence of a mixing step [66]. Finally, the processing time was often long since the heat needs to be transfer between the mould and material during heating and cooling stages. Some of these disadvantages of the process could be mitigated by good material mixing [67].

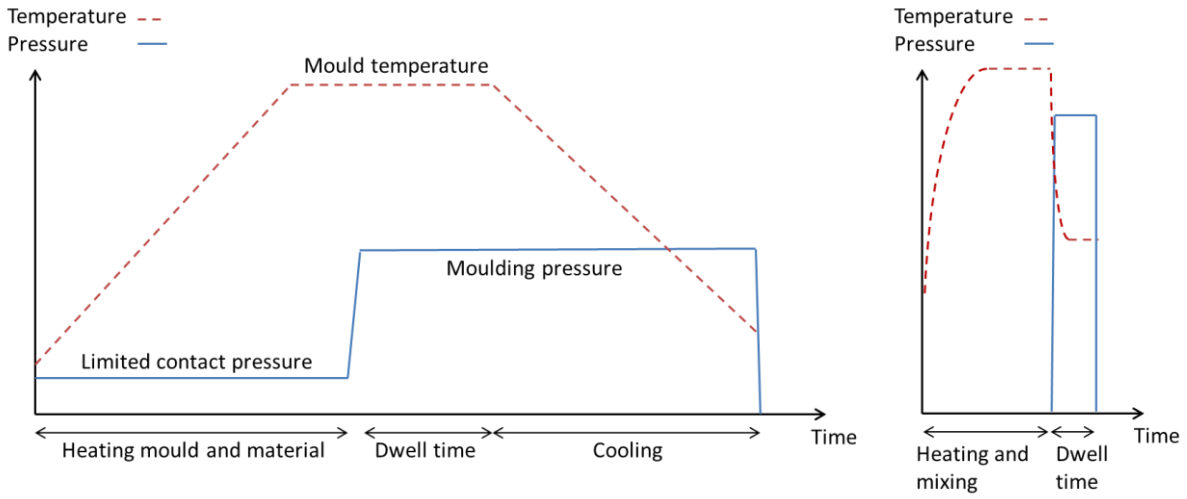

Figure 2.8 - Schematic representation of a typical non-mixed (a) and LFT mixed (b) compression moulding cycle

2.2.2 *Glass mat thermoplastics*

The use of Glass mat reinforced thermoplastic (GMT) is a matured process developed at the end of 1980s and represents a major market within the composite sector [68, 69]. The process consists of several steps, see Figure 2.9, starting by blending chopped long glass fibres with a thermoplastic polymer. After being heated and cooled under compression at a double belt press, a semi-finished product in plate form is produced. In a next step, this plate may be heated and subsequently compression moulded to form the final composite parts. Nesting and trimming might be necessary. The process is well suited for medium to large size products, large scale production, and cycle times around one minute. However, there are several disadvantages, like the amount of process steps, the cost intensive processing equipment and poor impregnation quality. The lack of mixing will induce similar difficulties as seen in DCM.

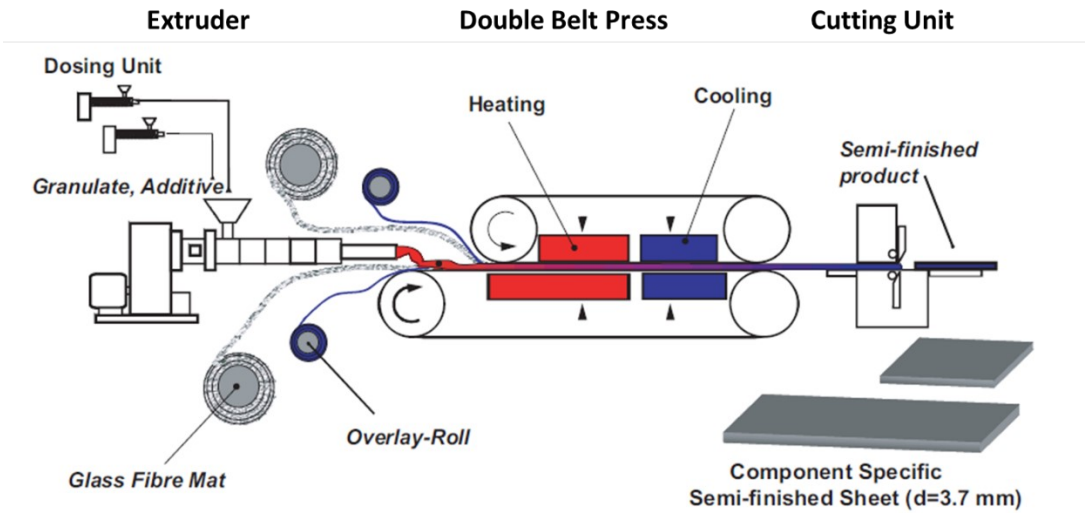

Figure 2.9 – Illustration of a GMT processing line for semi-finished products, source: [69]

2.2.3 *Injection moulding*

For both thermoset and thermoplastic matrix composites, mechanical grinding is commonly used to reduce the waste to small particles which can be used as filler, e.g. in injection moulding. Within injection moulding, fibre lengths are typically reduced by high shear forces to around 0.2 to 0.3 mm in the final product, resulting in reasonable fibre efficiency regarding stiffness, but low regarding strength and impact [8, 9, 70] (see Figure 2.1). Therefore, the recycling of thermoplastic composites by injection moulding does probably not lead to products that might be used in structural applications.

Alternatively, the extrusion of short or long fibre pellets semi-finished products is already performed by a commercial organisations [71]. However, as with all semi-finished products, this processing route adds one more extra process step, potentially leading to additional costs, polymer and fibre length degradation.

2.2.4 *Mixing compression moulding*

The long fibre thermoplastic (LFT) process uses pre-compounded thermoplastic matrix reinforced with long fibres in form of granules or pellets. The pellets are often cut from an extruded thermoplastic sheath around a fibre roving. A schematic representation of the mixing compression moulding (MCM), corresponding to the final cycle step, is similar to that one given in Figure 2.8b. The process consists of an extruder where material is simultaneously heated and gently mixed before injected or transferred to an isothermal stamping mould. Unlike injection moulding inducing high shear levels, the LFT process is especially designed for lower shear levels, to prevent fibre length degradation. This enables the manufacturing of parts containing longer fibres which features higher impact and strength properties [8, 9, 70, 72]. Therefore, LFT fills the gap between short fibres and continuous fibre in terms of property and price as is illustrated in Figure 2.10 [73]. Extensive work has been performed by Henning [72, 74–77] on a special version of LFT processes developed around the year 2000. This Direct LFT (LFT-D) has become the most used process compared to LFT and GMT [69, 78]. The LFT-D version features inline compounding and therefore eliminates the semi-finished product step (see Figure 2.11). Savings have been enabled by direct LFT in which raw materials like polymer and fibre are mixed and directly compression moulded in the same processing line. This partially omits logistics, leading to a simplified traceability of the material and need of semi-finished products like LFT pellets of plates. Reducing the process steps leads to a more cost effective process [79]. Beside the economical motivation, removing the semi-finished product and related process step also avoids a heating cycle which could lead to and increased environmental impact, polymer degradation and fibre length reduction.

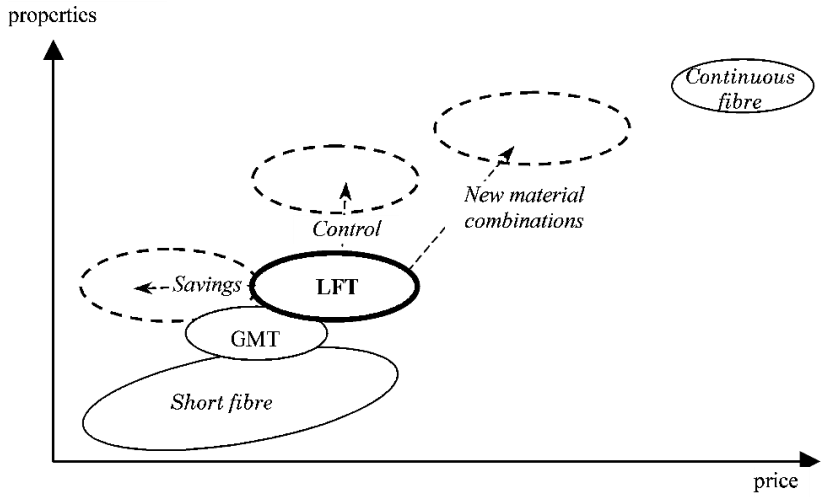

Figure 2.10 - Price-property relationship between different fibre reinforced thermoplastics. [73]

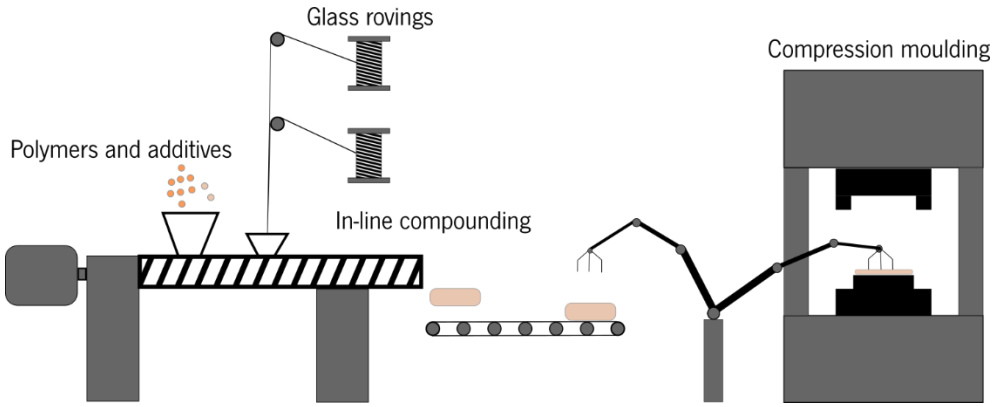

Figure 2.11 – Illustration of a direct LFT processing line for in-line compounding and compression moulding

2.2.5 *Recycling continuous fibre reinforced thermoplastics*

An overview of studies on the recycling of continuous fibre TPCs is presented in Table 2.1 (see Page 29). The list is compiled through screening of scientific and technical publications, and also incorporates more commercially sources such as websites and press releases of companies. The table shows the studied material, waste type, size reduction method and resulting fibre length. Furthermore, the Re-manufacturing technique with FVF and average fibre length after reprocessing is given when available. Finally, modelling, mechanical testing, manufactured applications and Life cycle and cost assessment (LCCA) are presented. The applications and LCCA are described in following sections.

A wide range of materials are considered, from high volume materials as G/PP to high value materials as C/PEAK and several types in between. The waste type is most often a multiply consolidated laminate or component and less frequent a single layer semipreg or prepreg. A size reduction step is present at all recycling solutions before the waste is re-manufacturing and results in fibre lengths between 0.1 and

100mm. Basically two types of methods can be distinguished: 1. an impact based size reduction such as hammer mills, cutting mills and granulators, which typically result in short fibre lengths (<5 mm) and 2. shear/cutting size reduction such as shredders and guillotines or choppers which typically result in longer fibre lengths (>5 mm) [80, 81]. One study, by Roux et al. [6], uses an electrodynamic fragmentation method, commonly found in mining.

The most common remanufacturing techniques are injection moulding, extrusion with compression moulding and DCM. A few use matrix dissolution to separate fibre and matric in combination with compression moulding. Some use a pelletising step as intermediate product. Fibre fractions are typically higher for compression moulding and lower for extrusion with compression moulding and injection moulding. The fibre length after reprocessing is often not available. From the offered data, injection moulding shows the most severe fibre length attrition. The fibre length reduction for extrusion with compression moulding is dependent on the type of extruder and is often significant. For direct compression moulding only, no reduction is observed when data was available and this is also assumed for the studies where no data was available. These observations fall in line with the results of Chu et al.[82] (see Figure 2.12), who studied the effect of processing method on the resulting fibre length in the material after processing.

Table 2.1 - An overview of studies or solutions concerning the recycling of continuous fibre TPCs. The list is ordered by the date of publication of the literature, website or press release. The lines in italic correspond to the recycling solution in this thesis. Overview adapted from [80]**.**

Material	Waste type	Size reduction	FL regrind (mm)	Re-manufacturing technique	FVF (%)	FL, after reprocessing (mm)	Modelling	Mechanical testing			Application	LCCA	Reference
								modulus (GPa)	strength (MPa)	toughness (J/m)			
G/PC	laminates	Liquid nitrogen + granulator	n/a	IM DCM	19-28	0.5 1.1	n/a	yes	yes	yes	n/a	n/a	Henshaw et al. [67]
G/PET	n/a	granulator	1-10	IM MCM DCM	23 23 23	0.08 0.14 0.5	yes	yes	yes	yes	n/a	n/a	Chu et al. [82]
C/PEEK	n/a	hammer mill cutting mill	0.1-1 0.1-3	IM DCM	24-43	n/a	n/a	yes	yes	n/a	n/a	n/a	Schinner et al. [83]
Flax/PP	production	cutting mill	n/a	MCM	13-35	n/a	n/a	yes	yes	yes	n/a	n/a	Schmachtenberg et al. [84]
C/PPS	weave trims	two-shaft shredder	1-18	MCM	33	n/a	n/a	yes	yes	yes	n/a	n/a	Janney et al. [85, 86]
G/PP	tape	two-shaft shredder	38	MCM	n/a	n/a	n/a	n/a	n/a	yes	n/a	n/a	Vaidya et al. [87]
C/PEEK	DCM UD tape component	Electrodynamical fragmenter	1-4	DCM	58*	no reduction	n/a	n/a	n/a	n/a	rotorcraft door hinge	n/a	Roux et al. [6] & Eguémann et al. [88]
C/PEEK	tape and laminate	Cut	3-19	DCM	59	no reduction	n/a	yes	yes	n/a	n/a	n/a	LeBlanc et al.[64]
G/TPU	n/a	n/a	5-25	DCM	45*	no reduction	yes	yes	yes	n/a	n/a	n/a	Rasheed et al. [26]
C/PEEK	semipreg laminated laminated	chopper n/a n/a	5-50 <10 <3	 Pelletising	50* 50* 25	n/a	n/a	n/a	n/a	n/a	rotorcraft door hinge, bracket and access panel	n/a	Teijin Carbon [89]
C/PPS	laminated	chopper + hammer mill	from <0.5 to 5-15	MCM IM	30-50	n/a	n/a	yes	yes	n/a	aerospace food-step and clip	n/a	Premium Aerotec [90], Lahr et al. Institut für Verbundwerkstoffe [91]
C/PPS	semipreg	chopper/guillotine	7.5-12.5	DCM	50*	no reduction	yes	yes	yes	n/a	aerospace access panel	n/a	Rasheed [5]
G/PP	laminated	chopper/guillotine	5-25	DCM	47*	no reduction	n/a	yes	yes	n/a	n/a	n/a	Moothoo et al.[92]

Table 2.1 -Continued

Material	Waste type	Size reduction	FL regrind (mm)	Re-manufacturing technique	FVF (%)	FL, after reprocessing (mm)	Modelling	Mechanical testing			Application	LCCA	Reference
								modulus (GPa)	strength (MPa)	toughness (J/m)			
C/PPS G/PP	laminated	two-& four-shaft shredders	10-30	MCM	20-35	little to no reduction	yes	yes	yes	yes	Aerospace access panel, bracket and safety shoe nose cap	yes	De Bruijn et al.[7, 93, 94] and Vincent [80]
G/PP	n/a	single-shaft shredder	20-100	DCM	n/a*	no reduction	n/a	n/a	n/a	n/a	product	n/a	Cetim [95]
C/PPS C/LMPEAK	laminated	n/a	<5	DCM	50	no reduction	n/a	n/a	n/a	n/a	product	n/a	Toray Advanced Composites [96]
C/PEEK	laminated	hammer mill four-shaft shredder	4.7-19 10-20	DCM	n/a	no reduction	n/a	yes	yes	n/a	n/a	n/a	Li et al. [97]
C/PPS	semipreg	four-shaft shredder	5-25	DCM	30-45	no reduction	n/a	n/a	n/a	n/a	n/a	n/a	Vincent et al. [98]
C/PP	LFT component	n/a	3	dissolution + CM	25	no reduction	n/a	yes	yes	n/a	n/a	n/a	Tapper et al. [99]
C/PPS	EoL	cryogenic grinder	<3	pelletising + IM pelletising + CM + thermoforming	n/a n/a	n/a	n/a	yes	yes	yes	bracket, cleat and Aerospace cockpit handle	yes	Leitat [100] Axyal [101]
C/PEI	LFT component	n/a	15-30	dissolution + solution impregnation + CM	50	no reduction	n/a	yes	yes	n/a	n/a	n/a	Liu et al. [102]
G/PMMA	component	granulator	<3	IM	13	n/a	n/a	yes	yes	n/a	n/a	yes	Cousins et al. [103]
G/PP C/PP G/PA	tape	chopper	<50	DCM	n/a*	no reduction	n/a	n/a	n/a	n/a	crash beam	n/a	Van Wees [104]

*: the remanufacturing step was realised without lowering the FVF of the initial waste

EoL: End-of-life, IM: Injection moulding, DCM: Direct compression moulding, MCM: Mixing compression moulding

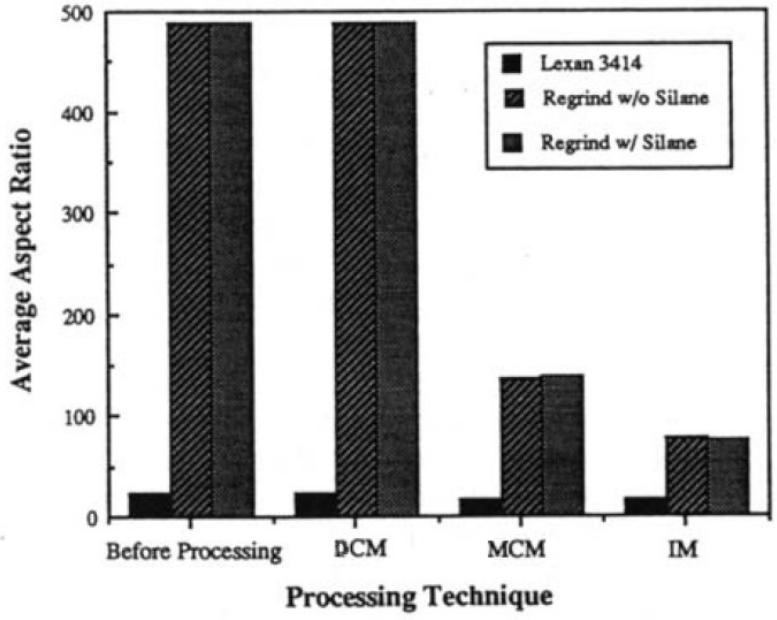

Figure 2.12 - The fibre length reduction for direct DCM, MCM and IM. Source [82]**.**

2.2.6 *Selecting the most suitable recycling route*

An overview of the previously discussed processes in Section 2.2 is given in Figure 2.13. Without mixing, size reduced waste material, e.g. flakes, can be directly process by direct compression moulding (as described in Section 2.2.1). Disadvantages are the low levels of homogeneity and long cycle time. This route is however widely described in literature and will therefore be included in this work for comparison. Processes with a mixing step on the other hand, offer a higher level of homogeneity and shorter cycle times. As described in Section 2.2.3, injection moulding leads to significant fibre length reductions resulting in lower mechanical properties. The recycling route involving semi-finished products results in an additional heating step which might cause degradation and involves the cost intensive processing equipment for GMT and fibre attrition for SFT or LFT Pellets. Considering the characteristics of MCM described in section 2.2.4, such as the benefits of mixing, the potential mechanical properties and short cycle time, this process was selected as object of this study as the most suitable recycling route and was benchmarked to the DCM route.

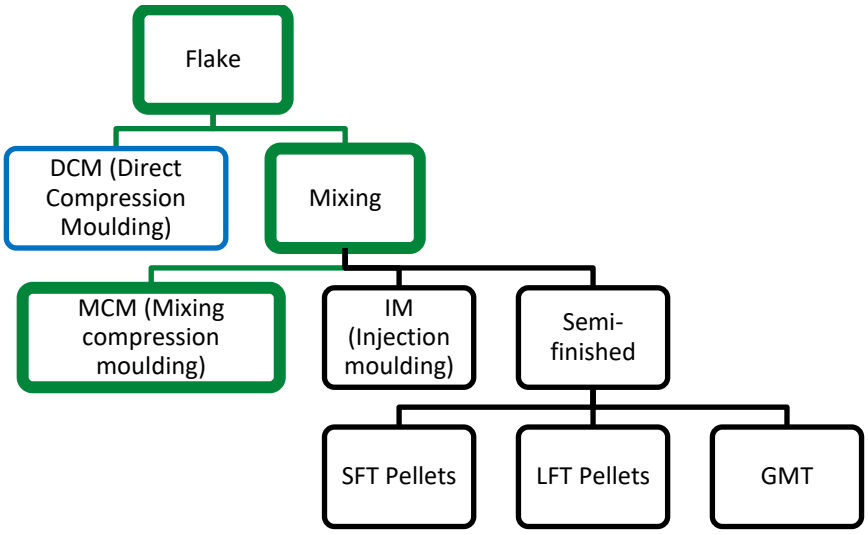

Figure 2.13 - Overview of various recycling routes. The most promising mixed compression moulded route is marked by a green thick line and the considered direct compression moulded route used as benchmarked in indicated in blue.

A schematic flow chart of these two recycling routes is given in Figure 2.14. A typical representation of pressure and temperature over time for both processing cycles is given in Figure 2.8. The mixing step enables the material to be heated outside of the mould. Therefore, the mould stands at a constant (isothermal) temperature, avoiding time-consuming heating and cooling cycles and thus the cycle time is typically in the order of minutes. The non-mixed moulding process requires not only the heating but also the subsequent cooling of the entire mould, resulting in a large energy consumption and a cycle time in the order of hours rather than minutes.

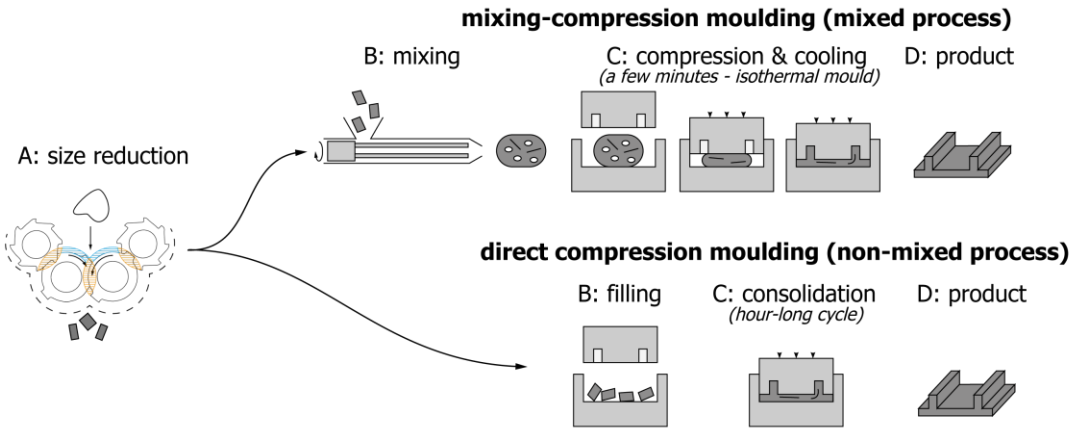

Figure 2.14 - Schematic flow chart of the mixed (top row) and non-mixed (bottom row) compression moulding recycling route.

Although the Direct LFT seems very suitable for recycling the shredded long fibre thermoplastics, the equipment costs are high [73]. This is not a problem for segments requiring high volume production rates, like the automotive, but less suitable for those involving lower production rates and that are currently available for recycling, as almost all other typically non-automotive markets. Therefore, a less costly

alternative capable of processing materials with high melt temperatures is required. In the current study, a low-shear mixing approach is explored, also referred to as Mixed compression moulding (MCM), using a small-scale and low-cost piston blender, originally developed by the Centre of Lightweight Structures in the Netherlands in 1998 [105] (see Figure 2.15). The equipment was developed to melt and mix LFT materials with minimal fibre breakage. Its simple construction results in a low-cost solution in comparison to the industrial equivalent. Unlike a typical extruder which uses a screw to mix and heat the material by shear, this device contains three rotating heated rods in a heated cylinder of 70 mm in diameter. The three rods are located at a different radius from the cylinder's centre. Since there is no plastification screw, the shear induced on the melt is very limited and thus fibre length can be maintained.

The material is fed into the heated cylinder via the hopper, after which a piston closes the cylinder by transferring the material to the centre of the cylinder. The material is not compressed, but compacted to fill the cavity by a filling fraction of 20% to 50% of the total volume. The rods start to rotate and are mixing and heating the material. Subsequently, the mixed material is ejected by the piston in form of a mixed dough or charge. After the mixing step, the molten and mixed material was rapidly transferred to a compression mould. Typical processing settings of this setup are a rotational speed of the rods of 5 to 20 rotations per minute (rpm) and a mixing and heating time of 5 to 20 minutes.

Compression moulding takes place directly after the charge is transferred to the mould for forming, consolidation and cooling. The moulds need to close at relatively high approaching speeds and high compression speeds of about 10 to 20mm/s [106]. During closing, the material flows and fills the mould cavity, after which the mould is kept closed at a pressure of minimal 50 bars during consolidation and cooling [73].

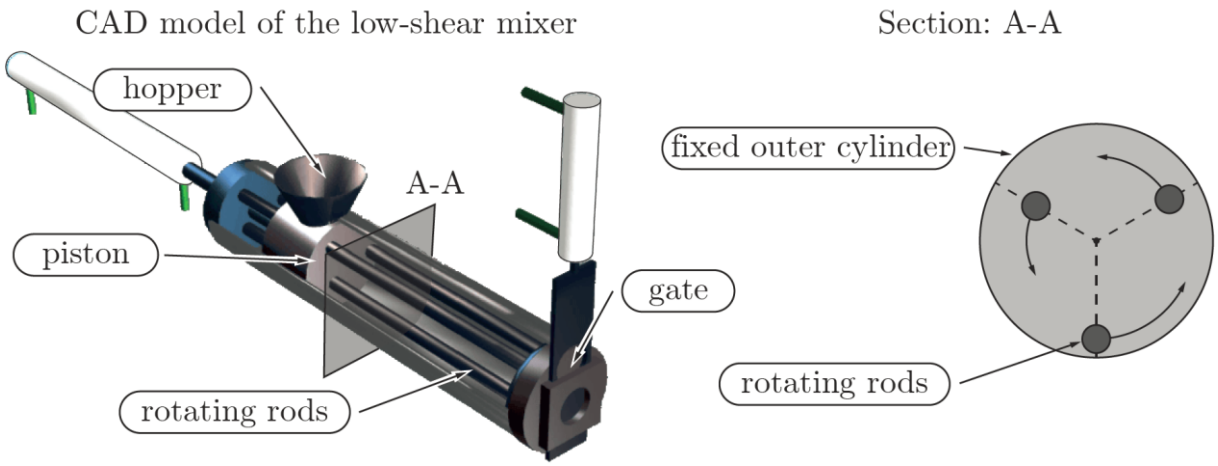

Figure 2.15 – A schematic representation of the low-shear mixing machine including a description of the main components [53, 105, 107]

Vaidya et al. studied mixing compression process for LFT material and applications in especially automotive, but also aerospace. Although not all publications are found to be very elaborate, they describe the use of various interesting topics, including the use of C/PPS [87, 108, 109]. In collaboration with Janney et al. the recycling of reclaimed carbon fibres and re-grind of PPS-based long fibre thermoplastic composites was also studied. Interesting results were found, e.g. after five consecutive regrind trials no degradation was seen in mechanical properties [85, 86]. This result was also found for G/PP material [106]. Henning also mentioned the possibility of recycling and states a specific extruder with a screw design was beneficial to preserve fibre length of large (12-50mm) shredded particles [68, 110].

Although some similarities can be found, laminated material of continuous fibres was barely recycled and experimental results were hardly compared to analytical models. This is surprising, as consolidated materials represent a large volume of the continuous fibre TPC waste, as described in Section 1.3.

2.3 Application

Various products made of recycled TPC and related materials are briefly discussed to present the current state of the art and opportunities for demonstrator products.

As presented in Table 2.1, some studies manufactured applications to demonstrate the possible products for recycled TPC waste, ranging from access panels (see Figure 2.17) and brackets, hinge or clips (see Figure 2.16) for aerospace to undefined products. The latter type is showed by research institute Cetim [95] and companies Toray Advanced Composites [96] and Van wees [104]. Little information is known about the application of these products. Material supplier Teijin provides sparse information on their recycled material and current applications. The C/PEEK material is categorised in three types: 1) Chips, which is single ply semipreg cut in rectangular flakes of 5 x 5 mm^2 to 50 x 50 mm^2, 2) Compound, which is a pellet of 30% fibre fraction by weight, and 3) Crushed, which is consolidated multiply post-industrial waste in size reduced to small flakes. It is unclear if these materials are already commercially available. The company displays a demonstrator for each of the material type. Chips were processed by Greene Tweed into a bracket (see Figure 2.16a). The compound was injection moulded into an aircraft wing access panel made from by Sintex NP Group (see Figure 2.17a).The crushed material was processed into a door hinge by Cross Composites but looks identical to the rotorcraft door hinge described by Roux et al. [6] and Eguémann et al. [88] which is also of C/PEEK material (see Figure 2.16b). These two studies provide more details on the rotorcraft door hinge and the latter study is the only one found which includes a description of a component test. A brittle failure mode was observed for the DCM part of recycled

material at a load which was 15% lower compared to a counterpart made of virgin chopped UD tape that showed a more ductile failure mode.

Three demonstrators have been made from C/PPS material in the Clean sky project RESET. The company Axyal [101] used DCM and CNC machining to process the material in a plate-like handle for the cockpit of a Dassault F5X airplane (see Figure 2.16c). At the technology institute Leitat [100], the coordinator of the RESET project, a bracket and cleat were injection moulded with the same material (see Figure 2.16d). In a similar approach to the RESET project, Lahr et al. [91] injection moulded C/PPS waste material from Premium Aerotec [90] into a food-step and clip for aerospace. Little information is known about these applications.

Previous work on access panel doors for aerospace has been performed with recycled composites by Rasheed [5] and Boeing [111] (see Figure 2.17b and c). The first is made by a DCM process and cutted carbon/PPS semipreg waste material. The part illustrates the design freedom by complex features, e.g. thickness transition, ribs, holes with bosses. The latter is made by virgin epoxy material and reclaimed carbon fibre from production of the 787 trailing edges and was mounted on the ecoDemonstrator 787 flight-test airplane wing. According to Boeing, it “marks the first time that recycled carbon fibre from aerospace parts has been remade into hardware qualified for commercial airplane flight.” [111] A third access panel is fabricated by CCS Composites [112] and is shown in Figure 2.17d. The panel is designed for the V-22 Osprey rotorcraft and is produced by DCM with virgin epoxy based BMC material. Although this application is not made from recycled or TPC material, interesting benefits are described that are possible due to the long discontinuous fibre material and compression moulding process, which is similar to recycled TPC. The compression moulding process allowed the design and fabrication of complex shapes in single process step. The geometric freedom enables ribs for stiffening and optimise load paths which is especially relevant for the highly loaded areas and the overall strength of the part. Like with the study of Rasheed, the parts can be supplied with integrated fasteners and features. Furthermore, the process allows for incorporation of lightning strike foils into the surface layer, as is visible in the figure.

a) Bracket made form Tenax® TPWF Chips by Greene Tweed [89]

b) A rotorcraft door hinge made of C/PEEK flakes obtained by Electrodynamical fragmentation. Source Roux et al. [6]

c) Source Axyal [113]

d) A Bracket and cleat made from recycled C/PPS material. Source Leitat [100, 114]

Figure 2.16 – Brackets, hinge and clips for aerospace

(a) OEM Aircraft wing access panel made from Tenax® Compound by Sintex NP Group. Material is recycled C/PEEK. Image courtesy: Teijin Carbon [89].

(b) Access panel with integrated design features like ribs, joggle and thickness transitions. The part is made out of C/PPS semipreg flakes by DCM. Image courtesy TPRC / Rasheed [5].

(c) Wing-access panels (bottom image) mounted on the Boeing ecoDemonstrator 787 flight-test airplane wing (top image) reclaimed carbon fibre material. Photo by John D. Parker and Image courtesy: The Boeing Co. [111].

(d) An access panel for the V-22 Osprey rotorcraft made from virgin chopped unidirectional carbon/epoxy prepreg material by DCM. Source: CCS composites and CompositesWorld [112].

Figure 2.17 - Access panels designed in previous studies

The overall conclusion of these products is that discontinuous fibres offers a geometric freedom which makes interesting design features for increased stiffness, optimised load distribution and material reduction by thickness transition possible. Often only limited information is available, which might be related to the involvement of commercial companies, but none of the products made of recycled TPC seem to be used in an application. Nevertheless, the two discussed access panel made from discontinuous fibres and thermosetting polymer offer interesting solutions and can replace current products of continuous fibre composites. When leveraging the geometric freedom of the discontinuous fibres and when taking waste material as a source, products made from recycled TPC will likely offer an interesting solution for several applications.

2.4 Life cycle and cost assessment

The environmental assessment of products is frequently carried out using Life Cycle Assessment (LCA) and is an established methodology supported by the International Standards Organisation (ISO). The method considers the environmental impact during all phases of a products lifetime. Typically, the following phases are described: material production, part production, use and End-of-Life (EoL) phase. Witik et al. [115] finds that the combination of LCA on environmental aspects with cost aspects is a worthwhile approach for comparing different materials and processes in terms of cost and environmental impact. The availability of inventory data for all phases is important and might be available in databases such as CES Edupack 2019 [116], Ecoinvent 2012 [117] and IDEMAT 2010 [118].

In an overview on LCA studies, Simões et al. [119] found that fibre reinforced polymer composites (FRPC) materials represent often the lowest environmental impact when compared to traditional materials such as metals. In some occasions, conflicting data was found and was explained to often originate from system boundary definition and EoL treatment. Including the disposal or EoL treatment phase often results in a negative influence for the FRPC compared to traditional materials [120, 121]. This reflects the fact that at EoL most FRPC are still deposited in landfills with little recycling or recovery being done [119]. The production of carbon fibre is known to be costly and energy intensive compared to other materials [122] [115]. LCA studies on carbon fibre show benefits in the use phase, but a large environmental impact in the material production phase [120, 123]. Pimenta et al. [124] drafted a comparison on the required energy for virgin and recycled material production of, in decreasing order of energy consumption: carbon fibre, aluminium, steel and glass fibre (see Figure 2.18). The production energy for carbon fibre is clearly the largest. The energy for recycling is similar for all materials, although for glass fibre no figure is given.

When recycling the carbon material after their primary application the impact of the material production phase can be spread over multiple applications [124].

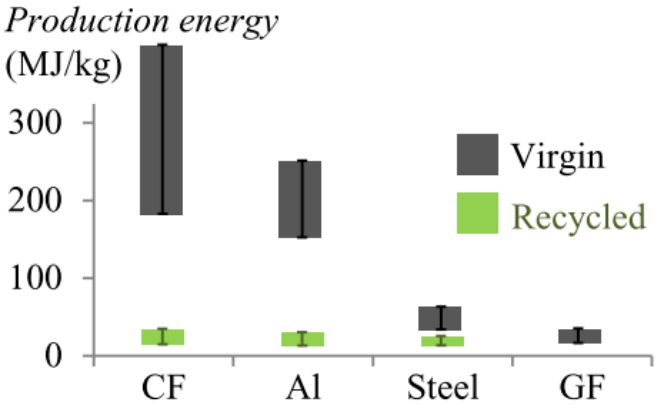

Figure 2.18 - Estimated ranges for energy consumption for material production [124]

Only a limited amount of studies has been found which describe the environmental impact by a life cycle assessment or cost of applications made of continuous fibre TPC. Some studies only give an indicative number or remark on the environmental impact or the cost of a part. For example, the popular article on the previously discussed wing access panel for the Boeing ecoDemonstrator program, briefly states an estimated CO2 reduction related to the production of the access panel of about a third by using reclaimed carbon fibre instead of virgin carbon fibre [111]. For the formerly mentioned access panel for the V-22 Osprey a cost reduction was noted by a significant reduced cycle time, coming from 8 hours for the hand-laid and autoclave cured sandwich construction, to under 30 minutes for DCM of the C/epoxy material.

From Table 2.1, only two studies describe a very limited economic or environmental assessment of recycling TPC material. Cousins et al.[103] evaluates the economic costs for a dissolution recycling method on material level. The material is a non-typical TPC, or more specifically PMMA or Elium® from Arkema. The solution is found economically feasible under certain conditions, e.g. labour cost and a resale price for PMMA of $2,5/kg which is similar to virgin. In the Reset project [100] the employment of 1 kg recycled C/PPS and C/PEEK in multiple demonstrators by the aircraft manufacturing industry is studied. However, current solutions or solutions made of virgin materials are not considered and therefore it is difficult to compare the impact of recycled material and the recycling process.

2.5 Conclusion and approach

The main goal of this PhD study is to develop a better understanding of the possibilities of continuous fibre TPC recycling. The research focuses on the optimum process for TPC waste to obtain the highest performance possible at lowest economic and environmental cost. Knowing the state of the art, a more

specific goal is to develop a new recycling route for continuous fibre TPC by analytical modelling and experimental validation of mechanical properties on material level followed by application and evaluation on product level.

In general, most of the studies focussing on recycling TPCs (presented in Table 2.1) investigated experimentally the mechanical performance of processed waste material. Some of them compare the results of recycled materials with virgin materials and others compare processing techniques. Only a limited amount of studies include modelling to predict the mechanical performance. There are a few demonstrators, but to the knowledge of the author, no study compares a final recycled part with a current product, meeting all requirements of a specific application or includes any economic and environmental impact assessment resulting from its use. Liu et al. [125] conclude in their review paper the following points:

- Re-manufacturing techniques and their relevant systems are still in their infancy
- The work focused on the optimal usage of the recyclates to improve the quality, or reduce the cost of a specific product is scarce
- Cost and environmental issues during the composite recycling are very important, therefore the developed approaches should not only be technically feasible, but also cost effective and environmentally friendly
- The energy and cost savings at the workshop level haven't yet been properly detailed in the literature related to the composite recycling area

Obtaining a better understanding of the material structure of TPC waste on the mechanical performance by modelling will be beneficial for many recycling approaches stated in Table 2.1 and will therefore be a relevant addition to the current state of the art. Optimising the recycling route and demonstrating the economic and environmental feasibility of potential applications will show the potential of recycling TPC waste and help industrial implementation, and are therefore included in this study.

2.5.1 *Modelling*

Modelling is only applied very limitedly in relation to the recycling of thermoplastic composites. In some studies, the Kelly-Tyson model for strength and a modified ROM or Halpin-Tsai model for modulus is used [5, 26, 82]. Most studies experimentally test the mechanical performance of the processed material. Lui et al. [125] states that there is "*a lack of mathematical models to depict the influence of variance of processing parameters on the quality of recyclates for recycling approaches".*

To find the optimum mechanical properties for waste material, the trade-off between long fibre length and homogeneous material needs to be studied. Therefore, the influence of fibre length, fibre content, fibre orientation, fibre dispersion and distribution on the mechanical performance is required. With this information a recycling route can be developed aimed at the requirements in the research question.

Existing models for the micromechanical modelling of stiffness and strength are described. Models that take into account the effect of fibre volume, fibre length and fibre orientation can be found in literature.

However, the influence of the degree of mixing is not typically taken into account, while it is known to have a significant influence on final composite properties. Therefore in this thesis, in Chapter 3, a method is proposed to further extended the existing models by taking into account the influence of fibre dispersion (through bundle size distribution) and fibre distribution (fibre volume distribution). In addition, as already integrated in some existing models, the effect of the fibre length distribution of the recycled material will also be included in the model to be developed so optimisation of the recycling route regarding mixing and fibre length is possible.

2.5.2 *Recycling route and experimental validation*

An overview of options to process discontinues fibres is given and current recycling methods to recycle TPCs are compared. A selection is made in Section 2.2.6. A low-shear mixing setup will be used in combination with compression moulding to process shredded flakes. Although some studies process TPC by mixing and compression moulding, laminated material of continuous fibres was barely recycled and experimental results were hardly compared to analytical models. Most of the studies processed material by DCM, which will occasionally be used to give refence to this commonly used process without mixing. Input of the modelling will be used to select the most suitable process parameters for the total experimental setup. With the new recycling routes in place, experimental tests will be performed to determine the stiffness, strength and impact toughness of the processed material (Chapter 4). The experimental results will be compared to the results of the model and offer validation of the technical feasibility of the recycling solution on material level

2.5.3 *Application*

To prove the translation of the technical feasibility from material level to product level, actual demonstrators are required. An application for high-end and high-volume markets shall be designed, manufactured and tested to functional specification of current application in Chapter 5. From the state of the art no products are found which are made of recycled TPC that are used in an application. But there

are studies on products made of recycled TPC and products made of related material combinations that stress the benefits related to the geometric freedom of discontinuous material. Therefore, the design shall utilise this geometric design freedom for aspects such as potential function integration, geometric stiffening and stress distribution.

2.5.4 *Life cycle and cost assessment*

By using a combined life cycle and cost assessment (LCCA) the cost financial cost, greenhouse gases (GHG) and cumulative energy depletion (CED) of the developed demonstrator products shall be determined in Chapter 6. By benchmarking the products to currently available alternatives, the function and value of the application is similar and the economic and environmental cost can be compared. With this information the research question can be answered.

Only a few studies offered limited information on the environmental and cost aspects of products made of recycled continuous fibre TPC. Even with reclaimed carbon fibre and virgin epoxy a significant reduction in GHG is claimed and virgin discontinuous fibres with epoxy already showed a cost reduction due to short cycle times of DCM in comparison to autoclave. When combining it with the manufacturing benefits of the TPC material, such as fast processing time and using recycled material, promising applications might be possible with the new recycling route.

The research question stays unchanged, but the scope is converged to the elements and approach described sections in 2.5.1 to 2.5.4.

2.6 References

[1] W. Schijve, "High performance at medium fibre length in long glass fibre polypropylene," *Plast. Addit. Compd.*, vol. 2, no. 12, pp. 14–21, 2000, doi: 10.1016/S1464-391X(00)80121-X.

[2] J. L. Thomason, "The influence of fibre length and concentration on the properties of glass fibre reinforced polypropylene: 5. Injection moulded long and short fibre PP," *Compos. Part A Appl. Sci. Manuf.*, vol. 33, no. 12, pp. 1641–1652, 2002, doi: 10.1016/S1359-835X(02)00179-3.

[3] U. Vaidya *et al.*, "Comparison of wet laid to other discontinuous processed carbon fiber thermoplastic composites," in *CAMX Conference Proceedings*, 2014.

[4] A. Sarhangi Fard, "Analysis and optimization of mixing inside twin-screw extruders," PhD Thesis, Eindhoven Univesity of Technology, 2010.

[5] M. I. Abdul Rasheed, "Compression molding of chopped woven thermoplastic composite flakes: a study on processing and performance," PhD Thesis, University of Twente, Enschede, The Netherlands, 2016.

[6] M. Roux, N. Eguémann, C. Dransfeld, F. Thiébaud, and D. Perreux, "Thermoplastic carbon fibre-reinforced polymer recycling with electrodynamical fragmentation: From cradle to cradle," *J. Thermoplast. Compos. Mater.*, 2015, doi: 10.1177/0892705715599431.

[7] T. A. De Bruijn, G. A. Vincent, and F. W. J. Van Hattum, "Recycling of long fibre thermoplastic composites by low shear mixing," in *SAMPE Europe*, 2016, pp. 540–546.

[8] T. A. De Bruijn, G. Vincent, and F. W. J. Van Hattum, "Recycling C/PPS laminates into long fibre thermoplastic composites by low shear mixing," in *Proceedings of the 21th Internatinoal Conference on Composite Materials ICCM21*, 2017.

[9] M. Selezneva and L. Lessard, "Characterization of mechanical properties of randomly oriented strand thermoplastic composites," *J. Compos. Mater.*, vol. 50, no. 20, pp. 2833–2851, 2016, doi: 10.1177/0021998315613129.

[10] P. Feraboli, E. Peitso, F. Deleo, and T. Cleveland, "Characterization of Prepreg-Based Discontinuous Carbon Fiber/Epoxy Systems," *J. Reinf. Plast. Compos.*, vol. 28, no. 10, pp. 1191–1214, 2009, doi: 10.1177/0731684408088883.

[11] M. Wijngaarden, A. Jongbloed, and J. de Vries, "Thermoplastic Compound Compression Molding," in *55th International SAMPE Symposium and Exhibition*, 2010.

[12] J. H. Phelps, "Processing-microstructure Models for Short- and Long-fiber Thermoplastic Composites," PhD Thesis, University of Illinois, 2009.

[13] C. L. TuckerIII and E. Liang, "Stiffness predictions for unidirectional short-fibre composites: review and evaluation," *Composites Science and Technology*, vol. 59, no. 5. pp. 655–671, 1999, doi: 10.1016/S0266-3538(98)00120-1.

[14] F. W. J. Van Hattum and C. A. Bernardo, "A model to predict the strength of short fiber composites," *Polym. Compos.*, vol. 20, no. 4, pp. 524–533, 1999, doi: 10.1002/pc.10376.

[15] H. L. Cox, "The elasticity and strength of paper and other fibrous materials," *Br. J. Appl. Phys.*, vol. 3, pp. 72–79, 1952.

[16] A. Kelly and W. R. Tyson, "Tensile properties of fibre-reinforced metals: Copper/tungsten and copper/molybdenum," *J. Mech. Phys. Solids*, vol. 13, no. 6, pp. 329–350, 1965, doi: 10.1016/0022-5096(65)90035-9.

[17] J. C. H. Affdl and J. L. Kardos, "The Halpin-Tsai equations: A review," *Polym. Eng. Sci.*, vol. 16, no. 5, pp. 344–352, 1976, doi: 10.1002/pen.760160512.

[18] G. P. Tandon and G. J. Weng, "The effect of aspect ratio of inclusions on the elastic properties of unidirectionally aligned composites," *Polym. Compos.*, vol. 5, no. 4, pp. 327–333, 1984, doi: 10.1002/pc.750050413.

[19] H. Krenchel, *Fibre Reinforcement: Theoretical and Practical Investigations of the Elasticity and Strength of Fibre-reinforced Materials*. Copenhagen, 1964.

[20] J. L. Thomason and M. a. Vlug, "Influence of fibre length and concentration on the properties of glass fibre-reinforced polypropylene: Part 1. Tensile and flexural modulus," *Compos. Part A Appl. Sci. Manuf.*, vol. 27A, pp. 477–484, 1996.

[21] C. L. Tucker III and E. Liang, "Stiffness predictions for unidirectional short-fiber composites: Review and evaluation," *Composites Science and Technology*, vol. 59. pp. 655–671, 1999.

[22] J. D. Eshelby, "The Determination of the Elastic Field of an Ellipsoidal Inclusion, and Related Problems," *Proc. R. Soc. A Math. Phys. Eng. Sci.*, vol. 241, no. 1226, pp. 376–396, 1957, doi: 10.1098/rspa.1957.0133.

[23] T. Mori and K. Tanaka, "Average stress in matrix and average elastic energy of materials with misfitting inclusions," *Acta Metall.*, vol. 21, no. 5, pp. 571–574, 1973, doi: 10.1016/0001-6160(73)90064-3.

[24] J. L. Thomason, M. a. Vlug, G. Schipper, and H. G. L. T. Krikor, "Influence of fibre length and concentration on the properties of glass fibre-reinforced polypropylene: Part 3. Strength and strain at failure," *Compos. Part A Appl. Sci. Manuf.*, vol. 27, no. 11, pp. 1075–1084, 1996, doi: 10.1016/1359-835X(96)00066-8.

[25] S. Kumar and J.-P. Kruth, "Composites by rapid prototyping technology," *Mater. Des.*, vol. 31, no. 2, pp. 850–856, Feb. 2010, doi: 10.1016/j.matdes.2009.07.045.

[26] M. I. A. Rasheed, B. Rietman, H. A. Visser, and R. Akkerman, "Experimental characterisation of recycled (Glass/TPU woven fabric) flake reinforced thermoplastic composites," in *19th International Comittee on Composite Materials*, 2013, pp. 3999–4010.

[27] K. S. Kumar, A. K. Ghosh, and N. Bhatnagar, "Mechanical Properties of Injection Molded Long Fiber Polypropylene Composites , Part 1 : Tensile and Flexural Properties," *Polym. Compos.*, vol. 28, pp. 259–266, 2007, doi: 10.1002/pc.

[28] G. W. Beckermann and K. L. Pickering, "Engineering and evaluation of hemp fibre reinforced polypropylene composites: Micro-mechanics and strength prediction modelling," *Compos. Part A*, vol. 40, pp. 210–217, 2009, doi: 10.1016/j.compositesa.2008.11.005.

[29] W. H. Bader, M. G., & Bowyer, "An improved method of production for high strength fibre-reinforced thermoplastics," *Composites*, no. July, pp. 150–156, 1973.

[30] S. W. Tsai and E. M. Wu, "A General Theory of Strength for Anisotropic Materials," *J. Compos. Mater.*, vol. 5, no. 1, pp. 58–80, 1971, doi: 10.1177/002199837100500106.

[31] S. R. Doshi and J.-M. Charrier, "A simple illustration of structure-properties relationships for short fiber-reinforced thermoplastics," *Polym. Compos.*, vol. 10, no. 1, pp. 28–38, 1989, doi: 10.1002/pc.750100105.

[32] G. A. Vincent, T. A. De Bruijn, S. Wijskamp, M. I. Abdul, M. Van Drongelen, and R. Akkerman, "Shredding and sieving thermoplastic composite scrap : Method development and analyses of the fibre length distributions," *Compos. Part B*, vol. 176, no. February, p. 107197, 2019, doi: 10.1016/j.compositesb.2019.107197.

[33] S. K. Garkhail, R. W. H. Heijenrath, and T. Peijs, "Mechanical Properties of Natural-Fibre-Mat-Reinforced Thermoplastics based on Flax Fibres and Polypropylene," *AppliedComposite Mater.*, vol. 7, pp. 351–372, 2000.

[34] S. G. Advani and C. L. Tucker III, "The Use of Tensors to Describe and Predict Fiber Orientation in Short Fiber Composites," *J. Rheol. (N. Y. N. Y).*, vol. 31, no. 8, pp. 751–784, 1987, doi: 10.1122/1.549945.

[35] G. B. Jeffery, "The Motion of Ellipsoidal Particles Immersed in a Viscous Flow," *R. Soc.*, vol. 102, 1922.

[36] F. Folgar and C. L. Tucker III, "Orientation Behavior of Fibers in Concentrated Suspensions," *J. Reinf. Plast. Compos.*, vol. 3, pp. 98–119, 1984, doi: 10.1177/073168448400300201.

[37] J. Linn, "The Folgar-Tucker Model as a Differential Algebraic System for Fiber Orientation Calculation," 2005.

[38] S. G. Advani, "The Use of Tensors to Describe and Predict Fiber Orientation in Short Fiber Composites," *J. Rheol. (N. Y. N. Y).*, vol. 31, no. 8, p. 751, 1987, doi: 10.1122/1.549945.

[39] H. C. Tseng, R. Y. Chang, and C. H. Hsu, "Numerical prediction of fiber orientation and mechanical performance for short/long glass and carbon fiber-reinforced composites," *Compos. Sci. Technol.*, vol. 144, pp. 51–56, 2017, doi: 10.1016/j.compscitech.2017.02.020.

[40] A. You, M. A. Y. Be, and I. In, "The use of micromechanical models to predict fiber reinforced plastics The Use of Micromechanical Models to Predict Fiber Reinforced Plastics," in *AIP Conference Proceedings 2055*, 2019, vol. 070016, no. January, doi: 10.1063/1.5084860.

[41] D. Dray, P. Gilormini, and G. Régnier, "Comparison of several closure approximations for evaluating the thermoelastic properties of an injection molded short-fiber composite," *Compos. Sci. Technol.*, vol. 67, no. 7–8, pp. 1601–1610, 2007, doi: 10.1016/j.compscitech.2006.07.008.

[42] J. Cintra and C. Tucker III, "Orthotropic closure approximations for flow-induced fiber orientation," *J. Rheol. (N. Y. N. Y).*, no. 39(6), pp. 1095–122, 1995.

[43] H. Chen and D. G. Baird, "Prediction of Young ' s Modulus for Injection Molded Long Fiber Reinforced Thermoplastics," *J. Compos. Sci.*, 2018, doi: 10.3390/jcs2030047.

[44] S. Toll and P. Andersson, "Microstructure of Long- and Short-Fiber Reinforced Injection Molded Polyamide," *Polym. Compos.*, vol. 14, no. 2, pp. 116–125, 1993.

[45] D. E. Spahr, K. Friedrich, J. M. Schultz, and R. S. Bailey, "Microstructure and fracture behaviour of short and long fibre-reinforced polypropylene composites," *J. Mater. Sci.*, vol. 25, pp. 4427–4439, 1990.

[46] C. Kuhn, "Molding of Fiber Reinforced Plastics Analysis and Prediction of Fiber Matrix Separation during Compression Molding of Fiber Reinforced Plastics," PhD Thesis, Universität Erlangen-Nürnberg, 2018.

[47] G. A. Vincent, T. A. de Bruijn, S. Wijskamp, M. van Drongelen, and R. Akkerman, "Process- and material-induced heterogeneities in recycled thermoplastic composites," *Submitt. to J. Thermoplast. Compos. Mater.*, 2019.

[48] B. N. Nguyen *et al.*, "Fiber length and orientation in long-fiber injection-molded thermoplastics - Part I: Modeling of microstructure and elastic properties," *J. Compos. Mater.*, vol. 42, no. 10, pp. 1003–1029, 2008, doi: 10.1177/0021998308088606.

[49] J. E. Spowart, B. Maruyama, and D. B. Miracle, "Multi-scale characterization of spatially heterogeneous systems: implications for discontinuously reinforced metal-matrix composite microstructures," *Mater. Sci. Eng.*, vol. 307, pp. 51–66, 2001.

[50] J. L. Kim, D.; Lee, J. S.; Barry, C. M. F.; Mead, "Microscopic measurement of the degree of mixing for nanoparticles in polymer nanocomposites by TEM images," *Microsc. Res. Tech.*, pp. 539–546, 2007.

[51] F. Van Hattum, C. Leer, O. Carneiro, and B. Maruyama, "Quantitative assessment of mixing quality in nanoreinforced polymers using a multi-scale image analysis method," in *8th ISTC*, 2006.

[52] M. Jawaid, S. Boufi, and A. Khalil, *Cellulose-Reinforced Nanofibre Composites*. Woodhead Publishing, 2017.

[53] G. A. Vincent, T. A. de Bruijn, S. Wijskamp, M. I. A. Rasheed, M. Van Drongelen, and R. Akkerman, "Characterisation and improvement of the quality of mixing of recycled thermoplastic composites," *Submitt. to Polym. Compos.*, 2019.

[54] J. L. Thomason, "The influence of fibre length and concentration on the properties of glass fibre reinforced polypropylene: 6. The properties of injection moulded long fibre PP at high fibre content," *Compos. Part A Appl. Sci. Manuf.*, vol. 36, no. 1, pp. 995–1003, 2005.

[55] M. Ericson and L. Berglund, "Deformation and fracture of glass-mat- reinforced polypropylene," *Compos. Sci. Technol.*, vol. 43, pp. 269–281, 1992.

[56] R. Rondeau and S. Reeve, "The effect of tows and filament groups on the properties of discontinuous fiber composites," in *44th International SAMPE Symposium*, 1999, pp. 1449–1460.

[57] J. M. Starbuck and L. B. Cataquiz, "Evaluation of Large Tow-Size Carbon Fiber for Reducing the Cost of CNG Storage Tanks," in *2000 Future Car Congress*, 2000, no. 724.

[58] J. S. Dahl, G. L. Smith, D. Q. Houston, D. Mi, S. Iobst, and L. Berger, "The influence of fiber tow size on the performance of chopped carbon fiber reinforced composites," in *SAMPE Conference Proceedings*, 2005.

[59] L. T. Harper, T. a. Turner, N. a. Warrior, and C. D. Rudd, "Characterisation of random carbon fibre composites from a directed fibre preforming process: The effect of tow filamentisation," *Compos. Part A Appl. Sci. Manuf.*, vol. 38, no. 3, pp. 755–770, 2007, doi: 10.1016/j.compositesa.2006.09.008.

[60] M. A. Tschopp, G. B. Wilks, and J. E. Spowart, "Multi-scale characterization of orthotropic microstructures," *Model. Simul. Mater. Sci. Eng.*, vol. 16, no. 6, 2008, doi: 10.1088/0965-0393/16/6/065009.

[61] M. Selezneva, K. Kouwonou, L. Lessard, and P. Hubert, "Mechanical properties of randomly oriented strand thermoplastic composites," *19th Int. Com. Compos. Mater.*, pp. 480–488, 2015, doi: 10.1177/0021998315613129.

[62] S. B. Visweswaraiah, M. Selezneva, L. Lessard, and P. Hubert, "Mechanical characterisation and modelling of randomly oriented strand architecture and their hybrids – A general review," 2018, doi: 10.1177/0731684418754360.

[63] D. DeWayne Howell and S. Fukumoto, "Compression molding of long chopped fiber thermoplastic composites," *Camx 2009*. 2009.

[64] D. Leblanc, B. Landry, M. Jancik, and P. Hubert, "Recyclability of randomly-oriented strand thermoplastic composites," *Iccm20*, no. July, pp. 19–24, 2015.

[65] M. I. A. Rasheed, B. Rietman, H. A. Visser, R. Akkerman, and F. W. J. Van Hattum, "Effect of overlap length on the mechanical properties of flake reinforced thermoplastic composites," *Camx 2015*, 2015.

[66] G. Vincent, V. Balakrishnan, T. A. de Bruijn, S. Wijskamp, and M. I. Abdul Rasheed, "Impregnation Quality of Shredded Semipreg after Compression Moulding," in *20th International ESAFORM Conference on Material Forming*, 2017.

[67] J. M. Henshaw, A. D. Owens, D. Q. Houston, I. T. Smith, and T. Cook, "Recycling of plastic thermoplastic composite material by injection and compression molding," *J. Thermoplast. Compos. Mater.*, vol. 7, no. 1, pp. 14–29, 1994.

[68] F. Henning, "Verfahrensentwicklung für lang- und endlosglasfaserverstärkte thermoplastische Sandwich- Bauteile mit geschlossenem Werkstoff-Kreislauf," PhD Thesis, Universität Stuttgart, 2001.

[69] M. Schemme, "LFT – development status and perspectives," *Reinf. Plast.*, vol. 52, no. 1, pp. 32–39, 2008, doi: 10.1016/S0034-3617(08)70036-5.

[70] E. Moritzer and G. Heiderich, "Mechanical recycling of continuous fiber- reinforced thermoplastic sheets Mechanical Recycling of Continuous Fiber-Reinforced Thermoplastic Sheets," in *AIP Conference Proceedings*, 2016, doi: 10.1063/1.4942328.

[71] Teijin, "New Thermoplastic Recycling Solution from Toho Tenax Europe," *Tokyo, Japan*. [Online]. Available: https://www.teijin.com/news/2017/ebd170307_03.html.

[72] F. Henning *et al.*, "LFTs for automotive applications," *Reinf. Plast.*, vol. 49, no. 2, pp. 24–33, 2005, doi: 10.1016/S0034-3617(05)00546-1.

[73] F. Van Hattum and S. Van Breugel, “LFT: The future of reinforced thermoplastics?,” *Reinf. Plast.*, vol. 45, no. 6, pp. 42–44, 2001, doi: 10.1016/S0034-3617(01)80208-3.

[74] A. Roch, T. Huber, F. Henning, and P. Elsner, “LFT foam - Lightweight potential for semi-structural components through the use of long-glass-fiber-reinforced thermoplastic foams,” *AIP Conf. Proc.*, vol. 1593, no. 2014, pp. 471–476, 2014, doi: 10.1063/1.4873824.

[75] M. Jauss, J. Schäfer, and F. Henning, “Neue Hochleistungsverbundwerkstoffe: Sandwichstrukturen mit Rezyklaten,” in *Strategien für die Produktion im 21. Jahrhundert*, 1997, pp. 14.1-14.9.

[76] A. Roch, T. Huber, F. Henning, and P. Elsner, “LFT foam - Lightweight potential for semi-structural components through the use of long-glass-fiber-reinforced thermoplastic foams,” vol. 471, no. 2014, pp. 471–476, 2014, doi: 10.1063/1.4873824.

[77] F. Henning, “Aufbereitung von glasfaserverstärkten Thermoplastsen-Rezyklateinsatz in hochwertigen thermoplastischen Bauteilen,” in *Strategien für die Produktion im 21. Jahrhundert*, 1997, pp. 38.1-38.7.

[78] H. Ning, N. Lu, A. A. Hassen, K. Chawla, M. Selim, and S. Pillay, “A review of Long fibre-reinforced thermoplastic or long fibre thermoplastic (LFT) composites,” vol. 6608, 2019, doi: 10.1080/09506608.2019.1585004.

[79] W. Krause, F. Henning, S. Tröster, O. Geiger, and P. Eyerer, “A Process Technologyfor Large Scale Productionof Fiber Reinforced Thermoplastic Components,” *J. Thermoplast. Compos. Mater.*, vol. 16, no. 4, pp. 289–302, 2003, doi: 10.1177/0892705703016004001.

[80] G. A. Vincent, “Recycling of thermoplastic composite laminates: The role of processing,” PhD Thesis, University of Twente, 2019.

[81] M. W. Biddulph, “Principles of recycling processes,” *Conserv. Recycl.*, vol. 1, pp. 31–54, 1976, doi: 10.1016/0361-3658(76)90005-9.

[82] J. Chu, J. L. Sullivan, and F. M. Co, “Recyclability of a Continuous E-Glass Fiber Reinforced Pol yca rbonate Corn posi te,” vol. 17, no. 4, 1996.

[83] G. Schinner, J. Brandt, and H. Richer, “Recycling Carbon-Fiber-Reinforced Thermoplastic Composites,” *J. Thermoplast. Compos. Mater.*, vol. 9, no. 3, pp. 239–245, 1996.

[84] E. Schmachtenberg and A. Helpenstein, “Recycling of natural- and glass-fiber reinforced thermoplastics,” in *Symposium and Exhibition International SAMPE*, 2004.

[85] M. Janney, J. Ledger, and U. Vaidya, “Long Fiber Thermoplastic Composites From Recycled Carbon Fiber,” in *44th ISTC*, 2012.

[86] M. Janney, U. Vaidya, R. Sutton, and H. Ning, “Re-Grind Study of PPS-Based Long Fiber Thermoplastic Composites,” in *SAMPE 2014*, 2014.

[87] U. K. Vaidya, K. B. Thattaiparthasarthy, S. Pillay, and H. Ning, “Automotive applications with cost-effective and recycled thermoplastic composites,” in *International SAMPE Technical Conference*, 2012.

[88] N. Eguémann, L. Giger, M. Roux, C. Dransfeld, F. Thiébaud, and D. Perreux, “Compression moulding of complex parts for the aerospace with discontinuous novel and recycled thermoplastic

composite materials," in *ICCM International Conferences on Composite Materials*, 2013, vol. 2013-July, pp. 6616–6626.

[89] Teijin Carbon, "Green innovations," 2016. [Online]. Available: https://www.teijincarbon.com/products/green-innovations?r=1.

[90] S. Black, "Thermoplastic composites 'clip' time, labor on small 233 but crucial parts," *Composites World*, 2015. [Online]. Available: https://www.compositesworld.com/articles/thermoplastic-composites-clip-time-labor-on-small-but-crucial-parts.

[91] R. Lahr and M. P. Päßler, "Workshop Recycling von CFK-Komponenten – Herausforderungen und Chancen," in *Workshop Recycling von CFK-Komponenten – Herausforderungen und Chancen*, 2016.

[92] J. Moothoo, C. Garnier, P. Ouagne, and C. Moulding, "Production Waste Management of Thermoplastic Composites Using Compression Moulding," no. August, pp. 20–25, 2017.

[93] T. A. De Bruijn, G. Vincent, and F. W. J. Van Hattum, "Recycling C/PPS laminates into long fibre thermoplastic composites by low shear mixing," in *ICCM International Conferences on Composite Materials*, 2017, vol. 2017-Augus.

[94] T. A. de Bruijn, G. A. Vincent, J. Meuzelaar, J. P. Nunes, and F. W. J. van Hattum, "Design, manufacturing and testing of a rotorcraft access panel door from recycled carbon fiber reinforced polyphenylenesulfide," in *SAMPE America 2019*, 2019.

[95] Cetim, "INDUSTRIE DURABLE," *Thermosaïc ®*. [Online]. Available: https://www.cetimgrandest.fr/industrie-durable/.

[96] Toray Advanced Composites, "Cetex ® Recycling Thermoplastic Composites," 2019. [Online]. Available: https://www.toraytac.com/media/e0c5c4b6-10bc-4aee-9649-5f94bd793504/mYFcJA/TAC/Documents/White Papers/Toray_Cetex_Recycling_Thermoplastic_Composites_White_Paper.pdf. [Accessed: 18-Jun-2020].

[97] H. Li and K. Englund, "Recycling of carbon fiber-reinforced thermoplastic composite wastes from the aerospace industry," *J. Compos. Mater.*, vol. 51, no. 9, pp. 1265–1273, 2017, doi: 10.1177/0021998316671796.

[98] G. Vincent, V. Balakrishnan, T. A. De Bruijn, S. Wijskamp, and M. I. Abdul Rasheed, "Impregnation quality of shredded semipreg after compression moulding," in *AIP Conference Proceedings*, 2017, vol. 1896, doi: 10.1063/1.5008006.

[99] R. J. Tapper, M. L. Longana, H. Yu, I. Hamerton, and K. D. Potter, "Development of a closed-loop recycling process for discontinuous carbon fibre polypropylene composites," *Compos. Part B Eng.*, vol. 146, no. June, pp. 222–231, 2018, doi: 10.1016/j.compositesb.2018.03.048.

[100] C. Aguilar, "RESET: Re-use of thermoplastic composite," *LEITAT Technology Center*, 2018. .

[101] Axyal, "Manufacturing of sheets and handles with pps recycled materials by thermostamping/thermoforming, RESET: Re-use of thermoplastic composite," 2018. [Online]. Available: https://projects.leitat.org/wp-content/uploads/2018/03/Présentation-RESET-23-03-2018-4.pdf. [Accessed: 01-May-2019].

[102] B. Liu, P. Zhu, A. Xu, and L. Bao, "Investigation of the recycling of continuous fiber-reinforced thermoplastics," *Thermoplast. Compos. Mater.*, pp. 3–15, 2018, doi: 10.1177/0892705718759388.

[103] D. S. Cousins, Y. Suzuki, R. E. Murray, J. R. Samaniuk, and P. Stebner, "Recycling glass fiber thermoplastic composites from wind turbine blades," *J. Clean. Prod.*, 2018, doi: 10.1016/j.jclepro.2018.10.286.

[104] P. Malnati, "Zero-waste: New process, equipment recycles prepreg, tape offal," *CompositesWorld*, 2019. [Online]. Available: https://www.compositesworld.com/articles/zero-waste-new-process-equipment-recycles-prepreg-tape-offal. [Accessed: 18-Jun-2020].

[105] A. Beukers, J. H. van Breugel, and F. J. Wiltink, "Device and method for the preparation of a mixture comprising of fibre-reinforced thermoplastic pellets. International Patent no. WO 00/02718; 2000."

[106] AZDEL Inc. Thermoplastic Composites, "Azdel Thermoplastic composites design and processing handbook," 1993.

[107] F. W. J. Van Hattum, J. P. Nunes, and C. a. Bernardo, "A theoretical and experimental study of new towpreg-based long fibre thermoplastic composites," *Compos. Part A Appl. Sci. Manuf.*, vol. 36, pp. 25–32, 2005, doi: 10.1016/j.compositesa.2004.06.031.

[108] U. T. Vaidya Kb; Pillay, Sb; Ning, H; Grow, Dt;, "Recycled long fiber thermoplastic composites for transportation applications," *SAMPE 2010 Conf. Exhib. "New Mater. Process. a New Econ.*, pp. 2–8, 2010.

[109] U. Vaidya, "Long Fiber Thermoplastics for Aerospace Applications," in *Conference CAMX 2015*.

[110] W. Krause, F. Henning, S. Tröster, O. Geiger, and P. Eyerer, "LFT-D – A Process Technology for Large Scale Production of Fiber Reinforced," *Thermoplast. Compos. Mater.*, vol. 16, no. July 2003, 2003, doi: 10.1177/089270503027645.

[111] N. Hulings, "From scrap to hatch : Recycled carbon fiber flies on ecoDemonstrator," *Our Environment, Boeing*, Dec-2014.

[112] S. Black, "Redesigning for simplicity and economy," *CompositesWorld*, Jan-2012.

[113] "Clean SKY WORKSHOP : Succesful projects for innovation and environment . RESET : Re-use of thermoplastic composite," no. March, 2018.

[114] G. Gardiner, "Recycled thermoplastic composites for production," *CompositesWorld*, 2019. [Online]. Available: https://www.compositesworld.com/articles/recycled-thermoplastic-composites-for-production.

[115] R. A. Witik, J. Payet, V. Michaud, C. Ludwig, and J. A. E. Månson, "Assessing the life cycle costs and environmental performance of lightweight materials in automobile applications," *Compos. Part A Appl. Sci. Manuf.*, vol. 42, no. 11, pp. 1694–1709, 2011, doi: 10.1016/j.compositesa.2011.07.024.

[116] Granta design Limited, "CES Edupack 2019 version 19.2.0." Cambridge, 2019.

[117] Swiss Centre for Life Cycle Inventories, "Ecoinvent v2.2 LCI data," 2012.

[118] Delft University of Technology, “Idemat 2010,” 2010.

[119] C. L. Simões, M. Vasconcelos, J. P. Nunes, and C. A. Bernardo, “Using a glass-fibre reinforced polymer composite in the production of sustainable water storage tanks,” *Int. J. Mater. Prod. Technol.*, vol. 52, no. 1/2, p. 162, 2016, doi: 10.1504/IJMPT.2016.073628.

[120] S. Das, “Life cycle assessment of carbon fiber-reinforced polymer composites,” *Int. J. Life Cycle Assess.*, vol. 16, no. 3, pp. 268–282, 2011, doi: 10.1007/s11367-011-0264-z.

[121] V. Khanna and B. R. Bakshi, “Carbon nanofiber polymer composites: Evaluation of life cycle energy use,” *Environ. Sci. Technol.*, vol. 43, no. 6, pp. 2078–2084, 2009, doi: 10.1021/es802101x.

[122] Y. S. Song, J. R. Youn, and T. G. Gutowski, “Life cycle energy analysis of fiber-reinforced composites,” *Compos. Part A Appl. Sci. Manuf.*, vol. 40, no. 8, pp. 1257–1265, 2009, doi: 10.1016/j.compositesa.2009.05.020.

[123] J. R. Duflou, J. De Moor, I. Verpoest, and W. Dewulf, “Environmental impact analysis of composite use in car manufacturing,” *CIRP Ann. - Manuf. Technol.*, vol. 58, pp. 9–12, 2009, doi: 10.1016/j.cirp.2009.03.077.

[124] S. Pimenta, S. T. Pinho, and P. Robinson, “Micromechanics of Recycled Composites for Material Optimisation and Eco-Design,” *18th Int. Com. Compos. Mater.*, pp. 1–6, 2011.

[125] Y. Liu, M. Farnsworth, and A. Tiwari, “A review of optimisation techniques used in the composite recycling area: State-of-the-art and steps towards a research agenda,” *J. Clean. Prod.*, vol. 140, pp. 1775–1781, 2017, doi: 10.1016/j.jclepro.2016.08.038.

3 Degree of mixing in micromechanical modelling

3.1 Introduction

In the Introduction and the state-of-the-art (Chapters 1 and 2), the background, motivation and the current level of development for TPC recycling was described. An important part of the goal of the thesis is to gain a better understanding of the possibilities of continuous fibre TPC recycling in order to find the optimum process for TPC waste leading to maximum performance. To obtain the optimum mechanical properties for waste material, the trade-off between long fibre length and homogeneous material needs to be studied.

Various analytical micromechanical models exist as is outlined in the state-of-the-art (Section 2.1). These models include fibre volume, fibre length and fibre orientation. The complex fibre structure of waste, the long fibres and the low level of shear during processing may however lead to non-homogenised composite materials and so, extension of these models is necessary to include the degree of mixing. The objective of this study is to include not only the influence of fibre length, fibre content and fibre orientation, but also consider the degree of mixing by implementing the effect of fibre dispersion and distribution on the mechanical performance. For the fibre dispersion and fibre distribution a BSD and FVD are considered, respectively. Since the waste material consist of flakes with a FLD, this was also included in the study. Various theoretical distributions, including upper and lower limits, are made for the FLD, BSD and FVD to study a broad range of potential solutions. Also, experimental data was available from Vincent et. al. that enabled to model the stiffness and strength with realistic FLD, BSD and FVD.

With the results from the models using the theoretical and realistic distributions, an experimental recycling route is developed aimed at the requirements in the research question (Chapter 4).

3.2 Method and materials

3.2.1 *Modelling method and properties*

Micromechanical modelling was used to predict stiffness and strength for the recycled thermoplastic composites used in this study. The Tandon-Weng [10] model was applied for stiffness and the Kelly-Tyson model for strength. Both were introduced in Section 2.1.1 and 2.1.2 respectively. As mentioned in Section 2.1, ideal elastic conditions were assumed, e.g. possible effects of fibre-matrix debonding, interfacial slip or matrix micro-cracking are not included. For the interested reader, detailed information on the used models can be found in [11, 12]. Additionally, a simple Modified Rule of Mixtures (M-ROM) is used for comparison. The method is modified to adapt for random in-plane fibre orientation by adding an orientation factor of (3/8) for the term accounting for the influence of fibres [13].

3.2.2 *Fibre orientation*

Three fibre orientation distributions were included in the study to show the influence of fibre orientation. Firstly, a UD fibre orientation with all fibres aligned is used. This orientation is often the starting point of any theoretical study and can practically be obtained when an alignment method is used [14], but it is not feasible in flow-dominated moulding processes in which fibres directions are changed by the flow itself. Secondly, a highly orientated fibre orientation, that can be found in slender parts with a large effect of fibre alignment due to the occurring flow in such processes [15], serves as an upper bound. Finally, a two-dimensional (2D) random orientation is studied to show the lower bound of orientation. Strong out-of-plane orientation is not often seen for components with thin reasonably thicknesses and is therefore not included. The three types of fibre orientation (see Section 2.1.4 for more information), corresponding components of the fibre orientation tensor and closure approximation used, are given in Table 3.1.

Table 3.1 - Orientation tensor components and closure approximation for the three selected fibre orientation states.

	Second order orientation tensor components						**Closure approximation**
	a_{11}	a_{12}	a_{13}	a_{22}	a_{23}	a_{33}	
Unidirectional	1	0	0	0	0	0	Quadratic [16]
Highly oriented	0.8	0	0	0.19	0	0.01	Fitted Cintra-Tucker [17]
2D random	0.5	0	0	0.49	0	0.01	Fitted Cintra-Tucker [17]

Since processing LFT material with limited flow typically exhibit a fibre orientation that closely resembles a random 2D fibre orientation (2D random), a method is required to predict the properties for this

orientation. The 'orientation averaging method' presented by Advani and Tucker [18] is used to account for the effect of fibre orientation. For the highly oriented and 2D random orientation a orthotropic fitted closure approximation, introduced by Cintra-Tucker [17] (see Section 2.1.4 for more information), is applied to allow calculating the fourth-order orientation tensors

3.2.3 *Material system*

A carbon fibre reinforced PPS (C/PPS) is the principal material system used throughout this study. It is occasionally compared to a glass fibre reinforced PP (G/PP). The constituent material properties of both material systems used for modelling are given in Table 3.2.

Experimental data of the Toray Cetex® TC1100 5HS C/PPS waste material is used as reference, see Figure 3.1 (left). The fabric is woven with 3K yarns. This material was collected at the manufacturing site and is a 3 mm thick consolidated laminate in a quasi-isotropic (QI) layup, containing a 50% FVF. The waste was shredded in-house using an Untha S20 low-speed two-shaft shredder with blades of 19 mm in width and no screen, for five consecutive times. The resulting flakes are shown in Figure 3.1 (right). A portion of the flakes was sieved with a multi-stage vibrating sieve with apertures of 2, 2.8, 4, 5.6, 8, 11.2, 16, 22.4 and 31.5 mm. Three batches were obtained: the batch denominated 'Sieved L' consists of flakes passing through the sieve with an aperture of 22.4 mm and rest on the sieve with 16 mm aperture. The batch denominated 'Sieved M', are flakes resting between the 11.2 mm and 8 mm aperture sieves and 'Sieved S' indicates a blend of flakes between the 5.6 mm and 2.8 mm aperture sieves. Finally, the flakes are diluted in the mixing process to lower the FVF with virgin PPS pellets of Celanese Fortron® 0214, which is the exact same polymer type as in the C/PPS composite flakes.

More information on the shredding and sieving of this material is available in the studies carried out by Vincent et al. [19, 20].

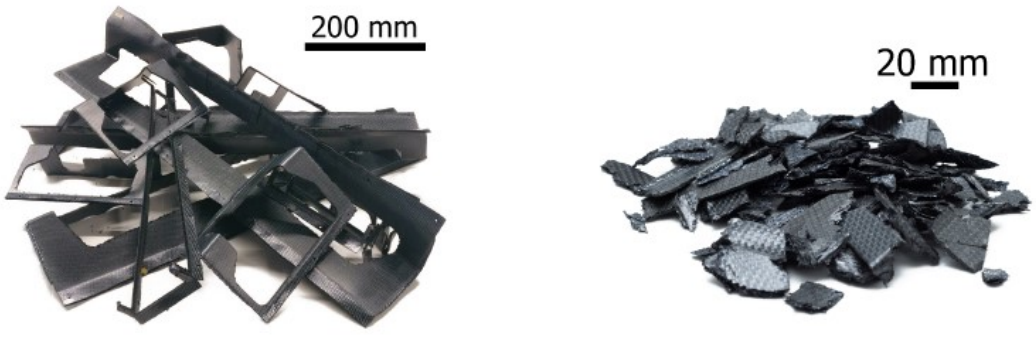

Figure 3.1 - Consolidated C/PPS waste material collected at manufacturing sites (left) and after shredding (right)

Table 3.2 - Material data used in the modelling

Property	Glass fibres	PP	Carbon fibres**	PPS***
Density (g/cm³)	2.56	0.91	1.76	1.35
Tensile Modulus (GPa)	70	1.3	230	3.8
Poison ratio	0.28	0.4	.28	0.36
Tensile strength (MPa)	3450	30	3530	90.3
Tensile strength at fibre failure*	-	30	-	57
Fibre diameter (µm)	15	-	7	-

* Calculated from fibre failure strain and matrix modulus for a G/PP and C/PPS combination
**Toray Carbon T300 Fibers America, Inc, "Torayca data sheet" CFA-001
***Celanese Fortron® 0214 datasheet

3.2.4 *Mixing process*

Experimental data on the mixing of recycled materials are used in this study. The considered recycling route consists of a low-shear mixing setup [7]. The mixing setup uses rotating bars (see Section 2.2.6) and is designed to reduce fibre friction by limiting the maximum shear level. Therefore, the degree of mixing is lower compared to extruder-based mixing setups, such as injection moulding. Realistic FVD and BSD data were obtained from a study by Vincent et al. [21]. Material was diluted to 20% FVF by adding virgin PPS pellets. The well- and poorly mixed materials were produced at a mixing time of 20 min and 10 min with a rotational speed of 15 rpm and 5 rpm, respectively. For both, the filling fraction (representing the ratio of air and material in the mixing cylinder) was 50% and the temperature was 360°C. These data are for mixed doughs before compression moulding.

No fibre attrition or impact on the mixing quality is assumed during compression moulding. This assumption is supported by Vincent et al. [22] who showed that no attrition was visible for the G/PP and it was very limited for the C/PPS, mostly during the compression moulding step. The mixing process therefore has only very limited influence on the FLD. The material was analysed as detailed in Section 2.1.6.

3.2.5 *Fibre length distribution*

In addition to using a constant fibre length, fibres in recycled TPC waste material were characterised by a fibre length distribution (FLD). Besides a range of fixed fibre lengths, several distributions were selected to study the influence of such a distribution. The FLD of the shredded material described in the previous section was characterised by Vincent et al. [19, 20], who used images of flakes to develop an image processing tool to obtain the FLD.

The FLD of non-sieved and Sieved S, M and L flakes are presented in Figure 3.2. To compare the results with a FLD of a material that is processed with fibre breakage a LFT pellet material processed by injection moulding (IM) from a study by Nguyen et al. [23] was included. The FLD is built by using a log-normal function, which captures the FLD well according to Nguyen, with fitting parameters m = −0.1967, s = 0.7977 and referred to as IM. The material contains a FVF of 19.2% and a nominal fibre length before processing of 13 mm. The distributions are discrete with a step size of 2 mm for the shredded material and 0.1 mm for the IM material.

It can be observed in Eq.5 that the fibre diameter is always present in combination with the fibre length, as part of the aspect ratio L/d. Assuming no correlation between the FLD and BSD, the distributions can be merged into an aspect ratio distribution.

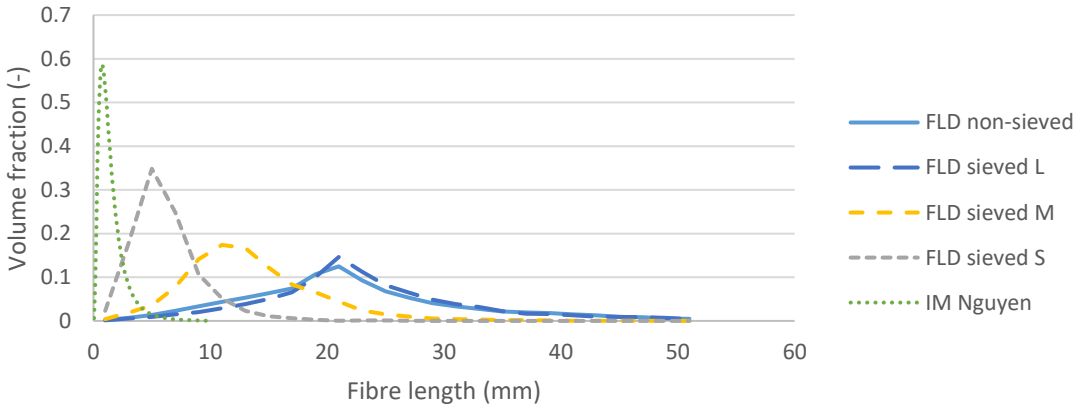

Figure 3.2 - Fibre length distributions of shredded material, one not sieved and three sieved material batches from Vincent et al. [20] **A fibre length distribution of material processed by injection moulding (IM) and characterised by Nguyen et al. is added** [23]**.**

3.2.6 *Bundle size distributions*

The influence of bundles is modelled by substituting the fibre diameter (d) by the bundle diameter (D) obtained from BSD as it may be seen in Figure 3.3. A square packing is assumed for the fibres in the

bundle leading to a fibre volume content of 78.5% in the bundle. Theoretically a maximum of 90.7% FVF can be obtained for a hexagonal fibre packing configuration [24]. This is however not considered realistic for bundles in the considered material. Figure 3.4 shows the bundle diameter for bundles of glass and carbon fibres expressed in µm and number of single fibres.

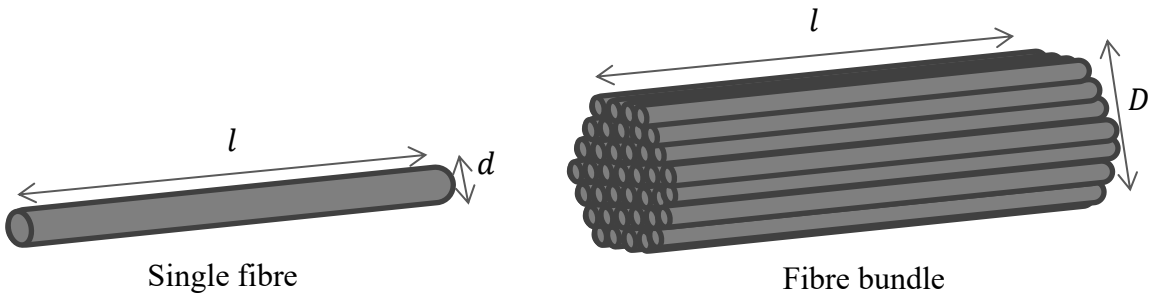

Figure 3.3 - A single fibre and fibre bundle with considered variables

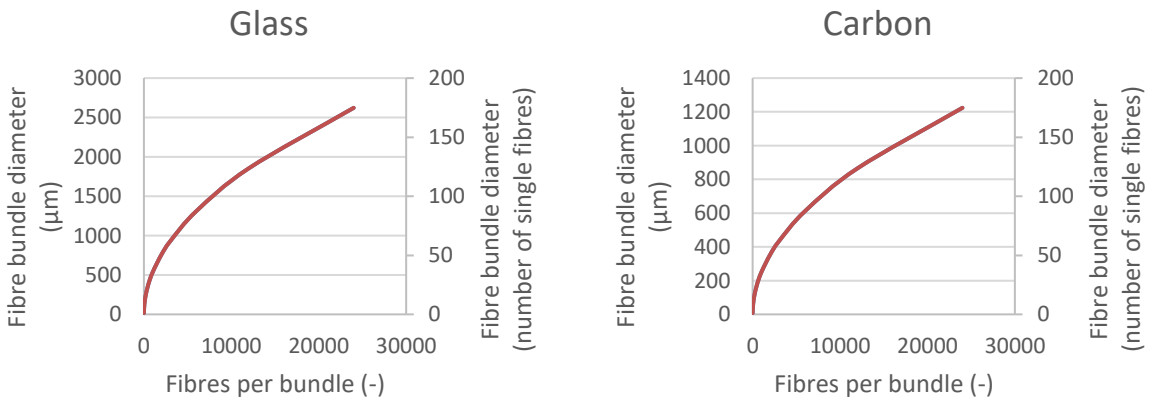

Figure 3.4 - Bundle diameter for bundles of glass (left) and carbon (right) fibres expressed in size and number of single fibres

The five different fibre-bundle distributions considered are presented in Figure 3.5. A constant fibre length of 10 mm was assumed for all distributions. Perfectly dispersed bundles, consisting of one fibre per bundle, used as default. A flat distribution consists with an equal volume fraction of bundles at every step. Two non-dispersed bundles were included to study the performance of non-mixed bundles. Firstly, a bundle of 3K fibres is involved because the considered waste material consists of such bundles. Secondly, a more cost-effective tow of 12K fibre is included. A Realistic 'good mix' (GM) and 'poor mix' (PM) material are considered, refereeing to a material mixed at mixing settings related to a good degree of mixing and to a poor degree of mixing respectively. For these PM and GM material, BSDs were obtained from a study by Vincent et al. [21] and corresponds to the Tests number 8 and 5, respectively, in Table 1 of his study.

Looking at Figure 3.5, the majority of the bundles in the GM distribution is dispersed to bundles of only a few fibres and contains only a limited fraction of non-dispersed bundles. The PM BSD still features a large fraction of small bundles, but also a substantial fraction of non- or poorly-dispersed bundles.

In order to take into account, the predominantly small to large bundle size in the model, the following BSDs were considered:

- A fully dispersed distribution of only single fibres
- A realistic bundle size distribution for 'good mix' (GM) material
- A realistic bundle size distribution for 'poor mix' (PM) material
- A flat distribution with an equal volume fraction of bundles at every step
- Non dispersed bundles of 3K fibres
- Non dispersed bundles of 12K fibres

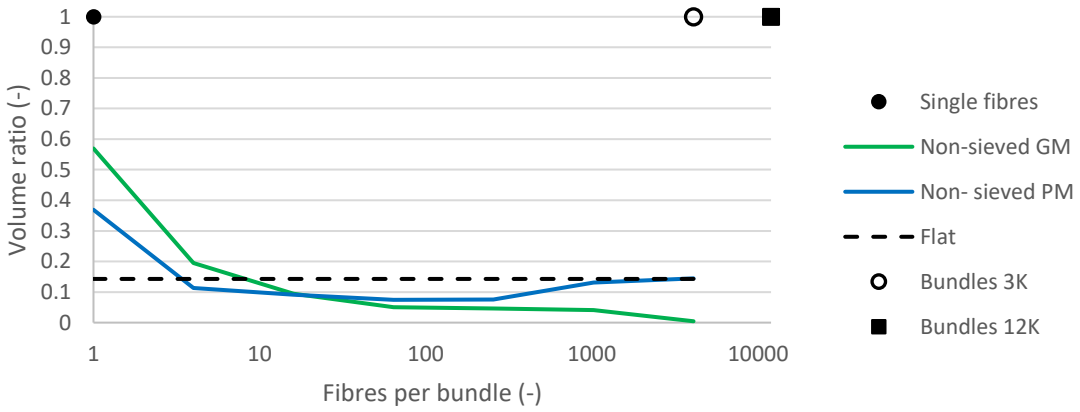

Figure 3.5 - The considered bundle size distributions

Experimental BSD data of sieved materials from Vincent et al. was used to study the influence of the FLD on the BSD and the influence of a combined fibre length and bundle size distribution (FLBSD) on the stiffness and strength. The data is presented in Figure 3.6 and covers the same sieved batches as considered in Section 3.2.5 for FLD.

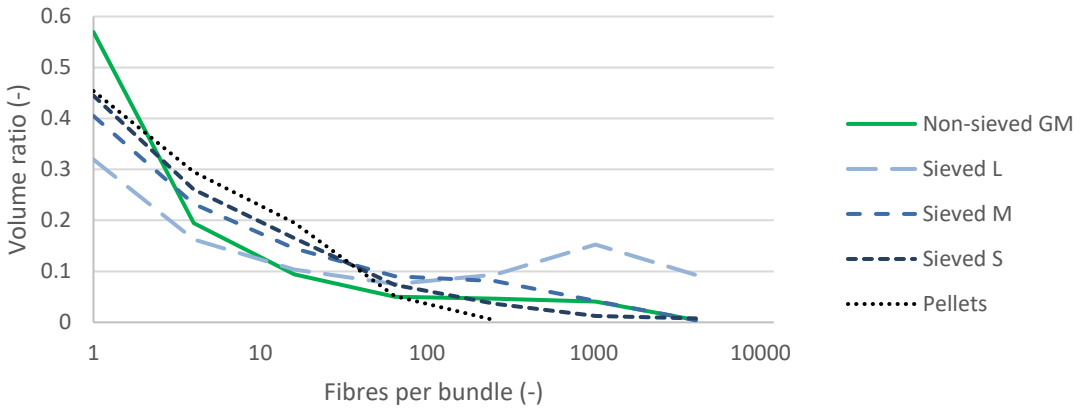

Figure 3.6 - Experimental data of Bundle size distributions for shredded flakes, three types of sieved shredded flakes and LFT pellets

3.2.7 *Fibre volume distribution*

Six different FVDs were considered to cover the complete range of FVDs that could exist in theory and practice. All six have an average FVF of 20% and are shown in Figure 3.7. Four are from a theoretical and two from an experimental origin. A fixed FVF value represents a FVD with no variation. A minimal variation FVD (min) is formed by two data points. The two experiment-based FLDs represent a GM and PM and exhibit a higher variation. These datasets were taken from a study of Vincent et al. [21], which correspond to test number 8 and 5 of the cited study and are of the same samples as considered in the BSDs, Section 3.2.6.

The experimental values were normalised to have an average of exactly 20% FVF. A flat distribution was added with larger variation than previous introduced FVDs. This theoretical distribution consisted of the same volume of length of every bundle size. The final FVD consisted of the maximum variation possible when the same quantity of resin rich and fibre rich material is considered, one half of the volume corresponds to a FVF of 2.5% and the other is 37.5%. The theoretical FVDs were described with a step size of 5%. Since the experimental FLDs are more complex, a step size of 2% was chosen.

In order to take into account the small to large variation of FVD in the model, the following FVDs were considered:

- A fixed value
- A distribution with minimal variation
- A realistic distribution for ‘good mix’ (GM) material
- A realistic distribution for ‘poor mix’ (PM) material
- A flat distribution, with an equal fibre content over the total range
- A distribution with maximal variation

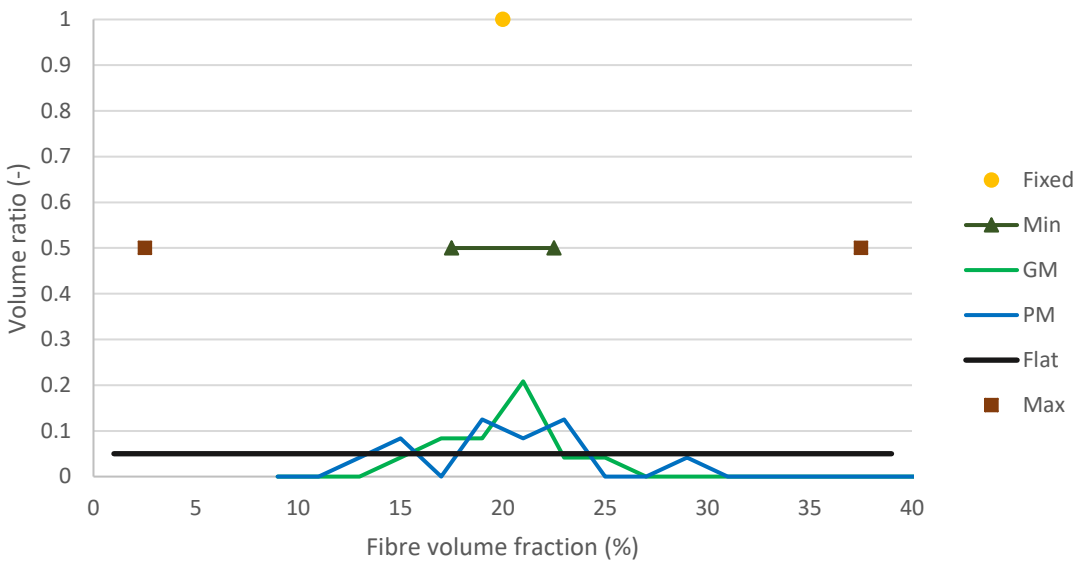

Figure 3.7 – The considered fibre volume distributions

3.2.8 *Combined FLD and BSD*

A new distribution was constructed to study the influence of a combined fibre length and bundle size distribution (FLBSD). No correlation between fibre bundles and fibre length was assumed for the uncoupled combination. The uncoupled FLBSD was made by computing a weighted average of the BSD at every individual FLD step. Five uncoupled distributions were plotted in terms of aspect ratio in Figure 3.8. In this graph, the FLD for non-sieved material and BSD for the GM and PM are taken from Sections 3.2.5 and 3.2.6 Combining the distribution of fibre length with the two bundle diameter distributions results in a shift to lower aspect ratios, especially for the PM material.

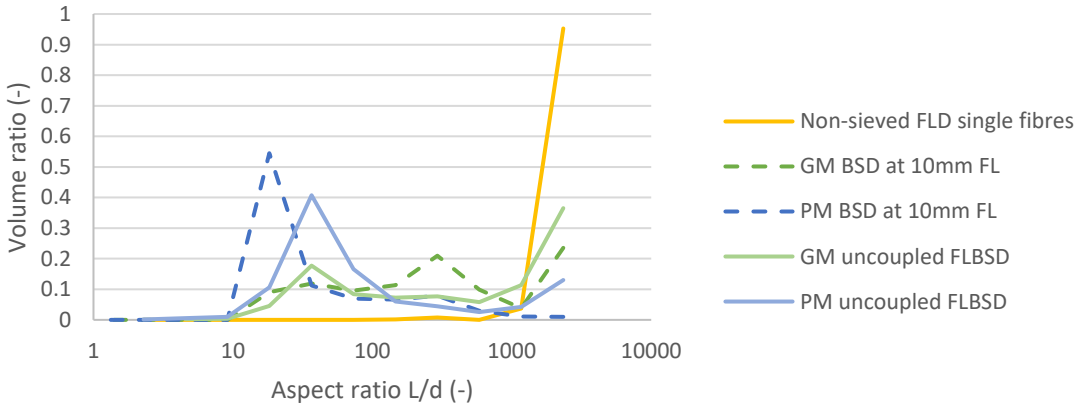

Figure 3.8 – Comparing FLD, BSD and combined uncoupled FLBSD of a GM and PM material

Coupled and uncoupled FLD and BSD combination

A second, coupled, type of FLBSD, can be made from the combination of FLD and BSD. Data on the BSD of sieved materials indicate that shorter fibres are more easily disentangled and therefore it is likely that shorter fibres in the FLD relate to the smaller fibre bundles. Subsequently, a higher fibre length correlates to larger fibre bundles. Hence, the coupled FLBSD was constructed by allocating the short fibres of the FLD to the small fibre bundles of the BSD for the same material. This automatically leads to an allocation of the long fibres in the FLD to the large fibre bundles in the BSD. The result is a narrower distribution of aspect ratios in comparison to an uncoupled FLBSD (see Figure 3.9).

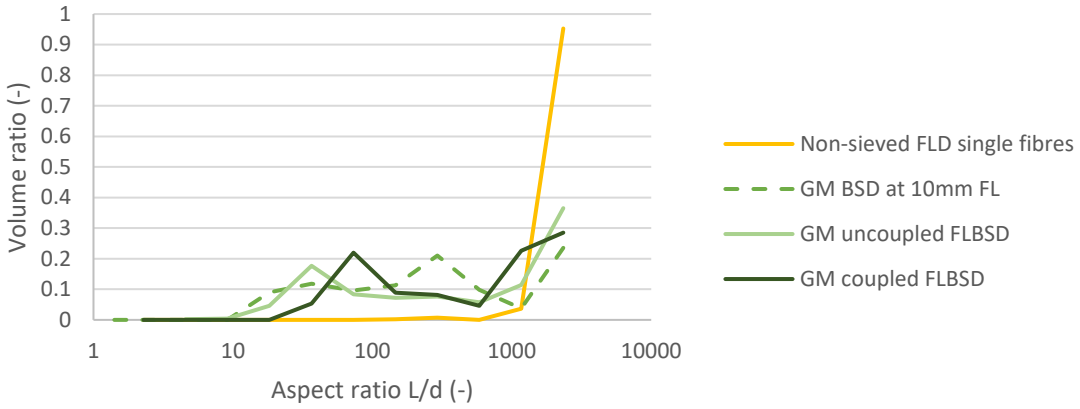

Figure 3.9 - Comparison of the FLD, BSD and coupled and uncoupled FLBSD of a GM

3.2.9 *Searching for the optimal distribution*

To find the best option in the trade-off between the fibre length distribution and the degree of mixing, four types of shredded C/PPS material were compared and benchmarked to virgin LFT pellets. The materials were processed in the same setup and at almost the same settings as the GM material described in Section 3.2.4. Only the mixing speed was slightly lower for the sieved materials, using 10 rpm instead of 15 rpm. The four types differ in FLD and therefore the mixing is influenced, as can be seen in the BSD (see Section 3.2.5 and 3.2.6). The uncoupled FLBSDs are given in Figure 3.10. The distributions of the materials are very different considering the FLD (see Figure 3.2) and BSD (see Figure 3.6) separately, because the combined FLBSD seem to level out these differences as it is depicted in Figure 3.10.

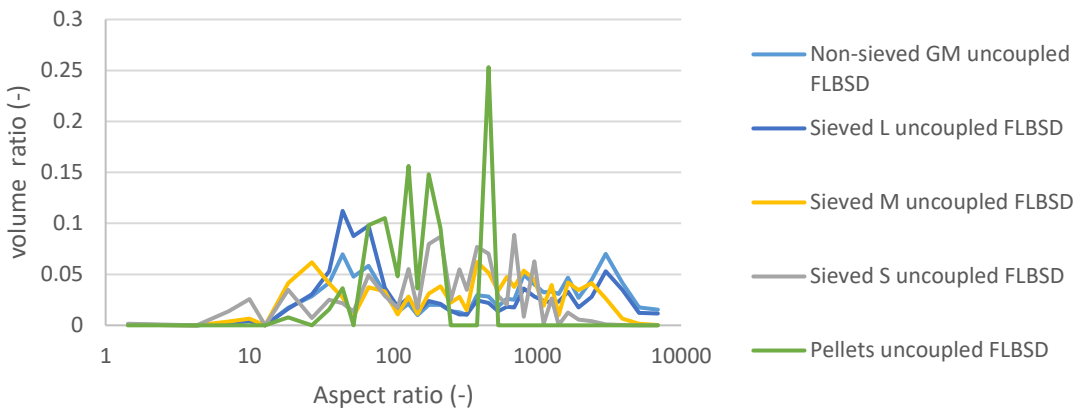

Figure 3.10 - Volume at aspect ratio for FLD, BSD and uncoupled combined FLBSD

3.2.10 *Overview of distributions*

An overview of all FLDs, BSDs, FVDs, coupled FLBSDs and uncoupled FLBSD used in this study is given in Table 3.3.

Table 3.3 - Overview of all distributions used in this study

	FLD	**BSD**	**FVD**	**Uncoupled FLBSD**	**Coupled FLBSD**
See Section	3.2.5	3.2.6	3.2.7	3.2.8+3.2.9	3.2.8
Theoretical					
Fixed / single fibre		X	X		
Min			X		
Flat		X	X		
Max (3K)		X	X		
Max (12K)		X			
Experimental					
GM (Non-sieved)	X	X	X	X	X
PM (Non-sieved)	X	X	X	X	
Sieved L	X	X		X	
Sieved M	X	X		X	
Sieved S	X	X		X	X
Pellets	X	X		X	
IM Nguyen	X				

3.3 Results of constant fibre length, volume and orientation

The described theories of Section 2.1 and 3.2 were used in combination with the data from Section 3.2. Before the distributions can be considered, the influence of various constant fibre lengths and fibre volume fractions on composite properties are modelled first as a benchmark. Additionally, the influence of fibre orientation was taken into account.

3.3.1 *Influence of fibre length and aspect ratio*

The strengths and stiffnesses are computed from the Mori-Tanaka and Kelly-Tyson models, as explained in Sections 2.1.1 and 2.1.2. The results are plotted for a range of 0% to 50% FVF in Figure 3.11. The mechanical properties are normalised to the ROM for continuous fibres as given by Equations 1 and 2, while neglecting the orientation and length factor. Unless otherwise stated a C/PPS UD material is considered. However, the results are expressed in terms of the aspect ratio to be more generally applicable.

The critical fibre length for C/PPS was computed using Eq 1. and was found to be 238 μm or an aspect ratio of 34.

The ROM serves as an upper limit since the properties corresponding to discontinuous fibres cannot outperform continuous fibres. For high aspect ratios the predicted properties for discontinuous fibres approach those ones predicted by the ROM for continuous fibres (see Figure 3.11 for aspect ratio >100). Notably, the moduli show values closer to the ROM for lower fibre aspect ratios compared to the values for strength. For the modulus, the values for discontinuous fibres are at 95% and 99% of the ROM values at an aspect ratio of 100 and 250 respectively. For the strength 95% and 99% are reached for an aspect ratio of 300 and 1700. At lower aspect ratios the normalised properties are significantly lower, a modulus of 50% and strength of 30% for a fibre aspect ratio of 15. At the critical fibre length of 34 aspect ratio the strength is close to 50% as is expected from the theory described in Section 2.1.2.

At a lower aspect ratio, the effect of fibre contents on the normalised modulus and strength property is visible.

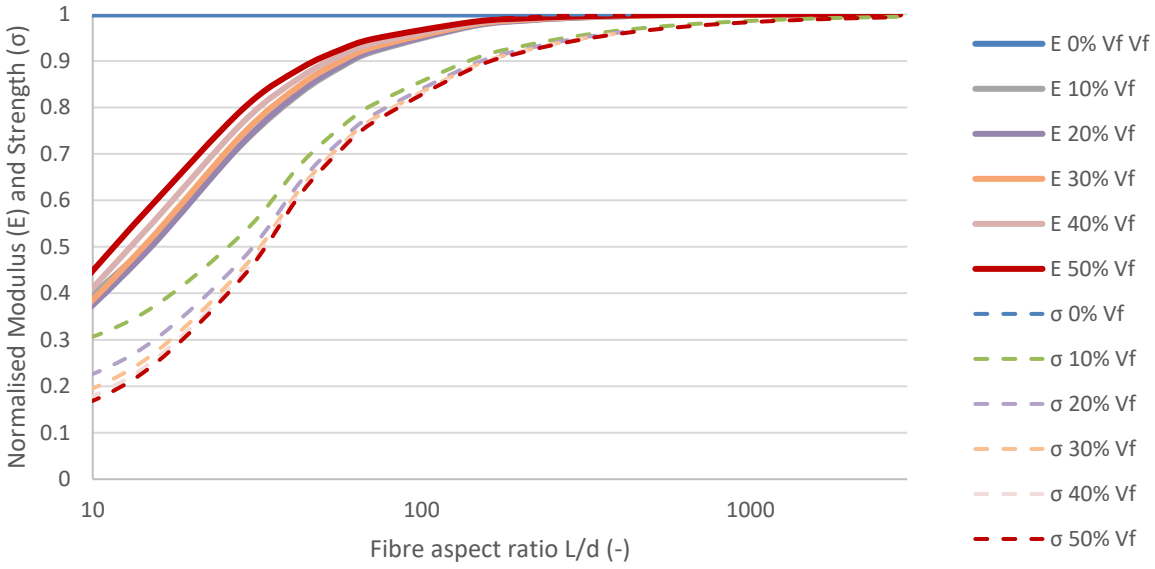

Figure 3.11 – Influence of the aspect ratio on the modulus and strength predictions for discontinuous fibres normalised to a prediction by ROM for continuous fibres. Plotted for multiple fibre contents. All for UD fibre orientation and C/PPS material system.

In Figure 3.12, the influence of fibre length on the modulus and strength is given for an UD fibre orientation and various fibre contents. The material is a C/PPS with 7 µm fibre diameter. Also, here the non-linear dependency on the length for both modulus and strength can be observed. The modulus levels become almost constant for fibre lengths between 200 and 2000 µm. For the strength there is first a large increase till a length of 300 µm, beyond this length the properties increase moderately until a length of several thousand µm for which no significant increase can be found. The non-linear relation indicates that applying an averaging method leads to improved predictions.

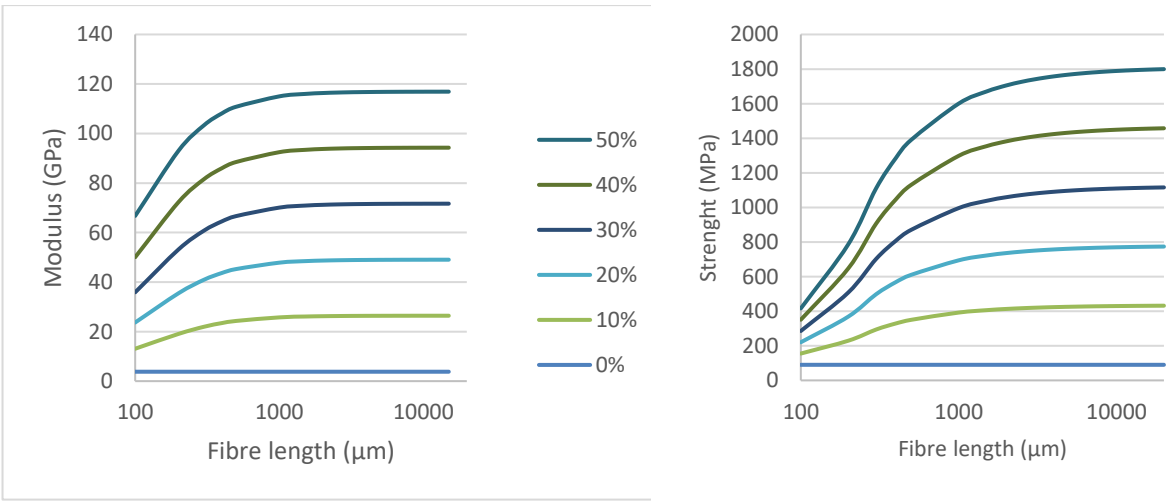

Figure 3.12 - Influence of fibre length on modulus (left) and strength (right) for UD C/PPS, plotted for various fibres contents.

3.3.2 *Influence of fibre content*

Modulus and strength predictions for discontinuous fibres were normalised to predictions by ROM for continuous fibres and are presented in Figure 3.13. As can be seen from the figure, the influence of the fibre content on the difference between discontinuous and continuous fibres is small, except for fibre aspect ratios below 20. For the modulus, an increasing fibre content results in higher normalised properties, while for strength this effect is contrarily. With the exception of non-reinforced polymer, which shows the exact same value as the ROM.

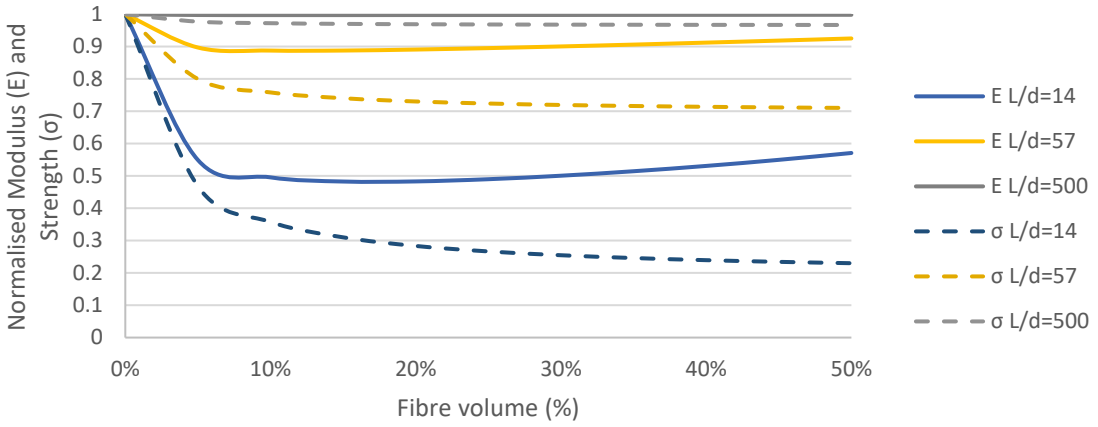

Figure 3.13 – Influence of the fibre volume on the modulus and strength predictions for discontinuous fibres normalised to a prediction by ROM for continuous fibres. Plotted for multiple fibre aspect ratios. All for UD fibre orientation and C/PPS material system.

In Figure 3.14, the influence of fibre length on the modulus and strength is depicted for a UD fibre orientation and various fibre contents. A linear effect between the fibre content and both modulus and strength can be observed, except for small fibre lengths of about 100 µm, where a slight non-linearity is observed.

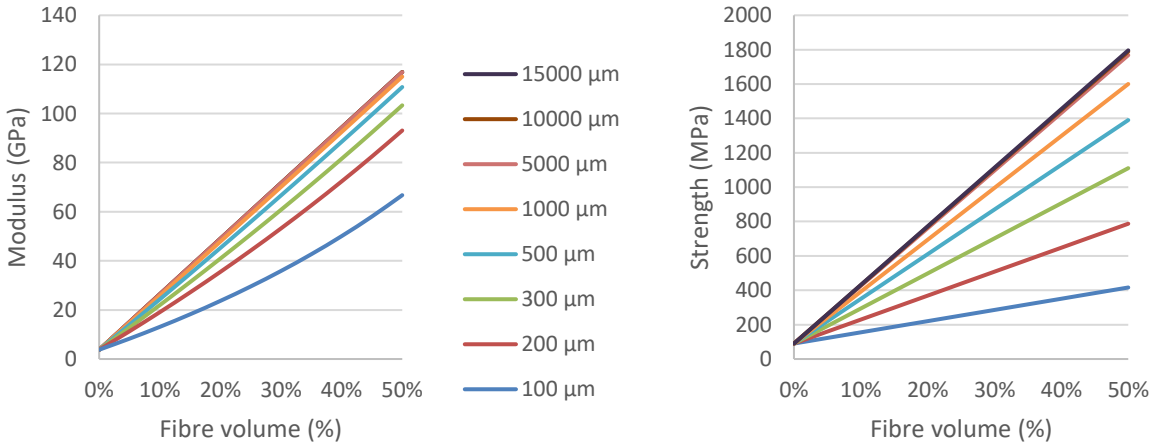

Figure 3.14 - Influence of fibre content on modulus (left) and strength (right) for UD C/PPS, plotted for various fibres lengths.

3.3.3 *Influence of fibre orientation*

Three different fibre orientation states were compared to study the influence of this variable. Besides the UD orientation which was used until now, a highly oriented and a 2D random orientation were compared.

The strengths and stiffnesses are computed from the Mori-Tanaka and Kelly-Tyson models, as explained in Sections 2.1.1 and 2.1.2 accounting for 2D random orientation as described in Section 3.2.2. These predicted stiffness and strength of discontinuous fibres over fibre length for 2D random fibre orientation are normalised to the ROM for continuous fibres and plotted in Figure 3.15, which is very similar to one obtained for the UD fibre orientation in Figure 3.11. However, for this fibre orientation, the ROM is enhanced with an fibre orientation factor of Krenchel ($\eta_o = 3/8$) to better extend the prevision to take into account 2D orientation, as is described in Equations 1 and 2 in Sections 2.1.1 and 2.1.2. The length factor in the ROM is neglected.

Results of the continuous fibre ROM outperforms the discontinuous fibres (Figure 3.15) as is also the case for UD fibre orientation (Figure 3.11). Normalised properties of a 2D random orientation show different results compared to a UD orientation. The increase of strength and stiffness with fibre length is less steep for the 2D random orientation (Figure 3.15) compared to the UD orientation (Figure 3.11). This results in a longer fibre aspect ratio to obtain 95% of the continuous fibre properties. Especially, strength properties at higher fibre contents do not approach the same values as UD oriented or continuous fibres.

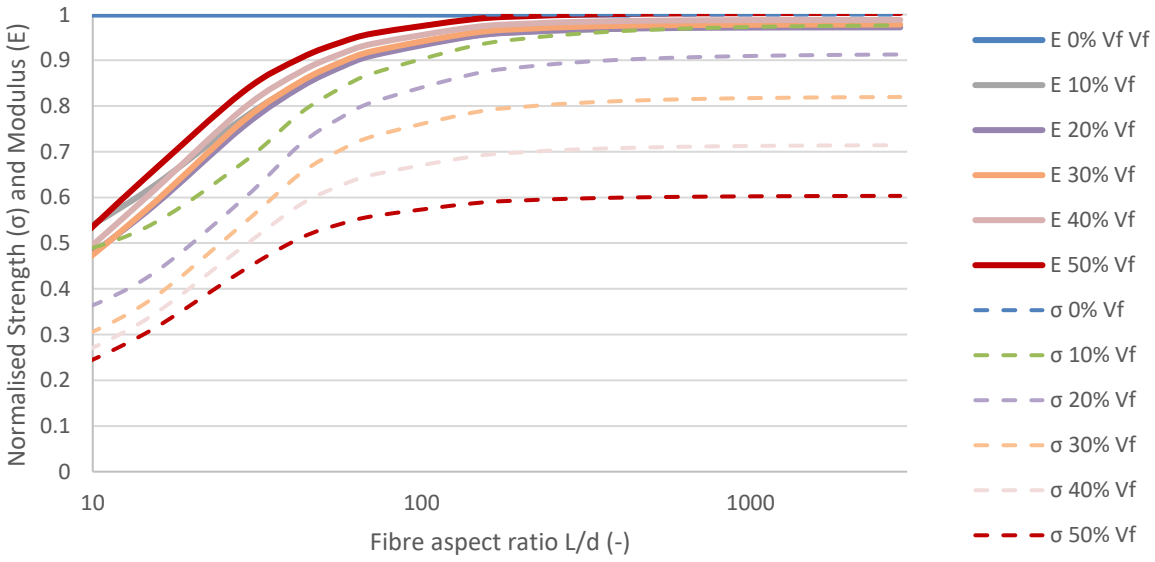

Figure 3.15 – Influence of the aspect ratio on the modulus and strength predictions for discontinuous fibres normalised to a prediction by ROM for continuous fibres. Plotted for multiple fibre contents. All for 2D random fibre orientation and C/PPS material system.

Moduli and strength of UD, highly-oriented and 2D random orientation distributions are compared for a FVF of 20% in Figure 3.16. For a fibre length of 100 μm, the properties of the highly oriented composites are 75% and 85% of the UD modulus and strength, respectively. For longer fibre lengths both decrease to roughly 70%. The 2D random equal 50% and 65% of the UD modulus and strength property, respectively, for a length of 100 μm and both decrease to 40% for longer fibres length.

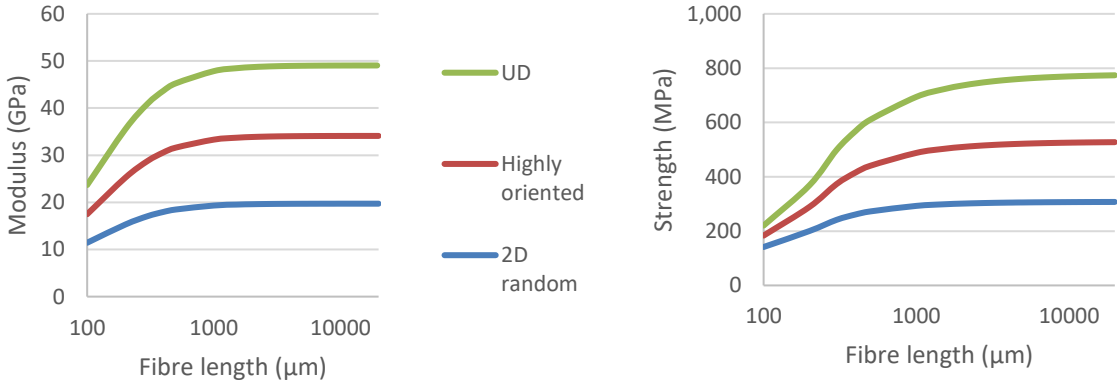

Figure 3.16 - Influence of fibre length on the modulus (left) and strength (right) for different fibre orientations at 20% FVF

In Figure 3.17, the modulus and strength predictions for a 1 mm long C/PPS and the various orientation tensors, as described in Section 3.2.2 are given versus the fibre content. The non-linear relation between fibre content and strength for more randomly oriented predictions is interesting. The non-linear relation indicates that applying an averaging method would lead to improved predictions. Instead of taking an average fibre volume, the effect of the fibre volume distribution on the composite properties should be taken into account. This is studied in Section 3.4.3.

The properties versus the fibre content for a 2D random orientation are plotted for various fibre lengths in Figure 3.18 to obtain a better understanding for which fibre lengths and volumes this non-linear behaviour exists. The results indicate a slight non-linear relation between fibre content and modulus for short fibre lengths. The non-linear relation is stronger for the strength, especially for longer fibre lengths.

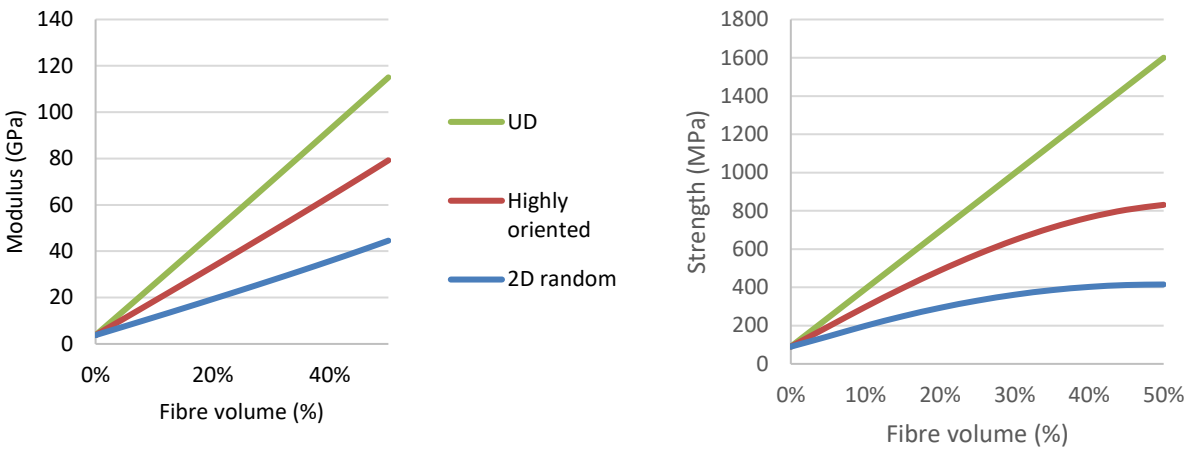

Figure 3.17 - Influence of orientation on modulus (left) and strength (right) for C/PPS of 1 mm fibre length

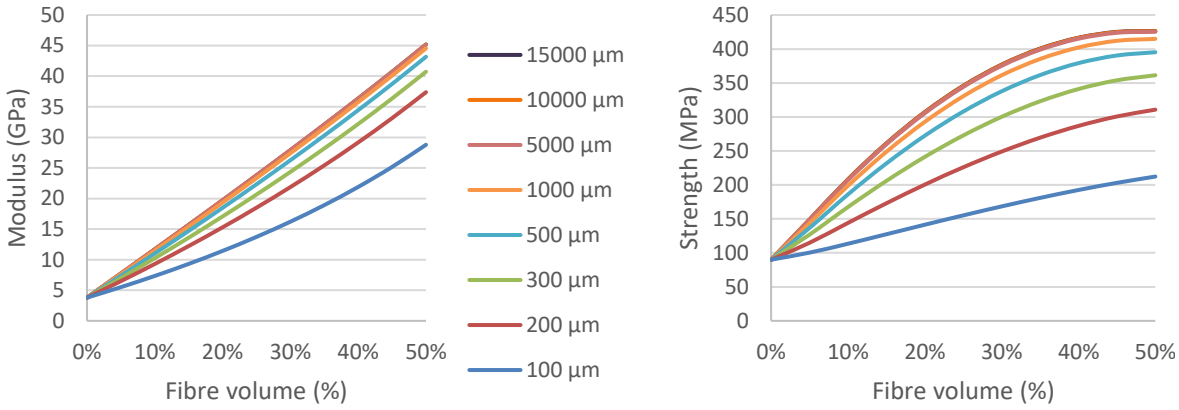

Figure 3.18 - Influence of fibre length on modulus (left) and strength (right) for 2D random C/PPS, plotted for various fibres lengths

3.3.4 *Conclusion*

As it can be seen, from the theoretical results shown in Figure 3.11 and Figure 3.15, composites with discontinuous fibres can be as strong and stiff as those with continuous fibres for high aspect ratios and UD orientation. Aspect ratios above 300 result in a modulus and strength of more than 99% and 95%, respectively, of ROM predictions for continuous fibres. Compared to these results for UD fibre orientation, lower strength values are found for a 2D random fibre orientation at higher fibre contents, when both normalised to ROM predictions.

The moduli and strengths are non-linear for aspect ratios below 100 and 250, respectively. For a single carbon fibre of 7 µm diameter, this corresponds to a fibre length of about 0.7 mm to 1.7 mm. However, the diameter is increased when bundles are considered and therefore also the required fibre length

increases. The non-linear relation indicates that applying an averaging method using a FVD leads to improved predictions.

3.4 Results for fibre length, fibre volume and bundle size distributions

The model presented in Section 2.1 and 3.2 was used in combination with the data from Section 3.2, to predict the effects of the FLD, FVD, BSD, coupled and uncoupled FLBSD on the stiffness and strength of recycled TPC material.

3.4.1 *Influence of fibre length distribution*

The results of the five different FLDs, as described in Section 3.2.5, are given in Figure 3.19. A fixed 10 mm fibre length is added for comparison. The moduli and strengths, except of the IM Nguyen, overlap and there is limited to no significant difference between the diverse FLDs. Calculated mechanical properties of the IM Nguyen show a small decrease, most notably for strength. The lower strength value is a result of the short fibres in the FLD of IM Nguyen, especially in the case of fibres significant shorter than 2 times the critical length (0.5 mm for C/PPS) as can be seen when looking back at the FLD in Figure 3.2 and the strength results of Figure 3.15. For a relatively long fibre length, of multiple times the critical length, its length does not have any influence on the modulus and strength. But bundle effects may have an influence considering the decreasing effect on the aspect ratio.

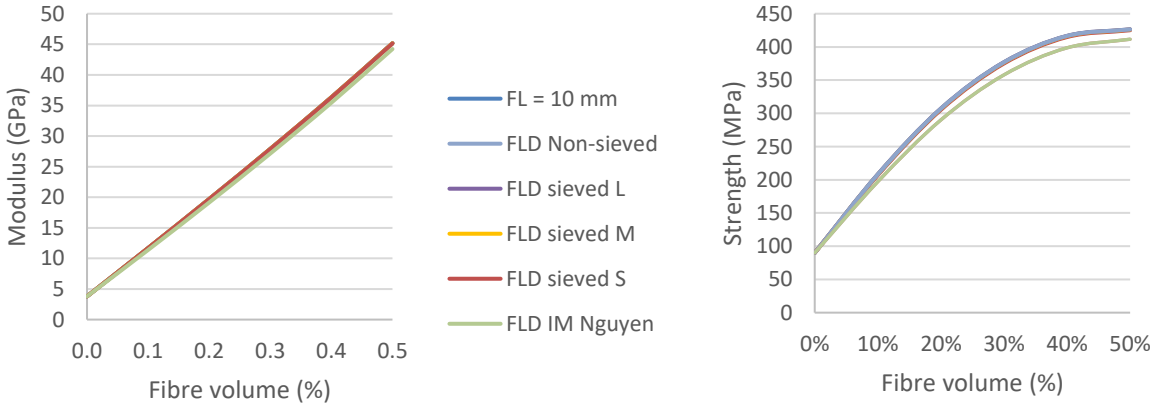

Figure 3.19 - Influence of fibre content on modulus (left) and strength (right) for 2D random C/PPS, plotted for various fibre length distributions.

3.4.2 *Influence of bundle size distribution*

The mechanical property predictions for the six BSDs described in Section 3.2.6 are plotted in Figure 3.20 and Figure 3.21 for UD and 2D random fibre orientation, respectively, to study the effect of bundle size. A clear influence can be observed for the different distributions on both modulus and strength. As expected from the results given for a constant fibre length in Section 3.3.1, the differences for strength are larger

than for the modulus. Compared to single fibres, the UD modulus of GM and PM material is about 11% and 21% lower respectively. For the UD strength the decrease is about 21% and 38%. For 2D random orientation the differences are smaller, with 9% and 17% lower modulus and 13% and 24% lower strength, for GM and PM respectively. For the flat BSD, the 3K bundles and especially the 12K bundles the differences are much bigger with about 30% to 50% for stiffness and 35% to 75% for strength.

Note that the fibre length in all cases is set to 10 mm, which is well above 5 times the critical fibre length (1.2 mm for C/PPS). This value was previously stated as a point where 90% of the strength was reached for the single fibre case. However, considering the BSD shows to have an impact at this 10 mm fibre length.

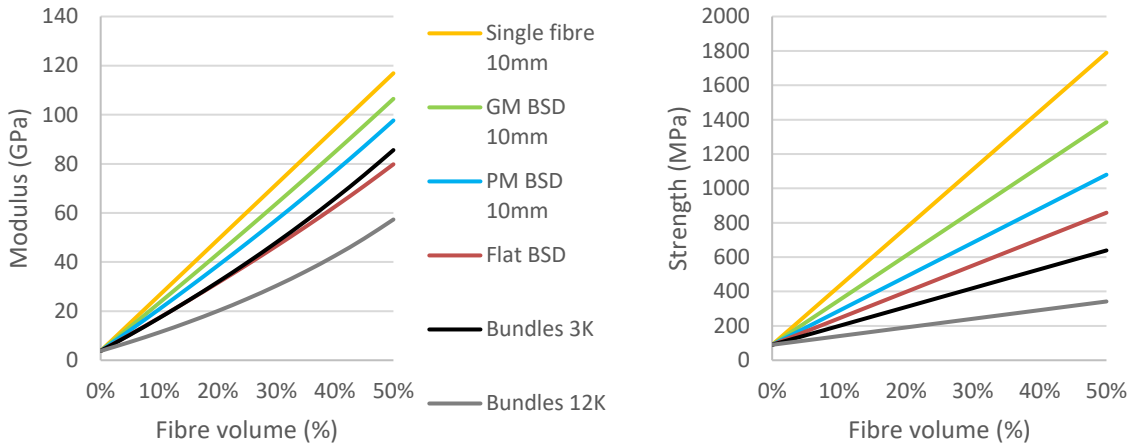

Figure 3.20 - Influence of fibre content on modulus (left) and strength (right) for UD C/PPS, plotted for various bundle size distributions.

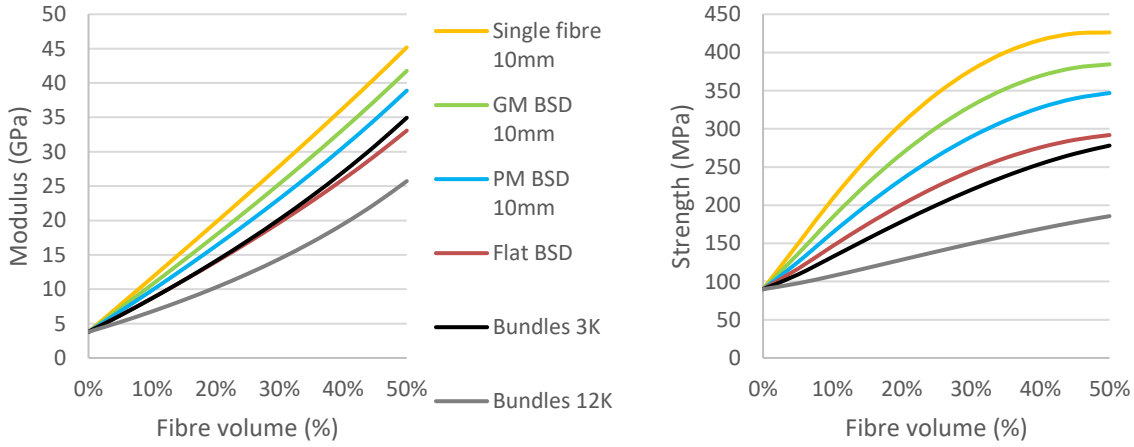

Figure 3.21 - Influence of fibre content on modulus (left) and strength (right) for 2D random C/PPS, plotted for various bundle size distributions.

3.4.3 *Influence of local fibre volume distribution*

Mechanical properties predicted by using the six FVDs from Section 3.2.7, are plotted in Figure 3.22 and Figure 3.23 for UD and 2D random fibre orientation, respectively. For UD fibre orientation and for the modulus predictions of 2D random the results for the six FVDs overlap. This was expected from the linear relation between the fibre content and the modulus as observed in Section 3.3.2. The strength of a 2D random fibre orientation, however, shows a non-linear behaviour and therefore also gives different results for the different FVDs. Nevertheless, only the theoretical maximum and the flat FVD show a clear difference. The more realistic FVDs, namely GM and PM that were derived from experimental data, give very similar results.

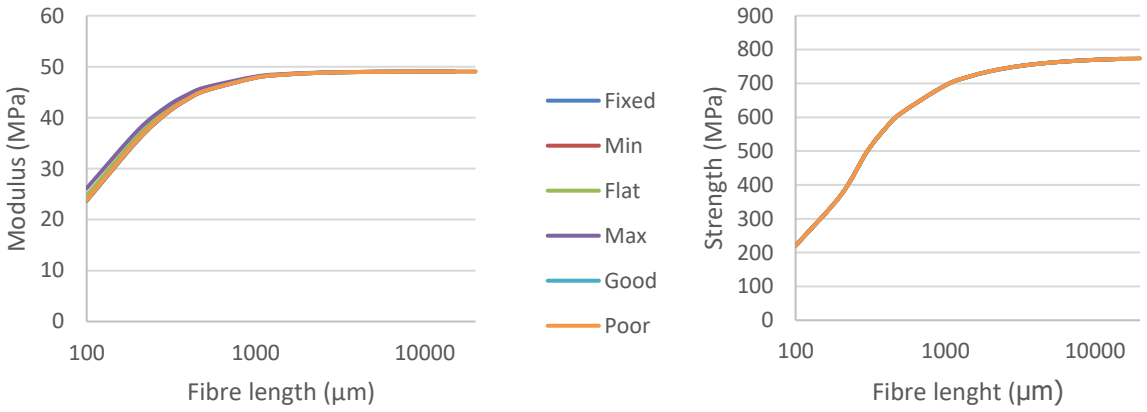

Figure 3.22 - Influence of fibre content on modulus (left) and strength (right) for UD C/PPS, plotted for various volume fraction distributions.

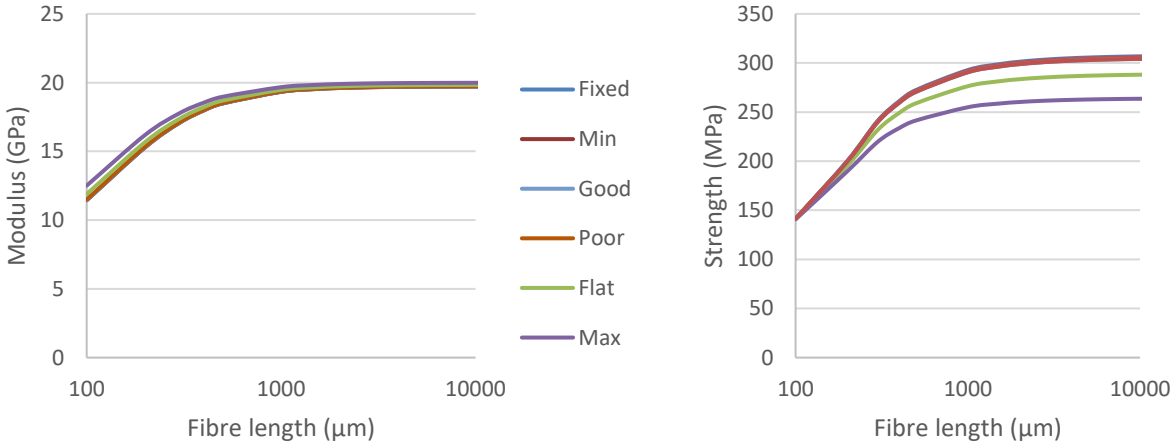

Figure 3.23 - Influence of fibre content on modulus (left) and strength (right) for 2D random C/PPS, plotted for various volume fraction distributions.

3.4.4 *Influence of combined FLD and BSD*

To further derive the importance of variations in homogeneity in the composites, the results of the combined uncoupled FLBSD are presented in Figure 3.24 for 2D random orientation. In these graphs, the data is compared with results for a single fibre, GM and PM materials of constant fibre length.

The combined FLBSD in respect to the separate FLD and BSD lead to mechanical properties which are higher than the properties predicted when considering only the BSD. These results fall in line with the input data, seen the fact that the aspect ratio of the combined FLBSD is also between the separate FLD and BSD.

For FVFs between 20% and 35%, the decrease in modulus between single fibre bundle to PM and GM material including the FLBSD is respectively 5% and 10%. For the strength the decrease is slightly bigger with 6% to 7% and 14% to 15% for the PM and GM materials, respectively.

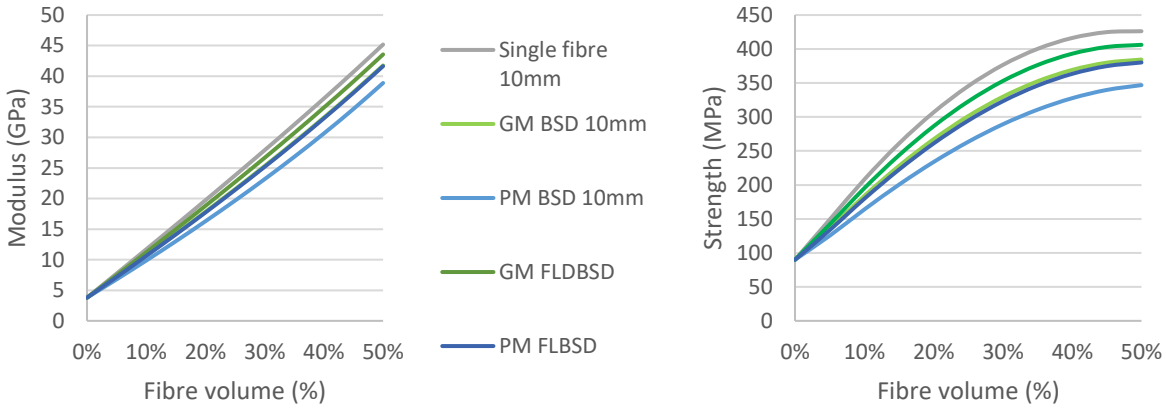

Figure 3.24 - Influence of fibre content on modulus (left) and strength (right) for 2D random C/PPS, plotted for a single fibre, BSDs at 10 mm fibre length and uncoupled FLBSDs. Showing the influence of a FLBSD combination. The PM FLBSD and GM BSD 10mm overlap.

Influence of coupling FLD and BSD

Finally, the influence of coupled to uncoupled FLBSD combinations is shown in Figure 3.25. As expected from the input data, seen the narrower distribution (the range of observed aspect ratio values is small) of the coupled FLBSD in respect to the uncoupled FLBSD, see Section 3.2.8, the coupled FLBSD predicts slightly higher properties in comparison to the uncoupled. Differences between the coupled and uncoupled are small, around 3%.

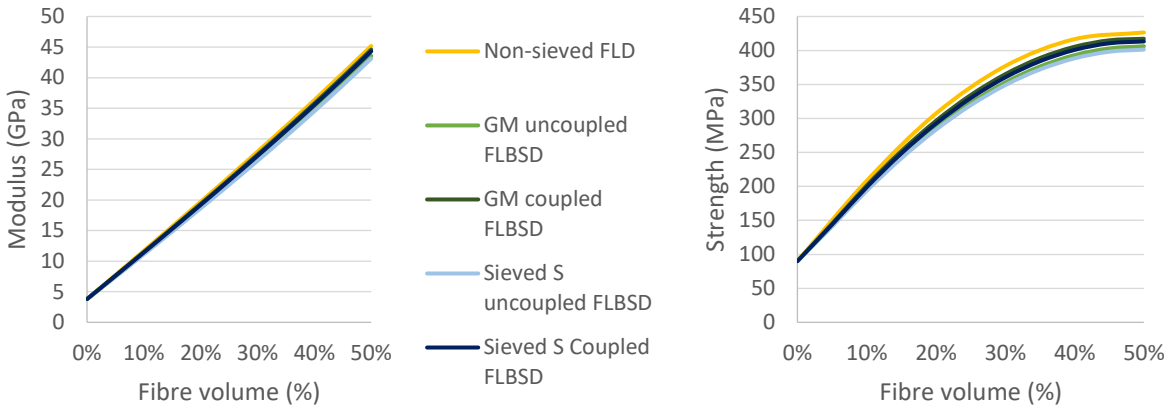

Figure 3.25 – Comparing coupled and uncoupled FLBSD for 2D random modulus and strength

3.4.5 *Searching for the optimal distribution*

As explained, getting optimised properties in discontinuous fibre composites is a trade-off between the fibre length distribution and degree of mixing. Therefore, four types of shredded C/PPS material were compared to find the best option. The combined uncoupled FLBSD input data used is given in Section 3.2.9. The results of the non-sieved batch, the three sieved batches, the single 10mm fibre and LFT pellets are presented in Figure 3.26 for 2D random fibre orientation.

The predictions of all distributions show a slightly lower modulus (5-6%) and strength (6-9%) value compared to single fibres of constant 10 mm length for FVF of 20-35%. No large difference is observed between the predicted results when using the different distributions. The pellets perform slightly better than the large flakes (Sieved L) with regard to modulus (3%) and strength (3-4%) for the given FVF. From the three sieved distributions, the medium-size sieved M performed slightly better than Sieved S and Sieved L. The non-sieved batch with a wide FLD distribution outperforms all sieved batches. Overall, no large differences are observed. Possible underlying explanations are discussed in Section 3.5.1.

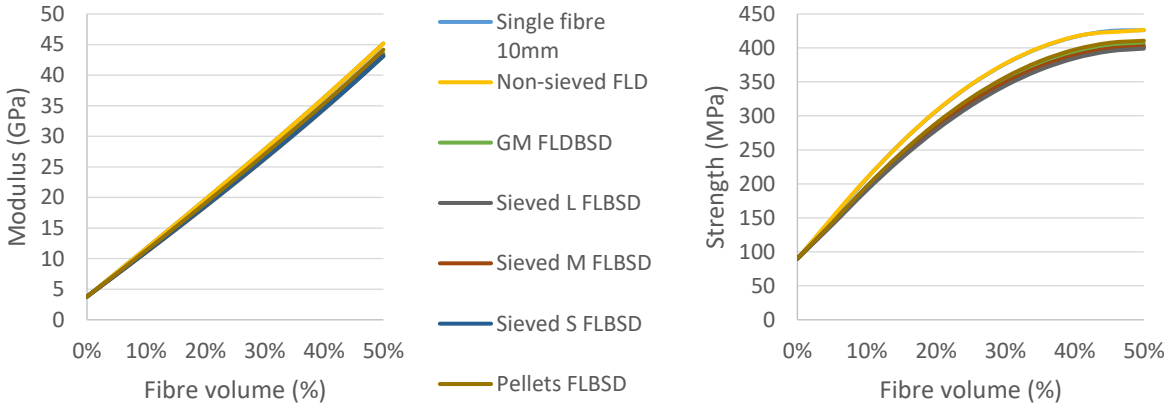

Figure 3.26 - Influence of five different FLDs considering both BSD and FLD for 2D random modulus and strength

3.4.6 *Influence of material system*

To study the influence of the material system, a G/PP composite was also considered. Although the properties of the constituent materials differ to those of the C/PPS, the approach and expressions do not change. Besides the difference in strength and stiffness of both matrix and fibre, less commonly expected differences originate from the fibre diameter and the matrix strength at fibre failure. However, as the critical fibre length of G/PP is 722 µm, about three times longer than the critical fibre length of C/PPS, the larger fibre diameter of the glass fibre results in a larger fibre lengths at which the stiffness and strength property reaches a plateau, as can be seen in Figure 3.27. Thus, incorporating the effect of fibre bundles in predicting properties is more critical.

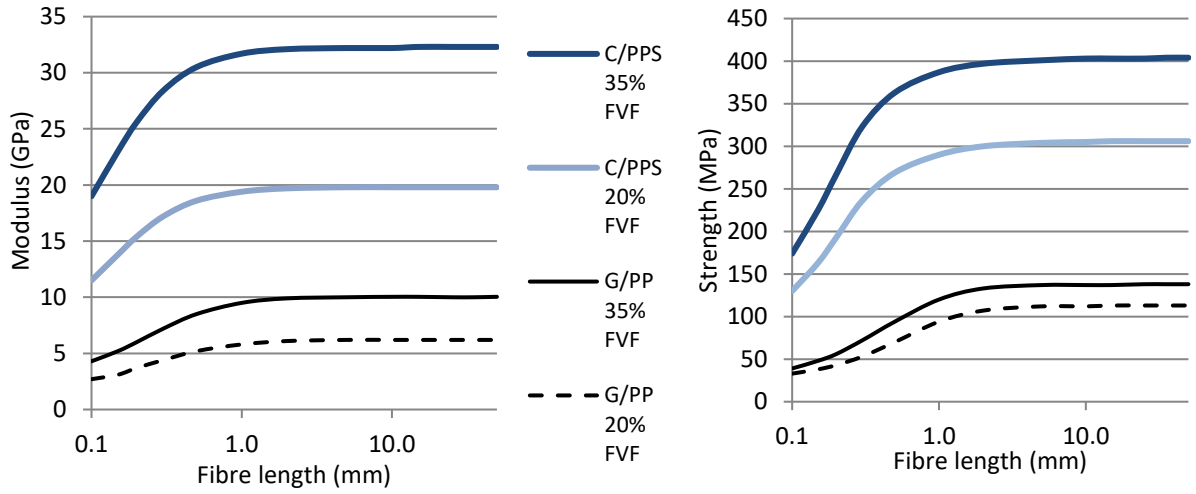

Figure 3.27 – Influence of material system on modulus(left) and strength (right) for a 2D random orientation

3.5 Discussion

In this chapter, theoretical and experimental FLD, FVD and BSD data were included in existing micromechanical models to allow for studying the influence of fibre length and degree of mixing, a trade-off in processing discontinuous fibre composites, on modulus and strength. Data of multiple FLDs and correlated FVD and BSD are compared to investigate the compromise between fibre length and degree of mixing. The results can provide more realistic mechanical data for design and application of recycled materials.

3.5.1 *The relation between dispersion, fibre length and fibre volume*

The models show that dispersion and therefor small bundle sizes favour mechanical performance, which is confirmed in literature [25–30]. Also Harper et al. [31] observed that maximising dispersion of large tows of 24K and 48K to produce preforms leads to increased mechanical performance. However, their study, along with other research [32–35] concluded that fibre packing considerations set an upper limit to the maximum fibre content practically feasible. This trade-off is confirmed by Kirupanantham [35], who modelled the effect of bundle diameter on stiffness and strength using shear-lag models and studied experimentally an epoxy carbon system by means of non-mixed compression moulding. He also observed that a high level of dispersion lead to greater macroscopic homogeneity and less manufacturing defects, such as waviness. However, he and others [36, 37] found that dispersed fibres are often lofted and therefore a large compression pressure is required to compact the more dispersed fibres.

The relation between dispersion and fibre length is studied by Vincent et al.[21]. He concluded that the FLD and BSD of the sieved batches indicate a relation between a FLD with predominately long fibres and a BSD with predominately large bundles. So, longer fibres tend to disperse less. Taking physical mixing phenomena into account, it is likely that bundles of shorter fibres are more easily to disentangled and disperse. Therefore, short fibres are probably related to small bundles and long fibres to large bundles.

As is described in Section 3.4.5, no large difference where found between batches of small flakes (with an average fibre length of 6 mm) and large flakes (with an average fibre length of 25 mm). The improvement of long fibres seems to be neutralised by the effect of the lager bundles due to a more difficult mixing. Better mixing is therefore interesting. Beside the dispersion and distribution, the aspect ratio is an interesting measure since it takes both BSD and FLD into account. It will still be interesting to also look at the BSD, since bundles can have both a negative and positive effect. A negative effect of them is that bundles lead not only to a decrease of the aspect ratio as is modelled in this study, but also result in elevated stress concentrations at their ends, as is described by Rondeau et al. [30]. A positive effect of

the presence of bundles is the enabling of a higher fibre packing. Therefore, the practically feasible maximum achievable fibre content is increased and lower compression pressures are required. For unimpregnated fibres it is possible to consider the option of aligned fibres in layers to achieve very high fibre contents [14, 38]. This could be considered as an ellipse with very large eccentricity.

Higher fibre volumes, longer fibres and high levels of dispersion lead to an increased performance. However, it is difficult to achieve all three.

3.5.2 *Variation and weakest link theory*

Variation of mechanical properties is expected to be large for wide distributions of FLD, BSD, FVD and FLBSD [39, 40]. A wider distribution represents a less homogeneous material, and therefore local effects that are not modelled in this study could lead to stress concentration for instance and ultimately to failure initiation.

The micromechanical modelling of strength in this study is based on the shear-lag theory. This theory considers the fibre failure and fibre pull-out failure mechanism. Variation of fibre strength can be implemented by including statistical model based on a Weibull distribution. The fibre is considered a chain in this approach. The strength of the chain is determined by the weakest link and tends to decrease as the number of links increases. Van Hattum et al. applied a three parameter Weibull distribution and found good agreement with experimental work [12]. A similar approach on the weakest link and size effect for bundles is evaluated by various authors [36, 41, 42]. Manderst et al. and Wisnom considered the strength and variability of carbon and glass fibre for single fibres and loose bundles [41, 42]. For loose (or dry) bundle, the matrix does not carry any load allowing progressive failure when the first fibre fails. Both used a Weibull strength theory according to a simple two-parameter model which was reasonably well in agreement with experimental data. Pimenta [36] developed a model including a hierarchical bundles organization and the fibre-matrix interfacial relation by a simplified shear-lag model. In this model the matrix does carry load. She found that the fibre-matrix interface leads to a lower variability by the size effect of bigger bundles compared to single constituent fibres and bundles result in initial strengthening. The experimental work of Pimenta on recycled composite material of reclaimed carbon fibre with epoxy resin showed a limited influence of bundles on stiffness and strength, but a large positive effect on toughness. The contradictive effect of lower strength for loose bundles and increasing toughness for composites with a strong fibre matrix interface is interesting to include in further study. The interface strength of the recycled composite material in this study is considered to be strong, since both fibre and matrix are recycled. Therefore, the influence was probably limited.

3.5.3 *Is simplification possible?*

It is interesting to see if an approach excluding averaging gives comparable results. Table 3.3 shows the average aspect ratio excluding and including BSD. Based on the latter, one may expect to find the best mechanical properties for the types with the highest average aspect ratio. The results however show that this simplification is not valid. Looking the ratio below the critical aspect ratio gives a reasonable relative estimation for the number of shredded flakes. This does not work for the pellets probably because they are more easily dispersed seen their UD structure. The results on aspect ratio at constant fibre length in Section 3.3 and literature, showed that the influence of aspect ratio on the mechanical performance reaches a plateau above 5 times critical fibre length. However, looking the ratio below at five times the aspect ratio, does not seem to bring improvement over only one time the critical aspect ratio. Therefore, it might be possible to obtain a quick indication by looking at the ratio of fibre volume below the critical aspect ratio compared to the total fibre volume, but more data should be analysed to obtain more confidence in such a rule of thumb.

Table 3.4 - Several key characteristics of concerning the aspect ratio and results on modulus and strength for 2D random orientation of non-sieved and sieved flakes

Material	average aspect ratio excl. BSD	average aspect ratio incl. BSD	ratio below the critical aspect ratio	ratio below 5x critical aspect ratio	Modulus @ 20% FVF (MPa) incl averaging FLBSD	Strength @ 20% FVF (MPa) incl averaging FLBSD
GM FLBSD	3306	1108	9%	37%	18.8	286
PM FLBSD	3306	447	22%	74%	17.7	261
Sieved S FLBSD	891	385	11%	39%	18.6	283
Sieved M FLBSD	1911	691	16%	34%	18.7	283
Sieved L FLBSD	3511	833	11%	52%	18.5	279
Pellets FLBSD	429	190	2%	65%	18.9	283

3.5.4 *Further study*

The experimental data used in this chapter to derive experimental FVD, BSD and FLBSD were collected from samples processed using a low-shear mixing method. This current prototype setup can be improved which will likely result in a better degree of mixing and therefore improved BSD. Thus moving the expected attainable properties more towards the higher aspect ratio region when looking at Figure 3.11 for UD and Figure 3.15 for 2D random fibre orientation.

The results in Section 3.4.5 indicate a balance in the trade-off between longer fibres (improving mechanical performance) and larger bundles (decreasing mechanical performance). Therefore, it would also be interesting to look at experimental FLD and BSD at shorter fibre length and with better mixing qualities in a comparable study to see if and when the balance will move towards higher or lower properties. For very short fibre lengths the aspect ratio will decrease inevitability, independent of the BSD, leading to lower mechanical performance as can be observed in Figure 3.11. In this case the fibres are likely to disperse perfectly, but the bundle diameter cannot be smaller than of one fibre. For very long fibres the bundle diameter will increase, but is limited to the initial tow size. Therefore the stiffness and strength will reach the plateau described in Figure 3.11 for UD and Figure 3.15 for 2D random fibre orientation. The aspect ratios of the used distributions are above 100 and therefore at the start of the horizontal plateau when looking at these figures.

The step size of the FLD is large in respect to the critical fibre length. A smaller step size could increase the effect of the smaller fibres and therefore lower the predicted modulus and strength. This is especially relevant for small fibre lengths, below two times the critical fibre length. Fibres of these lengths did not represent a significant part of the discussed experimental FLDs (typically << 1%). Regarding the BSD, a small step size at higher bundle sizes of BSD is important since this translates to lower aspect ratios and therefore the previous described analogy for FLD can be followed.

Experimental validation of the coupled FLD and BSD might be possible with the use of Micro-computed X-Ray tomography. But the large aspect ratio of fibres having 7 μm diameter, but lengths of over 20000 μm will result in high requirements regarding resolution, scanning volume and scanning time. The relative density difference between carbon fibres and PPS may be something to consider. This type of analysis can also provide a local fibre orientation distribution [43]. Alternatively, an empirical model as described by Chen et al. can be used to predict the effective bundle diameter for prediction of stiffness [25].

To improve the fibre orientation model, a combination of the Reduced Strain Closure and the Anisotropic Rotary Diffusion (ARD-RSC) model could be added [23]. This model was implemented by Phelps and Tucker [44] and later on further improved for long fibres by Tseng et al. [45] This model could improve the fibre orientation for LFT by slowing down the orientation kinetics [46]. However as modelling the orientation was not the focus of this work an ARD-RSC implementation is omitted.

The next step is an experimental validation by destructive testing of these theoretical results (Chapter 4). Applications of recycled TPC material are studied in Chapter 5. A parallel study on the effect of flakes and flake size on the squeeze flow and in-homogeneities is performed by Vincent et al. [22].

3.6 Conclusion

The relation of the fibre length and degree of mixing to the resulting composite's modulus and strength is modelled to obtain a better understanding of the influence of these variables for use in recycling continuous fibre thermoplastic composites.

A motivation was to determine the required fibre length for optimum mechanical properties. Based on a perfectly mixed material, a fibre length of roughly five times the critical fibre length is sufficient to obtain strength and modulus values close to those of continuous fibre composites. Therefore, FLDs do not have a big effect, except when a substantial volume is around or below two times the critical fibre length. And unless fibres are bundled together, drastically reducing the aspect ratio of the reinforcement.

A non-homogeneous material can be the result of a poorly mixed material as a consequence of low-shear processing to limit fibre attrition or due to the complex material morphology of the most common waste stream of flakes with woven structures. Several theoretical and experimental BSDs and FVDs were studied to investigate the influence of the degree of mixing.

BSD and FVD were observed for a lower degree of mixing. The effect of bundles was found to be substantial, with deviations in predicting stiffness and strength of tens of percent between using the theoretical and experimental distributions.

The influence of FVD shows to be very limited. Only theoretical distribution which are generally not realistic have an influence on strength for a 2D random orientation, most representative for moulded long discontinuous fibre composite.

For poorly mixed materials, when a combined FLD and BSD is assumed, the results present 10% and 15% lower modulus and strength values, respectively, than those predicted when a single fibre length and bundles of a single fibre are considered.

FLD of flakes of four different sizes were compared to find the optimal fibre length distribution for recycling. The distributions' average fibre length ranges from 6 to 25mm. Although the smaller flakes exhibit shorter fibre length in general, the improved degree of mixing in terms of BSD lead to higher mechanical property prediction for those small flakes. The results are very comparable when the combined FLBSD is considered.

Although these theoretical results should be experimentally verified, they show that flakes larger than 6 mm do not show an increased modulus and strength as compared to flakes of 6 mm. Flakes with longer

fibres show a higher level of bundles after processing. Modelling shows that the negative effect of the bundles on the mechanical properties is neutralised by the longer fibres. However, from the results of the BSD containing large bundles, it can be concluded that a higher level of mixing increases the mechanical properties. Consequently, this indicates that the optimal point in the trade-off between fibre length and degree of mixing covers a broad range due to the counteracting effects with the same order of magnitude of bundles and fibre length in the degrees of mixing. However, a higher degree of mixing, especially by an improved dispersion, at the cost of shorter fibre length may lead to higher mechanical performance.

3.7 References

[1] W. Schijve, “High performance at medium fibre length in long glass fibre polypropylene,” , vol. 2, no. 12, pp. 14–21, 2000, doi: 10.1016/S1464-391X(00)80121-X.

[2] J. L. Thomason, “The influence of fibre length and concentration on the properties of glass fibre reinforced polypropylene: 5. Injection moulded long and short fibre PP,” *Compos. Part A Appl. Sci. Manuf.*, vol. 33, no. 12, pp. 1641–1652, 2002, doi: 10.1016/S1359-835X(02)00179-3.

[3] U. Vaidya *et al.*, “Comparison of wet laid to other discontinuous processed carbon fiber thermoplastic composites,” in *CAMX Conference Proceedings*, 2014.

[4] A. Sarhangi Fard, “Analysis and optimization of mixing inside twin-screw extruders,” PhD Thesis, Eindhoven Univesity of Technology, 2010.

[5] M. I. Abdul Rasheed, “Compression molding of chopped woven thermoplastic composite flakes: a study on processing and performance,” PhD Thesis, University of Twente, Enschede, The Netherlands, 2016.

[6] M. Roux, N. Eguémann, C. Dransfeld, F. Thiébaud, and D. Perreux, “Thermoplastic carbon fibre-reinforced polymer recycling with electrodynamical fragmentation: From cradle to cradle,” *J. Thermoplast. Compos. Mater.*, 2015, doi: 10.1177/0892705715599431.

[7] T. A. De Bruijn, G. A. Vincent, and F. W. J. Van Hattum, “Recycling of long fibre thermoplastic composites by low shear mixing,” in *SAMPE Europe*, 2016, pp. 540–546.

[8] T. A. De Bruijn, G. Vincent, and F. W. J. Van Hattum, “Recycling C/PPS laminates into long fibre thermoplastic composites by low shear mixing,” in *Proceedings of the 21th Internatinoal Conference on Composite Materials ICCM21*, 2017.

[9] J. H. Phelps, A. I. A. El-rahman, V. Kunc, and C. L. Tucker, “A model for fiber length attrition in injection-molded long-fiber composites,” *Compos. Part A*, vol. 51, pp. 11–21, 2013.

[10] G. P. Tandon and G. J. Weng, “The effect of aspect ratio of inclusions on the elastic properties of unidirectionally aligned composites,” *Polym. Compos.*, vol. 5, no. 4, pp. 327–333, 1984, doi: 10.1002/pc.750050413.

[11] F. W. J. Van Hattum and C. A. Bernardo, “A model to predict the strength of short fiber composites,” *Polym. Compos.*, vol. 20, no. 4, pp. 524–533, 1999, doi: 10.1002/pc.10376.

[12] F. W. J. Van Hattum, J. P. Nunes, and C. a. Bernardo, “A theoretical and experimental study of new towpreg-based long fibre thermoplastic composites,” *Compos. Part A Appl. Sci. Manuf.*, vol. 36, pp. 25–32, 2005, doi: 10.1016/j.compositesa.2004.06.031.

[13] L. E. Nielsen, *Mechanical properties of polymers and composites vol. 2.* New York, 1974.

[14] D. Heider *et al.*, “Closed loop recycling of CFRP into highly aligned high performance short fiber composites using the TUFF process,” in *SAMPE Conference Proceedings*, 2019.

[15] J. F. O. Gara, G. E. Novak, and M. G. Wyzgoski, “Predicting the tensile strength of short glass fiber reinforced injection molded plastics,” in *10th Annual Automotive Composites Conference and Exhibition 2010*, 2010.

[16] D. Dray, P. Gilormini, and G. Régnier, "Comparison of several closure approximations for evaluating the thermoelastic properties of an injection molded short-fiber composite," *Compos. Sci. Technol.*, vol. 67, no. 7–8, pp. 1601–1610, 2007, doi: 10.1016/j.compscitech.2006.07.008.

[17] J. Cintra and C. Tucker III, "Orthotropic closure approximations for flow-induced fiber orientation," *J. Rheol. (N. Y. N. Y).*, no. 39(6), pp. 1095–122, 1995.

[18] S. G. Advani, "The Use of Tensors to Describe and Predict Fiber Orientation in Short Fiber Composites," *J. Rheol. (N. Y. N. Y).*, vol. 31, no. 8, p. 751, 1987, doi: 10.1122/1.549945.

[19] G. Vincent, T. A. de Bruijn, M. I. Abdul Rasheed, S. Wijskamp, and R. Akkerman, "Fibre length distributions of shredded thermoplastic composite scrap," *21th Int. Conf. Compos. Mater.*, no. August, pp. 20–25, 2017.

[20] G. A. Vincent, T. A. De Bruijn, S. Wijskamp, M. I. Abdul, M. Van Drongelen, and R. Akkerman, "Shredding and sieving thermoplastic composite scrap : Method development and analyses of the fibre length distributions," *Compos. Part B*, vol. 176, no. February, p. 107197, 2019, doi: 10.1016/j.compositesb.2019.107197.

[21] G. A. Vincent, T. A. de Bruijn, S. Wijskamp, M. I. A. Rasheed, M. Van Drongelen, and R. Akkerman, "Characterisation and improvement of the quality of mixing of recycled thermoplastic composites," *Submitt. to Polym. Compos.*, 2019.

[22] G. A. Vincent, T. A. de Bruijn, S. Wijskamp, M. van Drongelen, and R. Akkerman, "Process- and material-induced heterogeneities in recycled thermoplastic composites," *Submitt. to J. Thermoplast. Compos. Mater.*, 2019.

[23] B. N. Nguyen, S. K. Bapanapalli, V. Kunc, J. H. Phelps, and C. L. Tucker, "Prediction of the elastic-plastic stress/strain response for injection-molded long-fiber thermoplastics," *J. Compos. Mater.*, vol. 43, no. 3, pp. 217–246, 2009, doi: 10.1177/0021998308099219.

[24] P. C. Powell, *Engineering with Fibre-Polymer Laminates*, 1st ed. Springer Netherlands, 1994.

[25] H. Chen and D. G. Baird, "Prediction of Young ' s Modulus for Injection Molded Long Fiber Reinforced Thermoplastics," *J. Compos. Sci.*, 2018, doi: 10.3390/jcs2030047.

[26] D. E. Spahr, K. Friedrich, J. M. Schultz, and R. S. Bailey, "Microstructure and fracture behaviour of short and long fibre-reinforced polypropylene composites," *J. Mater. Sci.*, vol. 25, pp. 4427–4439, 1990.

[27] S. K. Garkhail, R. W. H. Heijenrath, and T. Peijs, "Mechanical Properties of Natural-Fibre-Mat-Reinforced Thermoplastics based on Flax Fibres and Polypropylene," *AppliedComposite Mater.*, vol. 7, pp. 351–372, 2000.

[28] J. L. Thomason, "The influence of fibre length and concentration on the properties of glass fibre reinforced polypropylene: 6. The properties of injection moulded long fibre PP at high fibre content," *Compos. Part A Appl. Sci. Manuf.*, vol. 36, no. 1, pp. 995–1003, 2005.

[29] M. Ericson and L. Berglund, "Deformation and fracture of glass-mat- reinforced polypropylene," *Compos. Sci. Technol.*, vol. 43, pp. 269–281, 1992.

[30] R. Rondeau and S. Reeve, "The effect of tows and filament groups on the properties of

discontinuous fiber composites," in *44th International SAMPE Symposium*, 1999, pp. 1449–1460.

[31] L. T. Harper, T. a. Turner, N. a. Warrior, and C. D. Rudd, "Characterisation of random carbon fibre composites from a directed fibre preforming process: The effect of tow filamentisation," *Compos. Part A Appl. Sci. Manuf.*, vol. 38, no. 3, pp. 755–770, 2007, doi: 10.1016/j.compositesa.2006.09.008.

[32] S. Toll and P. Andersson, "Microstructure of Long- and Short-Fiber Reinforced Injection Molded Polyamide," *Polym. Compos.*, vol. 14, no. 2, pp. 116–125, 1993.

[33] J. L. Thomason, "The influence of fibre length and concentration on the properties of glass fibre reinforced polypropylene : 7 . Interface strength and fibre strain in injection moulded long fibre PP at high fibre content," vol. 38, pp. 210–216, 2007, doi: 10.1016/j.compositesa.2006.01.007.

[34] J. L. Thomason, "The influence of fibre length and concentration on the properties of glass fibre reinforced polypropylene : 4. Impact properties," *Compos. Part A Appl. Sci. Manuf.*, vol. 28, pp. 277–288, 1996.

[35] G. Kirupanantham, "Characterisation of discontinuous carbon fibre preforms for automotive applications," PhD thesis, University of Nottingham, 2013.

[36] S. Pimenta, "Toughness and strength of recycled composites and their virgin precursors," PhD Thesis, Imperial College London, 2013.

[37] T. A. Turner, N. A. Warrior, and S. J. Pickering, "Development of high value moulding compounds from recycled carbon fibres," *Plast. Rubber Compos.*, vol. 39, no. 3–5, pp. 151–156, 2010, doi: 10.1179/174328910X12647080902295.

[38] M. Such, C. Ward, and K. Potter, "Aligned Discontinuous Fibre Composites: A Short History," *J. Multifunct. Compos.*, vol. 2, no. 3, pp. 155–168, 2014, doi: 10.12783/issn.2168-4286/2/3/4.

[39] J. S. Dahl, G. L. Smith, D. Q. Houston, D. Mi, S. Iobst, and L. Berger, "The influence of fiber tow size on the performance of chopped carbon fiber reinforced composites," in *SAMPE Conference Proceedings*, 2005.

[40] P. Feraboli, T. Cleveland, P. Stickler, and J. Halpin, "Stochastic laminate analogy for simulating the variability in modulus of discontinuous composite materials," *Compos. Part A Appl. Sci. Manuf.*, vol. 41, no. 4, pp. 557–570, 2010, doi: 10.1016/j.compositesa.2010.01.003.

[41] M. R. Wisnom, "Size effects in the testing of fibre-composite materials," *Compos. Sci. Technol.*, vol. 59, no. 59, pp. 1937–1957, 1999, doi: https://doi.org/10.1016/S0266-3538(99)00053-6.

[42] P. W. Manders and T. Chou, "Variability of Carbon and Glass Fibers, and the Strength of Aligned Composites," pp. 43–59, 1982.

[43] Y. Wan, I. Straumit, J. Takahashi, and S. V. Lomov, "Micro-CT analysis of internal geometry of chopped carbon fiber tapes reinforced thermoplastics," *Compos. Part A Appl. Sci. Manuf.*, vol. 91, pp. 211–221, 2016, doi: 10.1016/j.compositesa.2016.10.013.

[44] J. Wang and X. Jin, "Comparison of recent fiber orientation models in Autodesk Moldflow Insight simulations with measured fiber orientation data," *Proc. Polym. Process. Soc. 26th Annu. Meet.*,

2010.

[45] H. C. Tseng, R. Y. Chang, and C. H. Hsu, “Numerical prediction of fiber orientation and mechanical performance for short/long glass and carbon fiber-reinforced composites,” *Compos. Sci. Technol.*, vol. 144, pp. 51–56, 2017, doi: 10.1016/j.compscitech.2017.02.020.

[46] J. H. Phelps and C. L. Tucker III, “An anisotropic rotary diffusion model for fiber orientation in short- and long-fiber thermoplastics,” *J. Nonnewton. Fluid Mech.*, vol. 156, pp. 165–176, 2009, doi: 10.1016/j.jnnfm.2008.08.002.

4 Experimental study on the mechanical performance

4.1 Introduction

The mechanical performance of discontinuous fibre composites is theoretically predicted by the developed analytical model in the previous chapter. Besides considering various fixed fibre lengths, FVF and orientations, the model was developed for TPC waste by including FLDs, FVDs and BSDs. Results showed that stiffness and strength for fibre lengths longer than five times the critical fibre length approach values of those using continuous fibres. Where FVD has a limited influence on the stiffness and strength prediction, BSD showed to have a high impact on property prediction, especially when combined with a fibre length distribution.

The focus of this chapter is to experimentally test the technical feasibility of the recycling process on material level, as is proposed in the introduction (Chapter 1) and State of the art (Section 2.5.2). Literature on recycling of thermoplastic composite materials predominately consider non-mixed approaches [1, 2] (Section 2.2). A specific process, including a previously designed low-shear mixing process, was developed and applied to recycle TPC material with limited fibre friction in this research project [3, 4] (Section 2.2.6). Although the mixing process uses mixing rods instead of a conventional extrusion screw, it is similar to long fibre thermoplastic (LFT) processing, which is a technology thoroughly studied and embraced by industry for virgin discontinuous materials.

Another objective of this chapter is to study the mechanical performance of recycled TPC and validate the theoretical predictions. Determination of the stiffness and strength values that can be attained is relevant to explore new fields of application and, potentially, establish basic design values. A more specific goal is to study the influence of several variables on the mechanical performance of the processed material. The variables are chosen based on their proven influence shown in Chapter 3: fibre fraction, fibre length, fibre orientation, mixing process, material system and material structure. The results are compared to the theoretical predictions, including the influence of mixing as described in Chapter 3. When the developed

Parts of this chapter are reproduced with adaptions from "T. A. De Bruijn, G. Vincent, and F. W. J. Van Hattum. "Recycling C/PPS laminates into long fibre thermoplastic composites by low shear mixing", *21st International Conference in Composite Materials*, 2017." and "T. A. de Bruijn, G. A. Vincent, and F. W. J. van Hattum, "Recycling of long fibre thermoplastic composites by low shear mixing", SAMPE Europe, 2016."

recycling route is proven to be technical feasible on material level, it can be applied on product level to create multiple demonstrator products and showcase their capabilities (Chapter 5).

4.2 Method and materials

Two type material systems C/PPS and G/PP at various structures and dimensions are included in the current study. These materials are used in the DCM and low-shear mixing manufacturing processes described in Section 2.2. Specimens were submitted to flexural and impact tests. All samples produced with the mixing device will be referred to as mixed materials, mixed plates or mixed samples and the non-mixed materials as laminate, from here on.

Theoretical modelling

Micromechanical modelling was used to predict stiffness and strength based on a random two-dimensional (random2D) fibre orientation. The 'orientation averaging method' presented by Advani and Tucker [5] was applied to account for the effect of fibre orientation. An orthotropic fitted closure approximation was selected to calculate the fourth-order orientation tensors [6]. Fibre length, bundle size and fibre volume distributions are included to model the influence of a non-uniform fibre length and the effect of non-perfect mixing. More information on the employed models can be found in Chapter 3 [7, 8]. A modified rule of mixtures (MROM) was also used for comparison. The method was modified from the classic rule of mixtures to account for random in-plane fibre orientation [9].

4.2.1 *Material system*

As mentioned, two types of material systems were chosen: C/PPS was selected from the high-end market since it is the most common in aerospace [10] and G/PP was selected for the high-volume market since it is the most used TPC material in the composite sector [11]. These material systems are widely available at the industrial partners involved in this project (see Chapter 1 for more background information).

4.2.2 *Carbon fibre reinforced PPS*

Four types of C/PPS material were mixed and processed in this study: a shredded consolidated laminate, a cut powder-coated semipreg, a cut UD tape and LFT pellets. The waste of the first material was collected at the manufacturing site and is a 3 mm thick consolidated laminate of TenCate Cetex® TC1100 PPS in a quasi-isotropic (QI) layup of 5 harness satin, containing a 50% FVF (see Figure 4.1a). This waste was shredded in-house using an Untha S20 low-speed two-shaft shredder with blades of 19 mm in width and no screen, for five consecutive times. The resulting flakes are shown in Figure 4.2a. A portion of the flakes was sieved with a multi-stage vibrating sieve with apertures of 2, 2.8, 4, 5.6, 8, 11.2, 16, 22.4 and 31.5

mm. Three batches were obtained: the batch denominated 'Sieved L' consists of flakes passing through the sieve with an aperture of 22.4 mm and rest on the sieve with 16 mm aperture. The batch denominated 'Sieved M', are flakes resting between the 11.2 mm and 8 mm aperture sieves and 'Sieved S' indicates a blend of flakes between the 5.6 mm and 2.8 mm aperture sieves. More information on the shredding and sieving of this material is available in studies by Vincent et al. [12, 13]. The second material was a powder-coated semipreg of 50% FVF 5 harness satin as well, but consists of a non-consolidated single layer which was cut to flakes (see Figure 4.1b and Figure 4.2b). As with the consolidated laminate, the fabric was woven with 3K yarns. The consolidated flakes were diluted with Celanese Forton® 0214 PPS pellets and the powder-coated semipreg with the same polymer in powder form to obtain a lower fibre content of 20% FVF and 35% FVF, respectively. Only for the non-mixed semipreg flakes a powder version of the polymer was used. The third material was a TenCate Cetex® TC1100 UD tape, manually cut to strands of 5 mm, 10 mm and 20 mm length by a standard paper cutter (see Figure 4.3). The last material was LUVOCOM® 1301/XCF/30 pellets of 24.4% FVF, having fibres of about 3.5 mm in length (see Figure 4.2c). Virgin continuous fibre C/PPS laminates were included for benchmarking reasons. A non-shredded laminate was tested for comparison reasons.

For modelling purposes, the FLD and BSD data of Vincent et al. [14] was used as described in Section 2.1 and 3.2.

4.2.3 *Glass fibre reinforced PP*

Three types of G/PP material are used and shown in Figure 4.4: commercially available LFT pellets, virgin Twintex® (laminate) and recycled Twintex® (flakes). All types consist of E-glass fibre with a PP matrix. The fibre content for the Twintex® was 60% by weight (35% FVF) and the LFT pellets are in two versions, 40%w (19% FVF) and 60%w (35% FVF). The material was diluted with virgin PP pellets to obtain lower fibre fractions. The commercially available LFT pellets used, are 15mm long and are widely used in injection moulding. The comingled G/PP fibres of Twintex® have a 2/2 twill pattern, an aerial weight of 1485 g/m^2 and 1870 TEX (g/km). From this data a bundle size of 2k was estimated. The Twintex® material was compression moulded according to the settings of Table 4.1to form 2 mm thick consolidated $[(0/90)]_s$ laminates. To obtain the third material type studied, the consolidated plates were processed to 15x15 mm^2 flakes by laser cutting to guarantee a consistent size distribution. Subsequently the material was cleaned with alcohol.

Table 4.1 - List of all materials used in this study

		G/PP						C/PPS					
Class	Type	length (mm)	width (mm)	thickness (mm)	FVF (%)	orientation	structure	length (mm)	width (mm)	thickness (mm)	FVF (%)	orientation	structure
Continuous fibre material													
A	Virgin consolidated plate	-	-	2	35	0/90	2/2 twill	Continu-ous	-	3	50	QI	5HS
Discontinuous fibre materials													
B	Virgin pellets	7.5, 15	ø 2-3		19, 26*, 35	UD	-	3-4	ø 3,5		24.4	UD	
C	Virgin tape							5, 10, 20	0.2		50	UD	
D	Shredded consolidated laminate							FLD's in Section 3.2.5	3		35*, 50	QI	5HS
E	Cut powder-coated semipreg							15-25	0.2		35*, 50	QI	5HS
F	Cut consolidated laminate	15	15	2	19*, 35								

*diluted to lower FVF with virgin polymer

(a) (b)

Figure 4.1 - C/PPS Consolidated (a) and semipreg (b) waste material collected at manufacturing sites

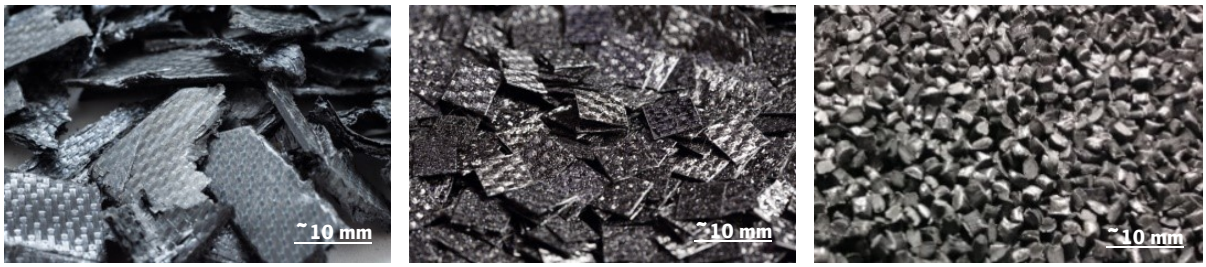

(a) (b) (c)

Figure 4.2 – C/PPS shredded consolidated laminate (a), cut woven semipreg (b) and cut UD pellets (c)

(a) (b) (c)

Figure 4.3 - C/PPS UD tape cut to 5 mm (a), 10 mm (b) and 20 mm (c) long strands

(a) (b) (c)

Figure 4.4 – G/PP consolidated laminated (a), cut consolidated flakes (b) and UD LFT pellets (c)

4.2.4 *Recycling process*

The materials in this study are processed by the three following types of manufacturing processes: low-shear mixing, DCM and stamp forming. The latter process was included for benchmarking reasons and only performed externally on virgin material of continuous fibre length (defined as "Class A" in Table 4.1). All materials with discontinuous fibre (defined as "Class B – F" in Table 4.1) were processed by low-hear mixing and referred to as mixed-materials. The recycled materials (defined as "Class D-F" in Table 4.1) were processed by DCM and are referred to as non-mixed materials. All materials including PPS were dried for a minimum of 2 h at a minimum of 100°C before processing.

4.2.5 *Low-shear mixing process*

The low-shear mixing machine described in Section 2.2.6 was used to melt and mix the material. Thereafter a piston extrudes the mixed material for further processing. The mixed dough was transferred to the centre of a 305x305 mm^2 cavity (see Figure 4.5), and compression moulded at the settings given in Table 4.2 to form plates. A distinction on well-mixed (or "good mix" - GM) material and poorly mixed (PM) material was made based on the results of the work from Vincent et al. [14] and are similar to the GM and PM materials as considered in Chapter 3. Transfer time between ejected dough and start of mould closure was timed to be typically 7 seconds.

Table 4.2 – Standard processing conditions, unless otherwise specified. PM refers to poorly mixed, GM refers to well mixed

	G/PP			C/PPS		
	Non-mixed	PM	GM	Non-mixed	PM	GM
Mixing temperature (°C)	-	230	230	-	320-360	330-360
Heating and Mixing time (min)	-	5-10	10-15	-	10-15	15-20
Mixing speed (rpm)	-	5	10-15	-	5	10-15
Heating rate (°C/min) (non-mixed)	15	-	-	15	-	-
Mould temperature (°C)	220	70-80	80	320	140-180	140
Dwell time (min)	4±1	3±1	3±1	15+15*	4±1	4±1
Moulding pressure (MPa)	0.5	4.5-20	4.5-20	1	4.5-21	4.5-21

*15 min dwell time heating, at limited pressure (<0.1 MPa), to obtain uniform temperature + 15 min dwell time under moulding pressure

4.2.6 *Direct compression moulding process*

The DCM described in Section 2.2.1 was used to form plates of non-mixed materials. The material was spread uniformly in a 250x250 mm^2 picture frame mould and was subjected to the moulding cycle as illustrated by Figure 2.8 a by using the processing conditions given in Table 4.2. Alternating layers of flakes and polymers were spread in the mould to improve the homogeneity of the sample for plates with a FVF

lower than the flake. See for several images during the DCM process and Appendix B for the processing conditions over time.

4.2.7 *Characterisation*

Materials described in Section 4.2.1 and manufactured by processes described in Section 4.2.4 are analysed by multiple types of mechanical tests and microscopical analysis. The majority of the testing was performed by flexural tests, supplemented with Charpy impact tests. Flexural tests have several advantages: simple specimen geometry and simplicity of performing the tests. No grips required and so less results need to be excluded as no specimens fail in a clamped area, as frequently happens in tensile tests. Optical microscopy and SEM are used to analyse the material structure and failure mode.

4.2.8 *Flexural test*

Two types of flexural loading geometries exist: four-point and three-point. The four-point loading geometry provides a constant bending moment between the central loading members. Therefore, the maximum stress is present over a larger section of the specimen in comparison to the punctual stress induced under the single loading member of the three-point test. Four-point is preferred because the larger section of maximum stress provides a more reliable and representative test for the non-homogeneous characteristics of discontinuous and recycled material because. Furthermore, the coinciding location of the maximum stress and the load introduction can potentially lead to undesired local stress concentrations. Thus, all flexural tests are performed under four-point ISO 14125, except for the G/PP Flakes and 35% FVF G/PP PM pellets which are tested by three-point bending test.

From the compression moulded plates, flexural and impact test specimens at a width of 25 mm were cut by diamond saw at the marked areas displayed in Figure 4.5. The thickness was 3 mm for the laminates and 3 to 5 mm for the mixed materials, except for the 50% FVF C/PPS plate, which was 7 mm thick. The edges were sanded and material was dried for several hours followed by a minimum of 12 hours on room temperature prior to testing. Four-point bending was performed according to ISO 14125 at a cross-head speed of 2 mm/min. A minimum of 5 specimens for each series was used to determine the flexural modulus and strength. The 7 mm thick plate, made of the shredded laminates, results in a major span over thickness ratio of 13.6, which was below the 16.5 prescribed by the standard. Shear effects may lead to an over prediction of mechanical properties, although no dominant shear effects were observed in the failure modes. For the continuous fibre laminates, two types of samples were tested: one with the oriented fibres of the outer layer aligned with the loading direction and one perpendicular to the loading direction. The span was according to the standard's Class II and Class III for G/PP and C/PPS material

respectively. Two types of samples were tested for the continuous fibre laminates, one with the oriented fibres of the outer layer aligned with the loading direction and one perpendicular to the loading direction.

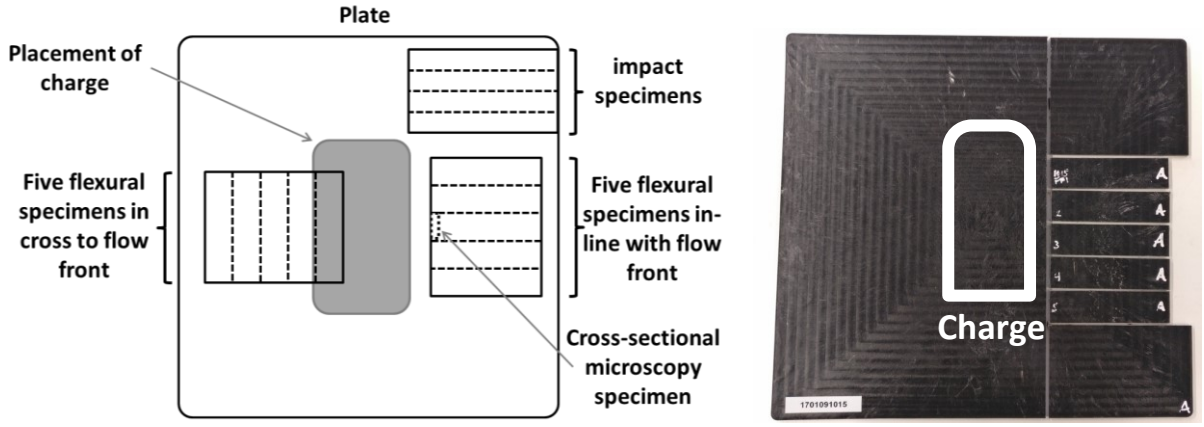

Figure 4.5 - An illustration (left) and image (right) of the plates produced by the low-shear mixing process, including an indication of the position where the charge is placed and samples for flexural and impact test within cut in-line- and cross to the flow direction and the cross-sectional microscopic sample is taken.

4.2.9 *Impact test*

Charpy impact tests were conducted in accordance with ISO 179-1e. Following the standard, a 7 J or 15 J hammer was selected dependent on the toughness of the specimen. The specimens were positioned edgewise at a support span of 20 times the thickness. Due to the long fibre reinforcement a width of 15 mm was chosen. Although the standard prescribes a number of 10 specimens per test, only 8 to 10 specimens were included for tests considering C/PPS material and 5 to 8 for tests considering G/PP material.

4.2.10 *Microscopy*

Optical microscopy analysis was performed to examine the material structure after mixing in general and the dispersion and distribution of fibres and fibre bundles in particular. Cross-sectional microscopic images were taken from the location illustrated in Figure 4.5.

To understand the failure mode and specifically study the fibre pull-out and fibre breakage, a scanning electron microscopy (SEM) was used. The SEM offers higher magnification, greater depth of field, and greater versatility than optical microscopy. The tested specimens were cut to fit inside the SEM analysis chamber. Two 5 nm conductive gold layers are deposited on the surface to be analysed by means of a Jeol JFC-1300 sputter deposition machine. Conductive tape was positioned to connect the specimen to the stub to enable discharging. The SEM analysis was performed on a Jeol JSM-6010LA machine.

4.3 Results and discussion

Flexural and impact test results are presented in this section. The outcome is presented for the materials specified in Section 4.2.1, manufactured with processes described in Section 4.2.4 and tested according to methods given in Section 4.2.8 and 4.2.9. Microscopic images were taken to visually inspect the processed materials. The results are used to study the effect of fibre fraction, fibre length, fibre orientation, degree of mixing and material structure in order to show the potential and processing window of the presented recycling route. The experimental results are compared to those ones obtained from the theoretical model for a 2D random fibre orientation of C/PPS and G/PP described in Section 3.3 and 3.4. The effect of material structure and processing method were assumed to be related to the degree of mixing and are therefore compared to the theoretically studied BSD and FVD results. An overview of Figures including all results is given in Appendix C.

4.3.1 *Influence of fibre fraction*

C/PPS

An increase in modulus and strength with the fibre fraction can be observed from Figure 4.6 and Figure 4.7, as was generally expected. At higher fibre contents, the increase of modulus along the fibre content limits off, while the strength of the poorly mixed material even declines. From Thomason [15] it is known that the mechanical properties of glass fibre composites with a high fibre aspect ratio, random orientation and a fibre content above 20% FVF level off due to fibre packing. Fibre packing limitations can result in a less homogeneous or poorly mixed material. A similar phenomenon as with G/PP will likely exist for carbon fibres, however the level at which it occurs might be different, in particular due to the smaller fibre diameter [24, 25]. The structure of woven continuous fibres enables a denser fibre packing, which is likely to contribute to the higher mechanical performance seen for *Virgin continuous fibre*. Two datapoints are given for the *Virgin continuous fibre* serie with QI layup, for the samples with a different outer ply orientation.

The experimental data is in line with the 2D random model for discontinuous fibres along the fibre content regarding overall trend and the order of magnitude of the values. The *Theory single fibre* shows the results for perfectly dispersed fibres with a FLD of the shredded material by S20 shredder. The *Theory 3K bundle 10 mm FL* version replaces the FLD of the previous stated series by a constant fibre length of 10mm and could be considered as a realistic worst-case scenario for both FLD and dispersion. The experimental results for strength are between these upper and lower bound scenarios, for modulus the *Flakes PM fall below the lower bound for the extremes of the tested FVF*. The differences between theoretical and experimental data of mixed materials is small for 20% to 26% FVF, but larger for 35% to 50% FVF. The 2D

random theory predicts, in contrary to the MROM, a nonlinear behaviour for strength at increasing fibre content, agreeing with the trend shown by the experimental data.

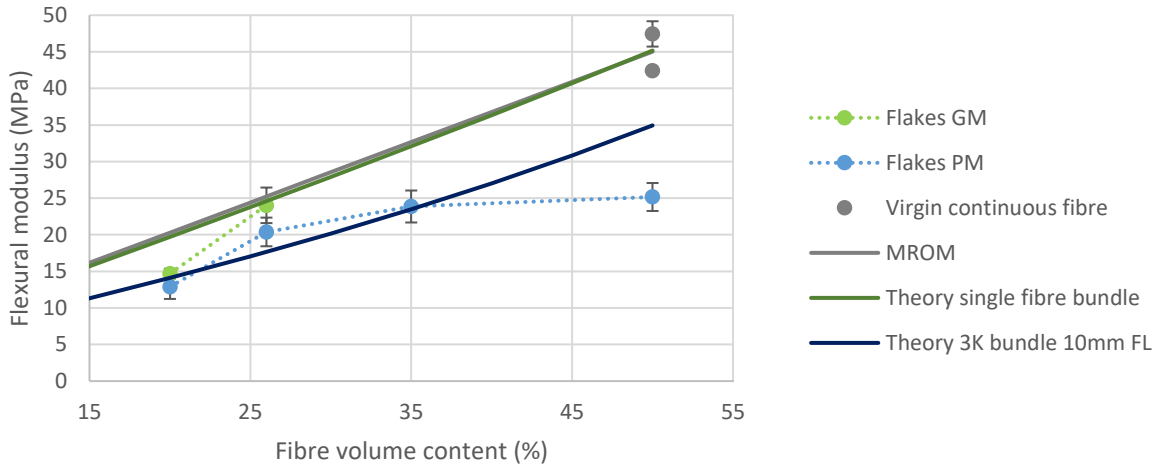

Figure 4.6 – Flexural modulus results for virgin continuous fibre materials, materials with discontinuous fibres for various structures, degrees of mixing and predictions of theoretical models. All C/PPS material. Error bars represent one SD.

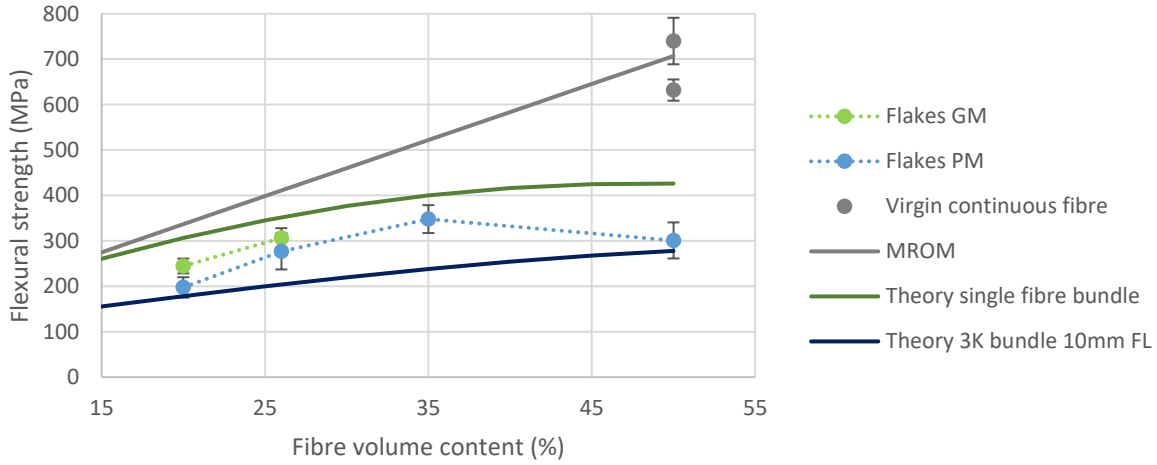

Figure 4.7 – Flexural strength results for virgin continuous fibre materials, materials with discontinuous fibres for various structures, degrees of mixing and predictions of theoretical models. All C/PPS material. Error bars represent one SD.

Cross-sectional microscopic images were taken from the location illustrated in Figure 4.5 and are presented in Figure 4.8. Black areas might be mistaken for voids, but are generally contaminations on the samples, see the enlargement in Figure 13. When comparing the mixed shredded laminates at different fibre fractions shown in Figure 4.8a and d-f, an increasing thickness is observed. At higher fibre content the mould cavity was not filled due to the increased viscosity, and since an equal volume of material was placed, the plates became thicker. Another observation is an increasing fibre bundle height for increasing fibre fraction, e.g. visible when comparing Figure 4.8a with e or f. The origin of this difference could be in the mixing and in the compression moulding step: a higher fibre fraction results in a higher viscosity and therefore reduced flow, which on its turn favours increased fibre bundle diameter.

(a) Mixed shredded laminate at 20% FVF

(b) Mixed cut semipreg at 20% FVF

(c) Mixed LFT pellets at 24,4% FVF

(d) Mixed shredded laminate at 26% FVF

(e) Mixed shredded laminate at 35% FVF

(f) Mixed shredded laminate at 50% FVF

Figure 4.8 – Cross-sectional microscopy of the processed C/PPS materials at a location shown in Figure 4.5. Black areas might be mistaken for voids, but are generally contaminations on the samples, see Figure 4.9.

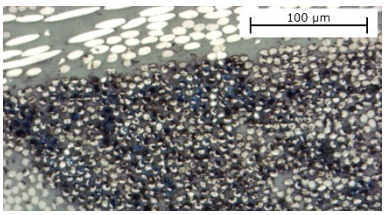

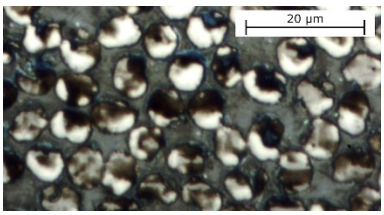

Figure 4.9 – Enlargement of the white marked area at the arrow in Figure 4.8 (f)

In the Charpy impact results in Figure 4.10, two FVFs of non-mixed semipreg and flakes are shown. The thick consolidated flakes show a decreased toughness with fibre content, while the semipreg shows an increasing toughness with FVF. The datasheet value for the C/PPS pellets of 24.4% FVF is 44 kJ/m² [17]. As a reference, 30% FVF glass filled injection moulded PPS has a Charpy impact toughness of 42 kJ/m² according to the datasheet [18].

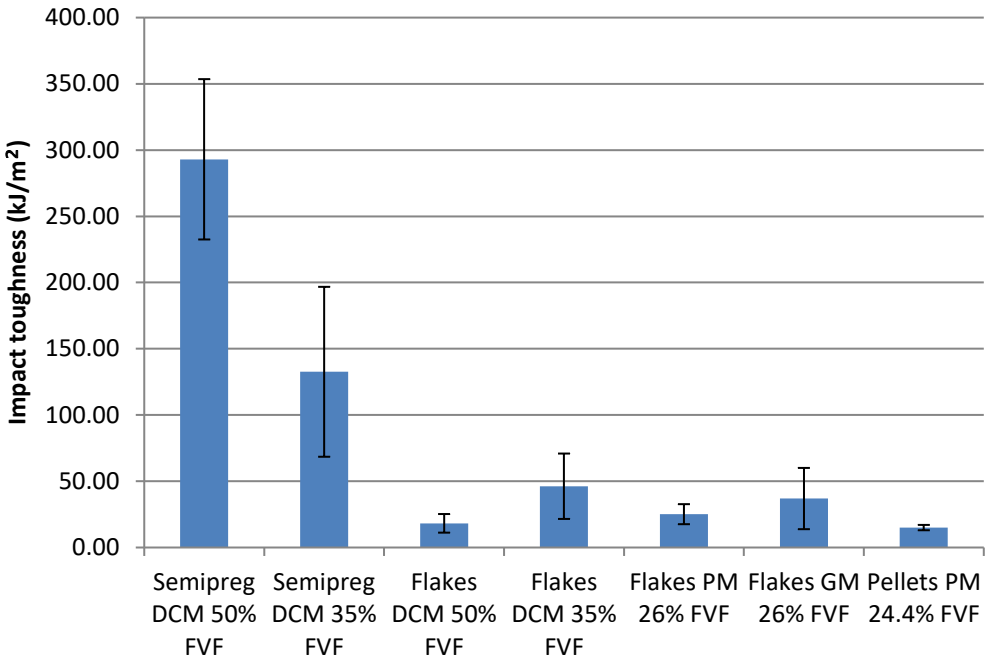

Figure 4.10 – Charpy impact toughness results for C/PPS materials with various FVF, structures and degrees of mixing. Error bars represent one SD. The datasheet value for pellets is 44 kJ/m² [17]**.**

G/PP

Results of the experimental flexural tests and theoretical models are given in Figure 4.11 and Figure 4.12 for G/PP material. As with C/PPS, an increase of modulus for higher FVF can be observed. The same is visible, too a less extent, for the strength of mixed material while the strength of the poorly mixed material even declines. The differences within the experimental data of mixed materials is small for 19%, but larger for 35% FVF. The standard deviation (SD) of poor mix materials increases at higher fibre content.

The *Theory single fibre* shows the results for perfectly dispersed fibres with a FLD of the shredded material by S20 shredder. For G/PP, the *Theory 2K bundle 15 mm FL* represents a lower bound scenario regarding a non-dispersed bundle size of the flakes, which is assumed to be 2K as described in Section 4.2.3. The constant fibre length of 15 mm is chosen since it equals the fibre length of both the cut flakes as the virgin pellets. The MROM is given as a reference. The trend of the experimental data generally follows the trend

of the 2D random model for discontinuous fibres. But, contrary to the C/PPS, there are experimental results that exceed the theoretical predicted upper bound.

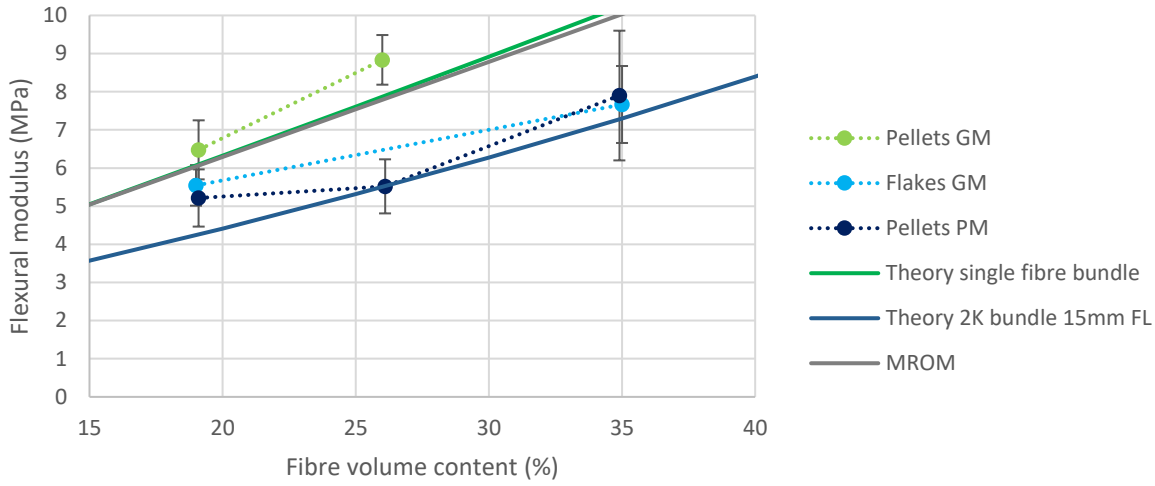

Figure 4.11 - Flexural modulus results for materials with discontinuous fibres at various degrees of mixing and predictions of theoretical models. All G/PP material. Error bars represent one SD.

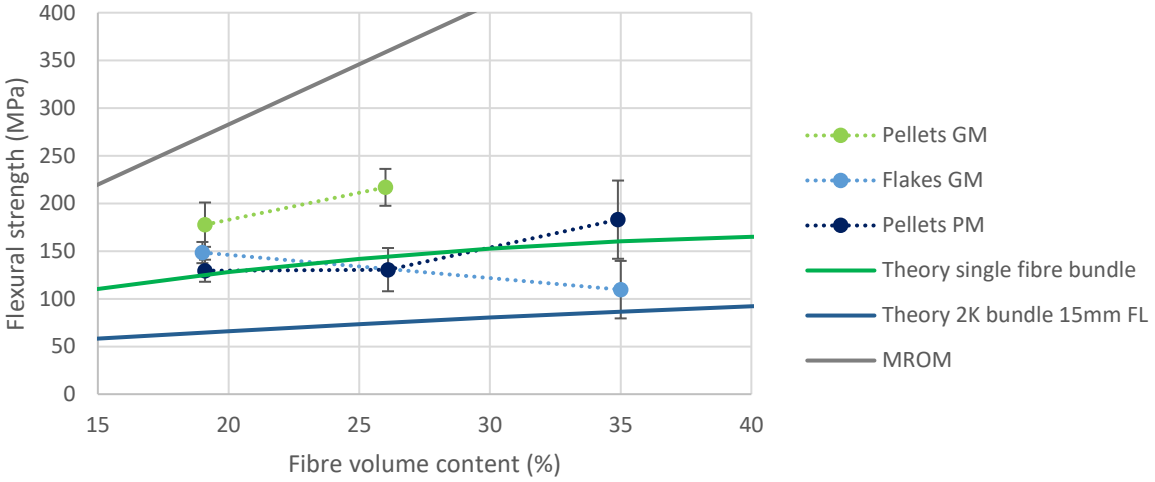

Figure 4.12 - Flexural strength results for materials with discontinuous fibres for various degrees of mixing and predictions of theoretical models. All G/PP material. Error bars represent one SD.

Charpy impact toughness results for various FVF and materials is shown in Figure 4.13. Like with modulus and strength, also impact toughness increases with FVF. The standard deviation is large, especially for the flake material. For any FVF, the flakes show a lower impact toughness compared to pellets.

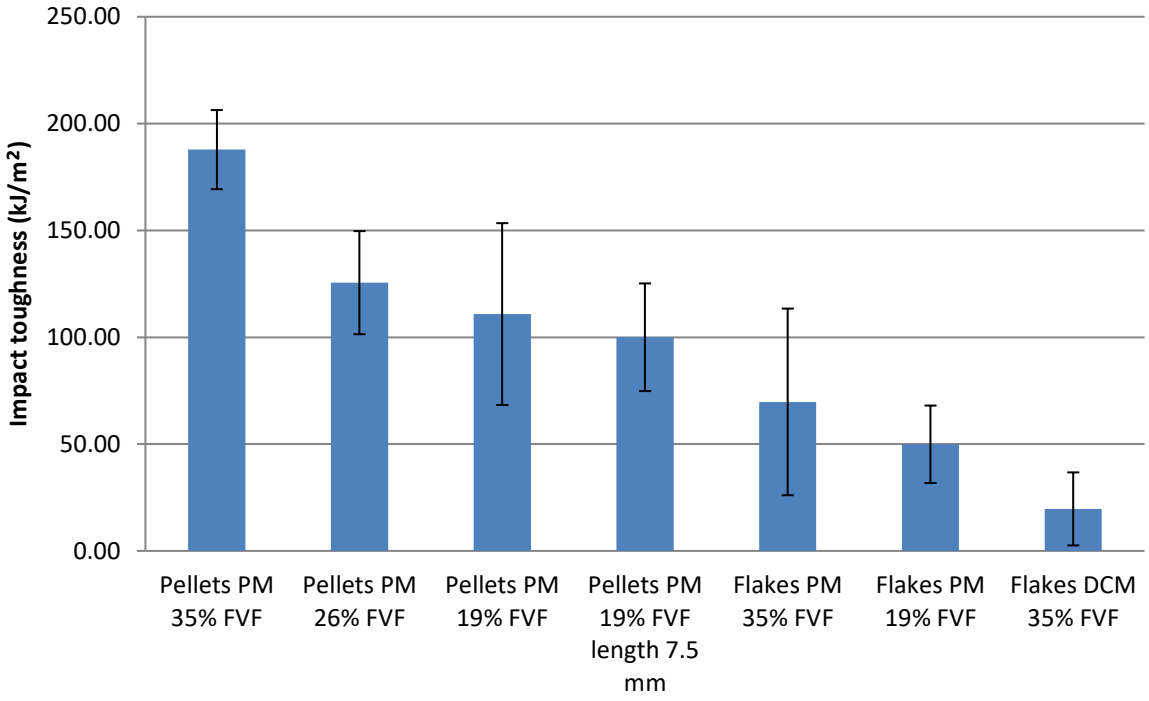

Figure 4.13 – Charpy impact toughness results for G/PP materials with various FVF, structure and fibre length. Error bars represent one SD. The datasheet value for 35% FVF Twintex® continuous woven fibre is 160 kJ/m² [19]**.**

4.3.2 *Influence of fibre length*

C/PPS

Experimental results and theoretical predictions of the influence of fibre length on the flexural modulus and strength is given in Figure 4.14 and Figure 4.15, respectively. All materials in the experimental work contain a fibre length above 5 times the critical fibre length (Table 4.1). The micromechanical model predicts a plateau for both modulus and strength above 5 times the critical fibre length, although the modulus reaches the plateau at a shorter fibre length (Section 3.3.1). As only limited amount of plates are tested and a large CoV (between 10 and 20%) makes it hard to conclude relations, the strength and modulus seem to be maximum at fibre lengths of about 10 to 15mm. For 5 and 10 mm fibre length the modulus for the UD tape is similar, but the strength increases (10%) on the interval. This could potentially be related to the later increase for strength already seen in theory, only at a longer fibre length due to bundle effects. For longer fibre lengths, both modulus and strength decrease for the sieved shredded flakes and UD tape. This could potentially be related to the decreasing mixing quality at long fibres lengths as is noted in Section 3.5.1. Another explanation could be found in the statistical effect known as weakest link theory, see Section 3.5.2. The theoretical predictions showed similar results for constant fibre lengths larger than 5 mm and the shredded flakes including a FLD (Section 3.4.1). One could speculate about the influence of the shape of the FLD on the mixing quality and therefore the formation of BSD. This could be

investigated by a study similar to that carried out by Vincent et al.[14] but would require an extensive and time-consuming analysis of cross-sectional microscopy observations.

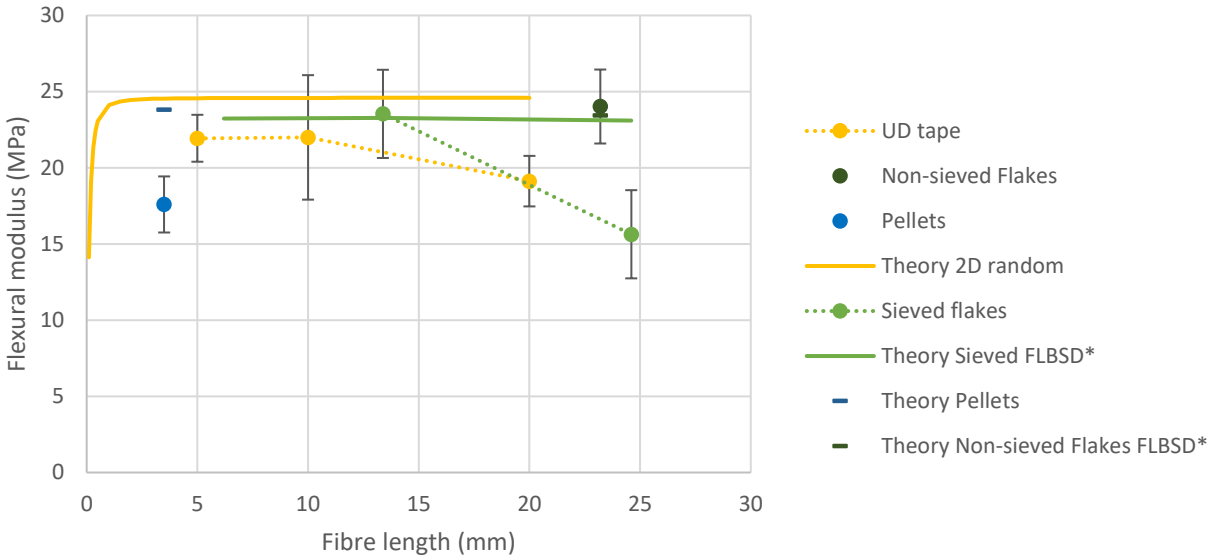

Figure 4.14 - Flexural modulus of mixed C/PPS at 26% FVF and various fibre lengths. Error bars represent one SD.

*) These results are computed with a FLD and are plotted at the average fibre length of the distribution. The Pellets of 24.4% FVF are normalised to 26% FVF. All materials were made with GM settings, except for the Pellets, which were PM.

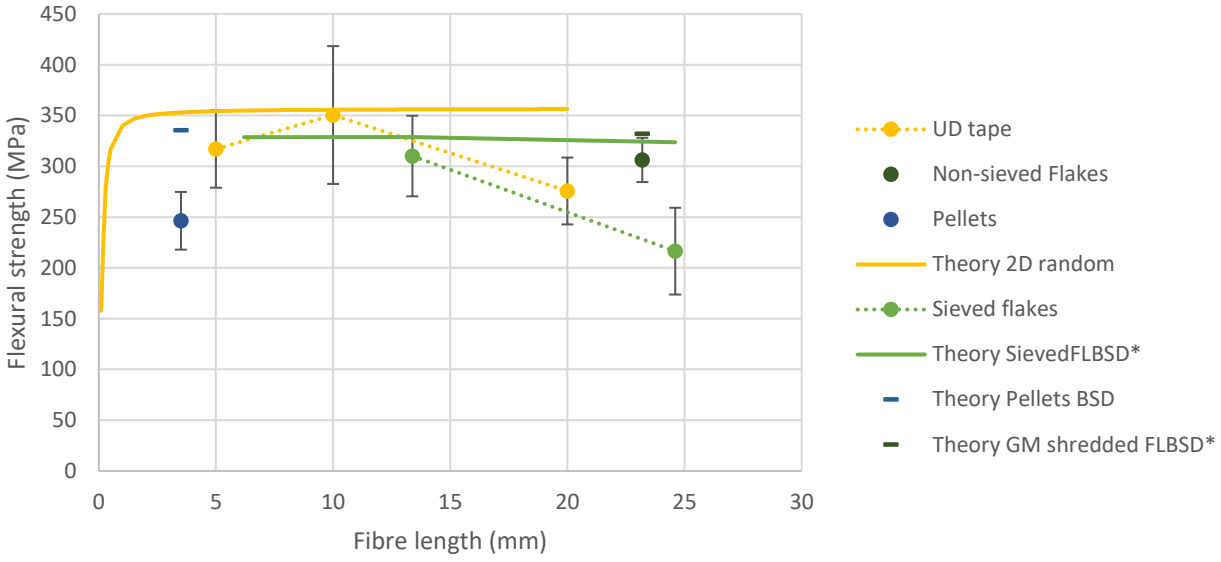

Figure 4.15 - Flexural strength of mixed C/PPS materials at 26% FVF and various fibre lengths. Error bars represent one SD.

*) These results are computed with a FLD and are plotted at the average fibre length of the distribution. The Pellets of 24.4% FVF are normalised to 26% FVF. All materials were made with GM settings, except for the Pellets, which were PM.

G/PP

Figure 4.16 shows the experimental and theoretical results for flexural modulus and strength for various fibre lengths. Both glass fibre lengths (15 and 7.5mm) used in the experimental work are on the theoretical predicted modulus and strength plateau, as is also the case for C/PPS. As predicted, the experimental results are similar for both used fibre lengths, but exceed the curves generated by the model to a far extent.

The impact results in Figure 4.13 show a very similar trend as stiffness and strength for fibre fraction, but slightly different for fibre length. Although the statistical analysis did not indicate a difference, the mean impact energy for a fibre length of 15 mm is slightly higher than for 7.5 mm. A larger influence of fibre length on impact in respect to modulus and strength is in agreement with that found by Thomason et al, describing that the influence of fibre lengths limits out at a longer length compared to stiffness and strength (see also Figure 2.1) [20].

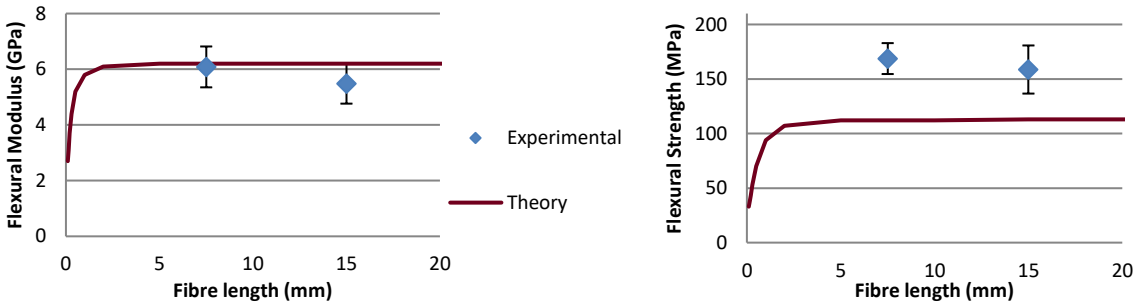

Figure 4.16 – Influence of the fibre length on the flexural modulus (left) and strength (right) of poorly mixed G/PP material at 26% FVF. The line represents the 2D random model described in Chapter 3. Error bars represent one SD.

4.3.3 *Influence of fibre orientation*

It is known that LFT compression moulding can generate flow induced fibre orientation anisotropic properties as a result [21]. A limited number of specimens, specimens oriented in flow and cross flow directions were tested to study the influence of this phenomena for C/PPS and G/PP. Five flexural specimens in each direction were cut as is illustrated in Figure 4.5. The C/PPS results are given together with theoretical predictions for UD, highly oriented and 2D random fibre orientation (see Section 3.3.3) in Figure 4.17 and Figure 4.18. Compared to the 2D random model, the experimental results perform slightly lower. The experimental results show a lower modulus (31%) and strength (17%) for the cross-flow direction in respect to the in-line flow. The standard deviation (SD) and CoV are similar. The results for G/PP are alike, although the difference between in-line and cross flow were very similar (28%) and fall in between the differences seen for C/PPS. The standard deviation of the G/PP results was however larger for the

cross-flow samples, compared to the in-flow samples. All other samples, and therefore also all other results presented in this thesis, were tested in the in-flow direction only, to save time. In-flow is chosen since the maximum loaded section of the specimens have a similar distance to the charge. For applications, the mould filling should preferably be chosen such that material flow is in the load orientation, e.g. by charge location and mould design. Note that the performed test is a flexural test and therefore the maximum stress is located at the upper and lower surface of the specimen.

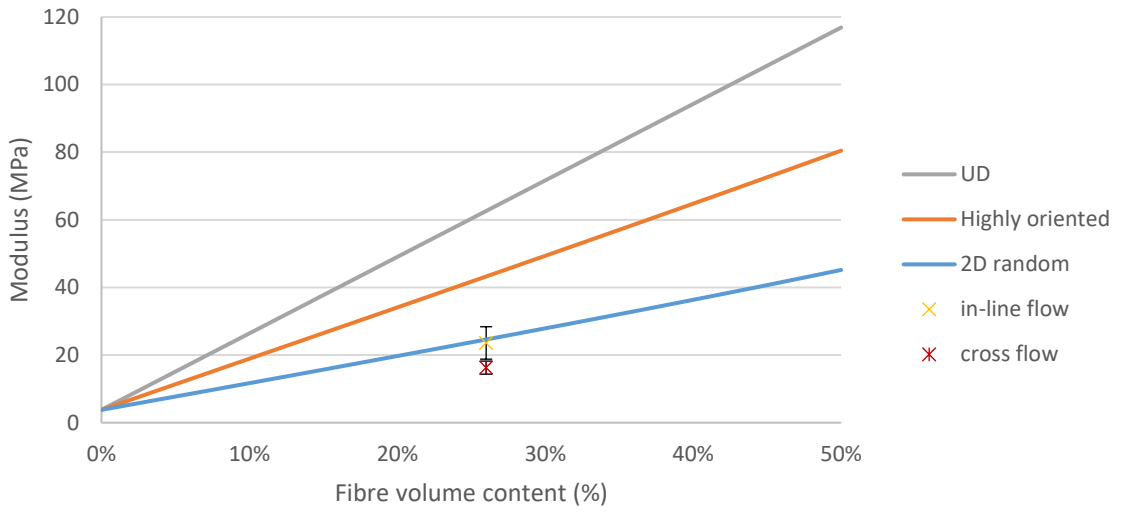

Figure 4.17 - Flexural modulus results for C/PPS with discontinuous fibres at various specimen orientation and predictions of theoretical models for various fibre orientation at 10 mm fibre length. Error bars represent one SD.

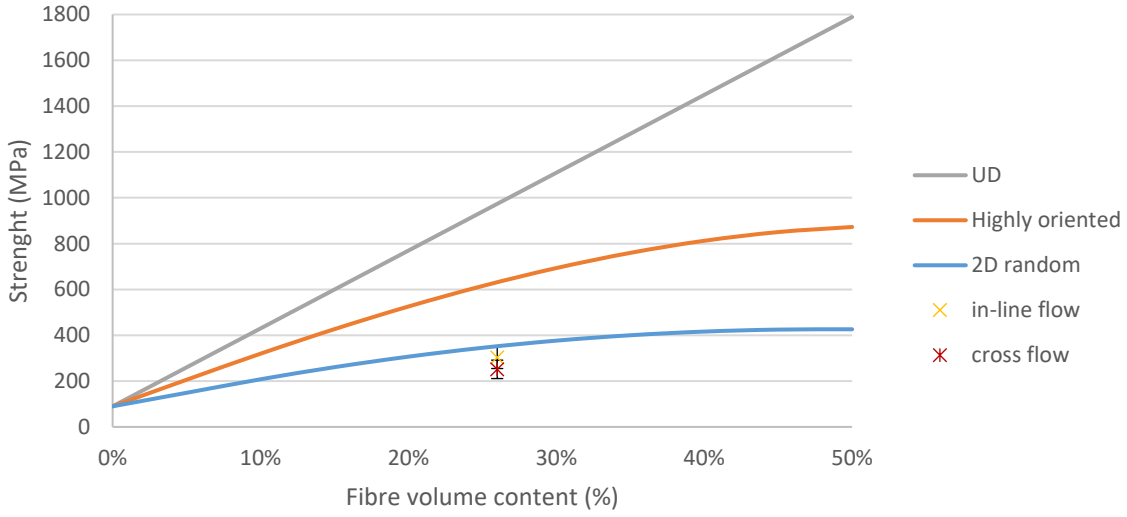

Figure 4.18 - Flexural strength results for C/PPS with discontinuous fibres at various specimen orientation and predictions of theoretical models for various fibre orientation at 10 mm fibre length. Error bars represent one SD.

4.3.4 *Influence of mixing process*

C/PPS

Experimental results regarding flexural modulus and strength of material that is processed by DCM and low-shear mixing at PM and GM settings are given in Figure 4.19 and Figure 4.20 respectively. The good mix material outperforms the poor mix material by 10-25% on modulus and strength. The variation for strength of good mix material (CoV = 7%) is also considerably better compared to the poor mix material (CoV = 11% and 14%) for a FVF of 20% and 26%.

Relevant results of the theoretical model of Chapter 3 are included. The *Theory single fibre* shows the results for perfectly dispersed fibres with a FLD of the shredded material by S20 shredder, representing an upper limit. The C/PPS *Theory 3K bundle S20 FLD* is based on the same FLD, but under lower bound dispersion, assuming all fibres to be in 3K bundles. The *10 mm FL* version is equal, but with a constant fibre length of 10mm and represents a realistic lower bound scenario for both FLD and dispersion. The *Theory GM FLBSD* and *PM FLBSD* are calculated using the FLD and BSD of GM and PM shredded material and should therefore be the closest to the experimental *GM flakes* and *PM flakes* results. The MROM is given as a reference.

The experimental data show the same trend and order of magnitude as the theoretical predictions, although the theoretical model overpredicts the results slightly. All mixed experimental results generally fall in between the upper bound given by the theoretical model of single fibres and lower bound of 3K bundles at 10mm fibre length for a FVF of 20-35%. The 3k bundle S20 FLD predictions are a more realistic lower bound scenario for the mixed materials since the appropriate FLD is used. The theoretical model including FLBSD at 20% and 26% FVF predicted a 6% higher modulus and 9% higher strength for GM material in comparison to PM material.

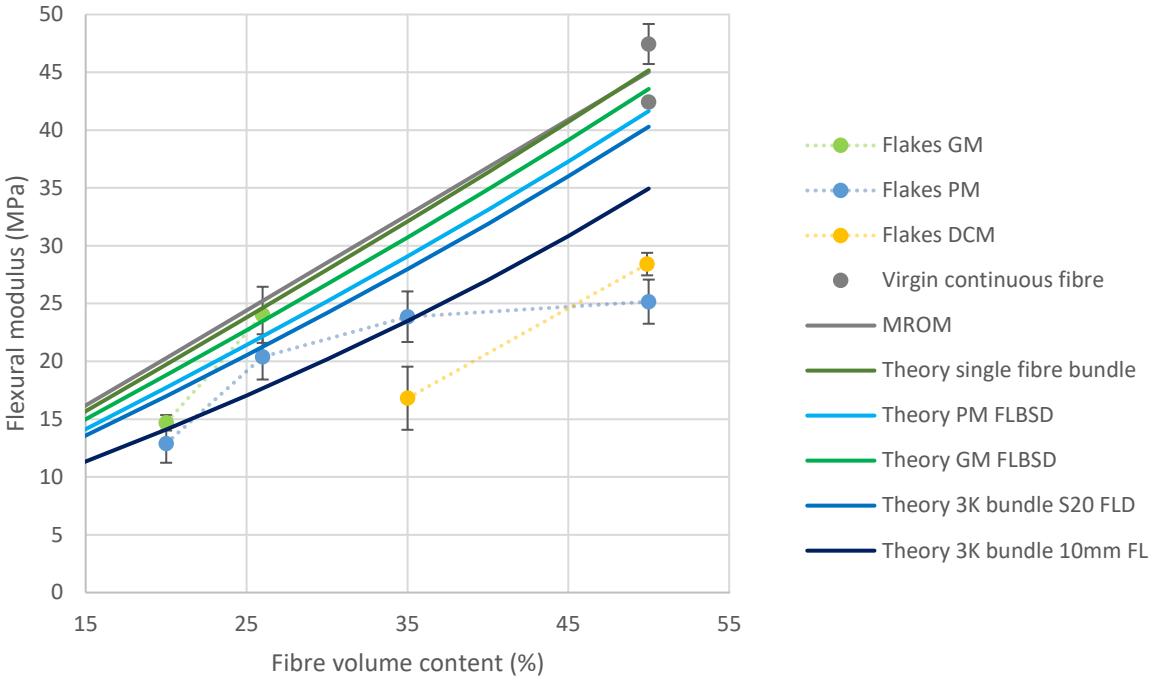

Figure 4.19 – Flexural modulus results for virgin continuous fibre materials, materials with discontinuous fibres for various structures, degrees of mixing and predictions of theoretical models. All C/PPS material. Error bars represent one SD.

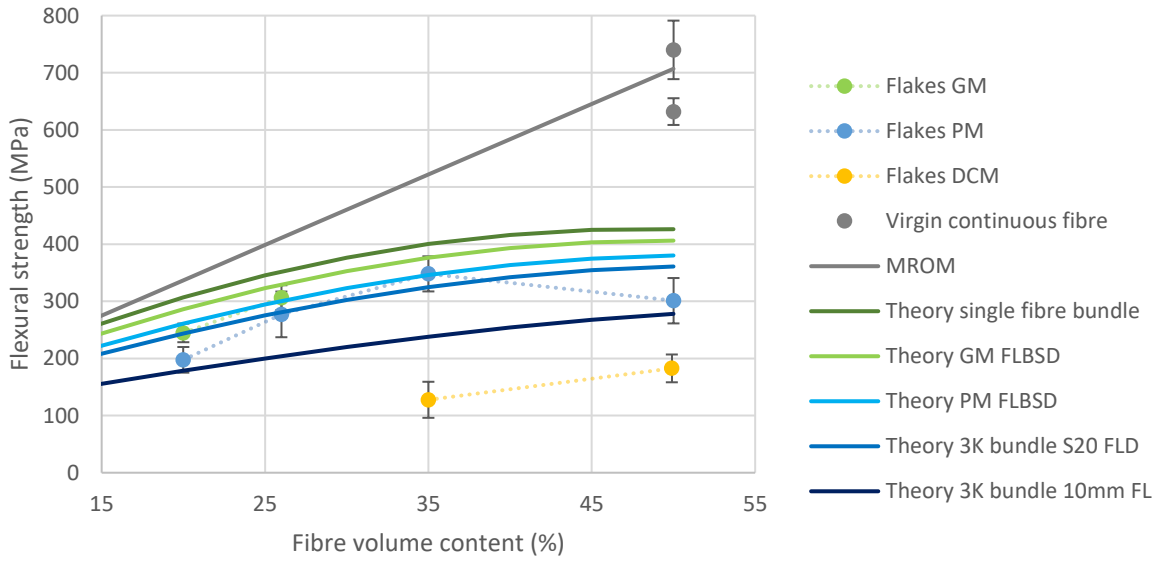

Figure 4.20 – Flexural strength results for virgin continuous fibre materials, materials with discontinuous fibres for various structures, degrees of mixing and predictions of theoretical models. All C/PPS material. Error bars represent one SD.

The flakes processed by DCM contain show a lower stiffness and strength compare to the mixed materials, with an exception for the modulus of 50% FVF, where the DCM processed material presents a higher stiffness than PM material. Especially the strength at 35%FVF is lower and the COV is generally higher

compared to the mixed materials. The plates produced from mixed material at 35% and 50% FVF where not completely filled, indicating a high viscosity. Other studies underline that mixed materials can be properly processed until 26%FVF and that above this fibre concentration especially strength levels can decline due to, among others, fibre-fibre interaction [15, 22]. For DCM it is difficult to blend in polymer material since only limit flow induce mixing exist which does not result in a homogenous material, potentially resulting in jamming of flakes and resin-rich areas resulting in lower strength values [1, 23].

As mentioned in the State of the Art (Section 2.2) multiple processing techniques are proposed for recycling C/PPS. These are ordered by increasing induced shear: DCM, low-shear mixing followed by compression moulding and extrusion by an LFT compounder followed by compression moulding. However, the low-shear mixing results in a modulus of 24GPa and a flexural strength of 348MPa at 35% FVF (see Figure 4.19 and Figure 4.20). A regrind study by Janney et al. using an LFT compounder, gives a modulus of 16 to 22 GPa and a flexural strength of 190 to 240 MPa at 34% FVF [24]. So, the low-shear mixing offers a higher value especially for strength. This might be related to the level of shear in the processing and therefor the fibre length in the tested specimens. The higher shear of the LFT compounder might result in a lower fibre length and therefore lower values, especially for strength. However, further study is necessary to investigate such hypothesis.

It can be seen that DCM allows using higher fibre contents and therefore also achieving higher moduli, possibly due to compact packing of fibre bundles. But the discontinuous structure obtained might result in more reduced strength levels [23]. Mixing, on the other hand, seems to limit the fibre content and therefore modulus, due to fibre packing problems. However, the strength is increased by the more homogeneous material structure. Nonetheless, mixing at high shear rates leads to reduced fibre lengths and therefore a strength reduction [25]. Further research is necessary to study the influence of processing in general and fibre length in particular.

G/PP

Looking at the mechanical properties of G/PP composite samples (Figure 4.21 and Figure 4.22), mixed samples perform consistently better than the non-mixed material for both flexural stiffness (24-60%) and strength (37-66%).

For G/PP the constant fibre length of 15 mm is chosen since it equals the fibre length of both the cut flakes as the virgin pellets. For G/PP, the *Theory 2K bundle 15 mm FL* represents a lower bound scenario regarding a non-dispersed bundle size of the flakes, which is assumed to be 2K as described in Section 4.2.3.

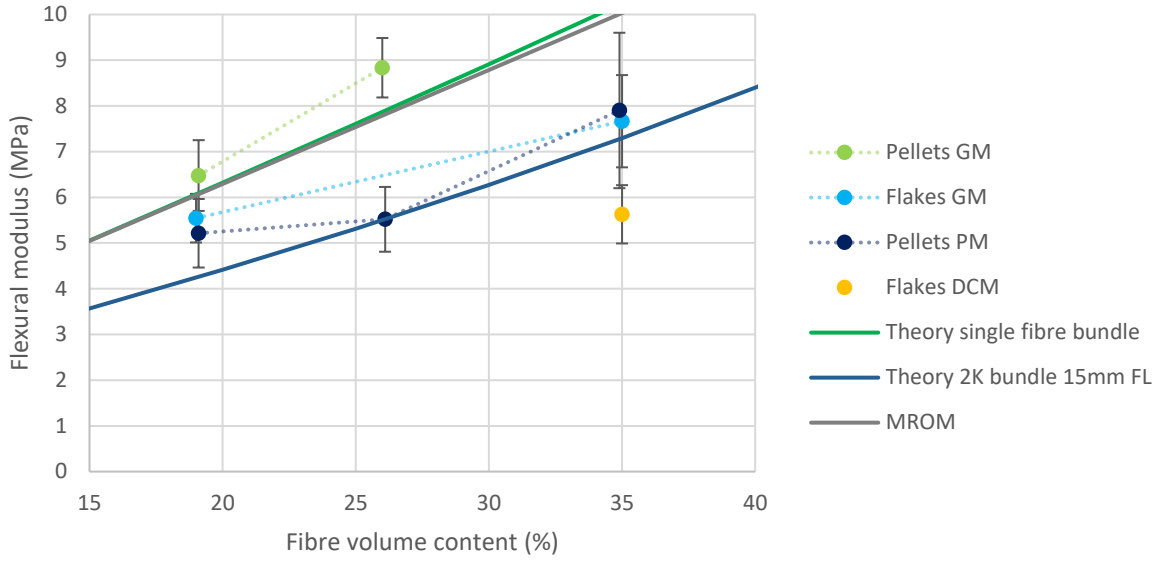

Figure 4.21 - Flexural modulus results for materials with discontinuous fibres at various degrees of mixing and predictions of theoretical models. All G/PP material. Error bars represent one SD.

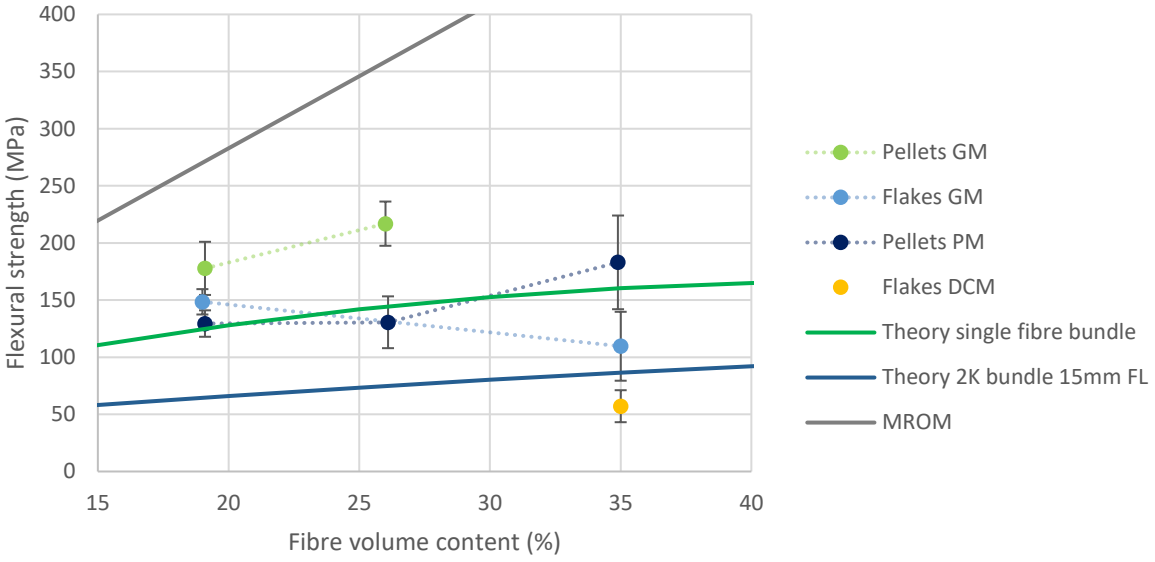

Figure 4.22 - Flexural strength results for materials with discontinuous fibres for various degrees of mixing and predictions of theoretical models. All G/PP material. Error bars represent one SD.

Correspondingly, the microscopic analysis shows a more homogenous distribution of fibres for the mixing process when comparing non-mixed (Figure 4.23) and mixed (Figure 4.24 and Figure 4.25) materials. Also, the void content illustrates that mixing results in an improved quality of the composite. Resin rich areas in non-mixed material can be seen in Figure 4.23. Fracture occurs in a matrix dominated section without fibres present to transfer the load. This weak spot is amplified by multiple flake edges, which result in stress concentrations limiting the material's strength values.

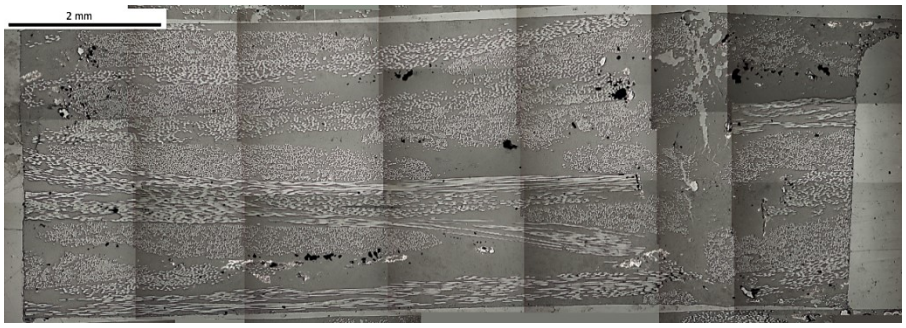

Figure 4.23- Cross section of compression moulded non-mixed flake material including a fracture area.

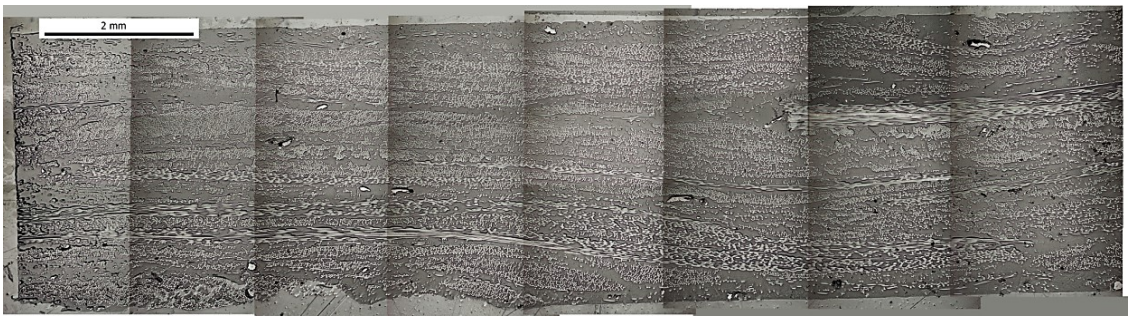

Figure 4.24 - Cross section showing the centre of a compression moulded mixed flake plate with 35%v fibre content.

Figure 4.25 - Cross section showing the edge of a compression moulded mixed pellet plate with 35%v fibre content.

The impact results for G/PP material processed by DCM, PM and GM are presented in Figure 4.26. The DCM process gives a result that is less than a third of the mixed material and also shows a very high COV. The pellets diluted with additional matrix show a lower toughness compared to non-diluted material with equal FVF. Pellets mixed at GM settings present a higher toughness and lower COV compared the pellets mixed at PM settings. So, when more mixing is involved, the toughness is higher for these samples.

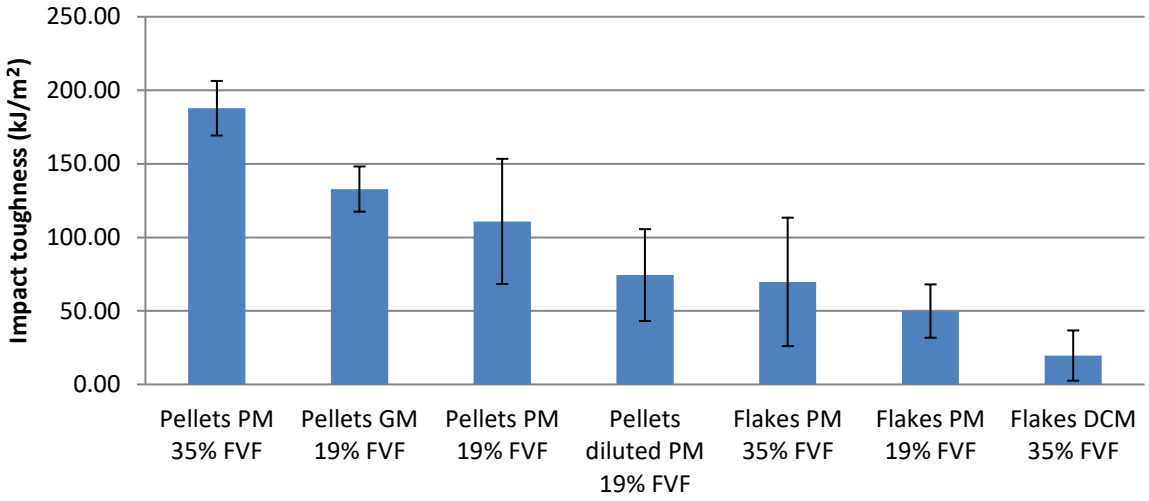

Figure 4.26 – Charpy impact toughness results for G/PP materials with various FVF, structure and degrees of mixing. Error bars represent one SD. The datasheet value for 35% FVF Twintex® continuous woven fibre is 160 kJ/m² [19]**.**

4.3.5 *Influence of input material structure*

C/PPS

To study the influence of material structures on the mechanical properties four material types were processed and tested (see Figure 4.27 and Figure 4.28 for modulus and strength results). Although the structure of the input materials is very different, the plates made by mixing of cutted semipreg and shredded laminate of 20% FVF have very similar properties, which are also in line with the pellet material.

From the cross-sectional micrographs depicted in Figure 4.8 a-c, the mixed shredded laminate and mixed cut semipreg look rather similar, while mixed pellets present a higher level of dispersion. This could be related to the unidirectional structure of the pellets, in which the fibres are not restricted by an entangled woven structure thus making fibre dispersion easier. Additionally, the limited fibre length could facilitate fibre movement, as studied by Thattaiparthasarthy et al. [26]. However, the plates fabricated with pellets tend to warp more, likely as a result of flow-induced fibre orientation which is less constrained by the short fibre length and UD structure.

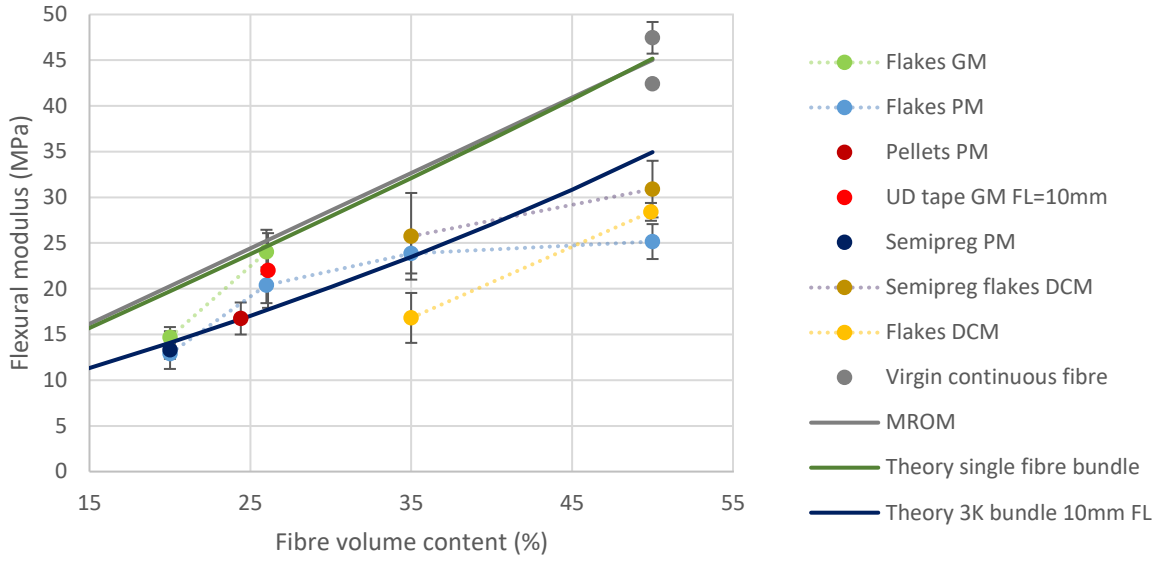

Figure 4.27 – The influence of input material structure on the flexural modulus is shown by including virgin continuous fibre materials, materials with discontinuous fibres for various structures, degrees of mixing and predictions of theoretical models. The virgin continuous fibre results are for a QI layup with a different outer ply orientation. All C/PPS material. Error bars represent one SD.

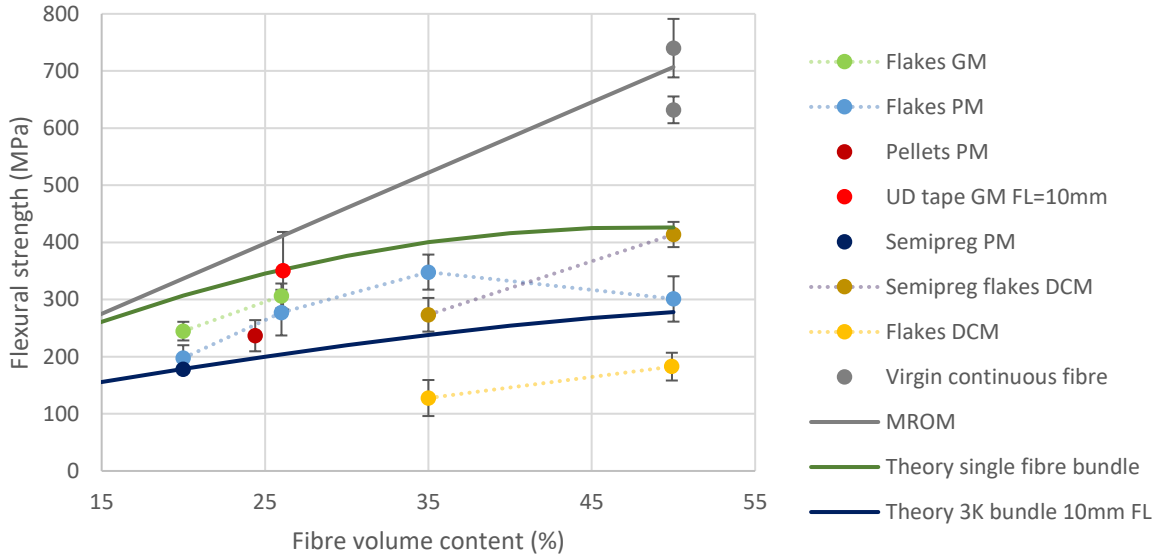

Figure 4.28 – The influence of input material structure on the flexural strength is shown by including virgin continuous fibre materials, materials with discontinuous fibres for various structures, degrees of mixing and predictions of theoretical models. The virgin continuous fibre results are for a QI layup with a different outer ply orientation. All C/PPS material. Error bars represent one SD.

For the non-mixed materials there is a clear distinction between the single-layered semipreg material and the multi-layered consolidated material. The first outperforms the latter on both stiffness (25%) and strength (122%). The poor performance of the multi-layered consolidated material might be linked to the

large thickness of the flakes (3 mm) in relation to the compression moulded plate (3.4 mm for 35% FVF and 3.7mm for 50% FVF). For semipreg this ratio is much smaller with a flake thickness of 0.2 mm and a compression moulded plate of 2.1 mm for 35% FVF and 2.3 mm for 35% FVF. This thickness ratio indicates a short path of tortuosity which is related to a poor strength by Rasheed et al. [23] and Selezneva et al. [27], see Figure 4.29.

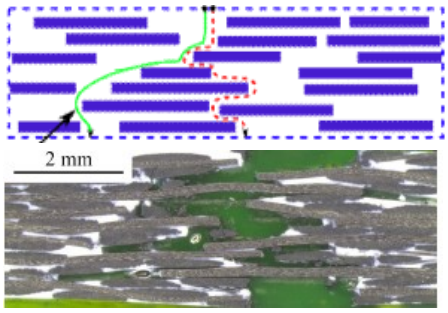

Figure 4.29 – Indication of the path of tortuosity with a hypothetical crack emanating from the top surface progressing in dashed or solid path (top) crack path leading to failure through flake pull out (interface failure) analogous to the dashed path in (bottom) [23]**.**

The virgin laminated material performs in line with the MROM and slightly lower compared to the datasheet values [28]. The orientation of the outermost layer, aligned with or perpendicular to the loading direction, is resulting in higher or lower measured properties, respectively. The virgin laminates outperform the mixed materials on stiffness and strength. Where the mechanical properties for mixed materials levels off out at high fibre fractions, the laminate with a structured fibre bundle pattern does not show such effects at 50% FVF. However, the design freedom when using mixed materials can enhance a part's performance due to geometric stiffening.

G/PP

For G/PP, the Twintex® flakes differ by their woven structure from the pellets. Also, the level of consolidation is different. In contrast to the flakes, the pellets are missing both the comingled structure of the base material and a pre-impregnation step as a beneficial side-effect of recycled material. The good mixed flakes perform show lower flexural modulus and strength values compared to good mixed pellets and are similar to the poor mixed pellets, see Figure 4.21 and Figure 4.22.

Images of mixed flakes (Figure 4.24) and pellets (Figure 4.25) show that the type of material has little influence on the general mixing result, a similar mixing quality is observed, although in Figure 4.25 a single poorly impregnated pellet is visible. These samples were made at poorly mixing settings: a mixing speed of 5 RPM and a heating and mixing time of 10 min.

Regarding the impact toughness given in Figure 4.26, a large difference is observed between the pellets and the flake material. The first showing a value which is more than twice as high as the latter.

4.3.6 *Failure mode*

The fracture surfaces of tensile tested specimens were studied by SEM to evaluate the failure mode. Specimens of plates produced at PM and GM settings were prepared according to the procedure described in Section 4.2.10. In Figure 2.2, a pulled-out fibre bundle can be observed in a post-mortem poorly mixed specimen. This gives an indication that the modification of the shear lag theory by replacing the fibre diameter by the diameter of bundles could be valid. Bundle pull-out is also observed by Pimenta [29]. The fracture surface of a GM C/PPS specimen is given in Figure 4.31. A higher level of fibre dispersion is visible for this GM material. Signs of single fibre pull-out can be observed by the long single fibres and holes (blue) and indication for fibre failure at the fracture surface is visible by short fibre ends (red).

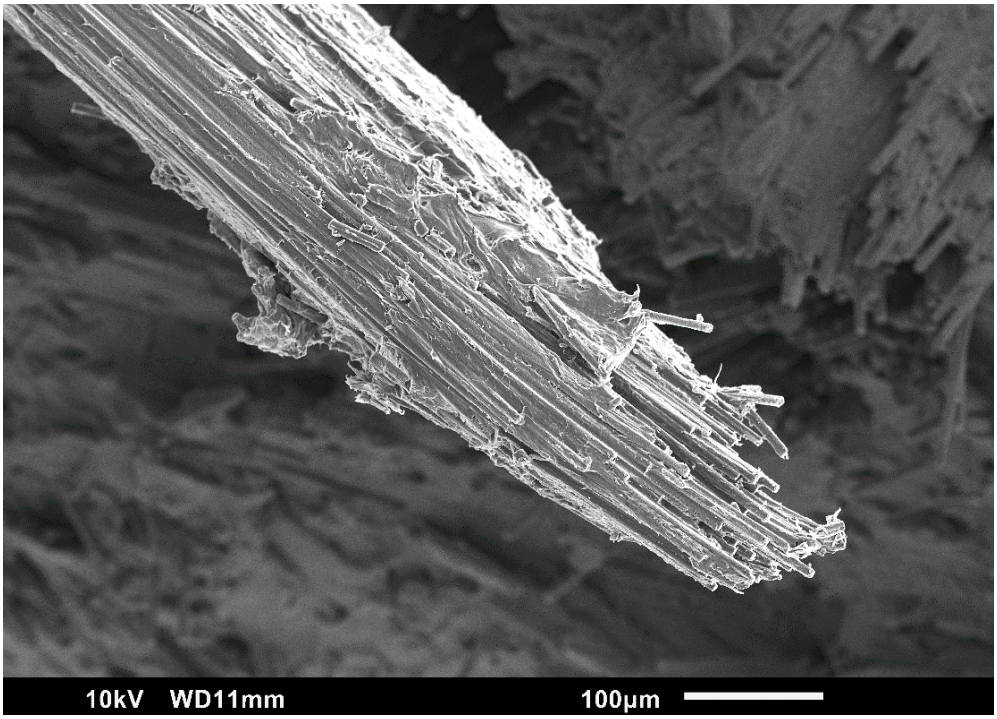

Figure 4.30 - SEM image of the fracture surface of a tensile tested specimen of PM C/PPS material showing a large bundle

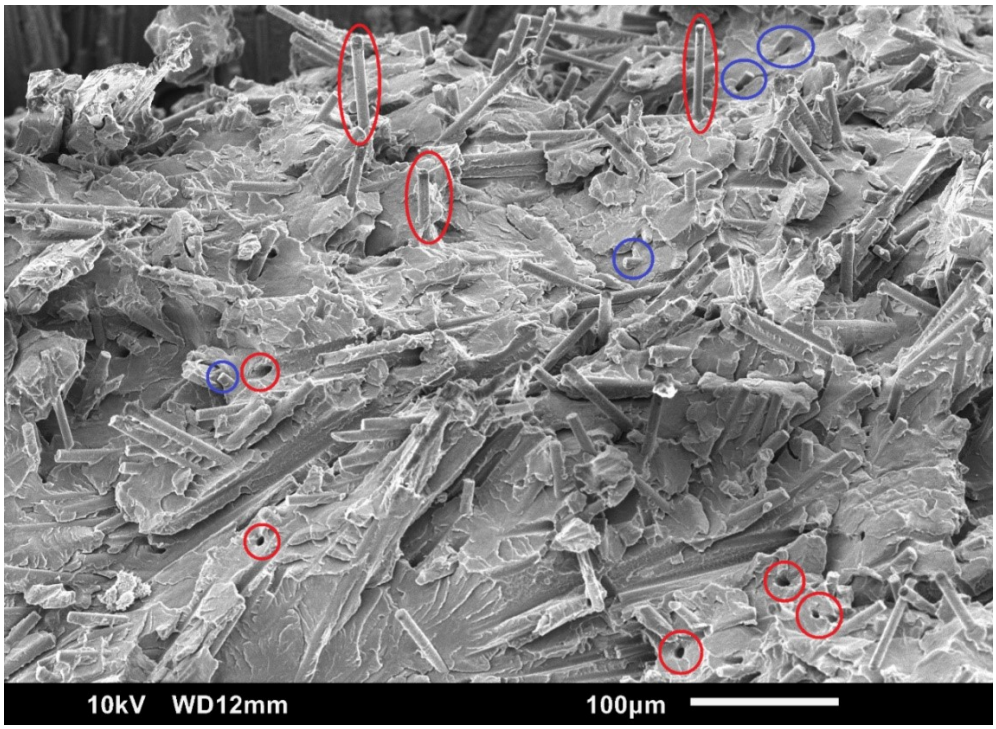

Figure 4.31 – SEM image of the fracture surface from a tensile tested GM C/PPS specimen. Long single fibre and holes are indicating a fibre pulled-out mechanism and are highlighted in red. Short fibres indicate fibre failure at the fracture surface and are highlighted in blue.

4.4 Conclusion

The recycling of C/PPS and G/PP was experimentally studied using both a direct compression moulding and a low-shear mixing process to retain the fibre length and thus mechanical properties. Flakes and pellets of various FVF, fibre length and structure were processed without mixing and at multiple mixing qualities to form plates. Specimens were cut for flexural and Charpy impact testing. The influence of FVF, fibre length, fibre orientation, mixing and material structure were analysed and compared to theoretical predictions of Chapter 3.

Overall, flexural modulus and strength increase with fibre content, at a rate similar to that predicted by analytical models. The strength of mixed materials levels off above 35% FVF are in agreement with theory. Non-mixed materials can be processed at higher FVF compared to mixed materials. The results show a smaller influence of fibre length on the modulus and strength, with slightly lower values below 5 mm and above 13 mm fibre length. All materials have a fibre length far above five times the critical fibre length and therefore the value predicted theoretically is constant. Test specimens cut in-line with material flow

show slightly higher properties compared to specimens cut in cross-flow direction and are close to theoretical predictions for 2D random orientation.

The modulus and strength of non-mixed materials is lower than mixed materials when normalised for FVF. Poorly mixed materials show consistently lower values than materials processed at good mixing setting. Differences due to mixing are larger for strength than for modulus. Results are in good agreement with theory. Experimental modulus and strength results for C/PPS are well in between the lower bound and upper bound scenarios predicted by theory. For G/PP material, the theory underpredicts especially the strength.

The structure of the input material shows a strong influence for non-mixed material compared to mixed materials: results for thick consolidated C/PPS material are lower compared to thinner semipreg material when processed by direct compression moulding, but similar when mixing is involved. Particularly the strength of non-mixed consolidated material is low.

Mixing results in a more homogeneous material, is less sensitive to material input and shows shorter cycle times. No significant difficulties were found during processing, underlining the robustness of the process studied.

4.5 References

[1] M. I. Abdul Rasheed, "Compression molding of chopped woven thermoplastic composite flakes: a study on processing and performance," PhD Thesis, University of Twente, Enschede, The Netherlands, 2016.

[2] M. Roux, N. Eguémann, C. Dransfeld, F. Thiébaud, and D. Perreux, "Thermoplastic carbon fibre-reinforced polymer recycling with electrodynamical fragmentation: From cradle to cradle," *J. Thermoplast. Compos. Mater.*, 2015, doi: 10.1177/0892705715599431.

[3] T. A. De Bruijn, G. A. Vincent, and F. W. J. Van Hattum, "Recycling of long fibre thermoplastic composites by low shear mixing," in *SAMPE Europe*, 2016, pp. 540–546.

[4] T. A. De Bruijn, G. Vincent, and F. W. J. Van Hattum, "Recycling C/PPS laminates into long fibre thermoplastic composites by low shear mixing," in *Proceedings of the 21th Internatinoal Conference on Composite Materials ICCM21*, 2017.

[5] S. G. Advani and C. L. Tucker III, "The Use of Tensors to Describe and Predict Fiber Orientation in Short Fiber Composites," *J. Rheol. (N. Y. N. Y).*, vol. 31, no. 8, pp. 751–784, 1987, doi: 10.1122/1.549945.

[6] J. Cintra and C. Tucker III, "Orthotropic closure approximations for flow-induced fiber orientation," *J. Rheol. (N. Y. N. Y).*, no. 39(6), pp. 1095–122, 1995.

[7] F. W. J. Van Hattum and C. A. Bernardo, "A model to predict the strength of short fiber composites," *Polym. Compos.*, vol. 20, no. 4, pp. 524–533, 1999, doi: 10.1002/pc.10376.

[8] F. W. J. Van Hattum, J. P. Nunes, and C. a. Bernardo, "A theoretical and experimental study of new towpreg-based long fibre thermoplastic composites," *Compos. Part A Appl. Sci. Manuf.*, vol. 36, pp. 25–32, 2005, doi: 10.1016/j.compositesa.2004.06.031.

[9] L. E. Nielsen, *Mechanical properties of polymers and composites vol. 2.* New York, 1974.

[10] J. Sloan, G. Gardiner, and M. Favaloro, "Webinar: Thermoplastic Composites in Aerospace Parts and Structures," *CompositesWorld*, 2019. [Online]. Available: https://www.compositesworld.com/events/details/41eef0b7-4495-492b-bb35-5ab94c961dfe. [Accessed: 16-Jun-2020].

[11] M. Biron, *Thermoplastics and Thermoplastic Composites: Technical Information for Plastics Users*. Elsevier Science & Technology, 2018.

[12] G. A. Vincent, T. A. De Bruijn, S. Wijskamp, M. I. Abdul, M. Van Drongelen, and R. Akkerman, "Shredding and sieving thermoplastic composite scrap : Method development and analyses of the fibre length distributions," *Compos. Part B*, vol. 176, no. February, p. 107197, 2019, doi: 10.1016/j.compositesb.2019.107197.

[13] G. Vincent, T. A. de Bruijn, M. I. Abdul Rasheed, S. Wijskamp, and R. Akkerman, "Fibre length distributions of shredded thermoplastic composite scrap," *21th Int. Conf. Compos. Mater.*, no. August, pp. 20–25, 2017.

[14] G. A. Vincent, T. A. de Bruijn, S. Wijskamp, M. I. A. Rasheed, M. Van Drongelen, and R. Akkerman, "Characterisation and improvement of the quality of mixing of recycled thermoplastic composites," *Submitt. to Polym. Compos.*, 2019.

[15] J. L. Thomason, "The influence of fibre length and concentration on the properties of glass fibre

reinforced polypropylene: 6. The properties of injection moulded long fibre PP at high fibre content," *Compos. Part A Appl. Sci. Manuf.*, vol. 36, no. 1, pp. 995–1003, 2005.

[16] J. L. Thomason and M. a. Vlug, "Influence of fibre length and concentration on the properties of glass fibre-reinforced polypropylene: Part 1. Tensile and flexural modulus," *Compos. Part A Appl. Sci. Manuf.*, vol. 27A, pp. 477–484, 1996.

[17] Lehmann-Voss, "Material datasheed of Lehmann-Voss LUVOCOM 1301XCF30 N PPS."

[18] Celanese, "FORTRON® PPS: Short-Term Properties Guide," 2016.

[19] Owens Corning, "Product information TWINTEX® T PP," 2008.

[20] J. L. Thomason, "The influence of fibre length and concentration on the properties of glass fibre reinforced polypropylene: 5. Injection moulded long and short fibre PP," *Compos. Part A Appl. Sci. Manuf.*, vol. 33, no. 12, pp. 1641–1652, 2002, doi: 10.1016/S1359-835X(02)00179-3.

[21] W. Schijve and A. Rüegg, "Long Fiber Thermoplastic Materials (LFT) – Material properties properly charactised," in *Internationale AVK-Tagung*, 2007, no. November, pp. 119–138.

[22] J. L. Thomason, M. a. Vlug, G. Schipper, and H. G. L. T. Krikor, "Influence of fibre length and concentration on the properties of glass fibre-reinforced polypropylene: Part 3. Strength and strain at failure," *Compos. Part A Appl. Sci. Manuf.*, vol. 27, no. 11, pp. 1075–1084, 1996, doi: 10.1016/1359-835X(96)00066-8.

[23] M. I. A. Rasheed, B. Rietman, H. A. Visser, and R. Akkerman, "Effect of overlap length on the mechanical properties of flake reinforced thermoplastic composites," in *CAMX 2015*, 2015.

[24] M. Janney, U. Vaidya, R. Sutton, and H. Ning, "Re-Grind Study of PPS-Based Long Fiber Thermoplastic Composites," in *SAMPE 2014*, 2014.

[25] U. Vaidya *et al.*, "Comparison of wet laid to other discontinuous processed carbon fiber thermoplastic composites," in *CAMX Conference Proceedings*, 2014.

[26] K. B. Thattaiparthasarthy, S. Pillay, and U. K. Vaidya, "Rheological characterization of long fiber thermoplastics - Effect of temperature, fiber length and weight fraction," *Compos. Part A Appl. Sci. Manuf.*, vol. 40, no. 10, pp. 1515–1523, 2009, doi: 10.1016/j.compositesa.2009.06.009.

[27] M. Selezneva, S. Roy, L. Lessard, and A. Yousefpour, "Analytical model for prediction of strength and fracture paths characteristic to randomly oriented strand (ROS) composites," *Compos. Part B Eng.*, vol. 96, pp. 103–111, 2016, doi: 10.1016/j.compositesb.2016.04.017.

[28] Ten Cate, "Technical datasheet: TenCate Cetex® MC1100 PPS Thermoplastic BMC." pp. 3–4, 2013.

[29] S. Pimenta, "Toughness and strength of recycled composites and their virgin precursors," PhD Thesis, Imperial College London, 2013.

5 Applications

5.1 Introduction

The previous chapter covered the experimental determination of the mechanical performance of recycled TPC materials. Results were found to be in-line with theoretical predictions (Chapter 3) and showed to increase with increasing fibre fraction; limited influence of fibre length for the studied interval and a larger influence of degree of mixing and material structure was found. Now the technical feasibility has been shown for recycling post-industrial TPC waste on material level, this chapter is focussed on the product level. The theoretically predicted mechanical properties found by the developed model described in Chapter 3 and the confirmation of this structural performance by the experimental tests on coupon level in Chapter 4 raises the question whether the developed recycling process and studied materials can be applied to create products with the same functionality as the currently used solution of virgin material.

To prove the translation of the technical feasibility from material level to product level, actual demonstrators are required for high-end and high-volume markets. As is described in the State of the art (Section 2.3), studies on parts made of related material-process combinations stress the benefits related to the geometric freedom of discontinuous material. Therefore, the design shall utilise this geometric design freedom for aspects such as potential function integration, geometric stiffening and stress distribution. Three demonstrators are described in this chapter. An aerospace access panel is designed, produced and tested to be mounted on a flying aircraft. The panel represents the high-end application field for recycled C/PPS material. In addition, a safety shoe nose cap was selected for the high-volume market and G/PP material. The latter is designed, manufactured and tested to the highest standards and benchmarked to a commercially available product. The most important criteria for the nose cap are impact resistance and strength, which are known advantages of LFT materials (see Chapter 1 and 2). A third demonstrator is an aerospace bracket, which is aimed to prove the geometric freedom of the material-

Parts of this chapter are reproduced with adaptions from "T.A. de Bruijn, G.A. Vincent, J. Meuzelaar, J.P. Nunes, F.W.J. van Hattum. Design, manufacturing and testing of a rotorcraft access panel door from recycled carbon fibre reinforced polyphenylenesulfide. *SAMPE America Conference 2019 Proceedings*, 2019, Charlotte, United States of America." and "I. ten Bruggencate, T.A. de Bruijn, G.A. Vincent, F.W.J. van Hattum. Design, manufacturing and testing of a safety shoe nose cap from recycled glass fibre polypropylene. *SAMPE Europe Conference 2019 Proceedings*, 2019, Nantes, France."

process combination. In the State of the art (Section 2.3), no products are found which are made of recycled TPC that are used in an application. However, the access panel and nose cap demonstrators described in this chapter are designed and tested to requirements for currently available applications. This enables to validate the technical feasibility of the recycling route to proven and real-world applications. It also allows for evaluating the value of the recycling route and product by economic and environmental impact assessment as is described in the objective of this thesis (Section 1.5) and studied in Chapter 6.

5.2 A rotorcraft access panel

5.2.1 *Introduction*

The access panel developed in this study is a part for a new rotorcraft [1, 2]. Specific values and details on loads, stresses and dimensions were not to be disclosed, due to the nature of the program, and are therefore omitted. The goal of this rotorcraft is to offer increased performance (speed, range, payload and agility) at affordable cost. To achieve these goals, composites are used throughout the structure (low weight, fatigue & corrosion insensitive). The access panels are created from the actual production waste of TPC components intended for the same rotorcraft structure (i.e. closed-loop recycling). The requirements for the access panels are fully representative for any aerospace part; including sufficient strength at ultimate load (UL), prescribed maximum deflection at limit load (LL) (to guarantee aerodynamic performance) and chemically and thermally resistant. The panel must fit the design space and needs to be interchangeable with the current panel made of thermosetting carbon epoxy prepreg composite by hand lay-up. The access panel is a rectangular non-structural component, with a prescribed thickness at the landing and is mounted by fasteners. The specific design goal is to minimise weight and cost of the panel.

On the rotorcraft, a number of identical panels are used, which will maximise cost and weight benefits in case of high-volume production of this type of parts made with the TPC-Cycle process.[1, 2]

The overall goal of this study is to design, manufacture, test and fly an aerospace part of recycled TPC material to show the technical and economic feasibility of the developed recycling solution.

5.2.2 *Development Approach*

The traditional ‘Building Block approach’ (as advocated in [3]) is chosen for the design and validation of this novel composite material and process (see Figure 5.1). Mechanical properties of the material were determined on coupon level (samples from flat plates of various FVF) and the results were used to create multiple conceptual designs. The concepts were evaluated by Finite element method (FEM) to select the

best concept for the detail design and the most critical design detail was selected and tested. In parallel, a manufacturing demonstrator, including a variety of stiffening geometries, was made to validate the processability of the design, select the final FVF and obtain samples for the detail test on the identified critical design feature. After these tests, the design concept was further optimised and frozen to produce the mould for actual part production. With this mould, a series of panels was produced; one representative panel was selected for the component test and two panels were selected for actual flight. The results are presented and discussed before the conclusion is given.

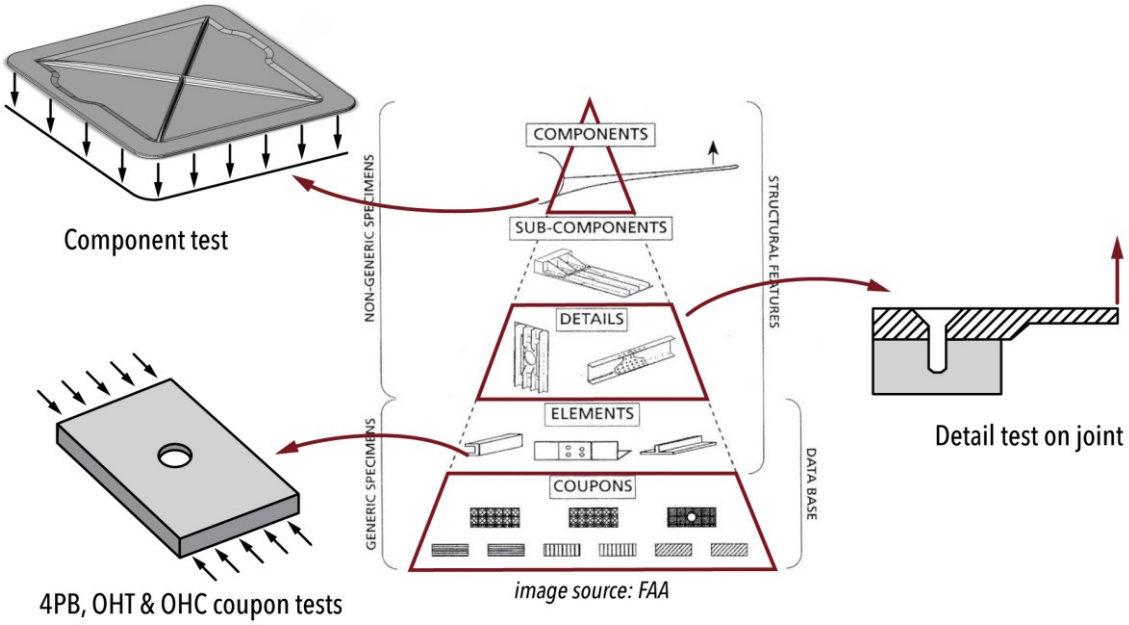

Figure 5.1 - Building Block test approach as followed for the recycled access panel, source: adapted from [3]

5.2.3 *Design*

From the requirements, the design is optimised for weight by reducing the thickness of the panel to the minimum producible thickness with the current process, and include ribs to obtain the required out-of-plane stiffness and distribute the stresses more equally over the fixation points.

Finite element model

FEM models for design iterations were made using the SolidWorks Simulation software package, which was chosen for its wide availability and ease-of-use, which significantly speeds up to the initial design iterations whilst given sufficiently accurate results. The final design was validated by a set of Patran/Nastran simulations. The prescribed aerodynamic pressures have been applied uniformly over the panel at LL and UL levels to verify stiffness and strength requirements, respectively. The boundary conditions are implemented by constraining three surfaces: the translation in out of plane direction of the

landing surface towards the landing, the fixation of the fastener shaft hole surface and the translation of the fastener countersink head surface in both directions. During the development, the successive FEM analyses have been updated with mechanical properties of increasing maturity as the process development continued in parallel.

Concept generation and selection

In order to be interchangeable with the original panels, the panel has a prescribed thickness and hole pattern for fasteners at the landing on the edge of the panel. The design of the middle section may be changed. Representative pictures of the part geometry are shown in Figure 5.2. Although the actual panel is slightly curved, a flat geometry is assumed for the first design iterations.

The first reference design is a thin non-stiffened panel to understand the benefit of extra geometric features and is show in Figure 5.2. The thinner middle section has the assumed minimum producible thickness of 2 mm. The design was evaluated using FEM for deflection and stress level. The deflection profile is visible in Figure 5.3 and shows a maximum deflection of about 170% of the allowable value. The major principal stress shows levels above the preliminary allowable values of the material properties at the location near the fasteners, especially the fasteners at the centreline, indicated in Figure 5.4. The high stress at the specific fasteners is a result of an un-even distribution of fasteners, which is part of the design requirements and thus cannot be modified. These first results show that the deflection criteria will be the main overall design driver, together with local stresses at the indicated fasteners.

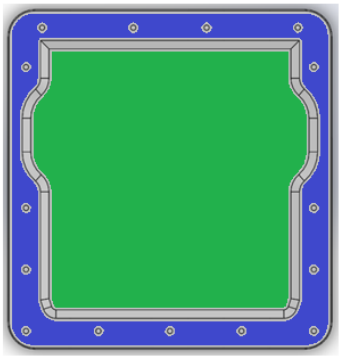

Figure 5.2 - The access panel with a prescribed location of fasteners and thickness on the edges (blue) and an inner section which is open for design (green)

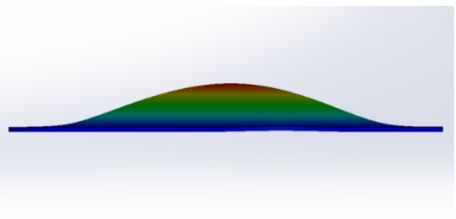

Figure 5.3 - Deflection of flat plate panel (not to scale)

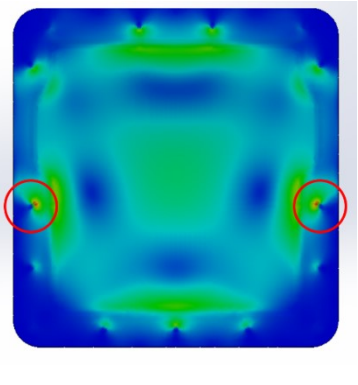

Figure 5.4 - The major principal stress distribution showing concentration at the fasteners indicated by a red circle. (blue correspond to a low and red to a high stress level)

Although stringers and ribs are generally implemented to increase geometric stiffening, ribs can also add value by redistributing the internal loads. The first reference design, with non-stiffened inner section, is shown in Figure 5.5. To increase the out-of-plane stiffness of the panel and reduce the stress level around

the two fasteners at the centreline, multiple stiffener concepts have been designed and evaluated using FEM. The concepts are numbered and shown in Figure 5.6. For the stiffener structure 1, the ribs are connecting holes of the panel to distribute the stress to these locations. When reaching the landing, the ribs spread out to limit stress concentrations. The concept 2 implemented a symmetrical design, similar to existing panel designs such as present on the Bell-Boeing V-22 [4]. From the stress distribution of concept 2, some ribs showed low levels of stress and are therefore removed for concept 3. In contrary to the first concept, the ribs in concept 2 and 3 are not connected to the thicker sides of the panel, which is generally not favourable considering the stress distribution at the stiffener ends. A second version, concept 3B is designed to compare the influence of the rib end. The size of the ribs in the concepts 1 to 3B is equal. The height and width of the ribs is decreased in concept 4 to study the influence of an increased number of smaller ribs. From the previously mentioned concepts 1-4, all showed an increased stiffness but local stress concentrations remained a point of attention. Option 4 gives the lowest stress level at the fasteners in the corners. In order to distribute the stresses more equally over the fixation points, two diagonal crossing ribs are designed to lead the loads towards the corners in concept 5.

The concepts have been compared on the maximum stress level at UL, mass and maximum deflection. Concept 5 was chosen because of the low weight, adequate stiffness and comparable overall stress to the other concepts. The design was further improved to the final design shown in Figure 5.7. Concept 2 and 3B showed a lower stress level but their weight is higher. Additionally, the manufacturability of concept 5 is more favourable, since the diagonal stringer cross increases the flow of material towards the corners.

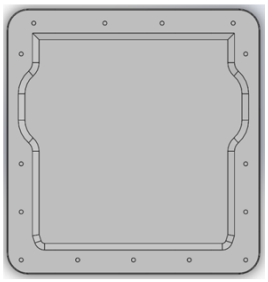

Figure 5.5 - Flat panel being the first reference design

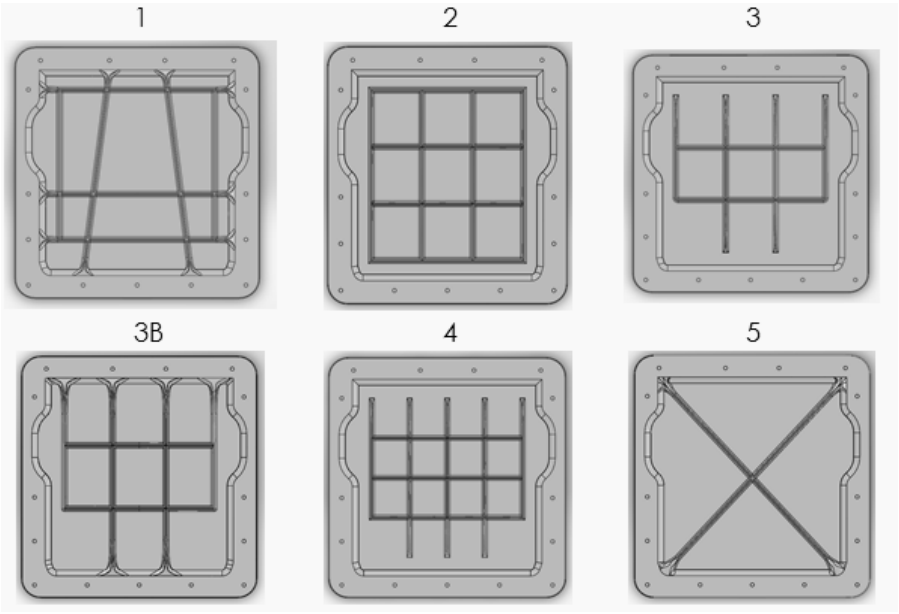

Figure 5.6 - Various concepts with different rib structures studied by FEM

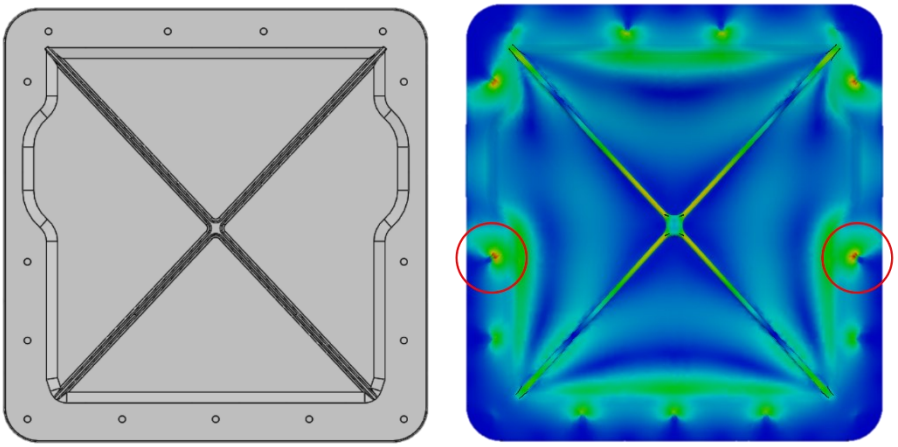

Figure 5.7 - The CAD model (left) and major principal stress distribution (right) of the final concept, red circles indicate stress concentration at fasteners

Detail design

Multiple variables of ribs are defined to ensure a good performance and production (see Figure 5.8). The maximum width (w) over base thickness (T) and height (h) over width (w) ratios are dependent on the flow of the material and can possibly lead to unfilled regions or matrix rich regions. Furthermore, a common result of wide ribs in respect to the base thickness are sink marks. The Azdel Inc. handbook [5] provide guidelines for a GMT process for G/PP, a material/process combination with similar artefacts as the current under study. Following these guidelines, a maximum height over width ratio of three should be

applied. Different rib configurations were tested and compared in Table 5.1 and the h/w of 9/3 was chosen. The problem of sink marks is limited since the coefficient of thermal expansion (CTE) of the used C/PPS material is low. The CTE for reinforced PP is 70-90 µm/m·K^{-1} and is 25 µm/m·K^{-1} for G/PP compared to 10 µm/m·K^{-1} for C/PPS. A radius at the bottom (r_B) of the ribs was added to improve material flow and to prevent fibre breakage. A top radius (r_T) is included to prevent unfilled or matrix rich corners. The draft angle (θ_d) enables demoulding and should be between 0.5° to 1.5° according to the Azdel Inc. handbook [5]. Since the coefficient of thermal expansion of the C/PPS material is lower, the draft angle is set at a higher angle of 2°.

The final design results in predicted a weight reduction of 9% with respect to the current baseline C/epoxy prepreg design. The deformation at LL is predicted to be within the stiffness requirements. Regarding strength, the stresses in the ribs are at an acceptable level, even compared to a conservative preliminary tensile strength value which has been statistically reduced for variation (B-value) and elevated temperature. The stress concentration at the fasteners is still above this value for plain tension, but was validated by a detail test.

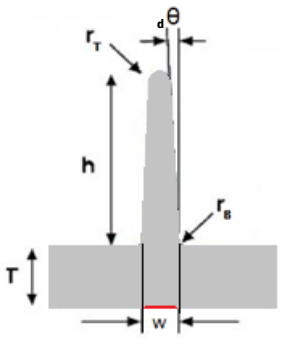

Figure 5.8 – Cross section of a rib, including relevant variables and the location of a potential sink marks (red).

Table 5.1 - Dimensions of the ribs in the manufacturing demo shown in Figure 5.9

Rib	Height (h) (mm)	Width (w) (mm)	Ratio (-)
A	6	3	2
B	9	2	4.5
C	7.5	2.5	3
D	9	4.5	2
E	9	3	3

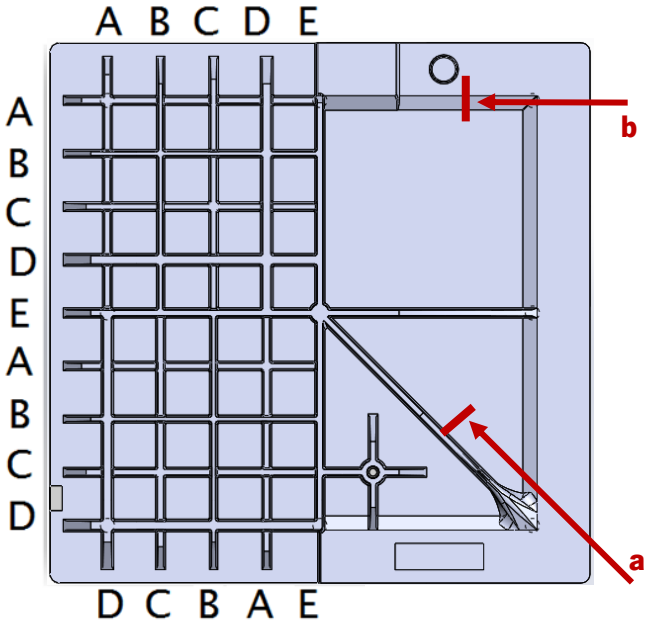

Figure 5.9 - Top view of the manufacturing demonstrator. The characters correspond to the dimensions of the ribs given in Table 5.1. The red annotations indicate the location where the cross-sectional microscopy samples were taken which are given in Figure 5.13.

Manufacturing demonstrator

A manufacturing demonstrator has been designed and produced to test the processing window of the material, design and process combination. Design guidelines for the processing of GMT G/PP were used in the design process and also served as a reference to choose the geometry near the processing limitations [5]. The manufacturing demonstrator as shown in Figure 5.9 was designed for three purposes:

- to manufacture the fastener section indicated as critical by FEM, that will be mechanically tested on detail level;
- to systematically test the manufacturability of the geometrical features. This includes thickness transitions, bosses, rib crossings and ribs with various width over height ratios of 1:2 to 1:4.5, see Table 5.1.
- To test the minimum thickness in relation to the maximum fibre content.

The set of ribs in the top left quarter are duplicated in a different order with respect to the centre of the plate, which is the location where the initial charge is placed. The second set of ribs is shifted vertically to the lower left part and mirrored horizontally, to evaluate the fill and flow behaviour dependent on the distance to the initial charge. In the right side of the panel, the edge and thickness transition are almost equal to the designed access panel to test this specific thickness transition. Additionally, the edge covers a section of steeper thickness transitions. The diagonal rib is identical to the one in the access panel. A more general view on this part is given in a previous paper [6].

5.2.4 *Materials and Methods*

Materials

The used material is post-industrial C/PPS waste. This material originates from the same structure as the access panel will be mounted on. The batch number and history of the material is therefore known, and enables the required traceability. Since the material is recycled near the production facility, the logistics are less complicated and prevent unnecessary environmental impact. This solution additionally implies a fixed supply and demand resulting in a lower risk from a business point of view.

Offcuts from a consolidated C/PPS laminate (TenCate Cetex® TC1100), consisting of multiple plies of 5 harness satin weave, are fed into an Untha S20 shredder for five consecutive times. The output of this low-speed two-shaft shredder with blades of 19 mm in width and no screen were long fibre length of 15 to 20 mm [7]. In this case, the offcuts were nesting residues of the ribs made by GKN Fokker. Flake sizes are automatically analysed and translated to a fibre length distribution by an in-house developed image processing tool. More information about the used shredding method and fibre length analysis is available in a study by Vincent et. al. [7]. The material is diluted with Celanese Fortron 0214 PPS pellets (i.e.

identical matrix as the recycled C/PPS laminate) to lower the FVF to 20%. Material data was gathered from the mechanical tests as described in Chapter 3, and used to predict the panel's strength and stiffness (see Table 5.2) [8].

At the start of the design process, only limited test data on mechanical properties of low-shear mixed C/PPS was available. The used data was obtained by 4-points bending tests in accordance with ISO14125 and is given in Table 5.2.

From the bending tests, it can be concluded that stiffness of the recycled material processed by low-shear mixing is reduced to roughly one-third of the baseline C/PPS material (quasi-isotropic laminate) due to the shorter fibre length and strongly reduced fibre volume fraction (20% versus 51%). For non-structural applications like this access panel, this is actually considered a benefit since a lower in-plane stiffness will prevent undesired load transfer into the panel; on the other side the out-of-plane stiffness can be tailored to the required value by means of integral stiffening offered by this technology.

Table 5.2 - Preliminary material properties deducted from 4-pnt bending test (all values Room Temp/average)

Material properties	Recycled C/PPS at 20% FVF
Density [kg/m^3]	1460
Flexural strength [MPa]	190
E-modules [GPa]	13
Poison ratio	0.3

Based on these tests, a conservative (lower) design value is derived for the preliminary design of the panel; the stiffness result has been used as reported. In further testing, both this preliminary stiffness and the assumed allowable strength need to be confirmed and updated as the process and product development progresses.

Manufacturing

The shredded C/PPS and PPS granulates were dried in a convection oven for a minimum of 2 h at 120 °C. Material was weighed and fed to the low-shear mixing device described in Section 2.2.6 [8, 9]. The mould was kept at an isothermal temperature in a 200 t press.

The manufacturing demonstrator was produced with a base thickness of 2 mm and 3 mm at 20%, 26% and 35% FVF to study the minimum producible thickness in relation to the FVF.

The access panels intended for flight tests were inspected, tested on component level, deburred and primed in the production facilities of GKN Fokker.

Mechanical Testing

Mechanical testing has been performed at Detail and Component Level. Limited Coupon Testing, in the form of 4-point bending test, was executed and is described in 4.2.8.

Detail Test

A dedicated test fixture, illustrated in Figure 5.10, was designed to test the critical design detail: bending of the laminate edge around the fastener in combination with tensile loading on the bolt. Although the load is introduced at a line instead of a distributed pressure, the local loading situation is similar. Six specimens were cut from a flat panel using a diamond saw and then sanded to clear the edges. The specimens were cut from the edges of the panel to correspond with the location of the critical design detail, as illustrated in Figure 5.4. This ensures that the flow dependent characteristics are similar. The hole and countersunk for the fastener were milled at the edge side of the component. The fasteners used were identical to those used in the real rotorcraft application. All tests were conducted at room temperature. The load was introduced by a 5 mm radius fixture at a cross-head speed of 2 mm/s in a universal testing machine (see Figure 5.10).

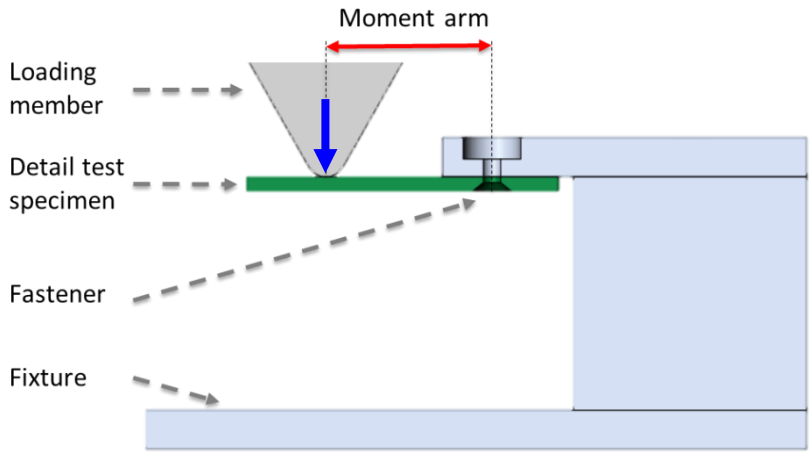

Figure 5.10 - Detail test setup

Component test

For this novel and unqualified technology, it was planned that final proof of strength was to be demonstrated by testing a representative panel up to failure or 300% of LL, whatever was to occur first. The load level of 300% of the design load is above UL and was selected to not only cover the usual safety factor, but also to address environment knockdowns (by temperature, moisture) and scatter. The test was conducted at room temperature.

Goals of the test were to proof sufficient strength at UL and to verify if the aerodynamic deformation requirement at LL was met. Moreover, the failure mode(s), if any, were to be investigated. In order to do so, a test set-up was created which is representative for both the support from the surrounding rotorcraft

structure as well as the aerodynamic loads sustained in flight: the panel was to be supported along its edges and subjected to a controlled (under)pressure; deformation was to be measured in the centre of the panel. During the test, the panel's critical stiffeners are loaded in tension (the critical failure mode from coupon tests). The test set-up is schematically depicted in Figure 5.11.

Since both the low-shear mixing process as well as the proposed inspection methods were new and unqualified, the access panels intended for actual flight were also subjected to a proof load of 100% LL using the same test set-up.

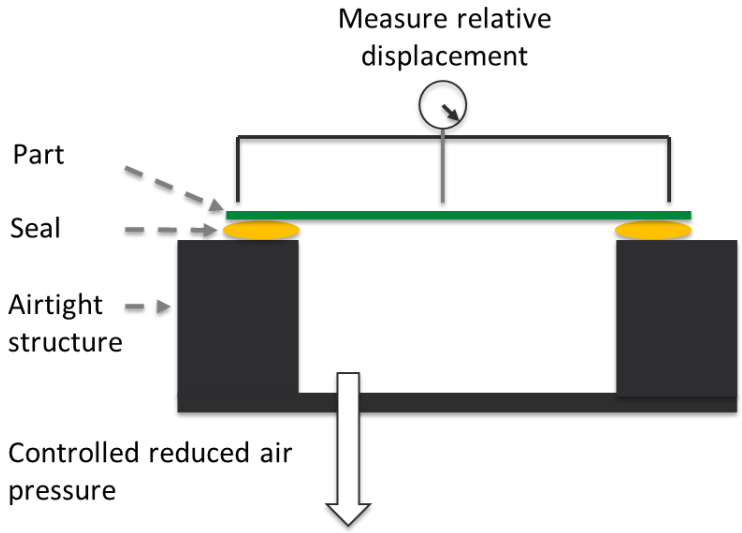

Figure 5.11 - Schematic test set-up for Component Test

5.2.5 *Results and discussion*

Manufacturing demonstrator

The manufacturing demonstrator shown in Figure 5.12 was produced at multiple thicknesses and FVF. Cross-sectional microscopy was performed to analyse the geometrical features of the manufacturing demonstrator moulded at a 26% and 35% FVF. Cross sections were made at a rib stiffener and a thickness transition, as indicated in Figure 5.9. Figure 5.13 (a) shows a fully filled stiffener with a 1:3 width over height ratio, without resin rich regions and without a visible sink mark. The gradual thickness transition is depicted in Figure 5.13 (b) and shows a similar result as seen on the stiffener: well dispersed fibres and a low void content. Especially at the thickness increase, fibres are more aligned along the mould surfaces, but a stronger out-of-plane orientation component is found in the mid-plane for thick sections.

The manufacturing demonstrator was produced with a base thickness of 2 mm and 3 mm at 20%, 26% and 35% FVF to study the minimum producible thickness in relation to the FVF. Results show that the

cavity is fully filled for 26% FVF at 3 mm thickness and for 20% FVF at 2 mm thickness. Short shots were observed for 35% FVF at 3 mm thickness and 26% FVF thickness 2 mm. Beside the thickness and fibre content, these results are likely to be dependent on part area, closing speed, and variables related to the viscosity; such as the material system, degree of mixing, the transfer time and material and mould temperatures.

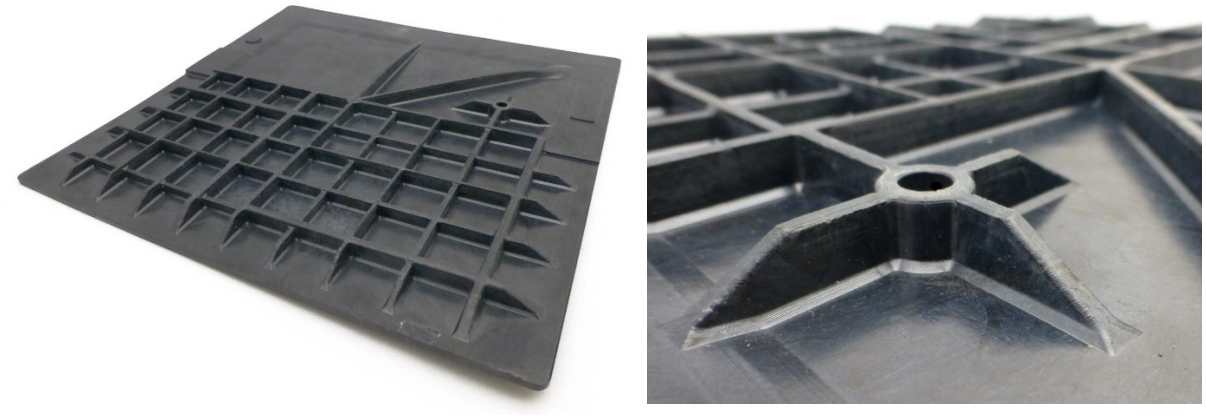

Figure 5.12 - A produced manufacturing demonstrator (left) and a close-up showing the thickness transition, ribs of various heights and intersections (right)

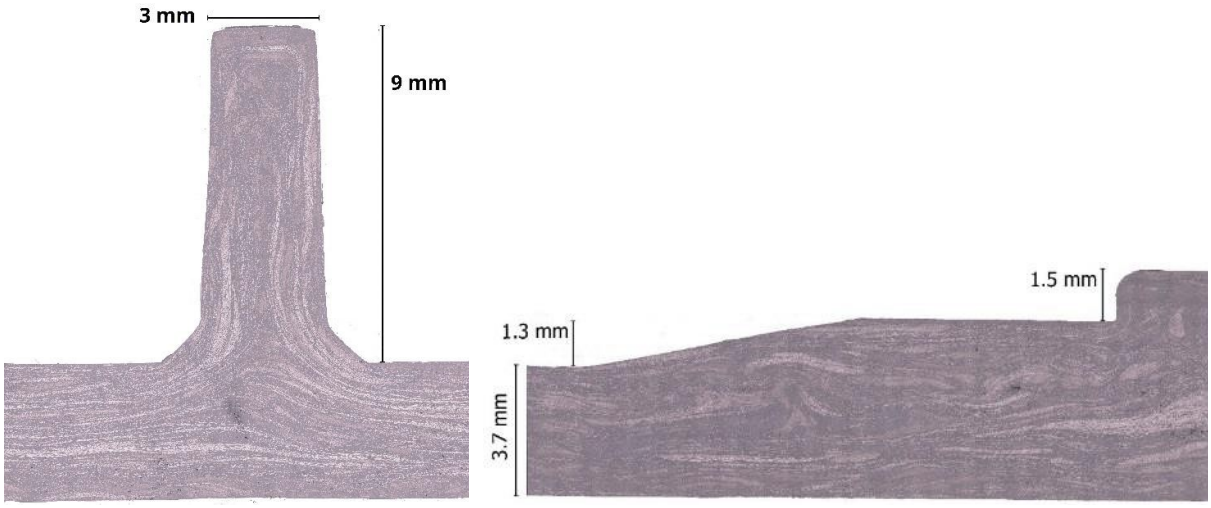

Figure 5.13 - Cross-sectional microscopy of a stiffener (a) and a thickness transition (b) at 35% FVF, the location with respect to the total panel is indicated in Figure 5.9.

Manufacturing access panel

Several access panels were manufactured by a preliminary process specification, see Figure 5.14. The production times were below 30 minutes per panel. The part is net-shaped and thus flash could be easily removed without NC trimming. This batch process and the use of a prototype low-shear mixer result in a part weight CoV below 5%. Warpage and small deviation of geometric accuracy were observed and could

partly be resolved by relaxation at elevated temperature. The mass of the part was as designed, resulting in a weight reduction of 9% compared to the current baseline panel.

Figure 5.14 - Designed and manufactured access panel for the rotorcraft. The landing area is coated with a light blue primer.

Mechanical Testing

Detail test

During the detail tests, all specimens showed consistent tensile failure at the fastener hole, as predicted (see Figure 5.7). The (gross) stress in the specimen at the location of the fastener is calculated considering the classic formula for determining the bending stress in a beam under simple bending. The cross-sectional area reduction of the fastener hole and stress concentrations phenomena are not included. The conservative average estimated bending stress at failure is 202 MPa with a CoV of 16%. These *gross* values (i.e. including the effect of the hole) correspond well with flexural strength data in Section 3.4. The data obtained in this study give great confidence regarding the structural integrity near the fastener.

Component test

Three representative panels were selected from the produced batch. From these panels, the 'least perfect' upon visual inspection was selected for the failure test. Air pressure under the panel was reduced in steps to 100% of LL and the deformation was measured. During subsequent load increases, audial observations (slight cracking noises) were made between 150% and 290% LL. Nevertheless, 300% LL was reached successfully and after 3 seconds, the load was removed. Figure 5.15 depicts the test in execution.

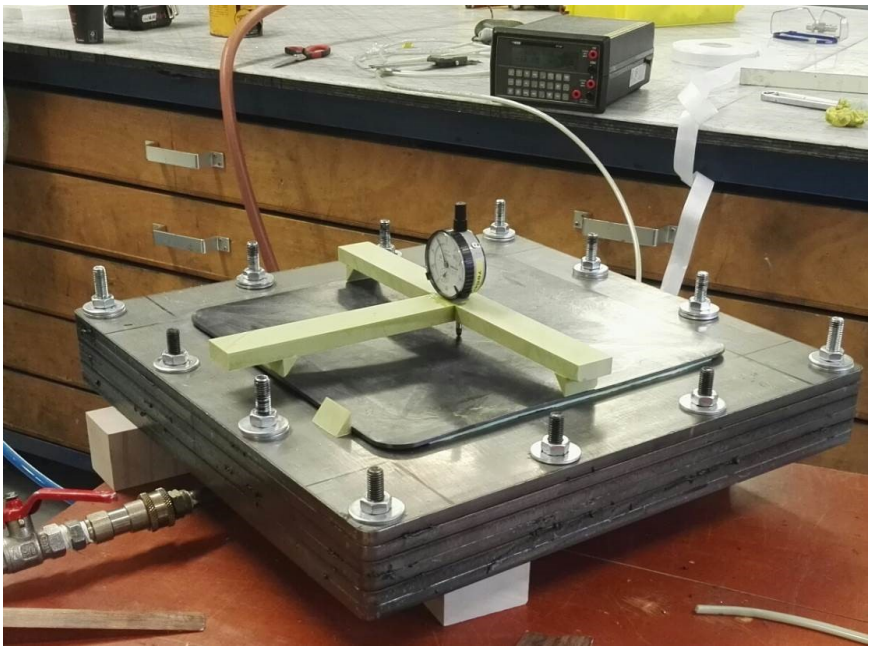

Figure 5.15 - Component test in execution

After removal of the tested panel, a detailed visual inspection was conducted at the stiffeners. Two small initial failures were detected at the expected locations: very small cracks originating from manufacturing imperfections at the surface near the stiffener crossing. Progression of the cracks stopped roughly halfway in the stringer, see Figure 5.16 for their location. As a result, the panel was able to sustain any further loading without subsequently failure. Moreover, the deformation at LL was within requirement and in line with FEM predictions. Consequently, the component test was successfully passed.

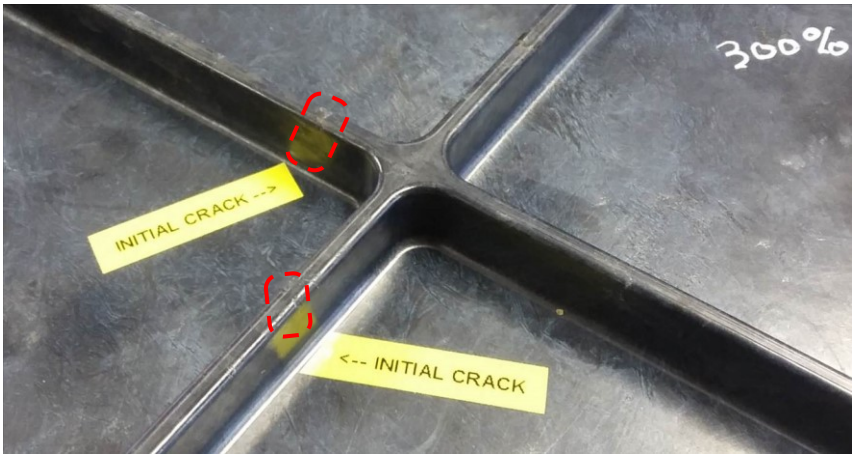

Figure 5.16 - Post-test inspection result (300% LL test), red circles indicate initial cracks

After the 300% LL test and inspection, the other two panels were proof-loaded to 100% LL. No observations were made during the test (no noises) and the post-test inspection did not reveal any defect or crack. Moreover, the stiffness of these panels was found to be according to specifications, with the deflection at

the centre within a 10% margin with respect to the requirement. Therefore, these two panels were approved for flight.

Further development

The developed application and its process demonstrates that similar solutions are feasible for high-end products. The potential environmental and economic benefits are estimated by a quick scan LCCA in the following Section 6.4. Thanks to the short cycle time, this process is also suitable for markets with larger volumes than aerospace. Currently, several actions are performed to evaluate the production process for serial production. Additional testing (especially coupon testing) and further industrialisation efforts (repetitiveness, geometrical stability) are foreseen necessary to qualify the process. Further attention is given to geometric accuracy. More detailed cost and environmental studies are being researched; quality control and inspection is also examined. At the same time, a feasibility study is executed to see if the applied approach and recycling route can be applied in other aerospace applications, such as (non-structural) fairings, covers & system brackets. The results regarding cost and weight reduction look very promising for several types of parts. On material level and possible function integration, interesting topics are hybrid structures including unidirectional tapes, integrated materials for lightning strike and galvanic protection.

The produced access panel have been successfully flight tested in 2020, together with the TPC control surfaces of which the waste originates, leading to the world's first flying fully recycled thermoplastic composite application in aerospace [10, 11]

5.2.6 *Conclusion*

The developed TPC recycling solution offers the possibility to retain long fibres and therefore high mechanical properties at short cycle times. The feasibility of this solution was proven by an access panel for a flying rotorcraft prototype. This panel has been designed against fully representative set of requirements, manufactured and successfully tested. TPC waste material of other components for the same rotorcraft have been recycled in the production of these access panels.

Desired complex features have demonstrated to be possible and offer the opportunity for stiffeners, which not only increase the geometric stiffness, but also enable to distribute stress more homogenously. In comparison to the current carbon/epoxy hand lay-up solution, the resulting product is 9% lighter, significantly more cost-effective and made of recycled material (fibre *and* matrix). Flight test demonstration with the recycled thermoplastic access panel installed on the rotorcraft was performed in 2020.

5.3 A safety shoe nose cap

5.3.1 *Introduction*

The recycling route, described in Section 2.2.6, is developed to retain long fibre lengths. As is discussed in the State of the art (Figure 2.1, Page 12), longer fibres especially result in higher strength and impact properties [12, 13]. A safety shoe nose cap (from now on referred to as nose cap) was chosen as a demonstrator, to show the developed recycling route is able to retain sufficient strength and impact properties and processing capabilities, not only for high-end applications, but also for more common and price-critical products. Recycled flakes, a nose cap and a safety shoe are shown in Figure 5.17. The standard for the heaviest class safety shoe nose, S3 classification, prescribes high requirements on compression and impact [14]. The production of this nose cap aimed at:

1. demonstrating the manufacturing feasibility of using recycled material for such product;
2. showing the possible process automation;
3. confirming the reduction in cycle time compared to similar products made of thermoset composites, and
4. determining potential weight reduction in comparison to current composites or steel nose caps.

To fulfil the objectives of this study, a current nose cap design was adjusted for the developed recycle route and manufactured with various materials. The produced nose caps, and a the commercially available nose cap, which was added as a benchmark, were tested according to the standard.

Figure 5.17 - The shredded flakes (left), a safety shoe (top) and the developed nose caps (bottom)

5.3.2 *Design*

Safety shoe nose cap design

Basic calculations and simulations were performed to validate the design, including hand calculations for deflection and tension. Simple FEM simulations showed a first impression of the location of the maximum stress and maximum displacement. For a separate set of nose caps, this location is locally reinforced with continuous fibre UD tape. One of the finite element simulations was performed using the ANSYS software package (see ahead Figure 5.32, Page 139). A load of 15kN is applied. The value of the stress, the location of the maximum stress and the deflection can be observed from this result.

For the design of the nose cap, three analyses were performed to verify and improve the manufacturability and to determine the position of the nose cap in the mould.

- Thickness analysis;
- Draft analysis;
- Undercut analysis.

Design mould

For the design of the mould the guidelines of the Azdel (GMT) Thermoplastic handbook [5] were followed. The most notable guidelines for the mould were:

- A minimal inner radius of 2 mm;
- minimal draft angle of 1 degree, preferred 3 degree;
- shut-off edge, space between the end of the material and closing of the mould (12.8 mm);
- a mould guidance before the mould is completely closed of 50 mm minimum;
- stop blocks, minimal surface of 1600 mm^2/100 t compression moulding force;
- cooling channels;
- press dwell time of 5-7 seconds per mm wall thickness [5]

A master mould including mould guidance, cooling channels and thermocouple was used, inside which the nose cape mould was placed. In Figure 5.18 the nose cap mould is given and in Figure 5.19 the complete set is depicted.

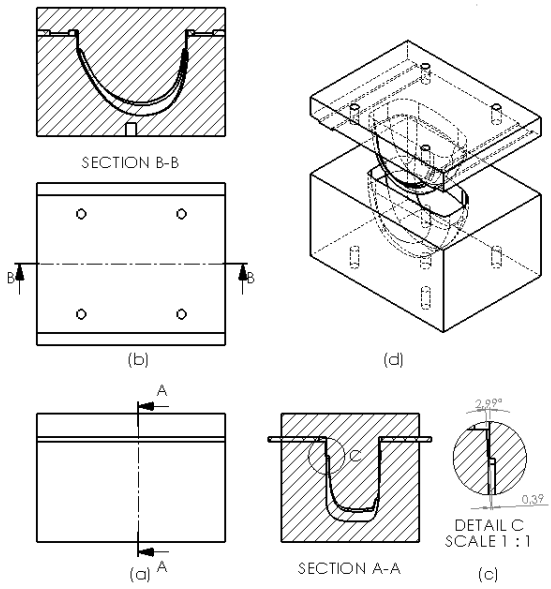

Figure 5.18 - Design of the safety shoe cap mould

Figure 5.19 - Safety shoe cap and master mould

5.3.3 *Materials and methods*

Materials

Three types of G/PP materials were used: Virgin pellets, recycled flakes and a combination of the pellets with UD tape reinforcement. The virgin pellets are commercially available long fibre thermoplastic (LFT) pellets of 15 mm length in 19% and 35% FVF, as is also described in Section 4.2.3. To test the effect of FVF on the nose caps' properties, nose caps were produced with LFT pellets of both stated FVF. The flakes originate from consolidated plates of 35% FVF woven commingled Twintex® material (see Figure 5.17). These plates were processed for five consecutive times in a four-shaft shredder without a sieve and fitted with 19 mm wide blades. More details and information about shredding these materials in general and the utilised setup in particular can be found in Section 3.2.3, as well as in [15]. The flakes were mixed with virgin PP to lower the FVF to 19%. A UD tape reinforcement was applied in combination with the LFT pellets in the third type of material. The UD pre-impregnated tape has a 35% FVF and was supplied by CompTape [16]. The assumption was made that the commercially available nose cap, used as a benchmark, was produced with glass fibres and an epoxy resin to determine the FVF from the resin burn out test results.

Manufacturing

The recycling route is demonstrated in Figure 5.20. In the first step, step A, the composite waste material is reduced in size to flakes, by e.g. a shredder. After the size reduction in step A, a specific quantity of material was placed in a mixing machine, step B, in addition to virgin resin. A detailed description of the

low-shear mixer can be found in 2.2.6. Subsequently, the heated dough is quickly transferred to the mould for forming. The processing settings are described in Table 5.3.

Table 5.3 - Processing conditions for the manufacturing of the safety shoe nose cap

	G/PP flakes and pellets
Mixing temperature (°C)	230
Heating and Mixing time (min)	10
Mixing speed (rpm)	5-10
Mould temperature (°C)	80
Dwell time (min)	1
Moulding pressure (MPa)	4.5

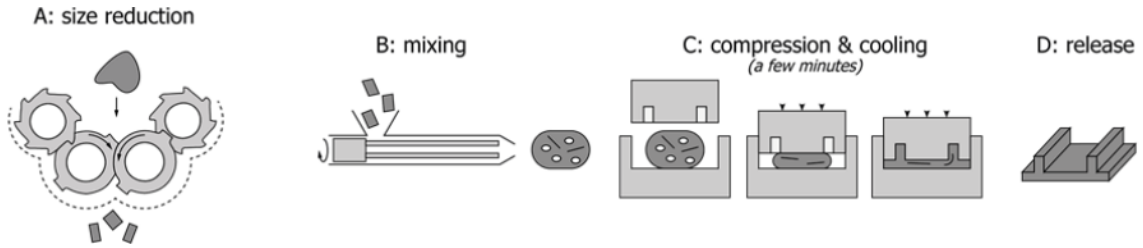

Figure 5.20 - Recycling process

A G/PP UD tape insert of continuous fibres was produced to reinforce the shoe locally with fibres in a preferred fibre orientation [17, 18] (see ahead Figure 5.26, Page 136). This insert was made by manually applying molten G/PP tapes on the male side of the mould by a hand applicator [19]. This device was developed in-house and was used to heat and position the UD tape under local pressure. The mass of the insert was 4 to 5 gr. To manufacturing the nose cap with insert, the insert was positioned in the female side of the mould and, prior to moulding, pre-heated to above melt temperature by an air gun to facilitate its bonding to the moulded material.

Safety shoe standards

The highest class of safety shoe nose cap was chosen for this demonstrator, which is the S3 classification. Two standards for personal protective equipment were used:

- Safety footwear (NEN-ISO 20345 2004) [14]
- Test methods for footwear (NEN-ISO 20344 2004) [20]

The nose cap is described in these standards as a 'safety toecap'. This term is defined as a component built into the footwear, designed to protect the wearer's toes against impact and compression. Two types

of safety footwear are distinguished: *protective footwear* and *safety shoes*. Safety shoes should be able to withstand an impact energy of 200 J ± 4 J and a compression load of 15 kN ± 0.1 kN [20]. For this research the latter safety class was chosen. At impact or maximum compression, a minimal internal clearance must be available underneath the test surface. This height depends on the shoe size, for a shoe size 43 this is 14.5 mm [14]. After the test, the tested surface may show signs of damage, but no light may shine through any potential cracks on the surface [14, 20].

Resin burn out test

Resin burnout tests were performed according to the EN ISO 1172/ ASTM D 2584 to determine and check the FVF. Furthermore, with this test an indication of the fibre structure and orientation can be obtained. Four type of nose caps were tested: a commercially available one which was added as a benchmark, a nose cap from recycled flakes at 19% FVF and nose caps from LFT pellets at 19% and 35%. The nose caps were placed in an oven with a temperature of 600˚C and remained there until no matrix material was visible. This resulted in a residence time of about 45 to 60 minutes.

Compression test

For the compression test, a test setup was designed and build according to the ISO 20344 standard, see Figure 5.21 [20]. Beside a general flat plate on top, it includes a specific fixture to keep the safety shoe nose cap into place at the bottom section. This fixture was designed to fit the compression test set up as well as the impact test set up. Mechanical testing was performed with the mixed and moulded nose caps, as well as with commercially available composite nose cap. This nose cap was used as a benchmark to compare the produced nose caps with a nose cap that is available on the market. Three specimens were tested for every nose cap type at a universal testing machine, with a speed of 5 mm/min, as described in the standard.

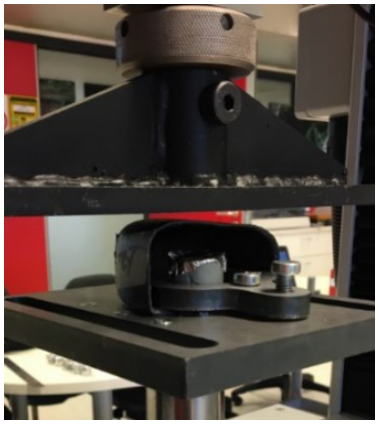

Figure 5.21 - Compression test setup

Figure 5.22 - Impact test setup

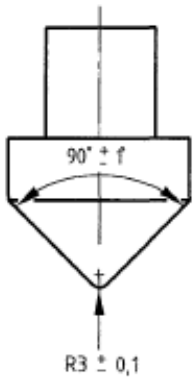

Figure 5.23 - Impact striker

Impact test

For the impact test, a test set up was designed and built according to the standard ISO 20344, Figure 5.22. The same bottom fixture was used as with the compression test. For the top section an impactor was designed and produced as prescribed in the standard. This impactor had to have a point of at least 60 mm long, the faces of which enclose an angle of 90 ± 1 degree. The top where the planes meet is rounded off with a radius of 3 ± 0.1 mm, see Figure 5.23. For the test a total weight of 20 ± 0.2 kg was required for the impactor and therefore used [20]. To check the impact energy, a high-speed video was used to measure the velocity just before impact. The recorded speed was 4.45 m/s, corresponding to an impact of 198 J. This is within the 200 ± 4 J specification prescribed in the standard. Three specimens were tested for every nose cap type.

5.3.4 *Results and discussion*

Manufacturing

About ten nose caps were produced with the process and material type described in Section 5.3.3 to enable the impact and compression tests. The low-shear mixer was filled with an amount of material sufficient for the production of three nose caps from one material batch. This led to a cycle time of about 5 minutes per nose cap. The following nose caps were manufactured:

- Pellets 19% FVF;
- Pellets 35% FVF;
- Flakes 19% FVF, Figure 5.24;
- Pellets 19% FVF + insert, Figure 5.27;
- Pellets 35% FVF thickened front, Figure 5.25.

The mass of the produced nose caps was measured and varied between 43.1 gr for Pellets 19% FVF + insert, to 61.9 gr for the nose cap with the thickened front. The mass of a commercially available thermoset nose cap was determined to be 69.1 gr and a similar steel nose cap was 86.4 gr. From these values it can be concluded that the produced nose caps are more than 10% lighter than the commercially available nose caps. Apart from this weight advantage, the production process of these recycled nose caps can potentially be highly automated. This may result in a less labour intensive production process in comparison to the commercial available nose caps that are likely to require more labour considering the high number of fabric patches at different orientations (see Figure 5.28). Also it would require less safety regulations since the thermoplastic matrix is safer to work with compared to thermoset process from a

chemical point of view, considering the Occupational Safety and Health Administration exposure and classification data in material safety datasheets of PP [21] and epoxy hardener [22].

Figure 5.24 - Produced nose caps of recycled material with 19% FVF

Figure 5.25 - Cross section of nose caps with a thickened front (left) and normal (right) FVF 35%

Figure 5.26 - Insert made of UD tape

Figure 5.27 – Nose caps with moulded with a UD tape insert

Figure 5.28 - The glass fibres of the benchmark nose cap after the resin is burned out show a structure of multiple patches

Figure 5.29 - The glass fibres of a nose cap made of recycled flakes after the resin is burned out show long fibres in random orientation

Resin burn out test

The method described in Section 5.3.3 was used to determine the FVF, the fibre structure and orientation of all tested nose caps, except the one with an insert and thickened front. The resin burn out test results are showed in Table 5.4. The produced nose caps differ maximal 1% FVF from the designed value. The commercially available nose caps have a considerably higher FVF in comparison to those produced in this study.

The burn out test revealed the layup of the commercially available nose cap (see Figure 5.28). Approximately 29 patches of woven glass fibre and different sizes were found. The patches are positioned under a 0/90° as well as a ± 45° angle in the commercially available nose cap. The majority of the fibres were found to be across the width of the nose cap. This means that the purchased nose caps have more fibres in the preferred direction than the produced ones in this study. The fibre structure of the nose caps made from recycled flakes and virgin pellets resembled a more a randomly orientated state (see Figure 5.29). These nose caps lost their shape after the resin burn out. When looking at the fibre structure, some bundles, but no flake structure could be identified.

Table 5.4 - An overview of the burn out and compression test results

Material nose cap	FVF from burn out test	Mean force first failure		Mean min. height under nose cap		Mean weight		Passed
	(%)	(kN)	SD	(mm)	SD	(g)	SD	
Pellets 19% FVF	19	12.5	1.03	12.5	1.03	43.1	1.45	X
Pellets 35% FVF	34	14.1	0.11	10.6	3.89	54.8	2.62	X
Purchased nose cap	52	N/A	N/A	27	0	69.1	0.44	✓
Recycled flakes 19% FVF	20	9.9	2.58	12.6	2.05	43.5	1.74	X
Pellets 19% FVF + insert	-	11.1	2.85	13.4	0.9	41.5	1.38	X
Pellets 35% FVF Thickened front nose cap	-	17.2	2.56	27	0.35	61.9	4.75	✓

Compression test

The universal test setup described in Section 5.3.3 and shown in Figure 5.21 was used for the compression tests. The results of the tests are given in Table 5.4. Three specimens were tested for all the different types of nose caps produced. The results show that only the purchased nose caps and the nose caps with the thickened front meet the S3 standards.

Typical force-displacement curves of the compression tests are visualised in Figure 5.30. This Figure shows that the purchased nose caps and the thickened front nose caps have a similar force displacement response. The same can be said for the nose caps of 19% FVF pellets. The nose cap made from recycled flakes fails at a lower load than the nose cap made from virgin material. This was expected from previous research, as the recycled material performs slightly lower than the virgin material, see Section 4.3.5. The nose caps from 35% FVF pellets performed better than the 19% FVF Pellets, indicating that the higher content results in a higher strength level. A relation which is in line with the results of Chapter 4.

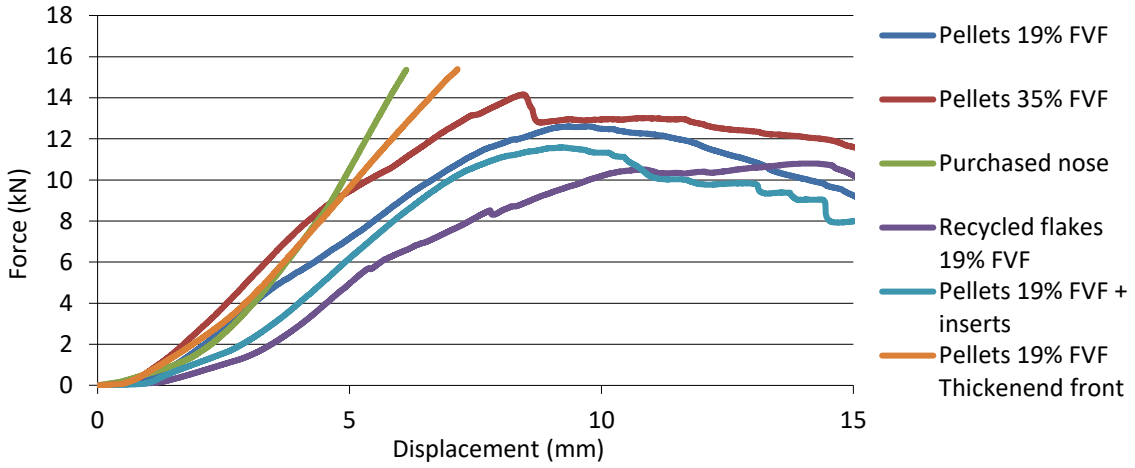

Figure 5.30 – Typical force displacement curves of the tested nose caps under compression

An example of the failure location is given in Figure 5.31. This can be compared to the simulations performed on the compression test, as shown in Figure 5.32. In the experimentally tested specimen buckling of the sides can be observed. This buckling occurs at the same location where the maximum stress is found in the simulation results.

Figure 5.31 – A nose cap made from 19% FVF pellets after the compression test

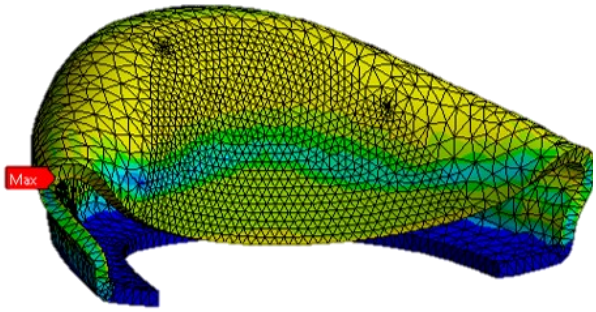

Figure 5.32 - Simulation results showing the stress distribution for a nose cap under a compression load of 15 kN and the location of maximum stress

Impact test

The universal test setup described in 0 and shown in Figure 5.22 was used for the impact test. The results are given in Table 5.5. Three type of nose caps passed the impact test: the nose cap from 35% FVF pellets, the nose cap with the thickened front and the purchased nose cap. In addition, it stands out that by adding the insert, the impact surface stayed intact. This is remarkable since the volume fraction of the insert is limited compared to the total nose cap. The insert is only 10%, with a weight of 4.4 gr in respect to the average mass of 43.5 gr for the nose cap with insert. Increasing the volume of the insert may lead to more desirable, among others, fibre orientation regarding the load scenario.

Table 5.5 - An overview of the impact test results

Material nose cap	Mean min. height under nose cap		Light through impact surface	Mean weight		Passed
	(mm)	SD		(g)	SD	
Pellets 19% FVF	14.3	1.06	Yes	43.1	1.45	X
Pellets 35% FVF	18.5	1.81	No	54.8	2.62	✓
Purchased nose cap	23.6	0.82	No	69.1	0.44	✓
Recycled flakes 19% FVF	12.0	2.17	Yes	43.5	1.74	X
Pellets 19% FVF + insert	14	1.36	2/3 No	41.5	1.38	X
Pellets 35% FVF Thickened front nose cap	21.2	0.90	No	61.9	4.75	✓

5.3.5 *Conclusion*

The results of the current research show that it is possible to produce safety shoe nose caps with the developed recycling process. It furthermore shows that it is possible to produce nose caps with recycled G/PP that meet the impact and compression requirements for S3 nose caps. The produced nose cap with the thickened front passed all the tests, in contrary to the other nose caps. Noticeably, the commercially available nose caps are heavier than the recycled nose caps. This gives way to include more material to further increase the mechanical performance of the recycled nose caps.

Further research needs to focus on producing the nose caps with the thickened front, producing nose caps at 35% FVF and the use of a larger G/PP tape insert so that fibres can be placed into the preferred direction, instead of the more random orientation typical for the compression moulding process. This will open the possibilities to produce safety shoe nose caps of S3 category with recycled material, with the low-weight benefit of composite nose caps in a process with high automation and short cycle time potential.

5.4 A Bracket

5.4.1 *Introduction*

Besides the access panel and the safety shoe nose cap, a third demonstrator was developed to showcase the capability of producing complex geometries. This demonstrator was especially aimed to test the possibility of using the developed recycling procedure in combination with the challenge of optimising the topology of complex shape products and was, therefore, less thorough described and not mechanically tested.

For this case, the aircraft engine bracket of the correspondingly named challenge organised by General Electric (GE) was selected [23]. The challenge aimed to test "crowdsourcing" of a design problem and aimed at utilising the geometric freedom of additive manufacturing to optimise the design of a titanium bracket through topological optimisation. The original design of the part was that given in Figure 5.33 and any new geometry developed should maintained the same functionalities and not exceeding the volume of the original part. Almost 700 designers submitted concepts and some achieved a weight reduction of 80% [23]. The second-best submission of all optimised designs is shown in Figure 5.34 and was made by Thomas Johansson.

Figure 5.33 - Original design of the GE aircraft engine bracket challenge, source: Carter et al. [23]

Figure 5.34 - An optimised design by Thomas Johansson from Sweden, ranked second in the contest, source: Carter et al. [23]

For the development approach the trinity of design, materials and processes as depicted in Figure 5.35 was chosen to develop a lightweight bracket. This triangle for lightweight design underlines the importance of all the following crucial paths to create reduced weight products: design, production and materials [24]. All of them are interrelated and typically none can be changed without causing impact on the others. All three aspects contribute to the creation of a final product with a low weight. For the design of concepts and analysis, topology optimisation is applied. The developed recycling process was selected as a production method with G/PP or C/PPS recycled discontinuous fibres and optionally locally reinforced by virgin UD fibre as material.

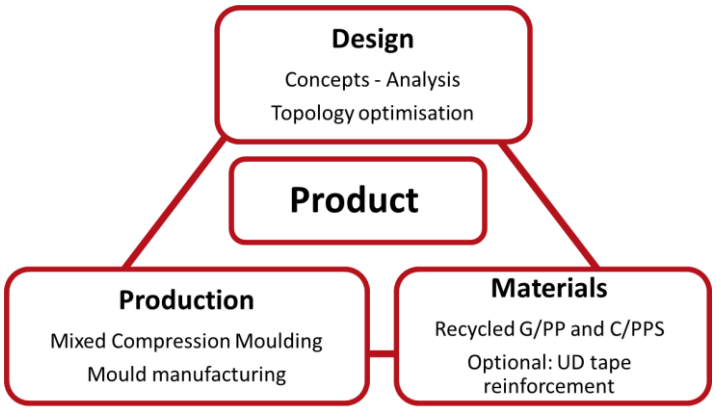

Figure 5.35 - The trinity of Design, Production and Materials is used to obtain a lightweight product [24]

5.4.2 *Design*

The design freedom is constrained by the production process through limitations related to the mould. Mould complexity is kept limited due to time and budget considerations. Therefore, the part release should be possible without sliding cores. From the material side the material flow and optional UD tape reinforcement was considered.

To obtain a better understanding of the influence of the separate load conditions on the topology optimised design solutions the following analysis a topology optimisation tool was applied. The four load conditions given in the challenge (see Figure 5.36) are separately applied to the design space to create four topology optimised designs by using Altair Inspire ™ software. Load conditions 1 and 2 lead to, among others, a bending load on the bracket. This might be a reason why the results for both conditions show full use of the top side of the design space, utilising full geometric benefits. For condition 2 also the lower side of the design space is used, resulting in a geometry close to a sandwich construction. The load of condition 3 is applied in a direction towards the fasteners of the bracket, resulting in a beam-like structure directly connecting the fastener locations with the location where the load is applied. The moment applied by load condition 4 results in a bending load in the bracket similar to, but with a different orientation from, conditions 1 and 2. This is likely the reason for the proposed solution with predominately material at the back and front, see Figure 5.36.

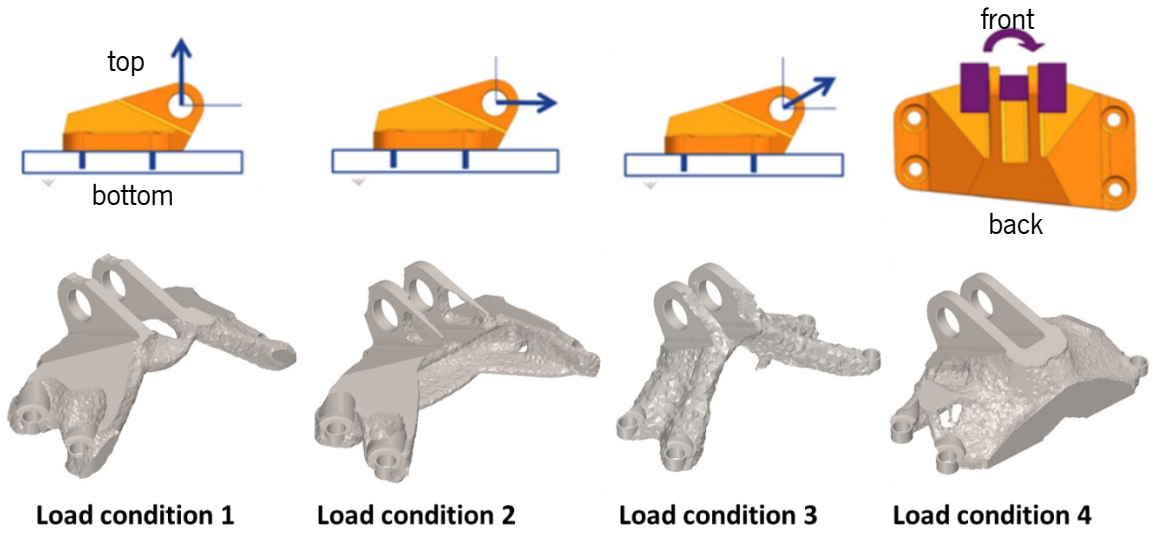

Figure 5.36 – The four load conditions prescribed by the GE bracket challenge are given in the top row and the related design solutions computed with Altair Inspire™ software are given in the bottom row

The top 10 best submissions for the challenge where evaluated to select the design. As previously mentioned, the design shown in Figure 5.34 of Thomas Johansson scored second-best and is almost 80% lighter than the original design showed in Figure 5.33 [23]. The design only needs a few adjustments to enable demoulding in the mix and compression moulding process developed in this research. Some additional modifications were made by introducing ribs for a smaller and more consistent thickness to minimise the influence of thermal shrinkage. A draft angle of 1° was added to all vertical surfaces to facilitate demoulding. The resulting CAD is given in Figure 5.37.

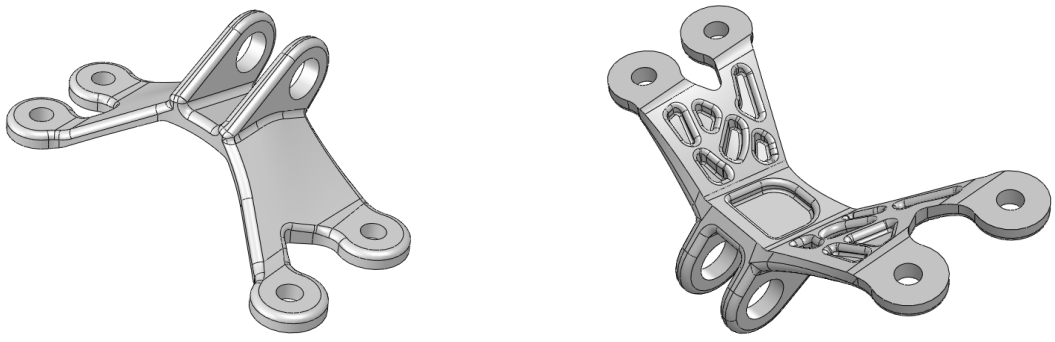

(a) (b)

Figure 5.37 - A top (a) and bottom (b) view of the CAD from the adjusted bracket for compression moulding

5.4.3 *Finite element modelling*

A simple FEM analysis is performed to study the stress distribution of the designed bracket. Solidworks® simulation software package was chosen for its wide availability and ease-of-use. A solid mesh with a mesh size of 1 mm was used in the bracket analysis. The load conditions of the GE challenge were reduced

since the design volume is limited to the original part and the original titanium material exhibit higher strength than the recycled G/PP material. A factor of 7.5 is determined by the ratio between the strength of titanium and the strength of recycled G/PP. With this factor taken into account, the load conditions become as described in Table 5.6.

Table 5.6 - Load conditions used for the FEM analysis of the bracket

Load Condition	Description
1	36 kN vertical up
2	38 kN horizontal out
3	42 kN at 42° from vertical
4	22 kN horizontal at intersection of centreline of pin and midpoint between clevis arms

The resulting Von Mises stress distribution for all load conditions are given in Figure 5.38. The stress distribution differs per load condition. In general, the stress values are below the assumed maximum allowable stress of 125 MPa in the majority of the bracket. However, stress concentrations exceeding the allowable stress can be observed at some specific locations. These locations correspond to those where most of the material is located in the results from topology optimisation (see Figure 5.36).

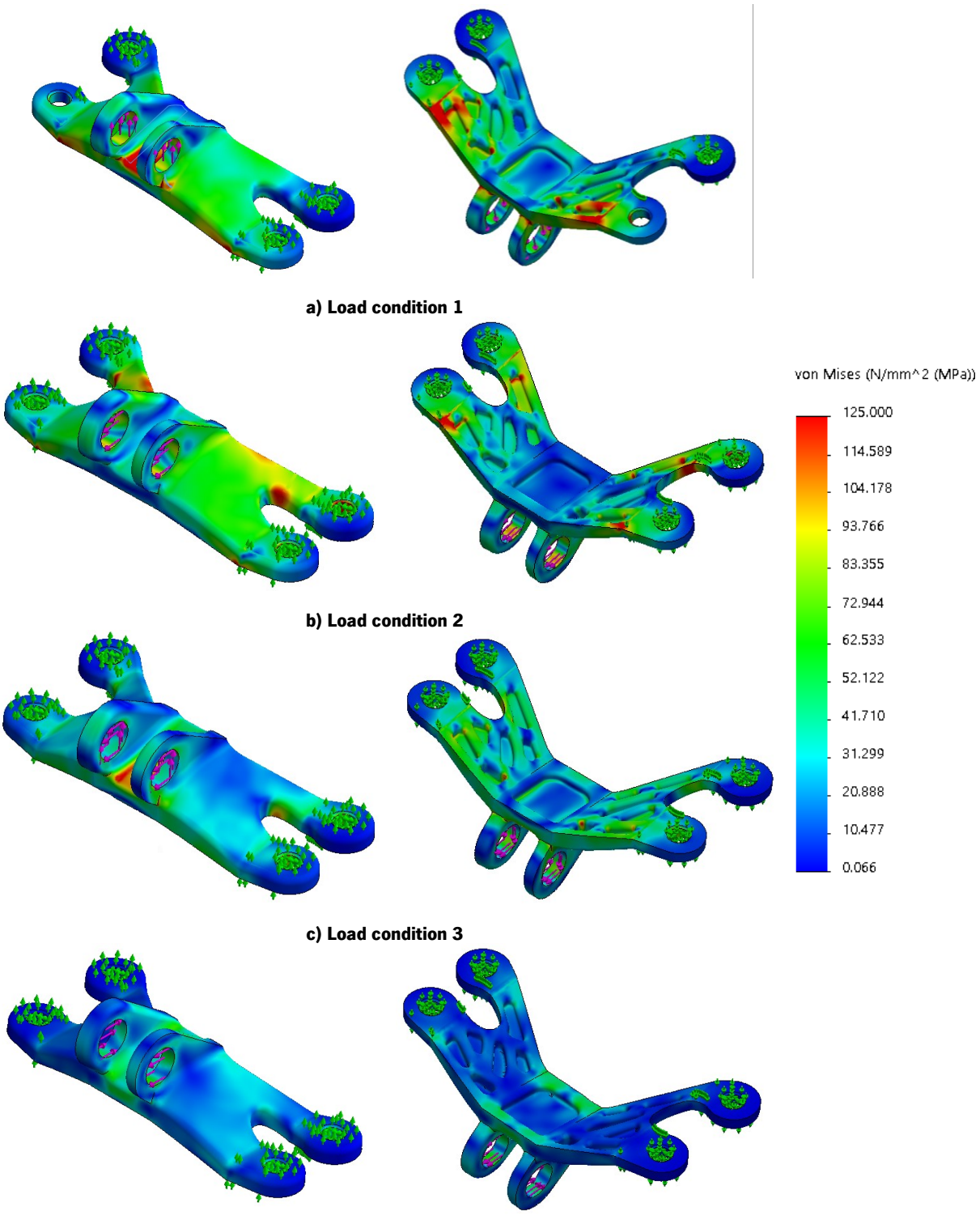

Figure 5.38 - Von Mises stress distribution for the four load conditions

5.4.4 *Processing*

To evaluate the processing route for the suggested solution, the shredded flake material from consolidated plates of 35% FVF woven commingled Twintex® where used, equal to the safety shoe nose cap application. The flakes were mixed with virgin PP to lower the FVF to 19%.

Based on the selected geometry, moulds were designed with inserts to facilitate the manufacturing of sharp edges, omit complex machine tooling and reduce production time. The inserts are depicted in Figure 5.39 by the in blue and grey coloured parts. In such conditions, the mould could be manufactured by only one ball head cutter by using one fillet radius for all non-sharp edges. All design guidelines described in Section 5.3.2 of the safety shoe nose cap are also applied to this mould. The CAD of both mould sides and including the mould inserts are shown in Figure 5.39.

The bracket was manufactured with a mixing temperature of 230°C for 10 minutes and a mixing speed of 10 rpm, in analogy to those used in the production of the safety shoe nose cap (see Section 5.3.3, Manufacturing). The material was compression moulded at 4.5 MPa pressure with a dwell time of 2 minutes and a mould temperature of 25°C.

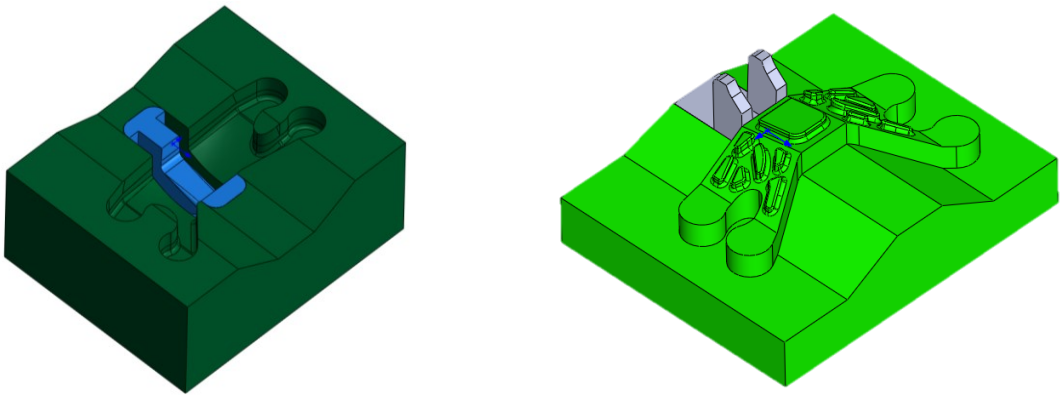

(a) (b)

Figure 5.39 – A CAD of the two sides of the mould are given in (a) and (b), a deviant colour is used to show the moulds insert to facilitate the manufacturing of the moulds

5.4.5 *Results and discussion*

The bracket designed in Section 5.4.2 was successfully manufactured with the material and manufacturing method described in Section 5.4.4. The produced part is shown in Figure 5.40. The total production time was 12 minutes, which is significant faster than additive manufacturing.

(a) (b)

Figure 5.40 - The top (a) and bottom (b) view of a produced bracket from G/PP material

Although, following this method, a significant weight saving is possible, further weight optimisation would be enabled by integrating UD continuous fibre tape inserts as is performed with the safety shoe nose cap (see Section 5.3.3: Manufacturing and 5.3.4: Manufacturing). Such an insert could improve the structural capabilities when orienting the aligned fibres of the UD insert in the load bearing direction. Multiple studies underline the weight-saving potential of UD inserts [25–27]. Beck [25], studied an injection moulded bracket including a UD insert. The UD tape insert connected the bushings for the fasteners, offering load introduction and fixation points for the insert manufacturing at the same time (see Figure 5.41). Although the insert was only 2.2% of the overall part weight, its introduction allows to increase the failure load by 2.5. Similarly, Thattaiparthasarathy et al. [26] saw and increase of mechanical performance when using the UD inserts as an alternative for ribs in a LFT plate. Katharina et al. [27] equally realised a weight reduction when applying local UD inserts in an over moulded part. The insert was placed in an unreinforced polymer to increase the bearing strength of a load introduction and compared to a glass fibre filled injection moulded polymer without the insert.

Figure 5.41 - A UD tape insert wounded around bushings for the fasteners (left) and an over moulded bracket (right). Image courtesy Fraunhofer ICT [25]

5.4.6 *Conclusion*

A bracket has been selected as a third demonstrator to show the manufacturing of a complex geometry. The part was designed for minimal weight. A mould was manufactured to enable the manufacturing of the bracket. The bracket demonstrates that the manufacturing of highly complex parts is possible with the developed recycling process. The production method has proven to allow enough geometric freedom to enable an optimised topology suitable to design complex shape parts, leading to significant weight savings and, unlike additive manufacturing, to the shorter manufacturing cycle times usually required by series production.

5.5 References

[1] GKN Aerospace, "GKN Aerospace's thermoplastic components flight tested on Bell V-280 Valor," 2020. [Online]. Available: https://www.gknaerospace.com/en/newsroom/news-releases/2020/gkn-aerospaces-thermoplastic-components-flight-tested-on-bell-v-280-valor/.

[2] GKN Aerospace, "GKN aerospace delivers thermoplastic composite components for Bell V-280 Valor," 2019. [Online]. Available: https://www.gknaerospace.com/en/newsroom/news-releases/2019/gkn-aerospace-delivers-thermoplastic-composite-components-for-bell-v-280-valor/. [Accessed: 20-Jun-2019].

[3] US Department of Transportation Federal Aviation Administration Advisory Circular AC20-107B, "Composite Aircraft Structure," 2009.

[4] S. Black, "Redesigning for simplicity and economy," *CompositesWorld*, Jan-2012.

[5] AZDEL Inc. Thermoplastic Composites, "Azdel Thermoplastic composites design and processing handbook," 1993.

[6] G. Vincent, T. A. de Bruijn, M. I. A. Rasheed, and S. Wijskamp, "Recycling thermoplastic composites using low shear mixing an experimental study on complex geometries," in *Conference proceedings 4th Inthernational Conference and Exhibition on Thermoplastic Composites*, 2018, no. October, pp. 30–31.

[7] G. Vincent, T. A. de Bruijn, M. I. Abdul Rasheed, S. Wijskamp, and R. Akkerman, "Fibre length distributions of shredded thermoplastic composite scrap," in *Proceedings of the 21th Internatinoal Conference on Composite Materials ICCM21*, 2017.

[8] T. A. De Bruijn, G. Vincent, and F. W. J. Van Hattum, "Recycling C/PPS laminates into long fibre thermoplastic composites by low shear mixing," in *Proceedings of the 21th Internatinoal Conference on Composite Materials ICCM21*, 2017.

[9] T. A. De Bruijn, G. A. Vincent, and F. W. J. Van Hattum, "Recycling of long fibre thermoplastic composites by low shear mixing," in *SAMPE Europe*, 2016, pp. 540–546.

[10] JEC Group, "A rotorcraft access panel made from recycled carbon PPS," *HOW IT'S MADE*, 2020. [Online]. Available: http://www.jeccomposites.com/knowledge/international-composites-news/how-its-made-rotorcraft-access-panel-made-recycled-carbon. [Accessed: 01-Jul-2020].

[11] H. Mason, "Recycled thermoplastic composite rotorcraft access panel takes flight," *Compositesworld*, 2020. [Online]. Available: https://www.compositesworld.com/articles/recycled-thermoplastic-composite-rotorcraft-access-panel-takes-flight. [Accessed: 26-Jul-2020].

[12] W. Schijve, "High performance at medium fibre length in long glass fibre polypropylene," *Plast. Addit. Compd.*, vol. 2, no. 12, pp. 14–21, 2000, doi: 10.1016/S1464-391X(00)80121-X.

[13] J. L. Thomason, "The influence of fibre length and concentration on the properties of glass fibre reinforced polypropylene: 5. Injection moulded long and short fibre PP," *Compos. Part A Appl. Sci. Manuf.*, vol. 33, no. 12, pp. 1641–1652, 2002, doi: 10.1016/S1359-835X(02)00179-3.

[14] International standard, "Personal protective equipment - Safety footwear ISO 20345," 2004.

[15] G. A. Vincent, T. A. De Bruijn, S. Wijskamp, M. I. Abdul, M. Van Drongelen, and R. Akkerman, "Shredding and sieving thermoplastic composite scrap : Method development and analyses of the fibre length distributions," *Compos. Part B*, vol. 176, no. February, p. 107197, 2019, doi: 10.1016/j.compositesb.2019.107197.

[16] "CompTape." [Online]. Available: http://www.compositetape.com/. [Accessed: 10-Oct-2019].

[17] T. A. De Bruijn and F. W. J. Van Hattum, "Cost-effective use of continuous fibre reinforced thermoplastic composites in plastic products," in *CAMX 2015 - Composites and Advanced Materials Expo*, 2015.

[18] K. B. Thattaiparthasarthy and U. K. Vaidya, "Processing & Characterization of Continuous Fiber Reinforcements Co-Molded With Long Fiber Reinforced Thermoplastics," in *SAMPE*, 2008, no. 4.

[19] T. A. De Bruijn and F. W. J. Van Hattum, "Cost-effective use of continuous fibre reinforced thermoplastic composites in plastic producs," in *CAMX Proceedings*, 2015.

[20] International standard, "Personal protective equipment - Test methods for footwear ISO 20344," Switzerland, 2004.

[21] Sabic, "Safety data sheet Polypropylene 522K-00900," 2015.

[22] Keystone Industries, "Material safety data sheet epoxy hardener KDP081808EPH," 2013.

[23] R. G. Carter, W.T., Erno, D.J., Abbott, D.H., Bruck, C.E., Wilson, G.H., Wolfe, J.B., Finkhousen, D.M., Tepper, A., Stevens, "The GE Aircraft Engine Bracket Challenge: An Experiment in Crowdsourcing for Mechanical Design Concepts," *Addit. Manuf.*, pp. 1402–1411, 2014.

[24] A. Beukers and E. van Hinte, *Lightness: the inevitable renaissance of minimum energy structures*, Fourth rev. Rotterdam: 010 publishers, 2005.

[25] B. Beck, "Local continuous-fiber reinforcement - tailored injection molding."

[26] K. B. Thattaiparthasarathy, S. Pillay, D. Bansal, H. Ning, and U. K. Vaidya, "Processing and characterization of continuous fibre tapes co-moulded with long fibre reinforced thermoplastics," *Polym. Polym. Compos.*, vol. 21, no. 8, pp. 483–494, 2013, doi: 10.1177/096739111302100802.

[27] K. Arnaut and A. S. Herrmann, "Tailored inserts based on continuous fibre for local bearing reinforcement of short fibre thermoplastic components," *Key Eng. Mater.*, vol. 742, pp. 82–89, 2017, doi: 10.4028/www.scientific.net/KEM.742.82.

6 Life cycle and cost assessment

6.1 Introduction

The environmental impact, economic cost and expected increasingly stringent legislation were drivers to start the development of the recycling route which is studied in this thesis, see Section 1.1. More background information can be found in the state of the art for LCCA (Section 2.4 and 2.5.4). Several studies concerning the LCA of composites in general and a few available examples specific for TPC materials and parts are described.

The objective of this thesis was to find the recycling route for processing post-industrial TPC waste leading to maximum cost effectiveness and minimum environmental impact. The mechanical performance on material level was studied analytically and experimentally in Chapter 3 and 4 respectively. In the previous chapter the access panel was designed, produced and tested as an example for the high-end application field for recycled C/PPS material. The geometric freedom of the material-manufacturing-method combination showed to be an instrument enabling a product with the required functionality while made of recycled material with inferior material properties. The developed application even proved to be lighter compared to the current solution. In addition, a safety shoe nose cap was selected for the high-volume market. With geometric adjustments it was possible to produce a nose cap meeting all requirements at equal weight as the commercially available benchmark. So, the previous chapters demonstrated the technical feasibility of the recycling route on material and product level. In this chapter the latter part of the objective is assessed, by evaluating and comparing the economic cost and environmental impact by GHG and CED of the recycled material to currently used alternatives. Three levels are considered: 1) On the material level, mechanical property and environmental data was collected and compared; 2) On a functional level, these materials were also compared by evaluating the impact of flat plate and rib designs with equal bending stiffness; 3) For the part level the developed aerospace access panel and safety shoe nose cap were selected.

6.2 Method

A quick scan LCCA [1] was used because an estimation of the impact was considered sufficient at this stage. This provides an indication of the total impact and how it is distributed for different scenarios that are considered. The method follows the structure and guidelines of the international standard for Environmental management and Life cycle assessment (ISO 14044:2006). First the goal and scope were defined, thereafter a functional unit selected and subsequently a material flowchart as a base for the life cycle inventory developed to include the life cycle phases of material, production, transport, use and end of life. In the environmental analysis the cumulative energy demand (CED, in MJ) and greenhouse gases (GHG, in CO_2-equivalents) are taken into account. The cost price is estimated by applying the same framework as for the environmental assessment and includes overhead costs. The impact of recycling is allocated to the product made out of recycled materials by integrating the cost and environmental impact of the transport and treatment of the waste material necessary to transform the waste into input material for the product made of recycled materials. The selected end-of–life treatment of waste for products made by both virgin and recycled materials is chosen to be incineration with energy recovery, as this is most common today in the Dutch recycling sector for composite materials without an industrialised recycling method [2].

6.3 Impact on material and design feature level

The following section gives an overview on material data: mechanical properties, price and environmental impact. The data is presented in a way to compare the materials by a property important for designing, in this case the bending stiffness.

6.3.1 *Comparison on material level*

Eight materials are compared on three type of properties in Figure 6.1. The figure shows, from left to right along the horizontal axis, first the mechanical properties, then the environmental impact and economic cost per mass unit and finally the environmental impact and economic cost per specific stiffness. The eight materials can be divided in four groups:

1. Injection moulded virgin C/PPS and G/PP material at 20% FVF (25% and 40% by weight respectively) and with a short fibre length (SF) below 5 mm, indicated by C/PPS (SF) and G/PP (SF).
2. MCM recycled C/PPS and G/PP material at 20% FVF and with a long fibre length (LF) over 5 mm, indicated by C/PPS (LF) recycled and G/PP (LF) recycled.
3. Aluminium 713.0 T5 and steel AISI 1095
4. G/epoxy and C/epoxy in a quasi-isotropic (QI) layup at 44% and 52% FVF respectively (63% and 65 respectively by weight)

Group 1 materials are very similar to the ones studied in this thesis (group 2). However, the virgin materials are processed by injection moulding and have therefore a shorter fibre length. Group 2 represents the recycled materials used in this research. Group 3 represents metal alloys, which are widely used for structural applications. Continuous fibre epoxy-based material systems (group 4) are typically used when continuous fibres are considered and can be found in the current and benchmarking scenario of the applications considered in Section 6.4 and 6.5. All economic and environmental data in this section (6.3) is obtained from CES Edupack [3]. Note that the injection moulded virgin C/PPS and G/PP properties are likely to originate from specimens having a high fibre orientation tensor in the loading direction, resulting in higher mechanical properties than what can be achieved in perpendicular directions (see Section 2.1.4). This has a strong effect on the stiffness and strength properties and therefore also when comparing materials 'per unit bending stiffness'. A tabular representation including a more elaborate description and specific sources of the data per kg and per specific stiffness of material can be found in Appendix D.

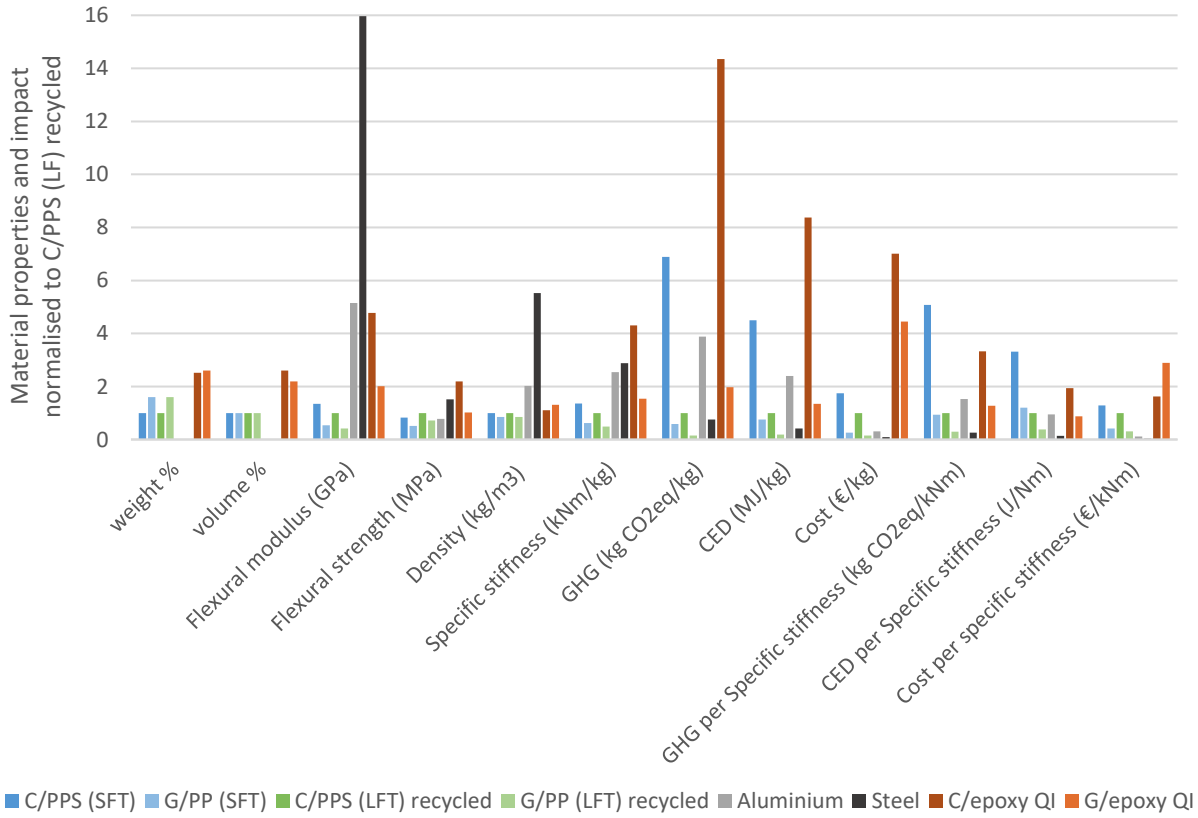

Figure 6.1 - Material properties, environmental and cost impact per mass unit and per specific stiffness, all normalised to the C/PPS (LFT) recycled material. Note that a higher value is generally preferable for mechanical material properties, but generally unfavourable for density, environmental impact and economic cost. SFT is injection moulded short fibre and LFT is MCM long fibre length.

Looking from left to right at the properties and environmental impact shown in Figure 6.1, the flexural modulus of metals is particularly high compared to all other materials and especially the discontinuous

glass fibre materials show a low value. With regard to strength, the values show less variations. The density of the materials shows a similar profile as the flexural modulus, but this property has an inverse effect on the specific stiffness. Therefore, the values for specific stiffness show less variations. The only exception is C/epoxy, which exhibits a high modulus and low density. However, the cost for C/epoxy is the highest, whereas the cost for steel is the lowest. The specific stiffness of the recycled C/PPS and glass-based composites is 2 to 5 times lower compared to values for metals and virgin carbon/epoxy. As for density, high values affect the impact both on environmental and economic cost, and are thus generally unfavourable. The high impact on CED, GHG and cost of the virgin carbon fibre materials (C/epoxy and C/PPS SF) stand out. The discontinuous glass fibre-based materials and steel show a low value on these indicators. The trade-off between the flexural modulus and the cost of density, CED, GHG or economic cost are presented on the right side of Figure 6.1. Again, the lowest values are found for discontinuous glass fibre materials, aluminium and especially steel. Recycled carbon and glass fibre materials show a lower GHG, CED, and Cost per specific stiffness compared to their virgin thermoplastic or epoxy-based counterparts.

This comparison shows that carbon/epoxy is best with regard to specific stiffness and steel is best when environmental and economic costs are taken into account. However, when looking at the specific stiffness per property, a simple linear relation between the properties is assumed, where geometric effects can result in a non-linear relation for functional applications dominated by flexural stiffness requirements, as discussed in the following section.

6.3.2 *Comparison of flat beam profiles*

For structural applications, the mechanical performance of materials is important. However, the functionality of an application is, besides the constituent materials, also determined by other factors. It is therefore favourable to compare on functionality rather than on material properties only. This is a similar approach as the analysis on the characteristic of "mechanical efficiency" (η_e) performed by Ashby [4] and Beukers et al. [5], who come to the following relation of Young's modulus (E) and density (ρ) for solid beams in compression, bending and buckling:

$$\eta_e = \frac{\sqrt{E}}{\rho} \tag{1}$$

One example of a functional requirement for the structural performance of an application is the bending stiffness. For many applications, e.g. the access panel, this bending stiffness (*K*) is an important criterion and consists of a 'material part' given by the Young's modulus (*E*) and a 'geometric part', represented by the moment of inertia (*I*).

$$K = EI \tag{2}$$

Where the moment of inertia of a rectangular cross-section is given by:

$$I = \frac{bt^3}{12} \tag{3}$$

To compare the functionality of applications, rather than material alone, the following example is made. A solid flat beam with equal width (*b*), in this case set at 10 mm, is selected. If it is assumed to be required that the beam has a bending stiffness of 2 Nm^2. A bending stiffness resulting in typically used thicknesses. The needed thickness (*t*) to achieve this bending stiffness may then to be calculated by substituting equation 2 in equation 3 and rewriting for *t*:

$$t = \sqrt[3]{\frac{12K}{Eb}} \tag{4}$$

Thus, the mass (m) per meter length for all materials can be calculated using the density, the width and equation 4 for the thickness:

$$m = \rho \cdot b \cdot \sqrt[3]{\frac{12K}{Eb}} \tag{5}$$

Figure 6.2 shows the environmental impact and cost for a flat beam design of the eight materials per meter length, with an equal bending stiffness of 2 Nm^2. Only the impact and cost of the material production phase is considered, no part production. The four discontinuous fibre materials with the "rib" suffix are discussed in the next section.

In comparison to the results on specific stiffness and impact for specific stiffness given in Figure 6.1, the results for a flat beam profile presented in Figure 6.2 show a stronger advantage for a low density and a

smaller advantage for a high Young's modulus. This can be explained by the geometric stiffening effect of a higher thickness as a result of materials with a lower stiffness, see equation 4. This non-linear effect is in line with equation 1 from Beukers et al. and equation 5. The results show that steel is the heaviest solution, at roughly twice the mass of the beam made of other materials, while on material level steel shows the highest specific stiffness, after C/epoxy. The C/epoxy material offers the lightest design for the beam. All other materials show a fairly similar mass.

The mass results directly influence the CED, GHG and cost impact with a linear relation. However, due to the high material cost per kg carbon fibre-based materials display a high GHG, CED and cost impact. Especially the recycled G/PP shows a low impact.

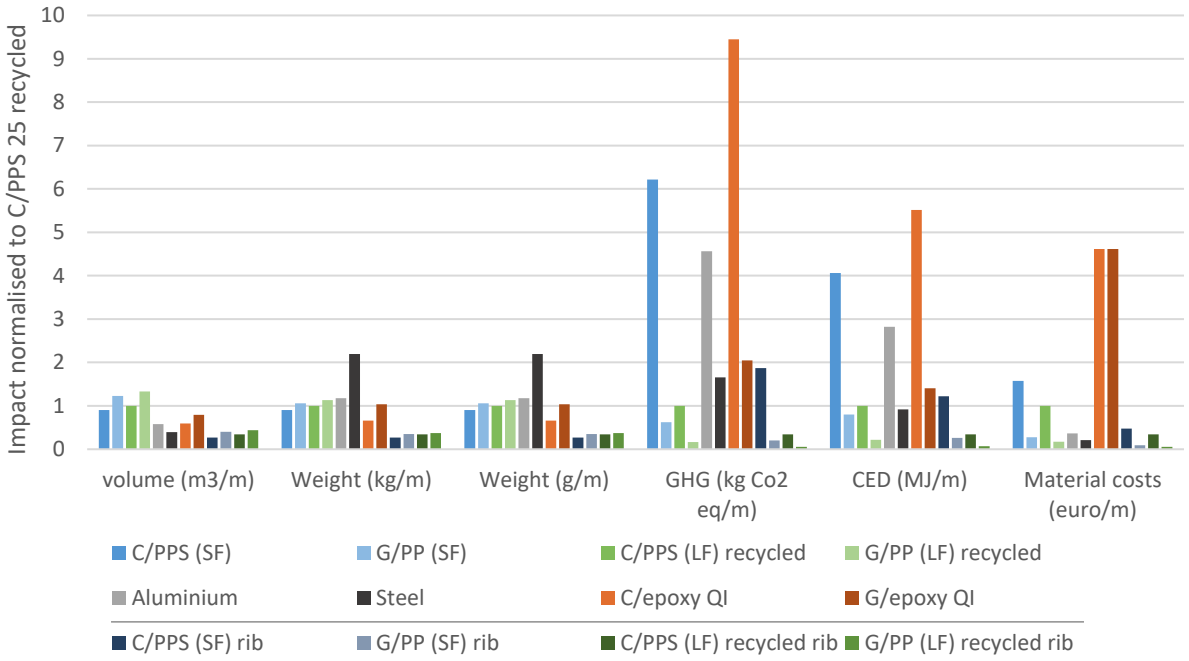

Figure 6.2 - The influence for various material types on the mass, environmental and economic impact per meter length. The geometry is a flat beam or, when indicated by a "rib" suffix, a rib geometry as in Figure 6.3. All with a bending stiffness of 2 Nm² and a width of 10mm. SF is injection moulded short fibre and LF is MCM long fibre length.

6.3.3 *Comparison of T-shaped profiles*

The use of ribs allows for stiffening a construction. With discontinuous fibre reinforced thermoplastics in an injection or compression moulding process, ribs can be realised without adding any significant processing time and cost.

In this section, a T-shaped profile is used as example. It is assumed that the T-shaped profile has a wall thickness (t), a rib height of three times the thickness making the total height four times the thickness

(3t+t) and a width of 1 cm, see Figure 6.3. The thickness (t) is calculated for the reference bending stiffness K = 2 Nm². The results are given in Figure 6.2 and Appendix D.

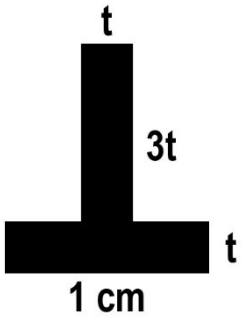

Figure 6.3 – Cross section of the considered rib geometry and associated dimensions

Comparing these values with the results for equal bending stiffness and the same materials, but a flat beam profile in Figure 6.2, a lower mass and therefore also a lower environmental impact and cost can be achieved. These solutions can also outperform other materials in terms of mass, including the generally used carbon fibre epoxy composite material, where the addition of ribs is more difficult to achieve due to constraints of continuous fibre reinforced plastic composites and the hand lay-up process.

Thus, when taking the full set of parameters influencing functionality into account during design optimisation, recycled materials can enable products with lower weight, lower environmental impact and lower economic costs.

6.4 Application: access panel

Now that there is insight on material and design level, an access panel made of recycled thermoplastic composites is analysed for the high-end aerospace industry. Different scenarios are described and analysed using quick scan LCA methodology and cost price calculation, as described in Section 6.2. The following three scenarios are considered:

I. Hand-laid panel made of virgin C/epoxy material – the current fabrication method
II. Direct compression moulded access panel made of recycled C/PPS material, which is a previously suggested recycling method [6], see Section 2.2.1 and 2.3, including Figure 2.17b.
III. Mixed and direct compression moulded panel made of recycled C/PPS + virgin PPS material - the currently applied recycling method proposed in this work, see Section 5.2.

6.4.1 *Goal and scope definition*

In this study, the life cycles of three scenarios for a specific access panel of an airplane were analysed and compared. The scenarios only differ in the materials and manufacturing processes used. The first one is the original one, a panel made of virgin material. The other two are redesigns made from recycled material. The overall goal of this study is to determine the environmental gain, if any exists, by using recycled material and the corresponding required process. The following phases are taken into account: material production, part production, transport, use and end-of-life. All scenarios require part quality evaluation by non-destructive testing (NDT), which is included. Maintenance, R&D, installation and dismantling phases were excluded from the study.

The *functional unit* used in this study is an access facility for the inspection of an airplane wing with a lifespan of 30 years or 28,000,000 km.

6.4.2 *Life cycle inventory*

All panels are assumed to have the same mass of 0.5 kg. However, as shown in Section 5.2.5, it is possible to develop a version made of recycled material with a mass reduction of 9% and therefore the results for that case are presented in Section 6.4.4. Since it is considered that such a mass reduction might not always be possible, the majority of the study was performed assuming an equal mass. This section describes the life cycle inventory of the three scenarios previously defined. Due to the different characteristics of the materials used, the production method of the scenarios varies.

The environmental impact of the use phase is estimated by calculating the impact of transporting 0.5 kg (the estimated panel mass) by a large business jet for 28,000,0000 km. Environmental data from CES Edupack 2019 [3], Ecoinvent 2012 [7] and IDEMAT 2010 [8] was used. When no CO_2-emission data was

available, the following conversion ratio was used 1 MJ = 0.19 kg CO_2-equivalent, according to Ecoinvent, for the energy mix in the Netherlands [7].

For the cost calculations a 15% overhead and 20% profit margin were assumed. Small deviations are explained by rounding the numbers. The processing costs were based on machine, operating and handling costs, obtained from CES Edupack 2019 [3] and internal communication [9]. A production of 2400 parts per year, for 20 years was assumed. This makes the costs for the mould per part negligible. Fuel cost was estimated by assuming 30000 flight hours of a 25000 kg business jet consuming 1900 l/h at a price of 0.34 €/l [10]. More details on the sources used can be found in Appendix E.

Scenario I: Hand-laid panel made of virgin epoxy and carbon fibre material

In this scenario, illustrated by a material flowchart in Figure 6.4, the panel is produced by hand lay-up of prepregs made of virgin material. 50 parts are cured per cycle of 3 hours in an autoclave [9]. Carbon fibres are impregnated with epoxy in a prepreg step, where 5% material loss is taken into account. The prepreg is cut resulting in 15% material loss and positioned on the mould, vacuum-bagged and cured in an autoclave. Thereafter the part is debagged, trimmed (7% material loss) and a non-destructive test (NDT) is performed. It takes 0.625 kg of material for the production of a 0.5 kg part. Nylon foil, which is used a vacuum sealant, is included in the study as an aiding material, other consumables such as bleeder, peel plies and tapes are neglected since these are considered of little impact. The processing time of the hand lay-up process is estimated to 75 min, at an average of 74,35 €/h including cooled storage, cutting, hand layup, vacuum bagging, debagging, trimming, and 35% overhead and profit. The cost of the autoclave is estimated at 150 €/h and 3 hours are necessary to produce the 50 parts. All data originate from internal communication within the TPC-Cycle project [9]. More information can be found in the material flowchart in Figure 6.4 and Appendix E.

Scenario II: Direct compression moulded panel made of recycled material

In this scenario the panel is made of recycled C/PPS semipreg as studied by Rasheed [6]. As shown in Figure 6.5, C/PPS waste material is transported for 100 km to be shredded. The impact of shredding is based on Woldt [11]. In the shredding process, 5% material loss is taken into account [9]. The shredded flakes are heated and formed by direct compression moulding. For this step also 5% material loss is taken into account [9]. It will take 0.56 kg of material for the production of a 0.5 kg part. To determine the CED and GHG the energy consumption is calculated by including the energy loss due to convection of the mould [12], the heating of the mould, applying the pressure and heat loss during dwell. With 89%, most

energy is consumed by heating the plates and mould with a combined mass of 700 kg, the mass is calculated using the dimensions of the mould. The successive phases are assumed to be the same as for scenario I. The life cycle is illustrated in Figure 6.5. Processing cost for direct compression moulding is estimated to 120 €/h for a cycle of 2 hours, excluding 35% overhead and profit [9]. More details can be found in Figure 6.5 and Appendix E.

Scenario III: Mixed and compression moulded panel made of recycled + virgin material

This is the production method as described in Section 2.2.1. The method can process both shredded prepregs and consolidated laminates. Compared to scenario II a mixing step is added to heat and mix the composite material before compression moulding in order to improve the fibre distribution and cycle time, see Figure 6.6. The environmental and cost data for moulding C/PPS are taken from CES Edupack [3]. In the shredding process 5% material loss is taken into account [9]. Virgin PPS material is added and mixed with the shredded C/PPS, and 2% of production waste are taken into account for the compression moulding step (measured during production). It will take 0.24 kg of shredded C/PPS and 0.31 kg PPS material for the production of a 0.5 kg part. Processing costs for mixing and compression moulding are estimated to 130 €/h and a cycle of 15 minutes per part, excluding 35% overhead and profit [9].

An important difference between scenario II and III is the method of heating the material. In scenario II, heating takes place inside the mould, requiring the mould to be heated above the melt temperature of the polymer and cooled for every part. For scenario III, the material is heated during the mixing phase. Subsequently, the hot material is transferred to a mould that can remain at constant temperature, thus avoiding multiple heating and cooling cycles which decreases both energy consumption and processing cycle time. The successive phases are assumed to be the same as for scenario I. The life cycle flowchart is illustrated in Figure 6.6 and more data in a tabular format can be found in Appendix E.

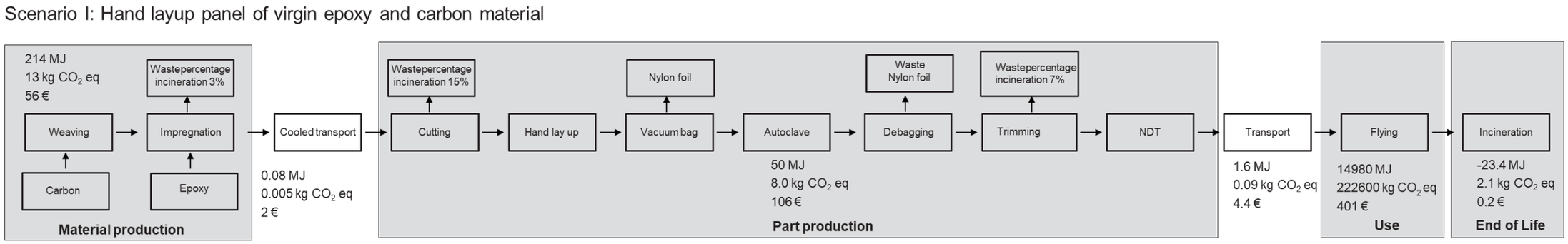

Figure 6.4 – Material flowchart of Scenario I: Hand lay-up panel of virgin material. The CED, GHG and economic impact are given for all four life cycles phases and transport

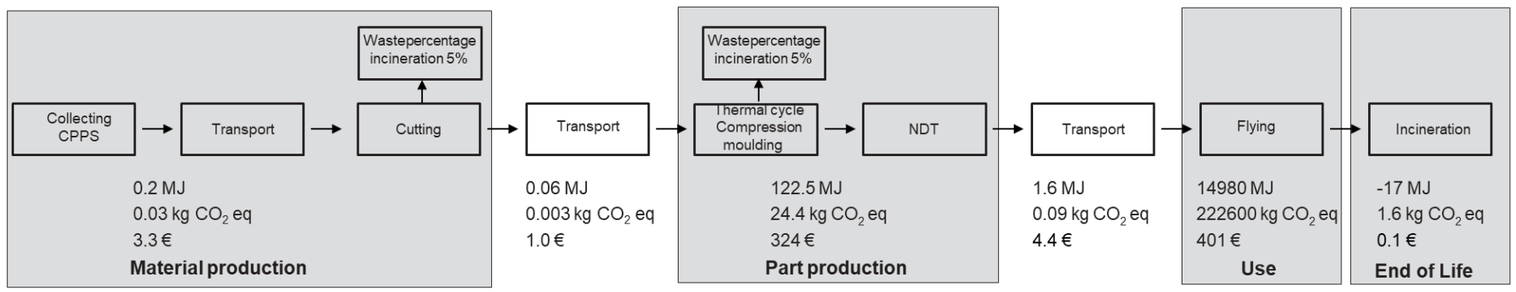

Figure 6.5 - Material flowchart of Scenario II: Direct compression moulded panel of recycled material. The CED, GHG and economic impact are given for all four life cycles phases and transport

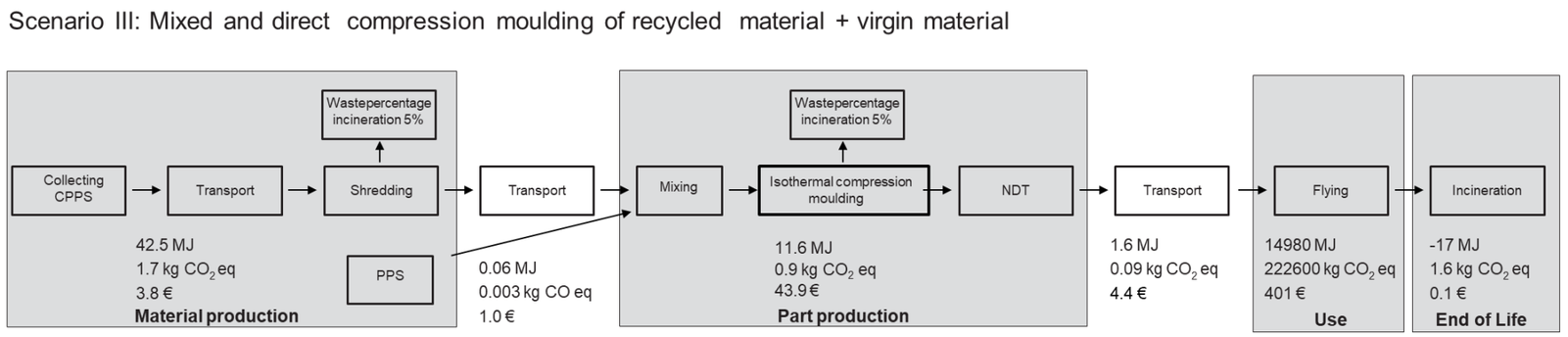

Figure 6.6 - Material flowchart of Scenario III: Mixed and compression moulded panel of recycled material + virgin material. The CED, GHG and economic impact are given for all four life cycles phases and transport

6.4.3 *Results*

With the Life cycle inventory discussed in the previous section, this section describes the results for the environmental impact with and without use phase. Furthermore, the economic impact is described and finally the overall results.

Environmental impact

In this section the environmental impact, as calculated following the methodologies described in Section 6.2 and using the inventory data of Section 6.4.2, is presented. As it can be seen in Figure 6.7 and Figure 6.8, the use phase has clearly the highest impact in all three scenarios and for both CED and GHG (>98% of total). Since the panel mass is assumed equal here for all scenarios, the impact is also equivalent. Section 6.4.4 shows the result for the case in of a mass reduction of 9%, since Section 5.2.5 shows that the recycled panel can be produced lighter. Beside mass, there is no influence on the use phase by the topics described in this thesis and therefore a comparison without the use phase is made between the three scenarios in the following section.

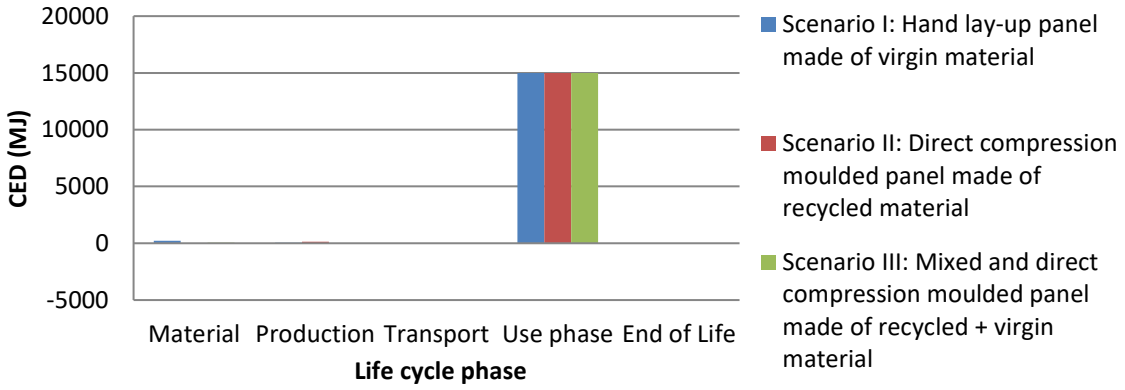

Figure 6.7 – Impact of scenarios on CED for all life cycle phases

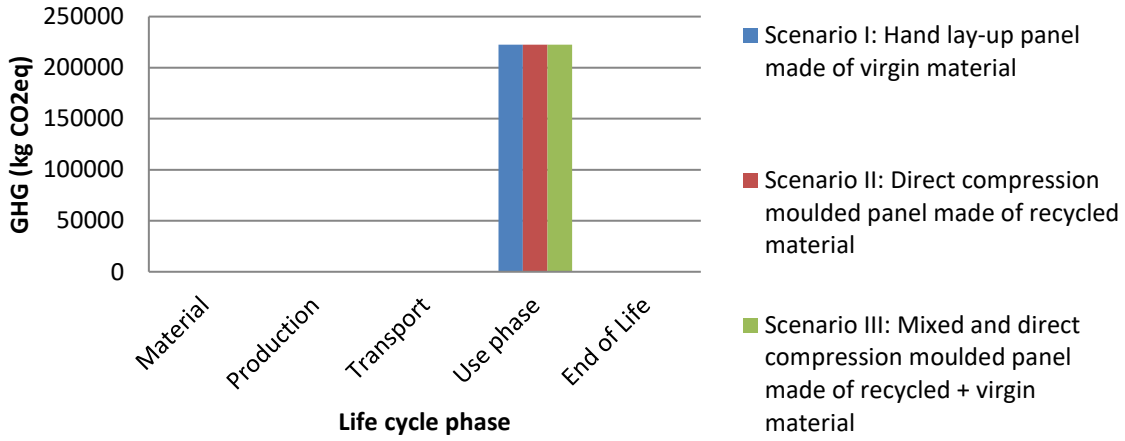

Figure 6.8 - Impact of scenarios on GHG for all life cycle phases

Environmental impact without use phase

Another comparison is made excluding the use phase. In this comparison, the major influence is the limited amount of virgin material in scenarios II and III, as presented in Figure 6.9 and Figure 6.10. This reflects the energy-intensive production process of virgin carbon fibre, presented in scenario I. Additionally, due to the high amount (25%) of material waste in the production process, scenario I uses even more of this virgin material. Scenarios II and III have far less material waste, each 7%. This 'near net shape production' is more in line with the waste prevention strategy from the EU waste framework directive [13]. A small effect of the added virgin polymer when 'diluting' the recycled material for processing in scenario III can also be observed. This effect isn't present in scenario II as the panel fully consists of recycled material.

The second scenario has a relatively high impact in the production phase. The large amount of GHG in this phase can be explained by the high amount of energy needed, i.e. for the heating cycles of the mould, and energy which is assumed to be used in the Netherlands.

The negative energy at the end of life for all three scenarios can be explained by assuming incineration with energy recovery as most likely scenario. It can be seen that more energy is recovered in scenario I due to the larger amount of waste generated. However, overall it can be observed that scenario III has the lowest impact with regard to energy use as well as greenhouse gases.

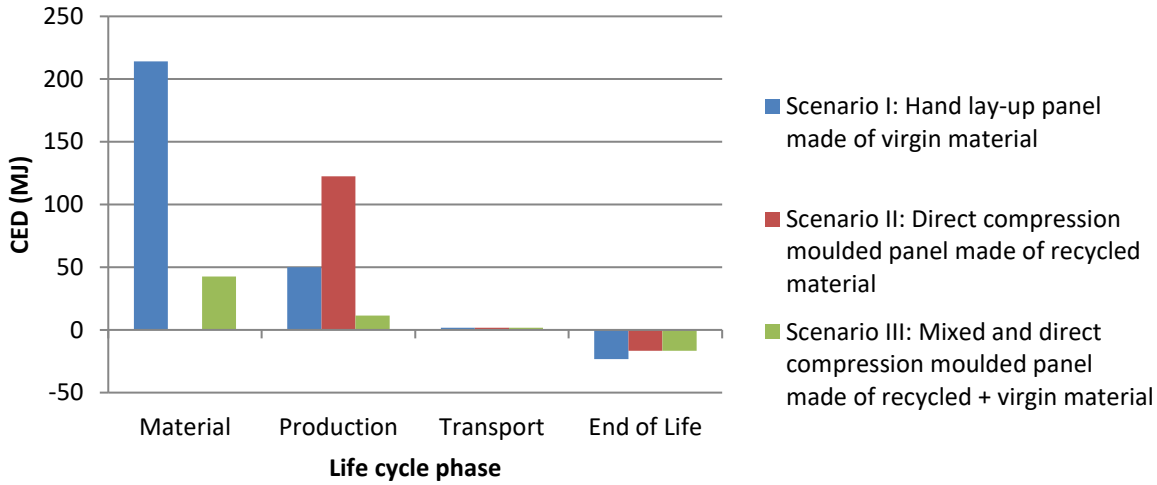

Figure 6.9 – Impact of scenarios on CED without use phase

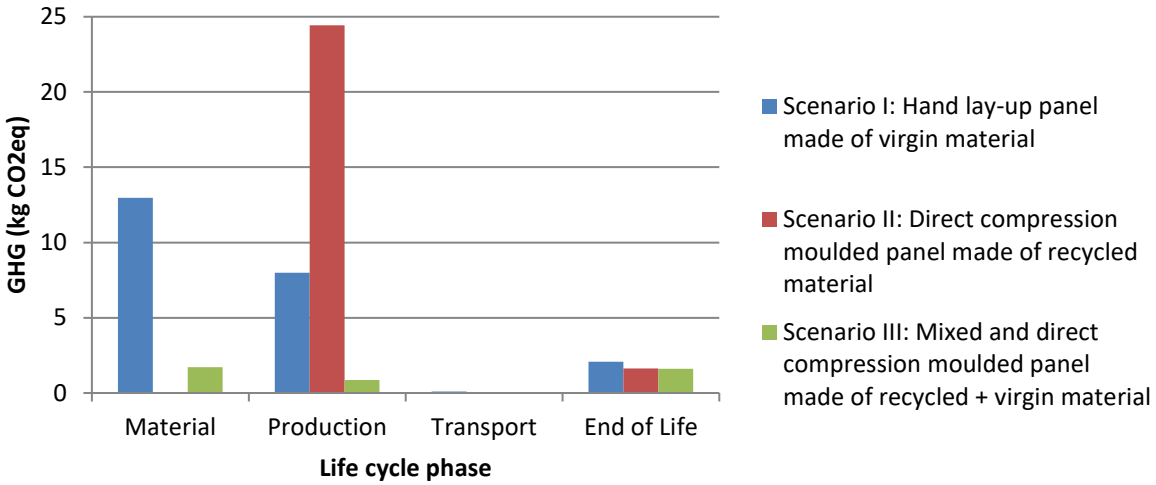

Figure 6.10 – Impact of scenarios on GHG without use phase

Economic impact

In this section the estimated costs related to the different life cycle phases for the three scenarios are presented. The cost per phase is presented in Figure 6.11 for all scenarios. The results show that the use phase, in this case fuel costs allocated to the panel, is again the most dominant phase with 69%, 54% and 86% for scenario I, II and III, respectively. Hereafter, the material and production costs have the highest contribution.

Scenario II has the highest cost for the entire life cycle as a result of the high production costs, and in particular due to the long heating cycle. The material phase of scenario I is highest, which can be explained by the price of 100% virgin material in comparison to the scenarios using recycled material. A second reason for a lower cost of scenario II and III in the material phase is the near net shape production, resulting in less waste as a trimming stage is not needed. To sum up, scenario III is, beside the environmental aspect, also favourable with regard to the economic impact.

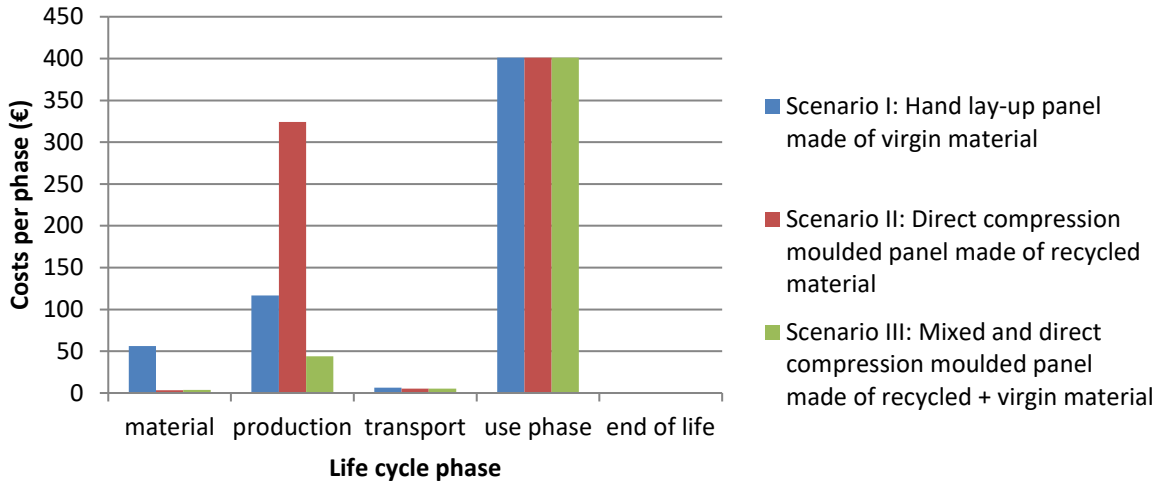

Figure 6.11 - Cost of access panel per life cycle phase for all scenarios

Overall results

A summary of the environmental and economic impacts for all scenarios are presented in Figure 6.12 to ease the comparison. The values are without the use phase and normalised to the current virgin material hand lay-up scenario. The impact of an access panel produced by the mixed and compression moulding process using recycled material with added virgin material (scenario III) is 84%, 81% and 64% lower for CED, GHG and economic impact, respectively, than the impact of scenario I (virgin material panel made by hand lay-up). Scenario III also shows a lower impact with regard to the DCM process of recycled material (scenario II), showing both the environmental and economic benefits of the process developed in the current study.

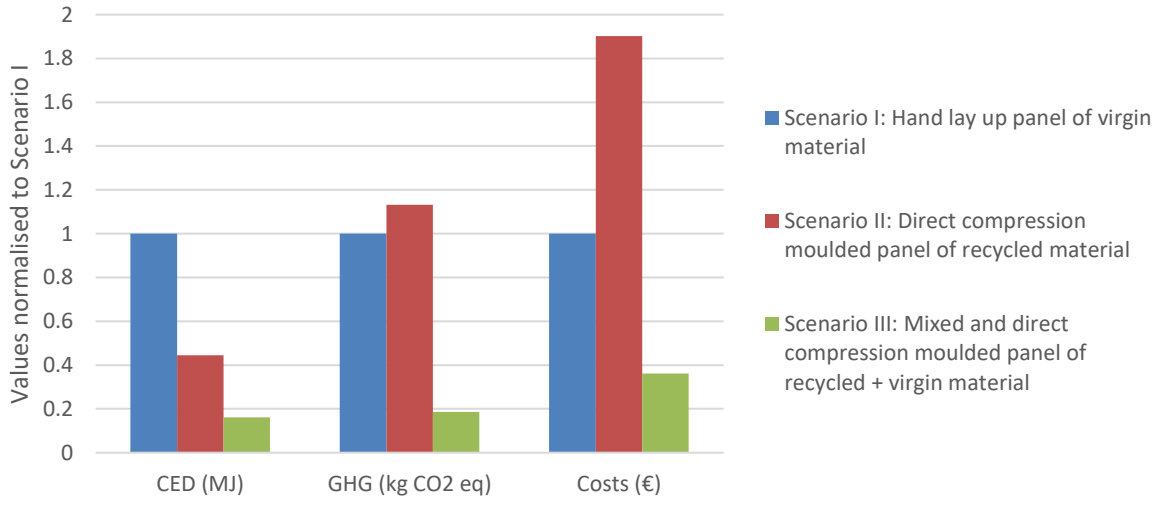

Figure 6.12 - Normalised environmental and economic impacts without use phase

6.4.4 *Mass reduction of redesigned parts*

As explained in Section 5.2.5, the actual redesigned parts allow for a mass reduction of 9% in comparison to the original access panel. For a fair comparison in the previous sections the panels were assumed to have the same mass. However, as an indication of the effect of a mass-optimised solution the impacts were recalculated and are presented in Figure 6.13. The results are again normalised to scenario I and include the use-phase. In comparison to the values presented in Figure 6.7 and Figure 6.8, a 9-10% reduction of the total environmental impact, both for CED and GHG, can be observed. The economic impact accounts for a 17% increase for scenario II and a 27% decrease for scenario III compared to scenario I, underlining the benefit of the process developed in the current study.

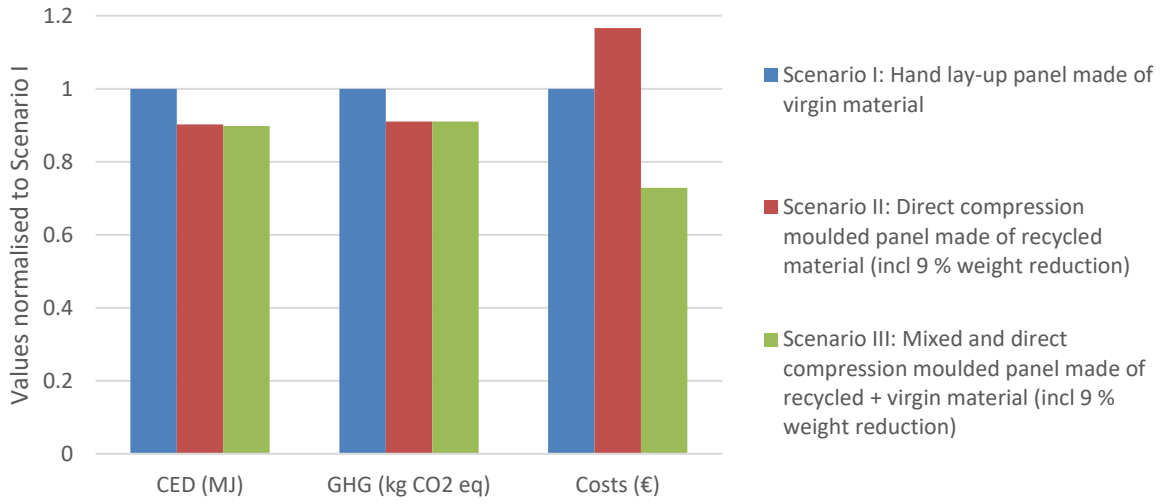

Figure 6.13 - Normalised environmental and economic impacts for all life cycle phases considering a 9% mass reduction for scenario II and III

6.4.5 *Discussion*

The ratio between GHG and CED of scenario I and II is dissimilar, see Figure 6.12. The difference can potentially be explained by the location of the energy production and associated GHG emission. The carbon fibre production in the material phase of scenario I is placed in Japan, because Japan is the main producer of carbon fibre worldwide [14], whereas the energy consumption during the production phase of scenario II is assumed to be taking place in the Netherlands. Energy in Japan is produced at a lower GHG emission in comparison to the Netherlands. The large influence of the energy mix of a specific geographic region on the GHG emissions for the production of carbon fibre is also mentioned by Witik et al.[15]

For scenario I, a number of 50 parts per autoclave cycle is assumed. This might be an overestimation. When a number of 15 is assumed, the results show an increase for the GHG (+74%), CED (+37%) and cost (+12%) impact of Scenario I. The results for 15 parts per autoclave cycle are presented in Figure 6.14. The GHG and CED of scenario I for the production phase is now slightly higher than of Scenario II. The cost of trimming in Scenario I might be higher for more complex parts. Since the production method of this scenario does not lead to a net shape part, costly CNC and special moulds will be required.

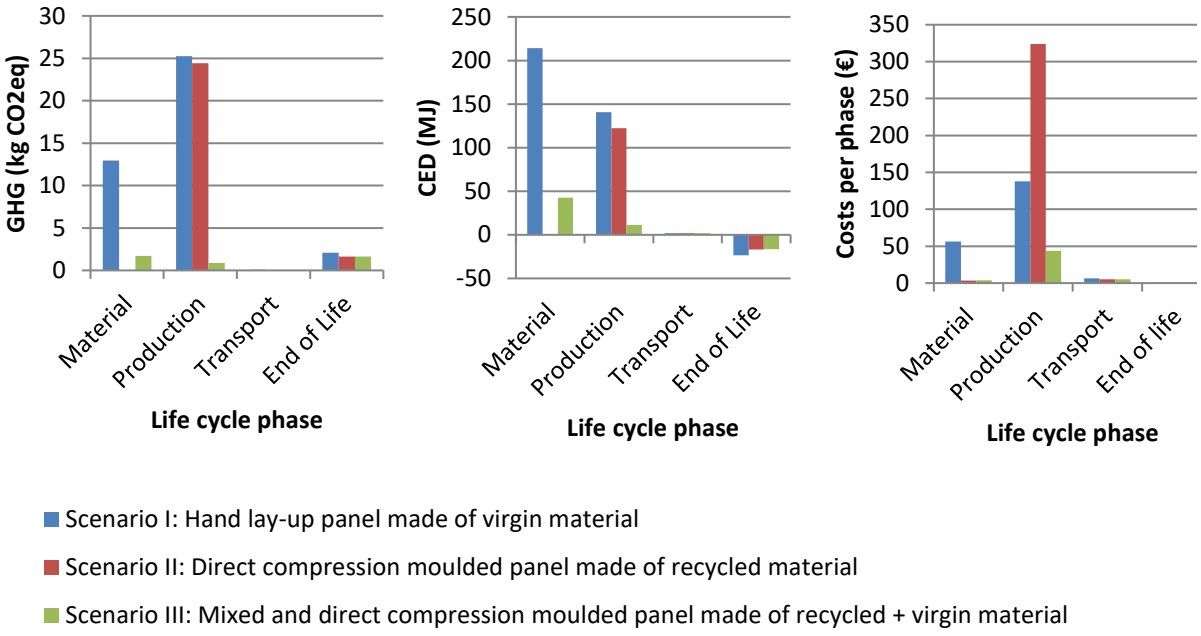

Figure 6.14 - The results when the number of parts in scenario I for autoclave cycle is adjusted from the initial 50 to 15. The GHG, CED and Cost impact per life cycle phase (excl. use phase) for all three scenarios. The production of Scenario I changed significantly to the results shown in Figure 6.9 to Figure 6.11.

The production phase of Scenario II could possibly be improved by making use of an induction heated mould. This technology would enable to heat only the surface of the mould touching the material, instead of heating the entire mould. The result would likely be a lower energy consumption and a quicker compression moulding step as advantages, but it would lead to a costlier production equipment and mould design.

The use of thermoplastic materials, the geometric freedom offered by discontinuous fibre composites and the compression moulding process used in scenario II and III could allow for benefits during successive processes and assembly. For example, the thermoplastic material allows for welding, in the process a lightning strike protection material could be integrated and the geometric freedom could allow for a design with function integration or one which is more favourable for installation. These potential benefits could influence the economic and environmental results but were not included in this study.

The cost related to waste management to ensure traceability of the material might become costly when the size reduction step is outsourced outside the manufacturing company where the waste is produced. This may lead to a higher waste material price compared to the 5 €/kg used in this study.

The majority of the results is presented without the use phase. Unlike environmental savings, most of the kerosene cost savings are associated to the end-user, whereas material, production and transport costs savings are directly linked to the part manufacturer. Hence, the economic impact of these phases, when all is equal, are most likely to be a critical factor for a part manufacturer's decision on which scenario to follow. Here, the lower economic impact in these phases of the process developed during this study (scenario III) shows clear benefits.

Environmental and economic data was not readily available during this study. The environmental data is often not known and economic figures are not easily shared since this data is often considered competition-sensitive information. Therefore, the accuracy of absolute figures may not always be high. However, the relative proportions between the scenarios are likely to stay valid since a similar method is applied for all three scenarios. Further research is required to collect more data of all scenarios. Also, additional environmental indicators should be involved and might enable an analysis including end-point effect by i.e. the Recipe method.

6.4.6 *Conclusion*

Looking at the environmental impact of the access panel at equal mass, the use phase has the largest contribution to the overall impact with over 98% for all scenarios. Therefore, lowering the mass is by far the best strategy to reduce the environmental impact. Since the studied access panel of recycled material actually features a mass reduction of 9%, the environmental impact for this case is 10-11% lower.

The second-largest factor in GHG and CED reduction comes from replacing the virgin C/PPS for recycled material, because the material extraction gives the second largest contribution to the overall impact. The type of process is important when recycled material is chosen. The isothermal mould of scenario III results in a lower environmental impact compared to the process of scenario II.

Regarding economic impact, the use phase (costs for kerosene) has again the highest contribution over the total lifespan, but the ratio is with 53-86% smaller compared to the environmental impact. Therefore,

reducing the mass of the panel results in the biggest reduction of cost. Second largest contribution is material costs, showing the potential for recycling.

Overall, the CED, GHG and economic impact, without the use phase, of an access panel produced by the developed method in this thesis (scenario III) account for a decrease of 84%, 81% and 64%, respectively, in comparison to the current scenario (scenario I).

6.5 Application: Safety shoe cap

In analogy to the C/PPS access panel, the safety shoe cap described in Section 5.3 was also analysed for its environmental and economic impact and compared to a commercially available counterpart. In contrast to the access panel which is meant for the high-end market, this application is designed for high-volume production, and therefore made of cost-effective G/PP bulk material. The following two scenarios are considered:

I. Resin transfer moulded safety shoe cap made of virgin G/epoxy material – the current fabrication method
II. Mixed and direct compression moulded safety shoe cap made of recycled G/PP + virgin PP material - the currently applied recycling method proposed in this work, see Section 5.3

6.5.1 *Goal and scope definition*

In this study, the life cycle of two safety shoe caps was analysed and compared. One, the commercially available shoe cap, is made from virgin materials: glass fibres and epoxy resin. The other cap is produced from recycled G/PP with additional virgin PP, see Figure 6.15. Their impact strength is similar as detailed in Section 5.3.4. It was assumed that the caps are produced in Brazil [16].

The goal of this study is to find out whether an environmental gain exists when using recycled material. The following phases are taken into account: material production, part production, transport, use phase and end-of-life. The use phase is assumed to have no impact because there is no maintenance or energy usage dedicated to the safety cap. Also, R&D, installation and dismantlement steps were excluded from the study since there was no data available and these steps are considered the same for both scenarios.

The *functional unit* used in this study is a toe protector capable of withstanding a compression force of 15 kN and an impact energy of 200 J for a single time [17].

Figure 6.15 – Safety shoe application with shredded material (left), a safety shoe (top) and the G/PP nose caps (bottom)

6.5.2 *Life cycle inventory*

This section describes the life cycle inventory of the two scenarios. See Figure 6.16 for caps of both scenarios.

In Section 5.3.4 it was shown that it is possible to design a version made of recycled material which also allows for a small mass reduction. However, considering that such a mass reduction might not be possible when a larger margin of safety is included, an equal mass was assumed in this study. Therefore, the environmental impact is based on a mass of 69 grams for both shoe caps. Environmental data from CES Edupack 2019 [3], Idemat [8] and EcoInvent v. 2012 [7] were used. When no CO_2 emission data was available, the following conversion ratio specific for the energy mix in the Netherlands was used 1 MJ = 0,19 CO_2, according to Ecoinvent V2-2, 2010.

The cost calculations are based on sales prices of individual parts which include 15% overhead and 20% profit margin. Small deviations can be explained by rounding numbers. The processing costs are based on machine, operating and handling costs. Wage in Brazil is assumed to be 5.74 €/h including overhead and profit [18].

Figure 6.16 - Two Safety shoe nose caps: left cap made of virgin glass/epoxy, right cap made of recycled G/PP

Scenario I: Safety shoe cap virgin material

In this scenario the cap is produced from virgin material by resin transfer moulding (RTM), see material flowchart in Figure 6.17. Glass fibres are produced and woven into fabrics. The weave is cut into 17 pieces and positioned in the mould (see Section 5.3.4). In this step, a material loss of 15% is taken into account. Then, epoxy is added to the glass fibres by resin transfer moulding. The part is demoulded and the edges are trimmed (5% waste assumed in the model). Now the safety cap is ready for assembly into the safety shoe. At the end of its lifespan the shoe with cap is considered to be incinerated with energy recovery. The resin transfer moulding setup is 45 €/h incl. overhead and profit, based on CES Edupack. It is assumed that four shoe caps are produced within 6 min. More detailed information can be found in Appendix F.

Scenario II: Safety shoe cap (recycled material + virgin material)

In this scenario the cap is produced by mixing and compression moulding recycled G/PP with added virgin PP, as described in Section 5.3.3 and illustrated in the material flowchart in Figure 6.18. Recycled G/PP is first shredded (assuming 5% waste [9]) before it is mixed and heated with virgin PP. Thereafter the heated material mix is compression moulded in an isothermal mould. After demoulding the net shaped product, the safety cap, is ready for assembly into the safety shoe. At the end of its lifespan the shoe with cap is considered to be incinerated with energy recovery. The mixing and compression moulding setup is 45 €/h incl. overhead and profit. Four shoe caps are produced every 4 min. The complete life cycle is illustrated in Figure 6.18.

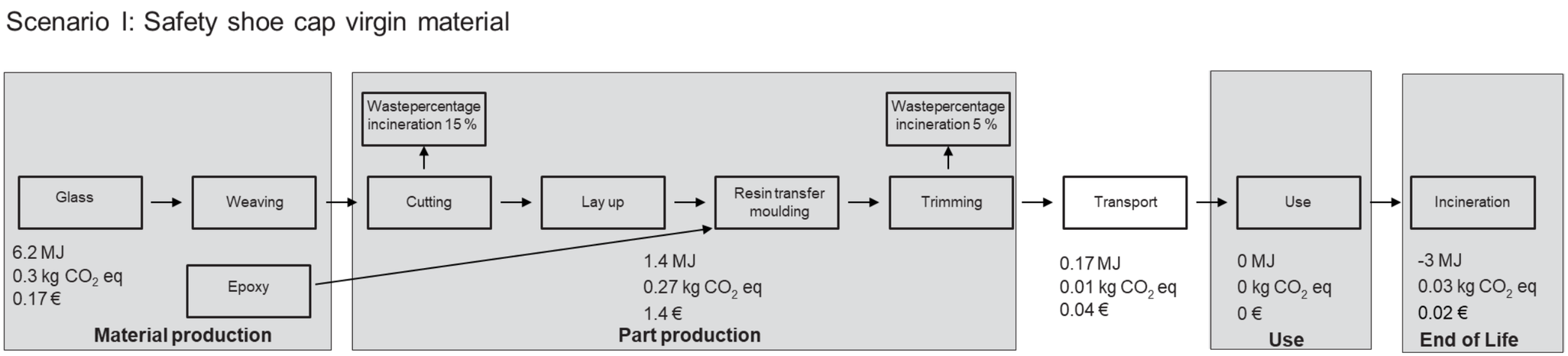

Figure 6.17 – Material flowchart of Scenario I: Safety shoe cap produced by resin transfer moulding of virgin material. The CED and GHG are given for transport and all life cycles phases, except the use phase.

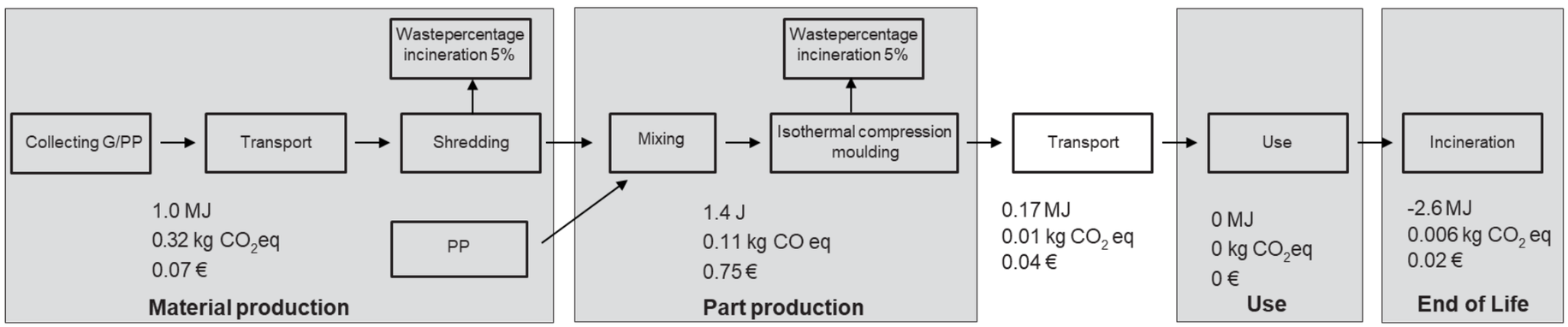

Figure 6.18 – Material flowchart of Scenario II: Safety shoe cap produced by mixed compression moulding of recycled + virgin material. The CED and GHG are given for transport and all life cycles phases, except the use phase.

6.5.3 *Results*

Environmental impact

The results for CED and GHG are presented in Figure 6.19 and Figure 6.20, respectively. The data shows that first the material, and then the production process contribute the most to the environmental impact. The difference between the scenarios is the largest for the material production phase. The impact of the material considered in scenario I is 6 and 10 times larger than of the material used in scenario II for CED and GHG respectively. When both material and part production phases are considered, Scenario I shows a three- and four-times higher impact for CED and GHG respectively. This can be explained by the energy intensive process for producing glass fibres and epoxy. The CED results for the end of life phase are negative, since energy is produced by combustion of the polymer. More energy is obtained in scenario II, since there is more polymer material (lower FVF) in the safety shoe cap considered in scenario I compared to Scenario II.

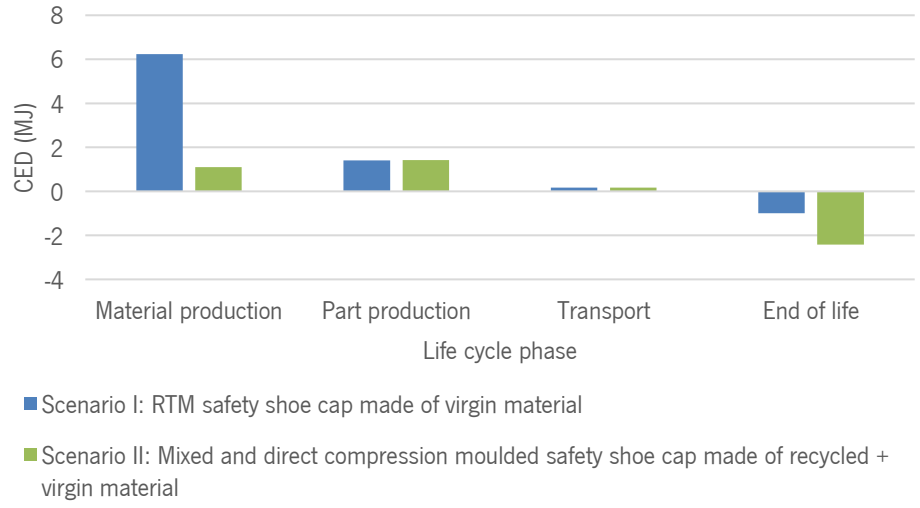

Figure 6.19 - Impact on CED for all life cycle phases

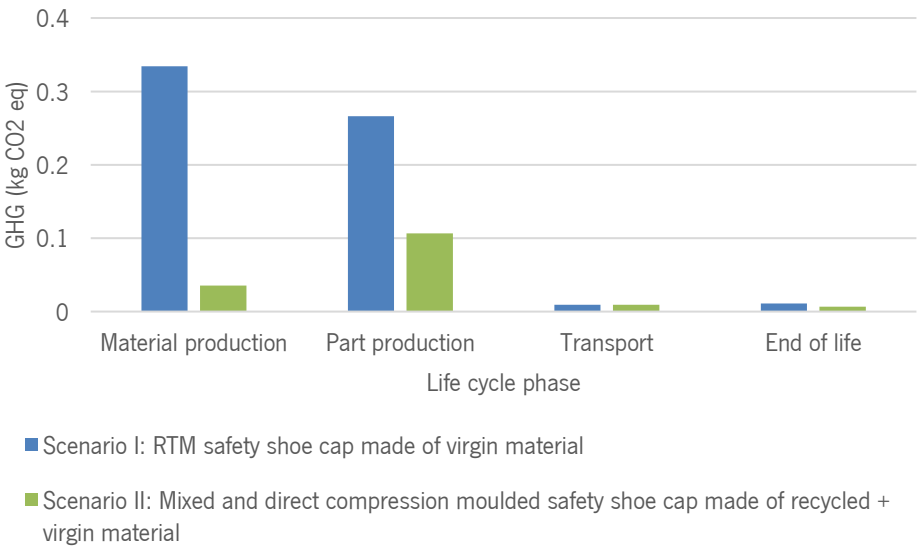

Figure 6.20 - Impact on GHG for all life cycle phases

Economic impact

The economic cost per phase for both scenarios is presented in Figure 6.21. Most of the costs results from the part production. For scenario I, cutting, lay-up and resin transfer moulding requires more time and is therefore more expensive compared to the mixing and compression moulding in scenario II. It can also be noted that transport and end-of-life hardly contribute to the overall costs.

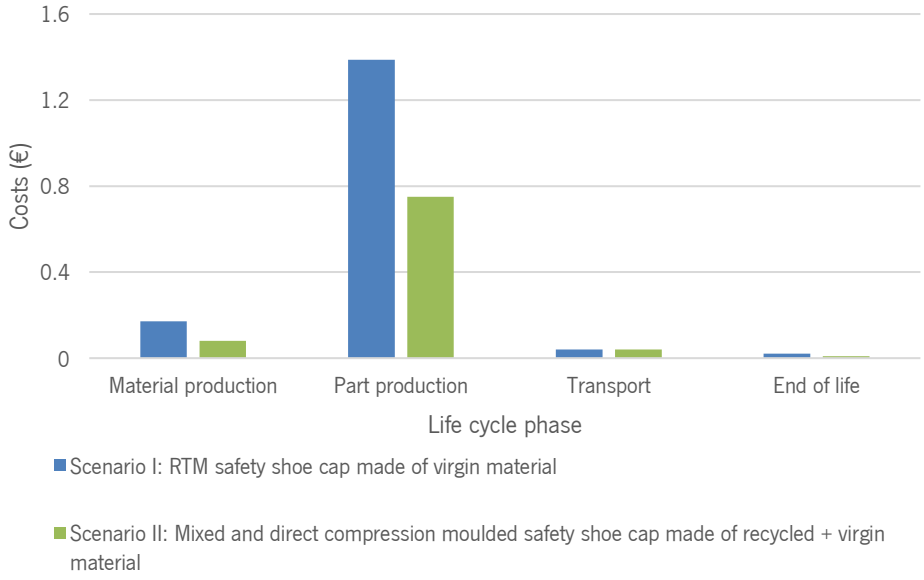

Figure 6.21 - Cost of safety shoe cap per life cycle phase

Overall results

In Figure 6.22, an overall comparison with regard to environmental and economic impact of both scenarios for the safety shoe cap is presented. The impact on CED for Scenario II is minimal due to the influence of energy recovery during the end-of-life. It can be observed that the safety shoe cap made from recycled thermoplastic composite material offers a significant environmental advantage and economic saving.

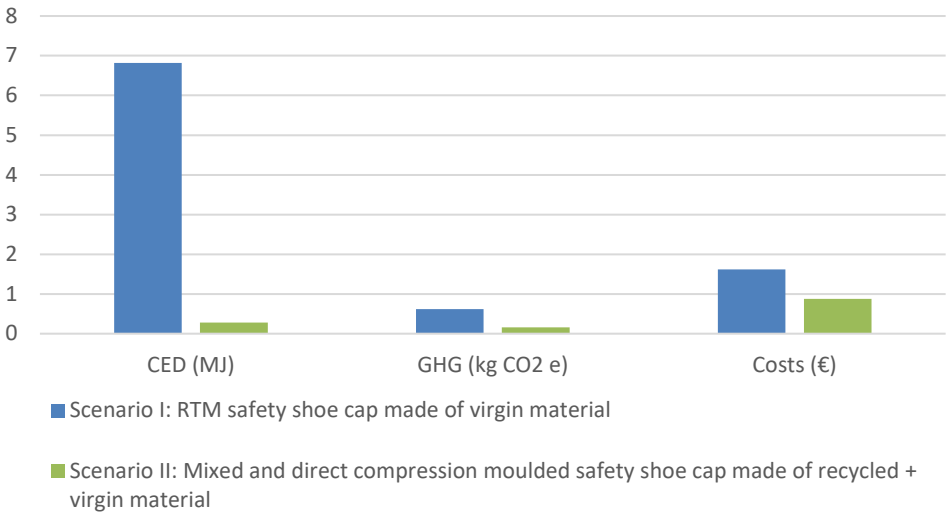

Figure 6.22 – Overview of environmental and economic impact for safety shoe cap

6.5.4 *Discussion*

One should take into account that due to estimations and uncertainty ranges in the data used, the outcomes of this study can be affected. Most uncertain assumptions made concern the transport and end-of-life phases, but not the material and production steps. As these latter phases have the largest influence on the environmental impact (Figure 6.20), it can be concluded that the environmental impact of the thermoplastic shoe cap is lower compared to the glass epoxy one. Further research is required to achieve a more comprehensive analysis, including more data for all scenarios, additional environmental indicators and end-point effect by i.e. the Recipe method. An option is to include the recycling potential of the thermoplastic material to a further extent into the model, by e.g. the use of recycled PP to dilute the G/PP during the mixing process or to consider recycling as an end-of-life scenario instead of incineration with energy recovery.

Regarding the economic impact, the labour-intensive production phase has the largest effect on overall costs. The total amount of time of manual labour is lower for scenario II and handling time can be even more reduced by automating the process. Emissions affecting safety and environment are potentially lower for scenario II as well, due to the nature of the materials used (thermoplastic versus thermoset). Compare for example the material safety data sheet of PP [19] and epoxy [20]. This might open the possibility to transfer the production to a country with a higher wage and more strict safety and environmental regulations, i.e. within Europe, without large impact on the economic benefits.

6.5.5 *Conclusion*

Concerning the environmental impact of a safety shoe nose, the study showed that the impact of the transport and end-of-life phase are low. As there is no impact during the use phase, the material and

production phase stand out. Here, the environmental impact of epoxy resin is higher compared to polypropylene. Besides, the resin transfer moulding process, used with resin, requires more energy in comparison to compression moulding. Finally, the thermoplastic material is recyclable, which is not the case for the thermosetting epoxy. Overall, scenario II has the least impact on the environment.

Regarding the economic impact, the glass epoxy process (scenario I) needs more handling time which results in a more expensive shoe cap in comparison to the G/PP press formed cap. In addition, the compression moulding process opens more possibilities for automation, potentially even further reducing these costs. Overall, the economic impact of the recycled thermoplastic shoe cap is lower compared to the impact of its thermoset counterpart.

6.6 Conclusion

The goal of this project was to determine whether the proposed manufacturing process in combination with the usage of post-industrial TPC waste leads to an improved cost-effectiveness and lower environmental impact for two selected applications. Both cost-effectiveness and environmental impact were studied in this quick scan LCCA, with CED and GHG as environmental indicators. For a more detailed insight in the environmental impact, a full life cycle assessment with more environmental indicators would be recommended. However, for the scope of the current study the used methodology is adequate.

For the impact on material and design feature level: recycled materials show a small advantage when comparing the effect on cost, GHG and CED on the material level. Considering the flexural stiffness, the advantage becomes larger, especially when geometric freedom for parts made of discontinuous fibres is utilised. Another benefit can be the low material density in minimum thickness applications that help designing a lighter product using this recycled material. Applications made using the recycling route, including also the processing step, show that even more cost, GHG and CED reductions are possible.

For the aerospace panel, reducing the mass shows the highest reduction of the total impact over the lifetime. Furthermore, results show that the environmental impact is reduced predominantly by using recycled materials. In addition, the costs are reduced primarily due to the short cycle time, and secondary due to a low price for recycled material in comparison to virgin material. The use of thermoplastic material instead of thermoset materials also reduces the amount of labour time, cycle time and consumables used in thermoset production processes. Overall, the proposed recycling route has significant benefits over the current solution with regard to environmental as well as economic impact.

The same logic applies for the safety shoe cap studied, for which the product involving recycled material outperforms its virgin counterpart both environmentally and economically. The latter even to such extent that local (e.g. EU) manufacturing might be an economically feasible option compared to outsourcing to low-wage countries.

In conclusion, the current chapter has shown that the newly developed process and recycling route of this study, besides offering technologically feasible solutions for existing structurally-loaded applications (see previous chapters), can also offer significant environmental and economic benefits in comparison to current technology for both high-end and low-end applications. Hence, it underlines the technical, economic and environmental feasibility of the technology studied.

6.7 References

[1] J. G. Vogtländer, *A practical guide to LCA*. Delft Academic Press, 2014.

[2] Ministry of Infrastructure and Water Management, "Sectorplan 11 Kunststof en rubber," vol. 3, no. 20150116, pp. 1–12, 2017.

[3] Granta design Limited, "CES Edupack 2019 version 19.2.0." Cambridge, 2019.

[4] M. Ashby, *Materials selection in mechanical design: Second edition*. 1999.

[5] A. Beukers and E. van Hinte, *Lightness: the inevitable renaissance of minimum energy structures*, Fourth rev. Rotterdam: 010 publishers, 2005.

[6] M. I. Abdul Rasheed, "Compression molding of chopped woven thermoplastic composite flakes: a study on processing and performance," PhD Thesis, University of Twente, Enschede, The Netherlands, 2016.

[7] Swiss Centre for Life Cycle Inventories, "Ecoinvent v2.2 LCI data," 2012.

[8] Delft University of Technology, "Idemat 2010," 2010.

[9] TPC-Cycle project partners *et al.*, "Internal communication within TPC-Cycle project meetings."

[10] International Air Transport Association, "Annual review 2017," Cancun, 2017.

[11] D. Woldt, "Zerkleinerung nicht-spröder Stoffe in Rotorscheren," PhD Thesis, Technischen Universität Bergakademie Freiberg, 2003.

[12] Ivaldi, "Heat loss by natural convection." [Online]. Available: http://www.ivaldi.fr/pages_anglaises/calcultherm-pertechalus.html. [Accessed: 01-Feb-2017].

[13] European parliament and the Council of European Union, "Directive 2008 98 EC on waste and repealing certain Directives," 2008.

[14] D. Walton, "Carbon Fiber: Japan's success story," *JEC Asia business review issue 4*, 2017. [Online]. Available: http://www.jeccomposites.com/events/jec-asia-2017/jec-asia-business-review/issue-4/carbon-fiber-japan-success-story. [Accessed: 10-May-2020].

[15] R. A. Witik, F. Gaille, R. Teuscher, H. Ringwald, V. Michaud, and J. E. Månson, "Economic and environmental assessment of alternative production methods for composite aircraft components," vol. 30, pp. 91–102, 2012, doi: 10.1016/j.jclepro.2012.02.028.

[16] "Private communication." .

[17] International standard, "Personal protective equipment - Safety footwear ISO 20345," 2004.

[18] J. Craenen, "MO: In Brazilië werken de meesten 44 uur per week voor 240 euro per maand," 2013. [Online]. Available: https://www.mo.be/wereldblog/jeff-craenen/brazilie-werken-de-meesten-44-uur-week-voor-240-euro-maand.

[19] Sabic, "Safety data sheet Polypropylene 522K-00900," 2015.

[20] Keystone Industries, "Material safety data sheet epoxy hardener KDP081808EPH," 2013.

[21] J. R. Duflou, Y. Deng, K. Van Acker, and W. Dewulf, "Do fiber-reinforced polymer composites provide environmentally benign alternatives? A life-cycle-assessment-based study," *MRS Bull.*, vol. 37, no. 4, pp. 374–382, 2012, doi: 10.1557/mrs.2012.33.

7 General Discussion

7.1 Introduction

The goal of this research was, as mentioned in the introduction, to develop a better understanding of the possibilities of continuous fibre TPC recycling and find *the recycling route for processing post-industrial TPC waste to maximum cost effectiveness and minimum environmental impact.*

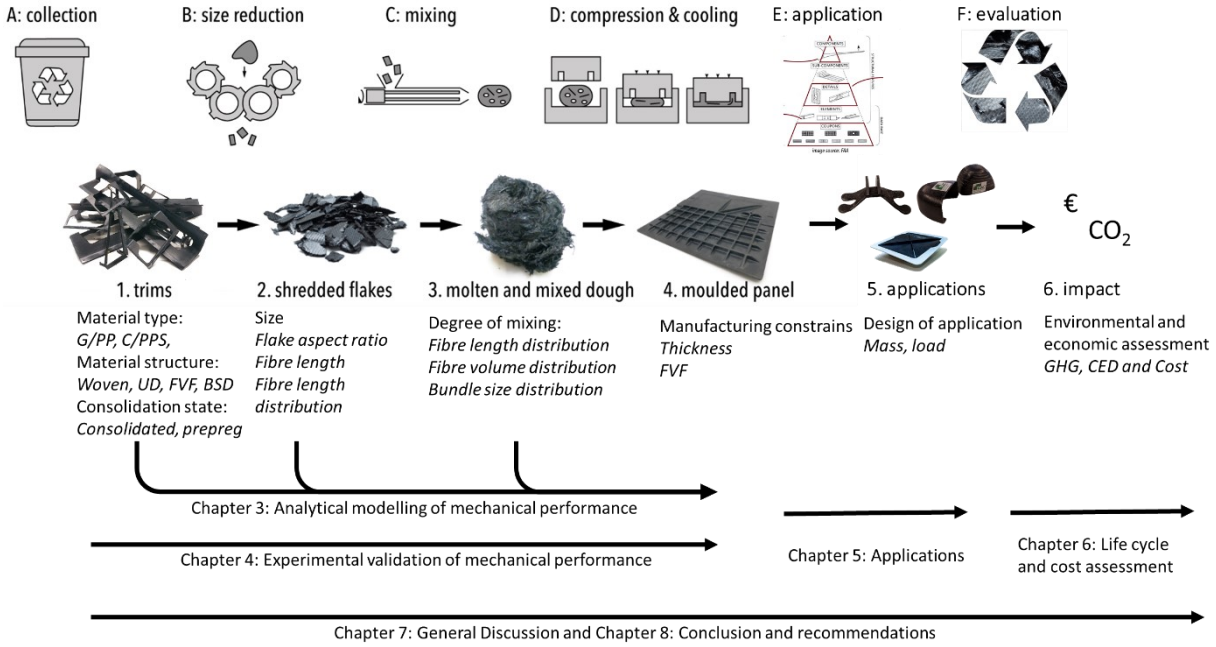

Figure 7.1 - Schematic flow chart of the developed recycling solution and the corresponding structure and correlation of this thesis. The top row illustrates the various process steps while the second row shows the material states in between. The studied variables are described in the third row and at the bottom the corresponding chapter reference is given.

During the study presented in this thesis a recycling route for thermoplastic composites was developed and studied. A general description of the developed route is presented in Figure 7.1. All steps of the route have been studied in detail from a theoretical, experimental and application point of view. The top row of the figure illustrates the process steps (A-F) from waste collection to evaluation and the second row shows the material states between each step (1-6), with directly underneath the studied variables in this thesis. The bottom row gives the corresponding chapter in this thesis.

The first step (A) corresponds to the material collection, for example trimmings or industrial waste. This defines the material type (e.g. G/PP and C/PPS in this thesis), material structure (e.g. woven, UD and initial bundle size) and consolidation state (e.g. consolidated laminate and powder coated prepregs). During the second step (B) the material is reduced in size to flakes, resulting in a certain fibre length distribution. At step C, the material is heated and mixed to a molten dough, which might have an effect on the fibre length distribution and will lead to obtaining quite diverse fibre volume and bundle size distributions. Subsequently, during step D, the dough is compression moulded to a part that will present the fibre orientation induced by the generated material flow. The relation between the variables in step A to D to the mechanical performance is analysed using the analytical model as described in Chapter 3. This model enables the determination of the optimal fibre length requirement and offers insight in the effects of the bundle size and fibre volume for maximising the mechanical properties. The same steps A to D are experimentally performed and described in Chapter 4 to validate the mechanical performance predicted by the analytical model. The application conceived in step E is described in Chapter 5. At this step the previous described information is used in combination with the maximum allowable FVF and minimum part thickness to design, produce and test the proposed application. The designed application is evaluated in step F to assess its environmental and economic impact. A schematic overview of the studies in this thesis and their correlation is given in Figure 7.1.

7.2 Theoretical prediction

To find the optimum mechanical properties for waste material, the trade-off of long fibre length and homogeneous material was studied in Chapter 3. Longer fibres are known to promote higher mechanical performance, but also require low-shear during mixing. The entangled structure of composite waste, especially for woven and consolidated materials, in combination with the low-shear mixing results in a non-homogeneous material with a given fibre volume and fibre bundle size distribution. This non-ideal situation is not often captured by current micromechanical models. In Chapter 3, existing micromechanical models are therefore extended to include not only the effect of fibre length distribution, but also from those resulting of the fibre volume and bundle size distributions. For each of these variables, multiple theoretically constructed distributions and also multiple experimental ones based on analysis of materials processed during the work were included. The goal of the theoretically constructed distributions was to determine the upper and lower bounds of the potential results. The distributions based on experimental work were included to allow studying the influence of the variable's distributions based on the studied recycling route.

In line with expectations and literature, the effect of fibre length on the mechanical properties is demonstrated and limits off for fibre lengths of more than five times the critical fibre length (1.2 mm for C/PPS and 3.6 mm for G/PP). Composites with discontinuous fibres can be as strong and stiff as those with continuous fibres for high aspect ratios and UD orientation (see Section 3.3.1).

Based on the theoretical constructed distributions, the FVD has a limited influence on the stiffness and strength prediction, BSD has shown to have a high impact on property prediction and may even lead to halved property values (Section 3.4.2). A BSD containing a relative large proportion of large bundles gives lower stiffness and strength compared to a BSD with a majority of smaller bundles, as was found in similar studies [1–6].

The experimental datasets of FLD, BSD and FVD included three flake sizes with an average fibre length between 6 and 22 mm and two combinations of mixing settings. The datasets of the three flake sizes show that bundles are more dispersed and fibres are more distributed for smaller flakes containing shorter fibres, underlining the trade-off of long fibre length and homogeneous material. The theoretical model predicts only limited differences (<2%) between the three datasets. The results indicate that, in the range of the dataset, there is little influence of the FLD and BSD. This could be explained by the plateau of maximum stiffness and strength achieved when fibres having at least five times its critical length are used or by a balanced effect from FLD and BSD, e. g. when their opposite effects are of similar magnitude. These results should be taken into account when in search of the most optimal fibre length. Due to the lack of available data on fibre lengths below 6 mm and above 22 mm, the interpretation of the results cannot be applied to smaller or larger fibre lengths. However, the data can be used as they are within the range of fibre lengths of interest to the current study.

The outcome of the experimental datasets of material processed at two different mixing settings show a larger difference (about 5-15%) in stiffness and strength values compared to the difference between the datasets of the multiple flake sizes. Material processed at “good” mixing settings (mixing for a longer time and higher rotational speed) results in higher strength and modulus predictions. The good mixed results approach the perfectly mixed single fibre bundle result up to about 10%, except for UD strength, for which the difference is larger (see Section 3.4.2). This suggests that there is potential gain for improving mechanical performance by enhancing mixing, at least from a theoretical point of view.

Interesting would be to study until what extent the mixing can be improved without attrition of the fibre. When larger shear rates are required to obtain a higher level of mixing, fibre wearing is more likely to

occur. Some attrition might not have a large influence of the mechanical properties, but what is the optimal balance between attrition and degree of mixing? More information on mixing devices and their effect on mixing is available [7, 8] and a twin screw set-up could be used to obtain a very uniform distribution of fibres, but can result in excessive fibre attrition leading to a pull-out failure mode on fibre level, which results in lower mechanical performance [9]. From Chapter 3, one can conclude that the fibre lengths, in any case, should stay above five times the single fibre critical length (~1.2 mm for C/PPS) to obtain near maximum performance regarding strength and stiffness. Impact requires longer fibre lengths [10, 11]. When the mixture is not perfectly dispersed and fibre bundles are present, the fibre length should be longer for maximum performance. When more detailed information is available on mixing and the effect on attrition the model described in Chapter 3 can be better used to predict the influence of the FLD, FVD and BSD on the mechanical properties.

There are several opportunities for improving the predictions. To improve the fibre orientation model, a combination of the Reduced Strain Closure and the Anisotropic Rotary Diffusion (ARD-RSC) models could be added [12]. This method was implemented by Phelps and Tucker [13] and later on further improved for long fibres by Tseng et al. [14] and could improve the fibre orientation for LFT by slowing down the orientation kinetics [15]. Also, the effect of the different ways of length-averaging [4] and fibre bending can be studied. The interfacial shear strength on the fibre-matrix interface highly influences the final composite strength. Since the determination of this property is difficult, further research into this matter is advised [16]. Furthermore, a higher sample frequency for experimental datasets of the FVD, the addition of the weakest link theory and fibre orientation trough thickness may offer additional opportunities for improvement, as is described in Section 3.5.2.

For more general use, a wide range of variables in the model can be changed e.g. the constituent materials, bundle size, fibre orientations and fibre volume fractions. Therefore, predictions for other materials than the studied C/PPS and G/PP can rather easily be computed, e.g. for materials of high volume consumption like the G/PA6, for C/PEKK if its predicted growth in aerospace is considered or new materials like C/LMPEAK [17]. Beside other materials, the model can also offer insight in the influence of processes, e.g. the influence of process induced fibre orientation on the mechanical properties or the influence of FLD, BSD or FVD in other mixing processes than considered in this thesis.

The model developed offers a better description of mechanical properties of nonhomogeneously mixed by including FLD, BSD, FVD and various combination in a micro mechanical model.

7.3 Experimental validation

The recycling of C/PPS and G/PP material was experimentally studied by using a recycling route expressly designed for that purpose, as is described in Chapter 4. Shredded or cut material was processed by low-shear mixing due to the focus on preserving long fibres to minimise downcycling and therefore, maximum cost effectiveness and minimum environmental impact. The mixing solution further contributes to these goals with an isothermal mould, which results in short cycle times to increase the cost effectiveness and minimum energy consumption to further minimise the environmental impact. Plates were manufactured at various degrees of mixing (non-mixed, poorly mixed and good mixed) and with various materials (FVF, fibre length and material structure). The mechanical properties were determined by flexural and Charpy impact tests on coupons. Direct compression moulding, without a mixing step, is often found in literature as a recycling process and therefore, the materials were also processed by this process to offer a comparison.

The recycling route was found feasible and the mechanical properties showed a strong relation with the FVF, as was described in Chapter 3. As predicted by the theoretical model, the strength of mixed materials levelled off above 35% FVF. The results comply with the theory that a higher quality of mixing leads to higher mechanical properties. The difference between poorly and good mixed material was similar to the predicted difference. It is difficult to verify the specific effect of FLD, BSD and FVD, since too many uncertain aspects contribute to the mechanical performance. The data suggests that a fibre length of 10mm and an FVF between 20% and 35% offer maximum performance. Overall, the experimental results show the same trends and order of magnitude as predicted values, validating the latter.

Analysis of the experimental data confirms that the mixed material offers higher mechanical performance than the direct compression moulded material for consolidated flakes. The difference between consolidated flakes and semipreg was limited for the mixing process studied, but significant for the direct compression moulding process. In the latter process, the semipreg performed better. The difference is particularly large for impact and larger for strength than for stiffness. The thin semipreg results in more overlapping flakes through the thickness of the material which likely effects the mechanical performance. This effect builds on existing evidence of Rasheed [18] that an increase of flake overlap leads to an increase in properties.

The experimental work showed that the recycling solution is capable of producing parts with structural performance and that mixing improves the mechanical performance of thick consolidated material.

Conversely, the properties are not close to the values of virgin continuous fibre composites of high fibre fraction, although the geometric flexibility might improve the feasibility of successful applications.

Sensitivity studies on the various process variables showed limited influence and underlines the robustness of the setup used. However, further study on the following items may improve the understanding on the effect of the process on the properties. The results show that the mechanical performance improves with the increasing of the degree of mixing, which is predominantly determined by rotational speed and time [19]. Therefore, it is highly recommend to have an answer for the following question: until what extent can the rotational speed, which predominantly determines the induced shear, be stretched before fibre attrition occurs? Extension of mixing time is not desired because of economics and potential thermal degradation of the polymer. Considering the semi-crystalline structure of PPS and the high cooling rate when the molten material is moulded in the isothermal mould, it is also recommended to study the level of crystallinity. The high temperature gradient may result in a lower level of crystallinity which is known to affect, among others, the stiffness and strength [20, 21]. Beside the crystallinity, also potential polymer degradation should be studied by thermal analysis. By including more tests (e.g. tensile tests, damage tolerance etc) and test conditions (e.g. elevated temperature, moisture etc) a higher level of understanding the mechanical performance and underlying factors can be obtained.

7.4 Application

Multiple demonstrator products were designed, produced and tested. The results show the capabilities of the developed recycling route by an aerospace access panel, a bracket and a safety shoe nose cap. The access panel presented the required functionalities by leveraging the geometric freedom of the material-manufacturing-method combination while made of recycled material with inferior material properties and was even lighter compared to the current solution. The bracket confirmed that complex geometries are possible. The safety shoe nose cap demonstrated the specified impact resistance and strength described in the standard for safety shoes after some geometric adjustments at equal weight as the commercially available benchmark.

Figure 7.2 - The three demonstrator products developed in this study: a bracket (left), two safety shoe nose caps (middle) and an access panel (right)

The mechanical properties predicted theoretically by the model described in Chapter 3 and validation by the experimental tests on coupon level in Chapter 4 for discontinuous fibres where considerably lower than of those of continuous fibre composites of the same constituent materials. However, the products developed which the recycled discontinuous fibres in Chapter 5 match the requirements on product level of the current continuous fibre versions at the same or even lower weight. These results show it is possible to substitute parts manufactured with virgin material comparable to the original material where the recycled material originates from. Hence, the waste material can be converted into a similar product meaning no downcycling occurs from a part level perspective.

The importance of the design-material-process approach [22] to the development of new products, common in composites engineering, is described in Section 5.4. Several aspects of this trinity for lightweight design have been applied in the three demonstrators. In the following section, further opportunities of exploring individual aspects of this trinity in order to contribute to promote the improvement of products are discussed.

Design

An important benefit of the material-manufacturing-method combination showed to be the geometric freedom. The manufacturing demonstrator showed it was possible to create complex features and ribs with a height over width ratios of 4.5 without fibre matrix separation. Unlike with injection moulding, the results demonstrate it is possible to mould thickness transitions from thin to thick sections and create ribs with a larger width than the base thickness of the panel without significant sink marks [23]. This freedom did not only enable the moulding of the topology optimised bracket design and the access panel with a lower weight compared to the current solution, but might also offer opportunities when the

surrounding parts may be adjusted. The geometric freedom can offer function integration at a new level compared to continuous fibre composites, enabling a similar effect of improvement to when a part designed for metal is produced in composite material without altering the design. This results often in a non-optimal solution which is not lighter or more cost effective than the original metal part (often called a "black metal design") [24]. Another related benefit of the geometric freedom is in the design for assembly. This step often represents substantial time and cost and the opportunity of more geometric freedom might translate in considerable savings.

Material

As the recycling route is not limited to the two materials described in this thesis, other TPCs can be processed, but may, amongst others, have a different viscosity and processing temperature. A further improvement of the applications is possible by integrating other materials for specific functions. In the safety shoe nose cap unidirectional tape was successfully co-moulded and multiple studies highlight the potential weight-saving of UD inserts [25–27]. A possible design for the access panel is shown in Figure 7.3. The UD tapes could be place in highly loaded sections or load paths of a part, e.g. ribs. Beside UD tapes, also blanks of continuous fibres may be used for larger area, combining the high mechanical performance of continuous fibres with the geometric freedom of discontinuous fibres in a hybrid product [28–30]. Especially when a sandwich structure can be created, these continuous fibre inserts can have a substantial effect on the strength and stiffness of a part. Additional layers might be co-moulded for further function integration, such as lightning strike or galvanic corrosion protection.

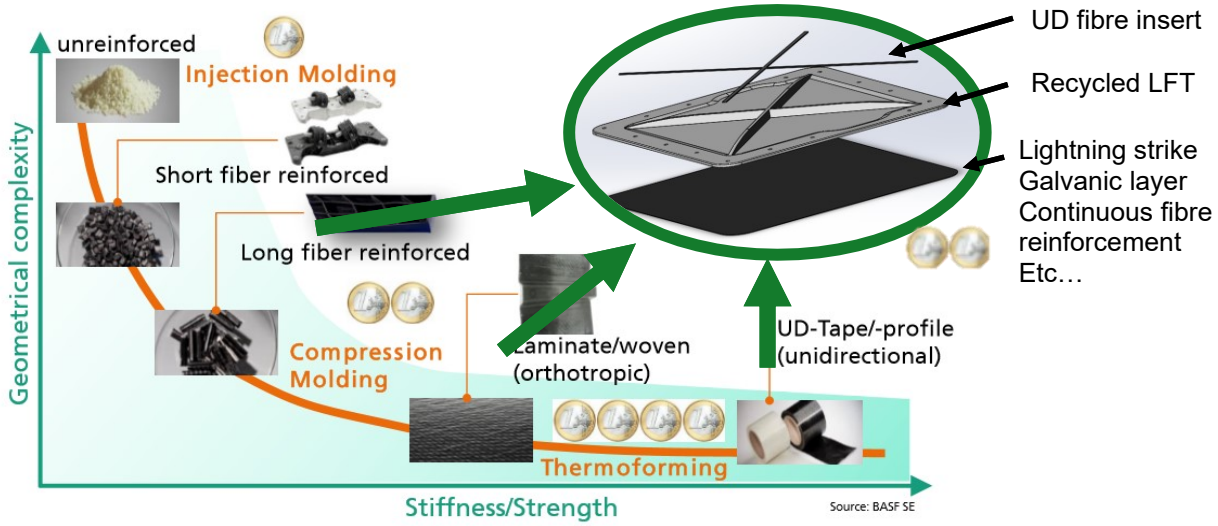

Figure 7.3 - The integration of a laminate and UD tape in the recycled LFT part might offer the benefits of the individual materials, such as geometrical complexity and high stiffness and strength in a hybrid solution. Layers for galvanic corrosion or lightning strike protection might also be co-moulded for additional function integration. Adapted from [31]**, image courtesy BASF SE**

Process

The experimental validation of the process used showed it is possible to use consolidated waste in structural applications with complex geometry. In combination with the short cycle time as a result of the isothermal mould, fast de-moulding and net shape manufacturing lead to interest from industry. However, several challenges were identified which will help the industrialisation of the recycling route. Four design of experiments are executed on mixing and compression moulding parameters for G/PP and C/PPS to gain insight on the processing window and the effect of the parameters on the mechanical performance and mixing quality. These studies are not elaborately described in this thesis since the results did not show a clear image. For the qualification and process specification a new study should be made in which the characterisation methods developed by Vincent et al. [32] will give more insight in intermediate steps.

Process modelling will help to develop more understanding of the process, increase the efficiency of the solution (e.g. weight, mechanical performance or cycle time) and investigate the feasibility of successful product for a specific material-process-design combination. The software package of Moldflow™ has the option to simulate the compression moulding of a charge. The software was used to a limited extent for the safety shoe nose cap and access panel. A flow analysis of the filling of the safety shoe nose cap mould is presented in Figure 7.4 and can be compared to the experimental flow analysis given in Figure 7.5. The latter image shows two orientations of the male mould and, from left to right side of the image, an increasing amount of processed material. The analysis can be used to, among others, study the filling sequence which is important for charge placement and mould design optimisation, e.g. regarding part orientation and shut-off edge. The fibre orientation result for a design concept of the access panel application is presented in Figure 7.6. The fibre orientation is important for the mechanical performance, force-deflection behaviour and warpage of the part. These two simulation results are just an example of what is possible. The simulation can be used for a wide range of other analysis, such as weld line prediction and total design of experiments on the influence of processing variables. For all analyses it is important to keep underlying assumptions in mind and verify the results experimentally when possible.

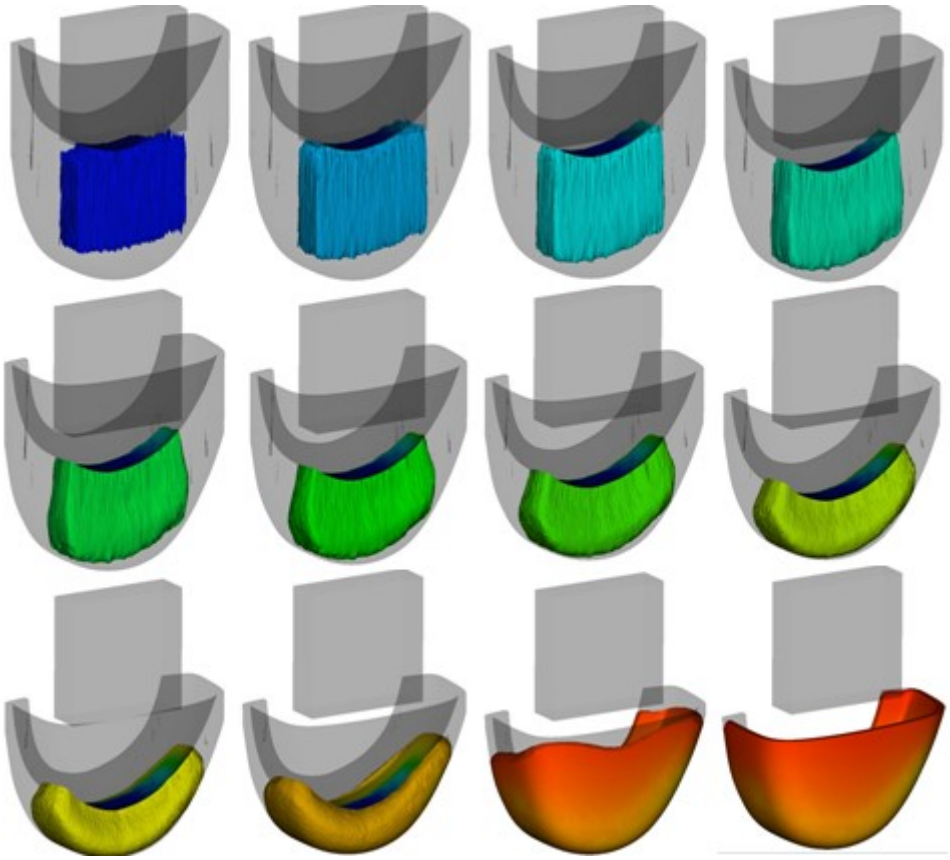

Figure 7.4 - Flow analysis simulation results showing multiple stages of the mould filling for the safety shoe nose cap, modelled in Moldflow™. The colour describes the fill time, the moment when the material is at that location for the first time.

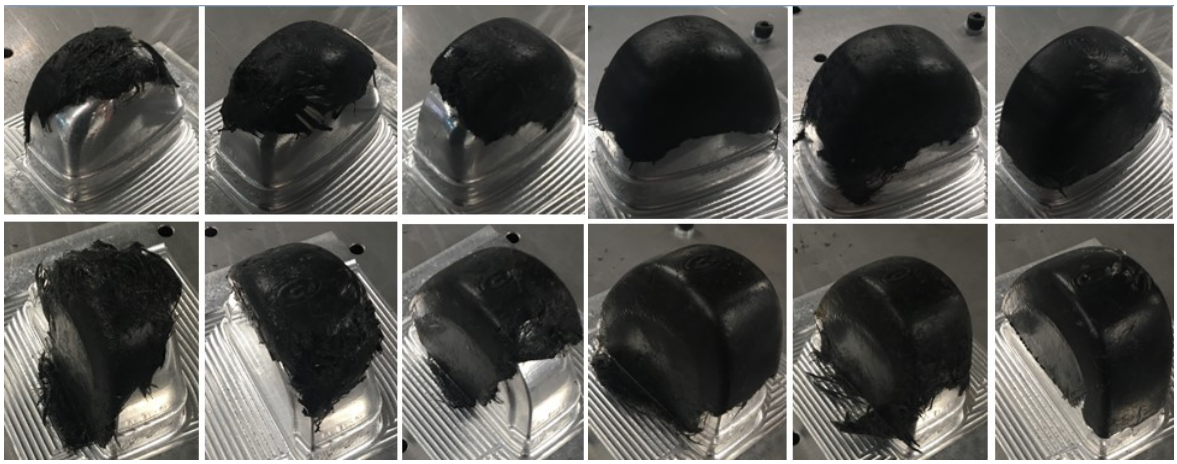

Figure 7.5 - Experimental flow analysis, the top and bottom line show different orientations of the male mould for the safety shoe nose cap. From left to right an increasing amount of material is processed. [33]

Figure 7.6 - Fibre orientation tensor results for a compression moulding simulation. A red colour indicates a highly oriented fibre orientation while blue colour indicates a 2D random orientation.

When utilising the described aspects of geometric freedom, material combinations and process simulation more successful applications are feasible. Typical application might involve brackets, clips and covers. Examples for an interesting high volume application is a manhole cover, recently Burek [34] studied the development of such product to replace the current cast iron solution, by making use of processes simulation software and combining recycled LFT material with a UD tape made with recycled polymer in a geometrically optimised design. For high-end applications in aerospace various opportunities are available which can be illustrated by several examples of companies offering solutions in the same field of applications, in which the companies often offer an alternative for metal products. At Sekisui Aerospace (previously Quatro Operations) cut UD C/PPS tapes are used as BMC to create stow bin brackets at 3500 units per month for the Boeing 787 by DCM process [35]. RTP company supplies G/PEEK material for overhead storage compartments brackets in Boeing 767 planes [36]. Greene Tweed produces similar type of products by DCM of BMC material for aerospace, but also for the oil and gas segment and general industry [37]. These products show discontinuous fibre composites offer interesting solutions and with the developed recycling route and mixing process the cycle time and material cost will be further reduced, resulting in a more cost-effective solution.

In addition of the described approach, results and opportunities, related processes such as LFT and GMT can offer further information to obtain guidelines for future development [23].

7.5 Evaluation

Throughout this thesis, the focus was on obtaining the recycling route for processing post-industrial TPC waste to maximum cost effectiveness and minimum environmental impact. In the life cycle and cost assessment in Chapter 6 the assessment of this goal is described. The results on material level, excluding the processing step, shows that the solution is not very competitive for most mechanical properties, but outperforms alternatives when a beam with a certain required stiffness is considered, especially when the geometric freedom is taken into account. The benefit of the solution is shown in the results of the LCCA on the access panel and safety shoe nose cap. Applications made using the recycling route, including the processing step, also show that significant GHG and CED cost reductions are possible.

Use phase in aerospace

Although the aerospace access panel made from recycled material by the mixing process showed a CED and GHG impact reduction of over 80% compared to the current solution during all life cycle phases except the use phase, the results showed that the vast majority of the life cycle environmental impact is during the use phase. So, while the carbon fibre production is very energy intensive, the recycling of the material by an energy efficient processing route does not directly translate in a large relative reduction (9-10%) of an aerospace application. The impact during the use phase is dominated by the weight of the product. The designed access panel in Chapter 5 showed to be 9% lighter and with the opportunities described in Section 7.4 and by using more testing for lowering the safety factor as described in Section 7.3, the design could be further improved potentially leading to an even lower weight. However, it will be very challenging in most aerospace applications to develop products of lower weight compared to current solutions by using recycled material with inferior material properties. Overall, using recycled material and the selected mixed recycling process will still offer GHG and CED reductions.

Cost

Since the use phase is less dominant for economic cost, the cost reduction of more than 60% in all phases except the use phase translates into a significant (27%) cost saving for the total life cycle. That discontinuous fibre reinforced composites can offer significant cost reduction is, besides the existing applications described in Section 7.4, also confirmed by a case study performed by Moniruzzaman of Sabic Innovative Plastics. He showed that an aircraft's interior food tray arm which was redesigned for discontinuous fibre material and injection moulding process can result in both a weight (about 45%) and cost reduction (19-77% depending on alloy of the benchmark) [38, 39].

The LCCA already includes the benefit of the recycled TPC flake material, the geometric freedom of the design, and, among others, the short cycle time and near net shape manufacturing of the process. But there are several possibilities to further reduce the environmental and economic impact. The previous stated recommendation on material, design and process in Sections 7.2-7.5 will translate in a lower impact. Additional reduction is possible by using recycled polymer to dilute the FVF of the TPC flake material and leverage function integration of surrounding parts or assembly steps or materials.

Although it was difficult to obtain accurate data which might affect the reliability of the exact figures of the performed LCCA, the overall conclusion is not likely to change. The LCCA shows the developed access panel and safety shoe nose cap have a lower environmental and economic impact than current solutions which proves that the recycling route can offer a cost-effective solution and low environmental impact for both high-end and high-volume applications.

7.6 General remarks

In addition to the topics stated in previous sections, some general remarks can be made to broaden the recycling of thermoplastic composites in the near future. The remarks originate from conversations with fellow researchers in the field of TPC [32], meetings within the TPC-Cycle project consortium or from related to research [40].

Thermoplastic composites are applied at increasing volume and although the material often enables a long product life time, there will be a moment in time when end-of-life waste becomes available in substantial volumes. A study on end-of-life-waste and waste including impurities is therefore advised.

An association of companies and institutes with a relation to the recycling of thermoplastic composites should be established, such as Plastic Recyclers Europe and the Association of Plastic Recyclers (North America). Preferably, the total supply chain should be presented. Goals should include standardisation, certification, preservation of material traceability, development and distribution of knowledge, creating more awareness of the recycling possibilities and increase the motivation for recycling, potentially by involving governments for encouraging the recycling by legislation.

7.7 References

[1] S. K. Garkhail, R. W. H. Heijenrath, and T. Peijs, "Mechanical Properties of Natural-Fibre-Mat-Reinforced Thermoplastics based on Flax Fibres and Polypropylene," *AppliedComposite Mater.*, vol. 7, pp. 351–372, 2000.

[2] H. Chen and D. G. Baird, "Prediction of Young ' s Modulus for Injection Molded Long Fiber Reinforced Thermoplastics," *J. Compos. Sci.*, 2018, doi: 10.3390/jcs2030047.

[3] D. E. Spahr, K. Friedrich, J. M. Schultz, and R. S. Bailey, "Microstructure and fracture behaviour of short and long fibre-reinforced polypropylene composites," *J. Mater. Sci.*, vol. 25, pp. 4427–4439, 1990.

[4] J. L. Thomason, "The influence of fibre length and concentration on the properties of glass fibre reinforced polypropylene: 6. The properties of injection moulded long fibre PP at high fibre content," *Compos. Part A Appl. Sci. Manuf.*, vol. 36, no. 1, pp. 995–1003, 2005.

[5] M. Ericson and L. Berglund, "Deformation and fracture of glass-mat- reinforced polypropylene," *Compos. Sci. Technol.*, vol. 43, pp. 269–281, 1992.

[6] R. Rondeau and S. Reeve, "The effect of tows and filament groups on the properties of discontinuous fiber composites," in *44th International SAMPE Symposium*, 1999, pp. 1449–1460.

[7] O. Galaktionov, "Optimization of distributive mixing: from prototype flows to industrial devices," PhD Thesis, Eindhoven University of Technology, 2002.

[8] A. Sarhangi Fard, "Analysis and optimization of mixing inside twin-screw extruders," PhD Thesis, Eindhoven Univesity of Technology, 2010.

[9] V. L. Bravo, M. R. Mcleod, and M. N. Bureau, "In-Line Compounding Experiments with Recycled Carbon Fibre Reinforcement," in *SAMPE Technical Conference Proceedings*, 2013, pp. 1–18.

[10] J. L. Thomason, "The influence of fibre length and concentration on the properties of glass fibre reinforced polypropylene: 5. Injection moulded long and short fibre PP," *Compos. Part A Appl. Sci. Manuf.*, vol. 33, no. 12, pp. 1641–1652, 2002, doi: 10.1016/S1359-835X(02)00179-3.

[11] W. Schijve, "High performance at medium fibre length in long glass fibre polypropylene," *Plast. Addit. Compd.*, vol. 2, no. 12, pp. 14–21, 2000, doi: 10.1016/S1464-391X(00)80121-X.

[12] B. N. Nguyen, S. K. Bapanapalli, V. Kunc, J. H. Phelps, and C. L. Tucker, "Prediction of the elastic-plastic stress/strain response for injection-molded long-fiber thermoplastics," *J. Compos. Mater.*, vol. 43, no. 3, pp. 217–246, 2009, doi: 10.1177/0021998308099219.

[13] J. Wang and X. Jin, "Comparison of recent fiber orientation models in Autodesk Moldflow Insight simulations with measured fiber orientation data," *Proc. Polym. Process. Soc. 26th Annu. Meet.*, 2010.

[14] H. C. Tseng, R. Y. Chang, and C. H. Hsu, "Numerical prediction of fiber orientation and mechanical performance for short/long glass and carbon fiber-reinforced composites," *Compos. Sci. Technol.*, vol. 144, pp. 51–56, 2017, doi: 10.1016/j.compscitech.2017.02.020.

[15] J. H. Phelps and C. L. Tucker III, "An anisotropic rotary diffusion model for fiber orientation in

short- and long-fiber thermoplastics," *J. Nonnewton. Fluid Mech.*, vol. 156, pp. 165–176, 2009, doi: 10.1016/j.jnnfm.2008.08.002.

[16] F. W. J. Van Hattum, "A study of the Mechanical Properties of Vapour Grown Carbon Fibres and Carbon Fibre-Thermoplastic Composites," PhD Thesis, Universidade do Minho, 1999.

[17] Ginger Gardiner, "PEEK vs. PEKK vs. PAEK and Continuous Compression Molding," *CompositesWorld*, 2018. [Online]. Available: https://www.compositesworld.com/blog/post/peek-vs-pekk-vs-paek-and-continuous-compression-molding. [Accessed: 04-Apr-2020].

[18] M. I. Abdul Rasheed, "Compression molding of chopped woven thermoplastic composite flakes: a study on processing and performance," PhD Thesis, University of Twente, Enschede, The Netherlands, 2016.

[19] G. A. Vincent, T. A. de Bruijn, S. Wijskamp, M. I. A. Rasheed, M. Van Drongelen, and R. Akkerman, "Characterisation and improvement of the quality of mixing of recycled thermoplastic composites," *Submitt. to Polym. Compos.*, 2019.

[20] S. Béland, *High Performance Thermoplastic Resins and their Composites*. William Andrew, 1990.

[21] F. C. Campbell, *Structural Composite Materials*. ASM International, 2010.

[22] A. Beukers and E. van Hinte, *Lightness: the inevitable renaissance of minimum energy structures*, Fourth rev. Rotterdam: 010 publishers, 2005.

[23] AZDEL Inc. Thermoplastic Composites, "Azdel Thermoplastic composites design and processing handbook," 1993.

[24] D. Weber-Steinhaus, "Why Switching to Composite Materials Requires a New Product Design," 2019. [Online]. Available: https://www.ansys.com/blog/switching-to-composite-materials-requires-a-new-product-design-black-metal.

[25] B. Beck, "Local continuous-fiber reinforcement - tailored injection molding."

[26] K. B. Thattaiparthasarathy, S. Pillay, D. Bansal, H. Ning, and U. K. Vaidya, "Processing and characterization of continuous fibre tapes co-moulded with long fibre reinforced thermoplastics," *Polym. Polym. Compos.*, vol. 21, no. 8, pp. 483–494, 2013, doi: 10.1177/096739111302100802.

[27] K. Arnaut and A. S. Herrmann, "Tailored inserts based on continuous fibre for local bearing reinforcement of short fibre thermoplastic components," *Key Eng. Mater.*, vol. 742, pp. 82–89, 2017, doi: 10.4028/www.scientific.net/KEM.742.82.

[28] D. R. Bruessel, H. Ernst, and M. J. D. Gmbh, "Tailored Long Fiber Thermoplastics (Tailored Lft) Developed for Series Production," in *49th international SAMPE symposium and exhibition*, 2004, p. pp.3122-3135.

[29] W. Krause, F. Henning, S. Tröster, O. Geiger, and P. Eyerer, "A Process Technologyfor Large Scale Productionof Fiber Reinforced Thermoplastic Components," *J. Thermoplast. Compos. Mater.*, vol. 16, no. 4, pp. 289–302, 2003, doi: 10.1177/0892705703016004001.

[30] F. Henning, "Verfahrensentwicklung für lang- und endlosglasfaserverstärkte thermoplastische

Sandwich- Bauteile mit geschlossenem Werkstoff-Kreislauf," PhD Thesis, Universität Stuttgart, 2001.

[31] F. Henning, "An integrated development approach to combine design, manufacturing and validation of high-pressure RTM composite structures," in *The 3rd SAMPE Asia Exhibition and Conference on Advanced Materials*, 2014.

[32] G. A. Vincent, "Recycling of thermoplastic composite laminates: The role of processing," PhD Thesis, University of Twente, 2019.

[33] I. ten Bruggencate, "Designing a safety shoe demonstrator," BSc Thesis, Saxion University of applied sciences, 2018.

[34] A. Burek, "Design and development of a composite tape reinforced access cover made of recyclates," MSc Thesis, Technische Universität Chemnitz, 2019.

[35] "Sekisui Aerospace." [Online]. Available: https://www.sekisuiaerospace.com/processes.

[36] RTP Company, "Aircraft Hinge Bracket." [Online]. Available: https://www.rtpcompany.com/aircraft-hinge-bracket/.

[37] "Greene Tweed." [Online]. Available: https://www.gtweed.com/.

[38] M. Moniruzzaman, "A design and performance study of metal replacement in aircraft food tray arms for aircraft weight reduction," *Aerospace manufacturing and design*, 2012. [Online]. Available: https://www.aerospacemanufacturinganddesign.com/article/amd0312-metal-aircraft-food-tray-arms/.

[39] Scott Stephenson, "Carbon fiber food tray arm: Better and cheaper," *Composites World, High-Performance Composites*, 2011. [Online]. Available: https://www.compositesworld.com/columns/carbon-fiber-food-tray-arm-better-and-cheaper.

[40] S. Pimenta and S. T. Pinho, "Recycling carbon fibre reinforced polymers for structural applications: Technology review and market outlook," *Waste Manag.*, vol. 31, no. 2, pp. 378–392, 2011, doi: 10.1016/j.wasman.2010.09.019.

8 Conclusion and recommendations

This thesis focuses on recycling of post-industrial continuous fibre reinforced thermoplastic composites, by investigating the theoretical prediction and experimental validation of mechanical performance and the application and evaluation of a developed recycling route. The ultimate aim was to find the recycling route for processing post-industrial TPC waste for maximum cost effectiveness and minimum environmental impact. The main conclusion from the research presented in this thesis are summarised below.

8.1 From theory

To define fibre length and mixing quality requirements, existing micromechanical models have been extended with fibre length-, fibre volume- and bundle size averaging to analytically predict stiffness and strength. A fibre length of roughly five times the critical fibre length is sufficient to obtain strength and modulus values close to those of continuous fibre composites. The effect of bundles was found to be substantial, with deviations in predicting stiffness and strength of tens of percent between using the theoretical and experimental distributions. The influence of FVD shows to be very limited. For poorly mixed materials, when a combined FLD and BSD is assumed, the results present 10% and 15% lower modulus and strength values, respectively, compared to perfectly mixed material with a homogeneous fibre length of 20 times the critical fibre length. The optimal point in the trade-off between fibre length and degree of mixing covers a broad range due to the counteracting effects with the same order of magnitude of bundles and fibre length in the degrees of mixing. However, a higher degree of mixing, especially by an improved dispersion, at the cost of shorter fibre length may lead to higher mechanical performance.

8.2 From practice

Experimental tests underline the importance of mixing for consolidated laminates and prove the possibility of reprocessing waste material. The low-shear mixing device is capable of disentangling the multi-layered and woven structure of consolidated flakes into bundles of varying size while preserving fibre length. The fibre fraction of flakes can be diluted by adding polymer. Flexural modulus and strength increase with fibre content, at a rate similar to that predicted by analytical models. The strength of mixed materials

levels off above 35% FVF and are in agreement with theory. Poorly mixed materials show consistently lower values than materials processed at good mixing settings.

Non-mixed materials can be processed at higher FVF compared to mixed materials. The modulus and strength of non-mixed materials is lower than mixed materials when normalised for FVF. The structure of the input material shows a strong influence for non-mixed material compared to mixed materials: results for thick consolidated C/PPS material are lower compared to thinner semipreg material when processed by direct compression moulding, but similar when mixing is involved. Particularly, the strength of non-mixed consolidated material is low.

Mixing results in a more homogeneous material, is less sensitive to material input and shows shorter cycle times. No significant difficulties were found during processing, underlining the robustness of the process studied.

8.3 From application

Although material properties are not directly competitive with virgin materials, the developed applications made of recycled material have proven to meet all tested requirements.

Produced safety shoe nose caps from recycled G/PP met the impact and compression requirements for S3 nose caps. UD tape inserts proven to be possible so that fibres can be placed into the preferred direction, instead of the more random orientation typical for the compression moulding process.

The production method has proven to allow enough geometric freedom to enable an optimised topology suitable to design complex shape parts, leading to significant weight savings and, unlike additive manufacturing, to the shorter manufacturing cycle times usually required for series production.

An access panel has been designed to meet fully representative set of requirements, manufactured and successfully tested. TPC waste material of other components for the same rotorcraft have been recycled in the production of these access panels. Desired complex features have demonstrated to be possible and offer the opportunity for stiffeners, which not only increase the geometric stiffness, but also enable to distribute stress more homogenously. In comparison to the current carbon/epoxy hand lay-up solution, the resulting product is 9% lighter, significantly more cost-effective and made of recycled material (fibre *and* matrix). Flight test demonstration with the recycled thermoplastic access panel installed on the

rotorcraft has been successfully performed, resulting in the world's first flying fully recycled continuous fibre thermoplastic composites application in aerospace.

8.4 From evaluation

The life cycle and cost assessment of the applications demonstrated a significant reduction in cost and environmental impact is possible.

Recycled materials show a small advantage when comparing the effect on cost, GHG and CED on the material level. Considering the flexural stiffness, the advantage becomes larger, especially when the geometric freedom for parts made of discontinuous fibres is utilised

For the aerospace access panel application, reducing the mass shows the highest reduction of the total economic and environmental impact over the lifetime. For the material and part production phase, the panel made from recycled material by the mixing process offers over 80% CED and GHG reduction and over 60% cost reduction compared to the virgin C/epoxy benchmark. For these two phases, the environmental impact can be predominantly reduced by using recycled materials, while for costs the near net shape and short cycle time characteristics in the part productions phase accounts for large reductions.

An equivalent conclusion for the safety shoe cap can be drawn, the product involving recycled material outperforms its virgin counterpart both environmentally and economically.

The results underline the technical, economic and environmental feasibility of the studied technology by significant benefits in comparison to current technology for both high-end and low-end applications.

Concluding, this study shows that recycling of continuous fibre thermoplastic composites is not only feasible, but offers opportunities for applications in the same field of application as products made from virgin material at a significant reduction in cost and environmental impact while even allowing for significant weight reductions when utilising the offered geometric design freedom.

8.5 Recommendations

This study shows it is possible to recycling post-industrial continuous fibre reinforced thermoplastic composites. Yet, additional research is suggested for further study. The present section proposes some recommendations for future work based on the results, discussion and conclusions of this thesis

- Improve the theoretical predictions by a higher sample frequency for the FVF, the addition of the weakest link theory and fibre orientation trough thickness.
- Improve the experimental setup to increase dispersion resulting in a higher mechanical performance. Since the fibre attrition was very limited, the shear during mixing may be increased.
- Perform more mechanical testing to decrease safety factors and increase the allowables used for design, e.g. tensile tests, damage tolerance tests and tests at elevated temperature.
- Study the degree of crystallinity for semi-crystalline material in produced parts and study the relation with the thermal cycle during processing.
- Study non-destructive inspection methods as it may offer an increased level of understanding of the quality of parts and is generally a default step in production within the aerospace sector.
- Explore the processing feasibility and effect on functional specifications of hybrid materials, e.g. including UD Tapes or woven laminates, Lightning strike protection, galvanic layer etc.
- Involve process simulation for optimising and understanding a broad range of aspects associated to the process, such as mould design, fibre orientation, warpage, weld line prediction and the effect of process parameters.
- Develop more applications to increase knowledge and awareness
- Test the applicability of design guidelines and knowledge of comparable processes, such as GMT and LFT.
- Update the LCCA with measured data and involve more environmental indicators
- Study how to treat end-of-life waste and waste including impurities and investigate the effect on the application
- Collaborate with partners in the supply chain, research and governmental institutes to obtain standardisation, preserve traceability of materials and increase the motivation for recycling of TPC.

8.6 Publications

The research presented in this thesis has resulted in a number of contributions in the field of recycling continuous fibre reinforced thermoplastic composites, which have been published as oral communications and peer-reviewed publications as listed in reverse chronological order below.

Journal Papers

- T.A. de Bruijn, G.A. Vincent, J. Meuzelaar, J.P. Nunes, F.W.J. van Hattum, "Design, manufacturing and testing of a rotorcraft access panel door from recycled carbon fiber reinforced polyphenylenesulfide", *SAMPE Journal*, March/April, 2020.
- G.A. Vincent, T.A. de Bruijn, S. Wijskamp, M.I. Abdul Rasheed, M. Van Drongelen, R. Akkerman. "Shredding and sieving thermoplastic composite scrap: Method development and analyses of the fibre length distributions." Published in: *Composites Part B: Engineering*, 176, 2019
- G.A. Vincent, T.A. de Bruijn, S. Wijskamp, M. van Drongelen, R. Akkerman. "Process- and material-induced heterogeneities in recycled thermoplastic composites." Submitted to*: Journal of Thermoplastic Composite Materials*, 2019
- G.A. Vincent, T.A. de Bruijn, S. Wijskamp, M.I. Abdul Rasheed, M. Van Drongelen, R. Akkerman. "Characterisation and improvement of the quality of mixing of recycled thermoplastic composites." Submitted to: *Polymer Composites*, 2019

Conference Papers

- I. ten Bruggencate, T. A. de Bruijn, G. Vincent, F.W.J. van Hattum, "Design, manufacturing and testing of a Safety shoe nose cap from recycled Glass fibre Polypropylene", *SAMPE Europe conference 2019 Proceedings*, 2019, Nantes, France.
- T.A. de Bruijn, G.A. Vincent, J. Meuzelaar, J.P. Nunes, F.W.J. van Hattum, "Design, manufacturing and testing of a rotorcraft access panel door from recycled carbon fiber reinforced polyphenylenesulfide", *SAMPE America Conference 2019 Proceedings*, 2019, Charlotte, NC, USA.
- G. Vincent, T.A. de Bruijn, M.I. Abdul Rasheed, S. Wijskamp, "Recycling thermoplastic composites using low-shear mixing: an experimental study on complex geometries," *ITHEC 2018 Conference Proceedings*, 2018, Bremen, Germany.

- G. Vincent, T.A. de Bruijn, M.I. Abdul Rasheed, S. Wijskamp, "Flow behaviour of recycled thermoplastic composites processed by low-shear mixing", *14th International Conference on Flow Processing in Composite Materials*, 2018, Luleå, Sweden.
- T. A. de Bruijn, G. Vincent, F. W. J. van Hattum, "Influence of low shear mixing settings on the mechanical properties of long glass fibre polypropylenen", *SAMPE Europe Conference 2017 Proceedings*, 2017, Stuttgart, Germany.
- G. Vincent, T. A. de Bruijn, M. I. Abdul Rasheed, S. Wijskamp, and R. Akkerman, "Fibre length distributions of shredded thermoplastic composite scrap", *Proceedings of the 21st International Conference on Composite Materials*, 2017, Xi'an, China.
- T. A. De Bruijn, G. Vincent, and F. W. J. Van Hattum, "Recycling C/PPS laminates into long fibre thermoplastic composites by low shear mixing," *Proceedings of the 21st International Conference on Composite Materials*, 2017, Xi'an, China.
- G. Vincent, V. Balakrishnan, T. A. de Bruijn, S. Wijskamp, M.I. Abdul Rasheed, "Impregnation Quality of Shredded Semipreg after Compression Moulding", *ESAFORM 2017: Proceedings of the 20th International ESAFORM conference on Material Forming*, 2017, Dublin, Ireland.
- T. A. De Bruijn, G. A. Vincent, and F. W. J. Van Hattum, "Recycling of long fibre thermoplastic composites by low shear mixing," *SAMPE Europe Conference 2016 Proceedings*, 2016, Liège, Belgium.

Other

- T. A. de Bruijn, F.W.J. van Hattum, "Rotorcraft access panel from recycled carbon PPS -The World's first flying fully recycled thermoplastic composite application in aerospace", Accepted for publication in: Reinforced Plastics, 2020

Awards

- CAMX 2019 "Unsurpassed Innovation Award" finalist. A rotorcraft access panel from recycled carbon PPS. Anaheim, CA, USA. September 2019. This submission was a collaboration between TPAC, GKN Fokker, TPRC and the other TPC-Cycle consortium partners.

Appendices

Appendix A. Images of non-mixed material during the DCM process

Figure A.1 and Figure A.2 show the material during the DCM process, as described in Section 4.2.6.

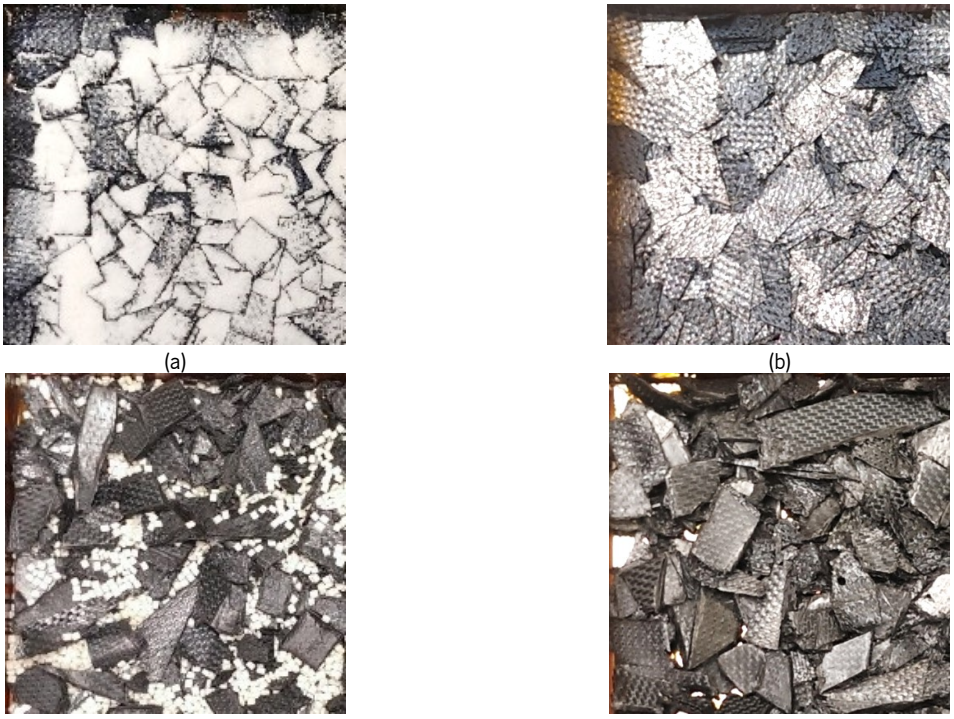

(a) (b) (c) (d)

Figure A.1 - Top left quarter of a mould before non-mixed moulding with semipreg (a+b) and consolidated flakes (c+d) C/PPS material at 35% FVF (a+c) and 50% FVF (b+d).

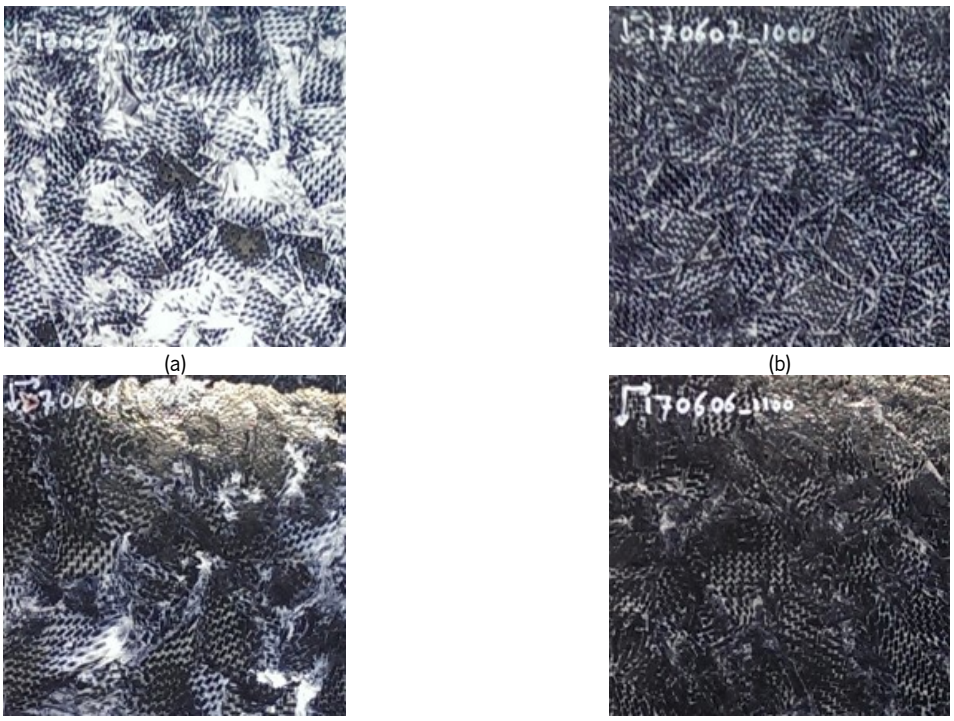

(a) (b) (c) (d)

Figure A.2 - Top left quarter of non-mixed compression moulded plates, made of semipreg (a+b) and consolidated flakes (c+d) C/PPS material at 35% FVF (a+c) and 50% FVF (b+d).

Appendix B. Processing of conditions for the DCM process.

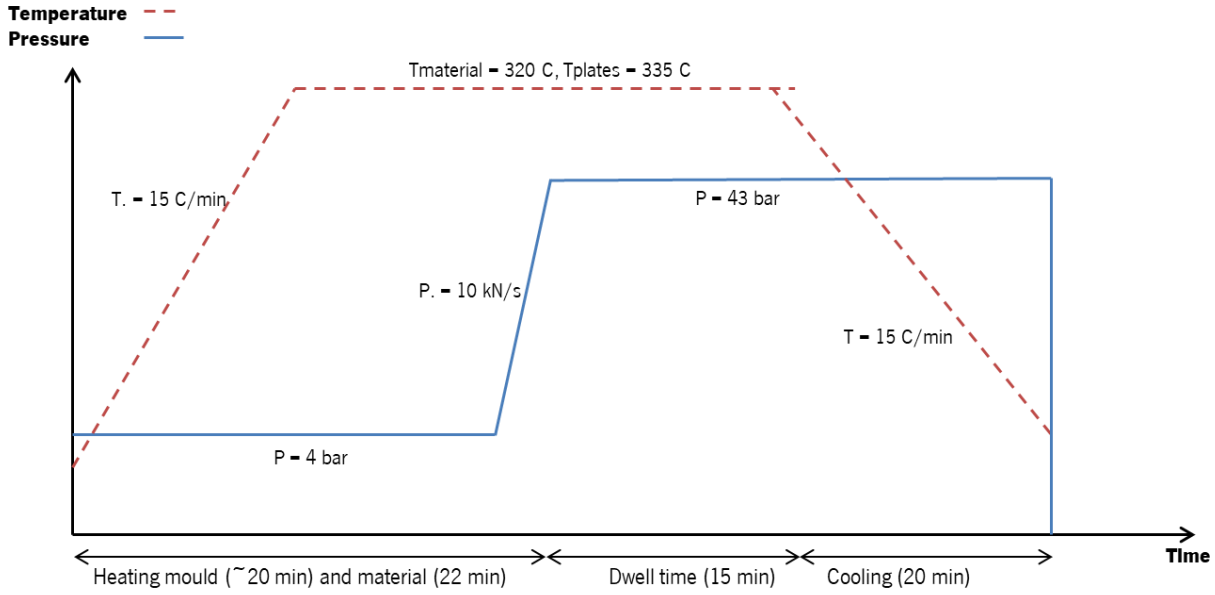

Figure B.3 The DCM processing conditions over time, as is referred to in Section 4.2.6.

Appendix C. An overview of all flexural results

All flexural modulus and strength results for C/PPS are given in Figure C.4 and Figure C.5, respectively, and for G/PP are given in Figure C.6 and Figure C.7, respectively. More details in Section 4.3.

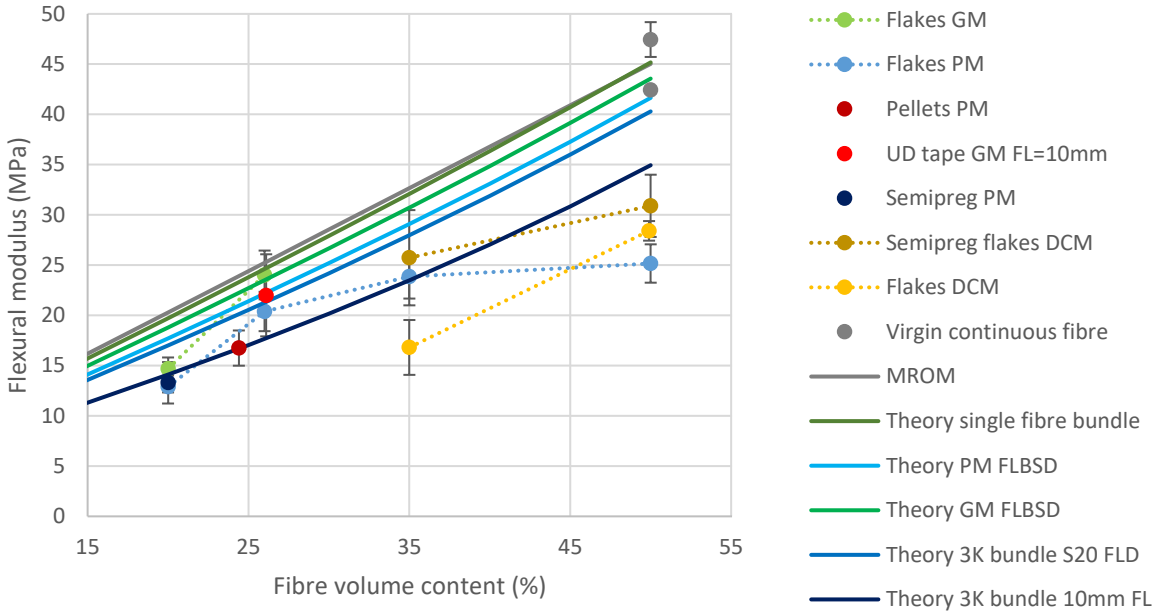

Figure C.4 – Flexural modulus results for virgin continuous fibre materials, materials with discontinuous fibres for various structures, degrees of mixing and predictions of theoretical models. All C/PPS material. The virgin continuous fibre results are for a QI layup with a different outer ply orientation. Error bars represent one SD.

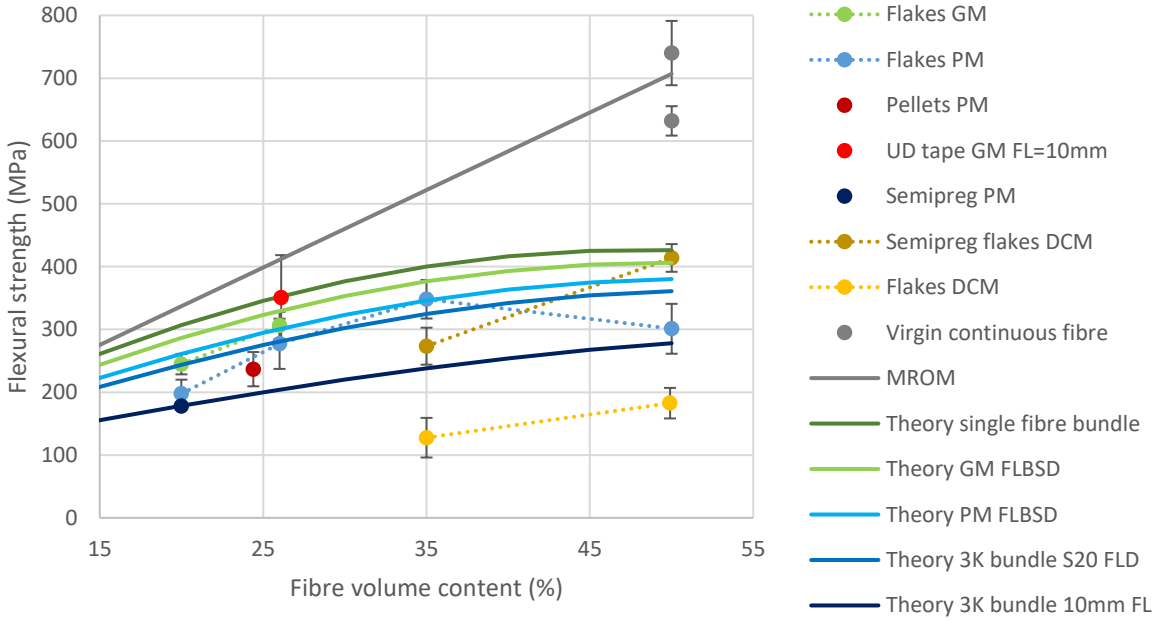

Figure C.5 – Flexural strength results for virgin continuous fibre materials, materials with discontinuous fibres for various structures, degrees of mixing and predictions of theoretical models. All C/PPS material. The virgin continuous fibre results are for a QI layup with a different outer ply orientation. Error bars represent one SD.

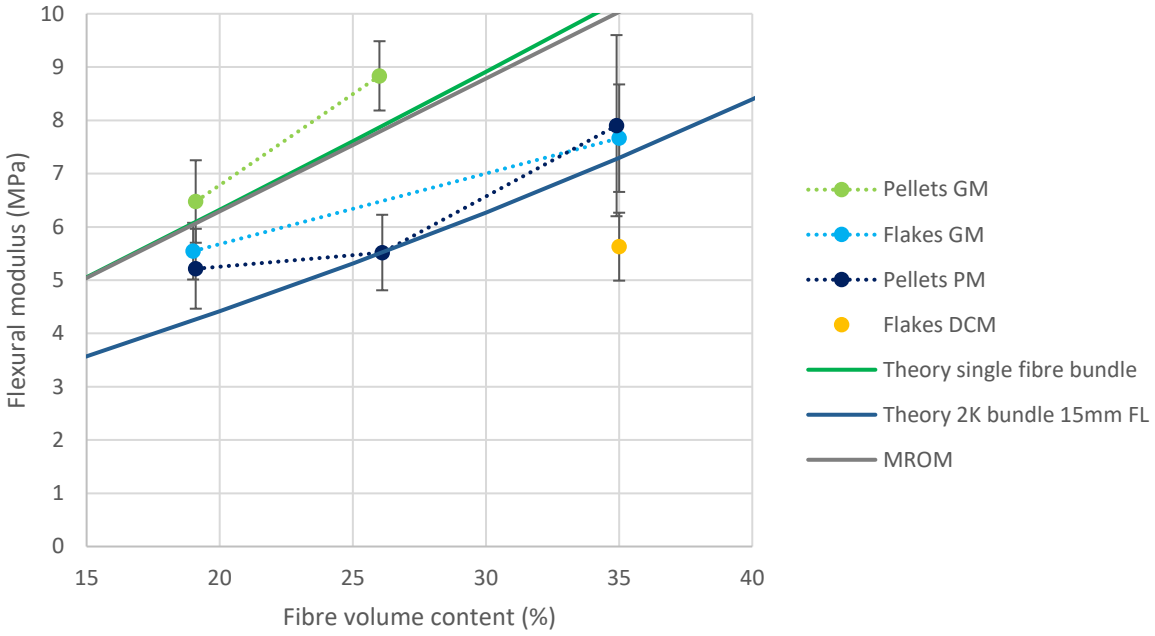

Figure C.6 - Flexural modulus results for materials with discontinuous fibres at various degrees of mixing and predictions of theoretical models. All G/PP material. Error bars represent one SD.

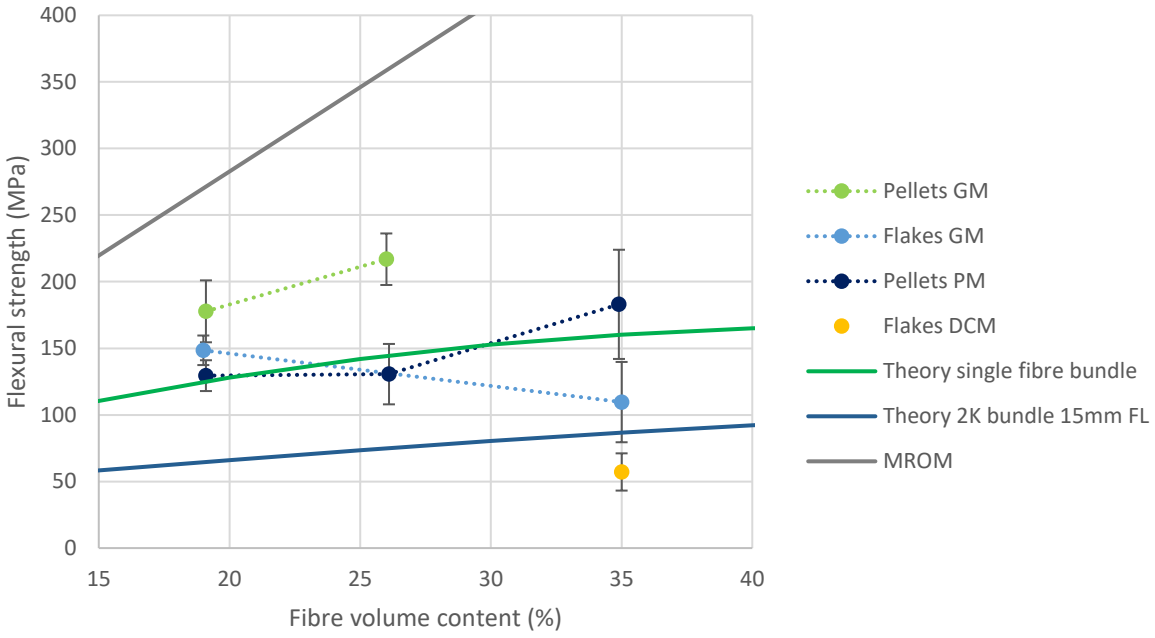

Figure C.7 - Flexural strength results for materials with discontinuous fibres for various degrees of mixing and predictions of theoretical models. All G/PP material. Error bars represent one SD.

Appendix D. Impact on material and design feature level

Table D.1 presents the material properties and environmental and cost impact on material level. Table D.2 and Table D.3 show the environmental and cost impact for a flat beam and T-shaped profile, respectively. More info can be found in Section 6.3.

Table D.1 - Overview of material properties and impact on GHG, CED and economic cost

Material	Fibre weight content (%)	Fibre volume content (%)	Fibre length (mm)	Density (kg/m3)	Flexural modulus (GPa)*	Flexural strength (MPa)*	Specific flex stiffness [illegible]	GHG (kg CO_{2eq}/kg)	CED (MJ/kg)	Cost (€/kg)	GHG per Specific stiffness (kg CO_{2eq}/kNm)	CED per specific stiffness (J/kNm)	Cost per specific stiffness (€/kNm)	Source
C/PPS SFT	25	20	< 5	1418	17.6	208.5	12.4	21.6	348	11.88	1.74	28.03	0.96	Average of CES PPS, 20%w and 30%w Carbon fibre
G/PP SFT	40	20	< 5	1220	6.965	128	5.7	1.84	58.35	1.79	0.32	10.22	0.31	CES PP homopolymer, 40%w glass fibre
C/PPS LFT recycled	25	20	> 5	1420	13	250	9.2	3.14	77.32	6.81	0.34	8.45	0.74	Cost: assuming 5euro/kg collection and logistics + 1 euro/kg shredding + cost based CES PPS, GHG/CED Ecoinvent V2-2, 2010 (cell 2313) and (cell 4138)
G/PP LFT recycled	40	20	> 5	1210	5.5	180	4.5	0.47	14.58	1.06	0.10	3.21	0.23	Cost: assume 0.5 euro/kg collection and logistics + 0.5 euro/kg shredding + cost based CES PP GHG/CED Ecoinvent V2-2, 2010 (cell 4138)
Aluminium	x	x	x	2880	67	194.5	23.3	12.2	186	2.12	0.52	8.00	0.09	CES Aluminium 713.0 permanent mould cast, T5
Steel	x	x	x	7850	207.5	380	26.4	2.37	32.35	0.65	0.09	1.22	0.02	CES Carbon steel, AISI 1095, annealed
C/epoxy 70(QI)*	63	52	∞	1575	62.15	549.5	39.5	45	647.5	47.75	1.14	16.41	1.21	CES Epoxy/HS carbon fiber, woven prepreg, QI lay-up
G/epoxy 70 (QI)*	65	44	∞	1860	26.2	255.5	14.1	6.185	104.8	30.35	0.44	7.44	2.15	CES Epoxy / E-glass fiber, woven prepreg, QI lay-up

*outer ply orientation unknown for QI layup

Table D.2 - The influence of a flat beam per meter length, with a bending stiffness of 2 Nm^2 and 10mm width, for various material types on the thickness, mass, environmental and economic impact

Material	Thickness *t* (mm)	Mass (g/m)	GHG (kg CO_2 eq/m)	CED (MJ/m)	Material costs (€/m)
C/PPS 25	5.1	73	1.58	25.4	0.87
G/PP 25	7.0	86	0.16	5.0	0.15
C/PPS 25 recycled	5.7	81	0.25	6.3	0.55
G/PP 40 recycled	7.6	92	0.04	1.3	0.10
Aluminium	3.3	95	1.16	17.7	0.20
Steel	2.3	178	0.42	5.7	0.11
C/epoxy QI	3.4	53	2.40	34.5	2.54
G/epoxy QI	4.5	84	0.52	8.8	2.54

Table D.3 - The influence of a T shaped profile per meter length, with a bending stiffness of 2 Nm^2 and 10mm width, for various material types on the thickness, mass, environmental and economic impact

Material	Thickness *t* (mm)	Mass (g/m)	GHG (kg CO_2 eq/m)	CED (MJ/m)	Material costs (€/m)
C/PPS 25	1.55	22	0.47	7.6	0.26
G/PP 40	2.3	28	0.05	1.6	0.05
C/PPS 25 recycled	1.95	28	0.09	2.1	0.19
G/PP recycled	2.5	30	0.01	0.4	0.03

Appendix E. Life Cycle Inventory of the access panel

Table E.4, Table E.5 and Table E.6 present the life cycle inventory of the access panel for scenario I, II and III, respectively. Further explanation can be found in Section 6.4.2.

Table E.4 - Access panel scenario I: Hand layup panel of virgin epoxy and carbon material

Item	Weight (g)	CED per access panel (MJ)	GHG per access panel (kg CO_{2eq})	Cost driven unit	Cost per access panel (€)	Source
Prepreg carbon fibres	625	214	12.96	90 €/kg	56.25	[21], Ecoinvent V2-2, 2010 (cell 4716)
Processing: Hand lay-up and autoclave	606	50.0	8.00	*	106.31	*
NDT				74.25 €/h	12.38	
Shipping and Cooled transport	500 and 625	1.72	0.09		6.37	Ecoinvent V2-2, 2010 (cell 4313 /cell 4138)
Fuel (use phase)	500	14980	222600	801.94 €/kg	400.97	Ecoinvent V2-2, 2010 (3998)
End of life (incineration)	687	-23.4	2.08	0.25 €/kg	0.17	[21], Ecoinvent V2-2, 2010 (cell 4863)
Total life cycle costs		15222	222623		582.43	
Access panel part (excl. Fuel (use phase))		242	23		181.46	

*Processing cost of Hand lay-up is estimated by 75 min of cooled storage, cutting, hand layup, vacuum bagging, debagging and trimming at an average of 74,35 euro per hour, incl. 35% overhead and profit. Autoclave is estimated at 150 euro/h, 50 parts per cycle of 3 hours, resulting in 9 euro per part.

Table E.5 - Access panel scenario II: Direct compression moulded panel of recycled material

Item	Weight (g)	CED per access panel (MJ)	GHG per access panel (kg CO_{2eq})	Cost driven unit	Cost per access panel (€)	Source
Shredded recycled C/PPS prepreg	556	0.23	0.03	Material 5 €/kg Shredding 1 €/kg	3.33	Ecoinvent V2-2, 2010 (cell 4138), D. Woldt[11]
Processing: Direct compression moulding*	525	122.5	24.4	175.5 €/h	324.00	
NDT				74.25 €/h	12.38	
Shipping	500	1.70	0.09	In NL 50 €/ 50 parts, sea 246 US$/50 parts	5.37	Ecoinvent V2-2, 2010 (cell 4313 / cell 4138)
Fuel (use phase)	500	14980	222600	801.94 €/kg	400.97	Ecoinvent V2-2, 2010 (3998)
End of life (incineration)	550	-16.8	1.63	0.25 €/kg	0.14	CES Edupack PPS 40% carbon fibre
Total life cycle costs		**15088**	**222626**		**746.18**	
Access panel part* (excl. Fuel (use phase))		**108**	**26**		**345.21**	

*Processing cost for direct compression moulding is estimated by 120 euro per hour for a cycle of 2 hours, excl. 35% overhead and profit.

Table E.6 - Access panel scenario III: Mixed and compression moulded panel of recycled + virgin material

Item	Weight (g)	CED per access panel (MJ)	GHG per access panel (kg CO_{2eq})	Cost driven unit	Cost per access panel (€)	Source
Shredded Recycled C/PPS	241	0.1	0.01	Material 5€/kg Shredding 1 €/kg	1.45	Ecoinvent V2-2, 2010 (cell 4138), D. Woldt[11]
Virgin PPS	309	42.4	1.71	7.45 €/kg	2.30	Ecoinvent V2-2, 2010 (cell 2313), cost CES Edupack PPS
Processing: Mixed and compression moulding	525	11.55	0.87	175.5 €/h	43.88	
NDT				74.25 €/h	12.38	
Shipping	500	1.70	0.09	In NL 50 €/ 50 parts, sea 246 US$/50 parts	5.36	Ecoinvent V2-2, 2010 (cell 4313 / cell 4138)
Fuel (use phase)	500	14980	222600	801.94 €/kg	400.97	Ecoinvent V2-2, 2010 (3998)
End of life (incineration)	550	-16.6	1.61	0.25 €/kg	0.14	CES Edupack PPS 40% carbon fibre
Total life cycle costs		**15019**	**222604**		**468.80**	
Access panel part (excl. Fuel (use phase))		**39**	**4.3**		**67.83**	

* Processing cost of mixed and compression moulding is estimated by 130 euro/h and a cycle of 15 minutes per part, excl. 35% overhead and profit.

Appendix F. Life Cycle Inventory of the safety shoe nose cap

Table F.7 and Table F.8 present the life cycle inventory of the safety shoe nose cap for scenario I and II, respectively. Further explanation can be found in Section 6.5.26.4.2.

Table F.7 - Scenario I: Safety shoe cap virgin material

Item	Weight (g)	CED per nose cap (MJ)	GHG per nose cap (kg CO_{2eq})	Cost driven unit	Cost per nose cap (€)	Source
Glass fibres	59.6	2.73	0.157	2 €/kg	0.12	Ecoinvent V2-2, 2010 (cell 1586)
Epoxy	23.2	2.98	0.153	2.27 €/kg	0.05	CES Edupack epoxy resin (unfilled)
Weaving	59.6	0.52	0.024	Incl. in glass fibre		Ecoinvent V2-2, 2010 (cell 4716)
Cutting				1 min	0.10	
Layup				1 min	0.10	
Resin Transfer Moulding*	72.5	1.40	0.267	1.5 min	1.10	CES Edupack advanced composites moulding
Trimming				1 min	0.10	
Transport Brazil to Netherlands		0.172	0.009	12500 km	0.04	Ecoinvent V2-2, 2010 (cell 4313)
(Use)					(0)	
End of life	69	-0.99	0.011		0.02	IDEMAT (cell 4849)
Total		**6.82**	**0.62**		**1.62**	

*The resin transfer moulding setup is 45 euro/h incl. overhead and profit and produces 4 nose caps every 6 minutes.

Table F.8 - Scenario II: Safety shoe cap (recycled material + virgin material)

Item	Weight (g)	CED per nose cap (MJ)	GHG per nose cap (CO_{2eq})	Cost driven unit	Cost per nose cap (€)	Source
Recycled G/PP	63.2	0.15	0.008	0.5 €/kg	0.03	Ecoinvent V2-2, 2010 (cell 4138) [7]
Virgin PP	12.7	0.95	0.025	1.335 €/kg	0.02	Ecoinvent V2-2, 2010 (cell 2314), cost CES Edupack
Shredding		0.01	0.002	0.5 €/kg	0.03	D. Woldt [11], CES Edupack PP 40% glass polymer moulding
Mixing and compression moulding*		1.42	0.11	1 min	0.75	CES Edupack PP 40% glass polymer moulding
Transport		0.17	0.009	12500 km	0.04	Ecoinvent V2-2, 2010 (cell 4313)
(Use)					(0)	
End of life	69	-2.4	0.008	0.25 €/kg	0.02	Idemat 2010 PP combustion
Total		**0.28**	**0.16**		**0.88**	

*The mixing and compression moulding setup are 45 euro/h incl. overhead and profit and produces 4 nose caps every 4 minutes.